Spatiotemporal Control of Mycobacterium Tuberculosis Cell Wall Biogenesis by the Peptidoglycan Synthase PonA1

Spatiotemporal control of *Mycobacterium tuberculosis* cell wall biogenesis by the peptidoglycan synthase PonA1

A dissertation presented

by

Karen Kieser

to

The Committee on Higher Degrees in Biological Sciences in Public Health

in partial fulfillment of the requirements

for the degree of

Doctor of Philosophy

in the subject of

Biological Sciences in Public Health

Harvard University

Cambridge, Massachusetts

April 2015

Professor Eric J. Rubin, MD, PhD Karen Kieser

Spatiotemporal control of *Mycobacterium tuberculosis* cell wall biogenesis by the peptidoglycan synthase PonA1

Abstract

Mycobacterium tuberculosis causes one of the most pernicious infectious diseases of humankind – tuberculosis, which is still a global problem in the 21st century. Drug-resistant *M. tuberculosis* infections are on the rise, necessitating novel drug development. A particularly fruitful avenue for drug development is the bacterial cell wall, as it is a structure required for bacterial survival and is accessible to small molecules. This complex structure must be dynamically remodeled every cell cycle to promote bacterial growth, and our understanding of how *M. tuberculosis* governs this process and the enzymes involved is rudimentary.

My work investigates how *M. tuberculosis* governs the synthesis and remodeling of an essential component of its cell wall – peptidoglycan. For cells to grow and divide, the peptidoglycan layer must be actively metabolized. Failures in the peptidoglycan structure result in cell lysis and death, which is why peptidoglycan synthesis is often targeted by antibiotics, such as penicillin. Hence, peptidoglycan must be static enough to resist interior turgor pressure and exterior insults (like antibiotics) and yet it must also be plastic enough to allow local restructuring to promote cell growth. How does the cell govern these paradoxical processes in both space and time to ensure survival?

I used a key peptidoglycan synthase, PonA1, to understand how *M. tuberculosis* engineers its cell wall during growth and division. PonA1 localizes to the cell septum during division, where it interacts with the essential peptidoglycan hydrolase RipA and modulates RipA activity during cell separation. PonA1 also localizes to the cell pole where it promotes expansion of the peptidoglycan layer of the cell envelope. I found that PonA1 is critical for the proper spatial organization of new pole growth and that phosphorylation of PonA1 modulates the rate of cell elongation at the pole.

In an effort to expand our understanding of how *M. tuberculosis* remodels its cell wall, I performed a whole genome mutagenesis screen to identify genetic partners of PonA1. I found factors critical for peptidoglycan synthesis, namely PonA2 and LdtB, a nonclassical transpeptidase that synthesizes the predominant crosslink in mycobacterial peptidoglycan. Further genetic and biochemical studies showed that simultaneous loss of PonA2 and LdtB is lethal to *M. tuberculosis*, suggesting an opportunity to develop chemotherapeutics targeting 3-3 transpeptidases like LdtB. These studies also suggested that enzymatic pathways that govern *M. tuberculosis* cell wall synthesis are spatially resolved.

My work identified genetic networks that govern cell wall construction in *M. tuberculosis* and showed the critical role of the peptidoglycan synthase PonA1 in controlling growth at the cell pole. Defining the spatiotemporal dynamics of key cell wall synthase proteins is important for understanding *M. tuberculosis*' physiology. My work expands our understanding of how a prevalent human pathogen governs the synthesis of its cell wall, a critical source for novel drug development.

Table of Contents

Dedication

This dissertation is dedicated to my parents, Laura and Robert Kieser, for their unswerving loyalty, love, and support. You both sacrificed much so that I could have much. Your desire for your children to achieve more than you were granted by life is the rock upon which my life is built. I am so grateful for all that you have done and continue to do for me. Thank you. I love you!

Acknowledgements

I thank my advisor, Dr. Eric Rubin, for his extraordinary guidance. I came to graduate school never having worked with bacteria and knowing little about genetics, and you have been an amazing support. You gave me invaluable tools for my scientific development and showed me how excellent science can be performed with kindness and goodwill. I am so grateful for the years of advice, encouragement, and care.

I also thank my dissertation advisory committee members Dr. Sarah Fortune, Dr. Marcia Goldberg, and Dr. Thomas Bernhardt for their excellent suggestions. I am grateful to have benefited from your wisdom, leadership, and exemplary science. I also thank Dr. Marcia Goldberg and Dr. Barbara Burleigh for crucial moments of advice and encouragement. You are incredible scientists and mentors, and my graduate school experience and science were the better for it. I thank my defense committee, Drs. Marcia Goldberg, Dyann Wirth, Barbara Burleigh, and Simon Dove, for their time and expertise at this juncture in my scientific career.

I am grateful to Dr. Zeynep Madak-Erdogan for her guidance and encouragement. You taught me the importance of pursuing goals with excellence and determination. Thank you for leading by example and for teaching me how to critically think about biology – and how to plan experiments with finesse. I will always be grateful for your unswerving confidence in my abilities and for your encouragement to pursue doctoral work, and at the highest level.

I am grateful to Dr. Simon Dove for his continued support. You have taught me so much – not the least of which is to believe in myself. Thank you for your limitless patience (even teaching me how to properly plate bacteria!) and encouragement to pursue good science. I am so appreciative of your mentorship and advice as I maneuvered through the difficulties of graduate school and science.

I have been fortunate to do my graduate work in a lab populated with wonderful people. To all of my past and current labmates – thank you! I especially want to thank Dr. Amy Barczak and Dr. Alissa Myrick for their friendship and guidance. Thank you for answering my innumerable queries with grace, kindness, and amazing advice. I respect you both immensely and am so grateful to have you as friends and role models. I am grateful to Dr. Michael Chao for teaching me the very basics of microbiology and bacterial genetics when I first joined the lab. I so appreciate your generosity, time, and intellectual

curiosity! I thank Dr. Cara Boutte for critical moments of mentorship (scientific and personal), and for your unflagging willingness to think through data, experiments, and papers. It's been such a pleasure to finish my PhD with you in the lab. To our technicians extraordinaire – Shoko Wakabayashi and Jess Pinkham – I am so grateful to also be able to call you friends. Thank you for making work in the BL3 more pleasant and for your generous help during experiments. I also thank Robin Basu Roy, Andrej Trauner, Brian Schuster, and Ravi Raju for making lab feel like a home at times.

I thank Dr. Thomas Bernhardt and Dr. David Rudner for generously allowing me to become a pseudo-lab member. I learned so much from both of you and from your labs. Thank you for stimulating conversations and excellent critiques of my data. I also thank members of the Rubin, Fortune, Bernhardt, Rudner, and Waldor labs for helpful discussions and thoughtful feedback on my work. You are amazing colleagues, and it has been a pleasure to have gotten to know and learn from all of you. And to Richa Gawande, Selasi Dankwa, Anthony Covarrubias, and Kutay Karatepe – wonderful fellow BPHers – I am honored to have you in my circle. You are extraordinarily gifted people, in so many ways, and graduate school would not have been the same without you. Thank you for your support!

And to my family and extraordinary friends: how lucky am I? You enrich me and my life in countless ways. Thank you!! I love you and am so indebted to each of you for the innumerable times that you have helped, guided, encouraged, supported, and sustained me these past 5 ½ years – this journey would have been impossible without you. I am especially grateful to Phil, Kathy, Suz, Andy, Holli, Ron, Lanae, Nic, Colleen, and Christine. Thank you for being such incredible parts of my life!

I am indebted to my wonderful partner (fiancé!), Daniel, without whom I would not have survived graduate school. Thank you for the innumerable pep talks, critical feedback, listening to late-night practice talks, and endless patience with last minute rescheduling due to experimental snafus. I am so grateful for your support on this road. You continue to make me a better scientist and, most importantly, a better person. I could not be more fortunate to share this life with someone who loves science, art, culture, and humanity as much as you do. Our journey together so far has been incredible, and I am delighted and grateful to be sharing this road together! I love you.

Chapter 1

Mycobacterial Cell Growth and Division

Section 1.1 Overview and Attributions

Overview

This chapter is composed of a review published in August 2014 in Nature Reviews Microbiology as well as a list of known factors involved in cell wall biogenesis in *M. tuberculosis*.

Attributions

I researched and wrote the review manuscript. Eric, several readers (see Acknowledgements), and Christina Tobin-Kåhrström (our editor at Nature Reviews Microbiology) provided editorial input.

Section 1.2 How sisters grow apart: mycobacterial growth and cell division

Karen J. Kieser[1] and Eric J. Rubin[1,2, ‡]

[1]Department of Immunology and Infectious Diseases, Harvard School of Public Health

[2]Department of Microbiology and Immunobiology, Harvard Medical School

Boston, Massachusetts, USA 02115

‡ Corresponding Author: erubin@hsph.harvard.edu

‡ Corresponding Author Present Address:

Harvard Institutes of Medicine, Room 1048

4 Blackfan Circle

Boston, MA 02115

(617) 432-3337

Abstract

Mycobacterium tuberculosis, the aetiologic agent of tuberculosis, owes much of its success as a pathogen to its unique cell wall and unusual mechanism of growth, which facilitate its adaptation to the human host and could play a role in clinical latency. Asymmetric growth and division increases population heterogeneity, which may increase antibiotic tolerance and the fitness of single cells. Here we review the unusual mechanisms of mycobacterial growth and cell wall biogenesis and discuss how these processes might affect *M. tuberculosis* survival *in vivo* and contribute to the persistence of infection.

Introduction

Mycobacterium tuberculosis is an extraordinarily successful human pathogen that infects up to one third of the global population [1] and causes one of the most recalcitrant bacterial infections of the modern era. Infection begins with the inhalation of aerosols containing *M. tuberculosis*, which are primarily taken up by alveolar macrophages, although other host cells can phagocytose the bacterium, including dendritic cells, monocytes and neutrophils [2,3]. A local proinflammatory response occurs in the lung, which results in the recruitment of additional monocytes and lymphocytes [3,4]. Assembly of these cells around infected macrophages generates a cellular mass, known as a granuloma, which is a pathological hallmark of tuberculosis (TB).

Granuloma histology is heterogeneous, even within a single individual, and ranges from cellular to caseous to fibrotic lesions [5]. Granulomas are traditionally considered an attempt by the host to control the infection, but the ability to restrict mycobacterial proliferation varies [6,7]. For example, caseating granulomas, which contain hypoxic centres [8], often rupture and release bacteria, which are then free to invade the surrounding host cells [4]. Furthermore, *M. tuberculosis* localizes to distinct regions within the granuloma [5], which also contain different subsets of immune cells. Thus, depending on the bacterial location and the immune cells present, the inflammatory response is likely to differ between distinct sites of the granuloma [9], which probably affects clearance of the infection. Inside macrophages, *M. tuberculosis* is usually found within a phagosome of variable maturation states [3] and encounters an arsenal of host defences, including phagosome acidification, antimicrobial peptides and reactive oxygen

species [4]. This range of distinct microenvironments exerts discrete selective pressures on individual bacterial cells, which suggests that mycobacteria need to adapt to ensure survival. How is such adaptation achieved? Recent work has revealed that mycobacterial cell growth and division produces heterogeneous daughter cells [10-13], which also undergo substantial cell wall remodelling during infection [14-17].

Proliferation of bacterial cells can be divided into two stages: elongation of the mother cell and division of the elongated mother cell into two daughter cells. In most bacteria, cell division is a symmetric process and produces daughter cells of the same size [18]. However, mycobacteria do not adhere to the "one-size-fits-all" rule and grow and divide in an asymmetric manner, which produces daughter cells of unequal sizes [10-13]. This trait might have been selected for, as cells of different sizes might have distinct survival advantages in the highly variable host environment.

As discussed below, the unique mode of mycobacterial elongation and division produces a population of daughter cells that vary in size, growth rate and cell wall composition [10-13], which functionally diversify the population. This phenotypic heterogeneity is further enhanced by cell wall remodelling processes that occur within the host [141-17]. Mycobacteria have an elaborate cell envelope comprised of several layers (Figure 1.1). Each of these layers displays different chemical modifications and the architecture of the cell wall is also molded through complex regulation. In the host, further remodelling occurs [14-17], which generates a population of cells that not only differ in size and growth properties, but also in the composition of their cell wall. This diversity is predicted to increase survival *in vivo* and has the potential to influence disease progression and clinical latency.

In this Review, we discuss the mechanisms and regulation of mycobacterial cell wall biogenesis, cell elongation and division. We also describe how these processes produce heterogeneity at the population level and consider the implications of single cell diversity for survival in the host.

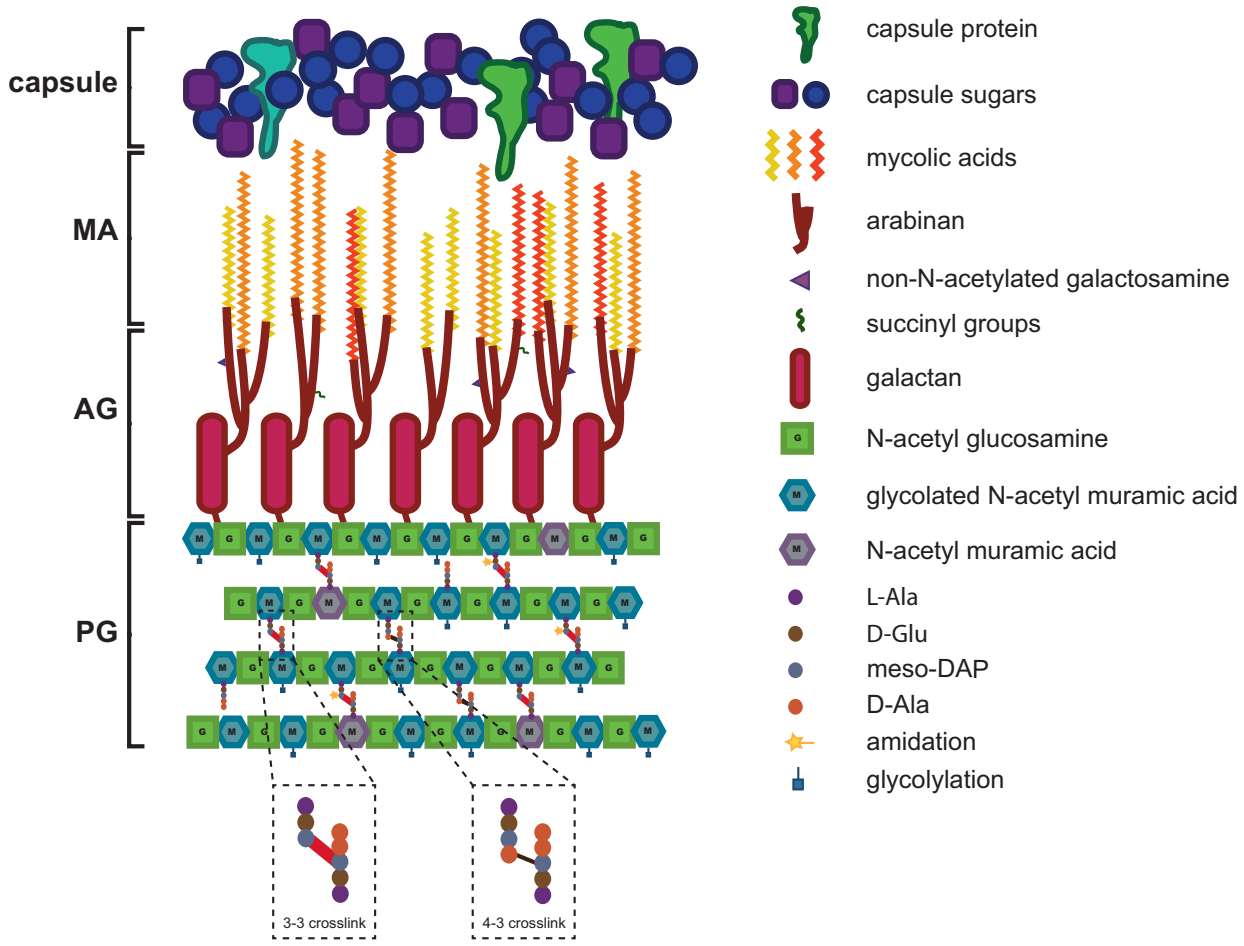

Figure 1.1. The mycobacterial cell wall. A thick layer of peptidoglycan (PG) covers the cell's plasma membrane (not shown). Mycobacterial PG contains unique chemistry, including glycolylation and amidation. The peptide crosslinks exist in two forms: as either 3-3 or 4-3 peptide crosslinks. Arabinogalactan (AG) is covalently crosslinked to the PG layer. The AG can be modified with succinyl moieties or non-N-acetylated galactosamines. A thick layer of mycolic acids (MA) are attached to the arabinogalactan layer and are thought to form an outermembrane like structure. During growth in more host-like conditions or during infection, the cell wall is surrounded with a capsule, which is composed of sugars and proteins.

The cell envelope of mycobacteria

The mycobacterial cell wall is a complex structure required for cell growth, resistance to antibiotics and virulence [76,105,106]. It is composed of three distinct macromolecules – peptidoglycan (PG), arabinogalactan (AG), and mycolic acids (MA) – surrounded by a non-covalently linked outer capsule of proteins and polysaccharides [23,76,105,107] (Figure 1.1; see Appendix 1 for more details). The high

density of lipids in the cell wall prevents accurate Gram staining and mycobacteria are referred to as acid-fast as they can be stained by acid-fast dyes, such as Ziehl-Neelson [23]. The cell wall is the most common target of antituberculosis drugs and many compounds that are in clinical use or are under development target enzymes that synthesize each layer of the cell wall [108].

The PG layer surrounds the plasma membrane and comprises long polymers of the repeating disaccharide N-acetyl glucosamine–N-acetyl muramic acid (NAG-NAM) that are linked via peptide bridges. The PG precursor Lipid II is generated in the cytoplasm [18,23] and is likely transported across the periplasm by the transmembrane protein MviN [21]. Unidentified hydrolases are required to open the PG mesh for the insertion of new precursors [18], which are added in an “inside to outside” manner [109]. The penicillin binding proteins (PBPs) PonA1 and PonA2 incorporate new subunits into the existing structure. Transpeptidases, such as PBPA, PBPB, LdtA and LdtB crosslink the newly inserted material [23]. Compared to other model bacteria, such as *Escherichia coli* and *Bacillus subtilis*, mycobacterial PG is heavily crosslinked. Up to 80% of the PG contains ‘nontraditional’ 3→3 peptide crosslinks instead of the ‘traditional’ 4→3 crosslink [72,75]. The PG polymer is also modified, such as glycolylation of NAM residues [73,110] and amidation of the D-Glu and meso-diaminopimelic acid (DAP) residues of the peptide side chain [72,111]. Amidation may mask recognition by the innate immune receptor Nod1, which has been observed in *B. subtilis* [112]. However, glycolylated NAM is efficiently recognized by Nod2 and induces the production of inflammatory cytokines in *M. tuberculosis*-infected macrophages [113,114].

A layer of AG surrounds the PG layer (Figure 1.1). Galactan comprises a repeating disaccharide unit of 6-D-Gal*f*β1→5-D-Gal*f*β and is synthesized by the galactofuranosyl transferases Glf, GlfT1 and GlfT2. Galactan is decorated with long arabinan polymers that are synthesized by the successive actions of DprE1, DprE2 [115], AftA, EmbA, EmbB and AftB [105]. Variability in arabinosylation exists, with some galactan chains remaining free of arabinan [116]. Arabinan chain termini are branched, a motif that is generated by the actions of AftD [117] and Rv1459 [105]. Arabinan can also be further modified by the addition of succinyl or unusual non-N-acetylated galactosamine (GalN) moieties [105]. The GalN

modifications are mainly present in pathogenic mycobacteria and may promote efficient infection, which has been observed in *Francisella tularensis* [74].

The majority of arabinan is ligated with long carbon chain mycolic acids (MA) [76,77,105], which form the characteristic thick waxy lipid coat of mycobacteria [23,118] and are major contributors to the impermeability of the cell wall [23,76,77] and virulence [76,100]. MA are formed from two fatty acids, a saturated shorter C_{20}-C_{26} α-branch that is connected to a C_{60}-C_{90} meromycolate branch. These branches are generated by the FASI and FASII [76,77,119]. FASI products are transferred to FASII for extension by the combined action of FabH, AcpM and FabD [76,77]. MA are then processed and matured by a cascade of enzymes [76,77,120,121] resulting in three distinct meromycolate variants: α-meroacids, methoxy-meroacids and keto-meroacids [76,77]. All three variants are required for full virulence during infection and have varying levels of saturation, cyclopropanation and oxygenation [76,77]. The inner membrane transporter MmpL shuttles MA to the cell surface [122-124] where the FbpABCD (Antigen85) complex ligates the MA monomer to AG [76,77,105]. While the coordination of MA and AG synthesis and insertion in the cell wall remains unknown, recent data suggest these macromolecules are produced and exported at the cell pole [19,125], where mycobacteria generate new cell growth.

Canonical cell growth in model organisms

The traditional model bacteria *Escherichia coli* and *Bacillus subtilis* have a vastly different cell wall architecture compared to mycobacteria and as such, cell wall synthesis and cell division rely on a different set of proteins. In *E. coli* and *B. subtilis* elongation occurs along the lateral cell wall and the elongation complex is comprised of PG synthases, lipoprotein modulators of PBP activity, cytoskeletal-like proteins and PG hydrolases [18,126-128]. PG synthesis is coordinated by bifunctional (*E. coli* PBP1a and perhaps PBP1b [18]; *B. subtilis* PBP1 [129]) and monofunctional (*E. coli* PBP2 [18]; *B. subtilis* PBP2a and PbpH [126]) PBPs (Table 1.1). The actin homologue MreB forms filaments underlying the elongation complex and facilitates elongation in *E. coli* and *B. subtilis*, which has two additional MreB homologues MreBH and Mbl [130], by guiding elongation complexes along the lateral wall [18,130] (Table 1.2). It has

Table 1.1. Major cell growth and division factors in *E. coli*, *B. subtilis*, and mycobacteria

	E. coli	*B. subtilis*	mycobacteria	function
elongation	PBP1a[18]	PBP1[126]	PonA1[28]	PG synthase
	PBP1b?[18]		PonA2?	PG synthase
	PBP2[18]	PBP2a[123]	LdtAB?[31]	PG synthase
		PbpH[123]		PG synthase
	Spr[124]			PG hydrolase
	YdhO[124]			PG hydrolase
	YebA[124]			PG hydrolase
		CwlO[125]		PG hydrolase
		LytE[125]		PG hydrolase
	MreBCD[18]	MreBCD[127]		structural protein
		MreBH[127]		structural protein
		Mbl[127]		structural protein
			Wag31[23]	structural protein
			CwsA[25]	structural protein
division	PBP1b[18]	PBP1[123]	PonA1[28]	PG synthase
	PBP1a?[18]		PonA2?	PG synthase
	PBP3[18]	PBP2b[123]	PBPA[30]	PG synthase
			PBPB[41]	PG synthase
	AmiABC[18]	LytC[135]		PG hydrolase
		LytD[135]		PG hydrolase
		LytF[135]	RipA[46]	PG hydrolase
			RpfB[47]	PG hydrolase
	ZipA[18]			structural protein
	ZapABCD[18,133]	ZapA[34]		structural protein
	FtsA[18]	FtsA[34]	FhaB[40]	structural protein
		SepF[34]		structural protein
	FtsQLB[18]	DivIBC[130]	FtsQ[22]	structural protein
	FtsW[18]	FtsW[34]	FtsW[22]	structural protein
	FtsZ[18]	FtsZ[34]	FtsZ[22]	structural protein
	FtsN[18]			structural protein
	FtsP[134]			structural protein
			CrgA[42]	structural protein
			CwsA[25]	structural protein

also been reported that interactions between FtsZ and MreB are necessary for appropriate cell division in *E. coli* [131], suggesting a potential mechanism for coordinating elongation and division.

Similarly to mycobacteria, polymerization of FtsZ initiates cell division in *E. coli* and *B. subtilis*. The divisome is mainly composed of PG synthases that construct the septum (*E. coli* PBP1b, perhaps PBP1a, and PBP3 [18]; *B. subtilis* PBP1 and PBP2b [35]), structural proteins (*E. coli* FtsW, FtsN, FtsQLB [18]; *B.*

subtilis FtsW, DivIBC [132]) and hydrolases that physically separate daughter cells (*E. coli* AmiABC [18]; *B. subtilis* LytCDF [133]). Other factors that regulate divisome formation are also involved [18,35,134]. Placement of the Z-ring is carefully controlled, and in *E. coli*, this is regulated by the MinCDE system during normal growth and by SulA when the SOS response is induced [134] (Table 1.2). In *B. subtilis*, the functional homologues of MinCDE (MinCD and DivIVA), together with EzrA, are responsible for determining the site of Z ring formation [35]. EzrA interacts with FtsZ and PBP1, suggesting that it may synchronize elongation and cell division in *B. subtilis*. The *B. subtilis* ClpXP protease also regulates Z-ring formation by inhibiting FtsZ polymerization [35]. The UDP-glucose transporter UgtP inhibits FtsZ polymerization during nutrient-limiting conditions, thereby coupling growth rate to cell division in *B. subtilis* [35]. The DNA-binding nucleoid occlusion factors (such as SlmA in *E. coli* [134] and Noc in *B. subtilis* [35]) also function in FtsZ placement and regulate Z-ring formation through direct interactions with FtsZ and coordination with the replication machinery, respectively [134] (Table 1.2).

Table 1.2 Cell morphogenesis systems in *E. coli*, *B. subtilis*, and mycobacteria

	E. coli	*B. subtilis*	mycobacteria
negative regulators of the Z-ring	minCDE, SulA	minCD and DivIVA, ClpX, UgtP, MciZ (sporulation)	FtsZ phosphorylation?, ClpX?, ChiZ?, Rv3660c?
positive regulators of the Z-ring	FtsA, ZipA, ZapABCD	FtsA, SepF, ZapA	FtsW?, FhaB (FipA)
nucleoid occlusion	SlmA	Noc	?
subcellular guidance of PG synthesis	MreBCD, RodZ, RodA, PBP2	MreBCD, RodZ, RodA	Wag31 (DivIVA)?, RodA?

Peptidoglycan synthesis & polar growth

Traditional model organisms, such as *E. coli* and *B. subtilis*, are rod-shaped bacilli in which elongation of a mother cell occurs along the cell body, followed by division at mid-cell to generate two equally-sized daughter cells. By contrast, elongation occurs at the cell poles in mycobacteria and results in the production of unequally-sized daughter cells (Figure 1.1).

Is polar growth symmetric or asymmetric?

All rod-shaped bacteria contain two poles: an old pole, which is inherited from the mother cell and a new pole that is synthesized during division. In mycobacteria, polar growth results in daughter cells of different sizes and two hypotheses were recently proposed to explain how this occurs [10,13] (Figure 1.2). One model reported that growth is unipolar owing to the extremely slow growth of the new pole relative to the old pole [10] and it is now recognized that both poles elongate but at different rates [10,13], thus giving rise to daughter cells of different sizes. The second model suggests that the growth rate of the old and new poles is symmetric for the majority of the cell cycle, but that growth predominantly occurs at the old pole after cytokinesis [13], thereby resulting in unequally-sized daughter cells. The use of different experimental conditions and methods for determining the timing of cell division could account for the deviating observations.

The evidence for the symmetric model was derived from the study of *Mycobacterium smegmatis,* in which polar elongation was measured between successive cytokinesis events [13] (Figure 1.2A). Because cytokinesis partitions the mother cell by separating the cytosolic contents, the authors reason that it is during this process that the two daughter cells are generated. To visualize cell growth, cells were pulse labelled with a fluorescent amine-reactive dye that stains the cell surface. The dye does not diffuse during cell growth and enables visualization of newly incorporated, unlabelled cell wall material over time [10,13]. Using this cell surface dye and a fluorescently tagged Wag31 (a protein that localizes to the division septum) the authors assessed polar growth in single cells over time using a microfluidics approach [13]. After cytokinesis (which is detected by Wag31 localization to the septum) but before the physical separation of the cells, growth occurs predominantly at the old pole (Figure 1.2A). After physical cell separation, both the new and old poles of the daughter cells elongate at the same rate until the following cytokinesis event [13].

In the second model, *M. smegmatis* polar elongation was measured between successive cell separation events (Figure 1.2B). Similarly to the previous study, a microfluidics device was used to monitor single cells stained with the fluorescent amine-reactive dye [10]. The marker does not obscure the initiation of

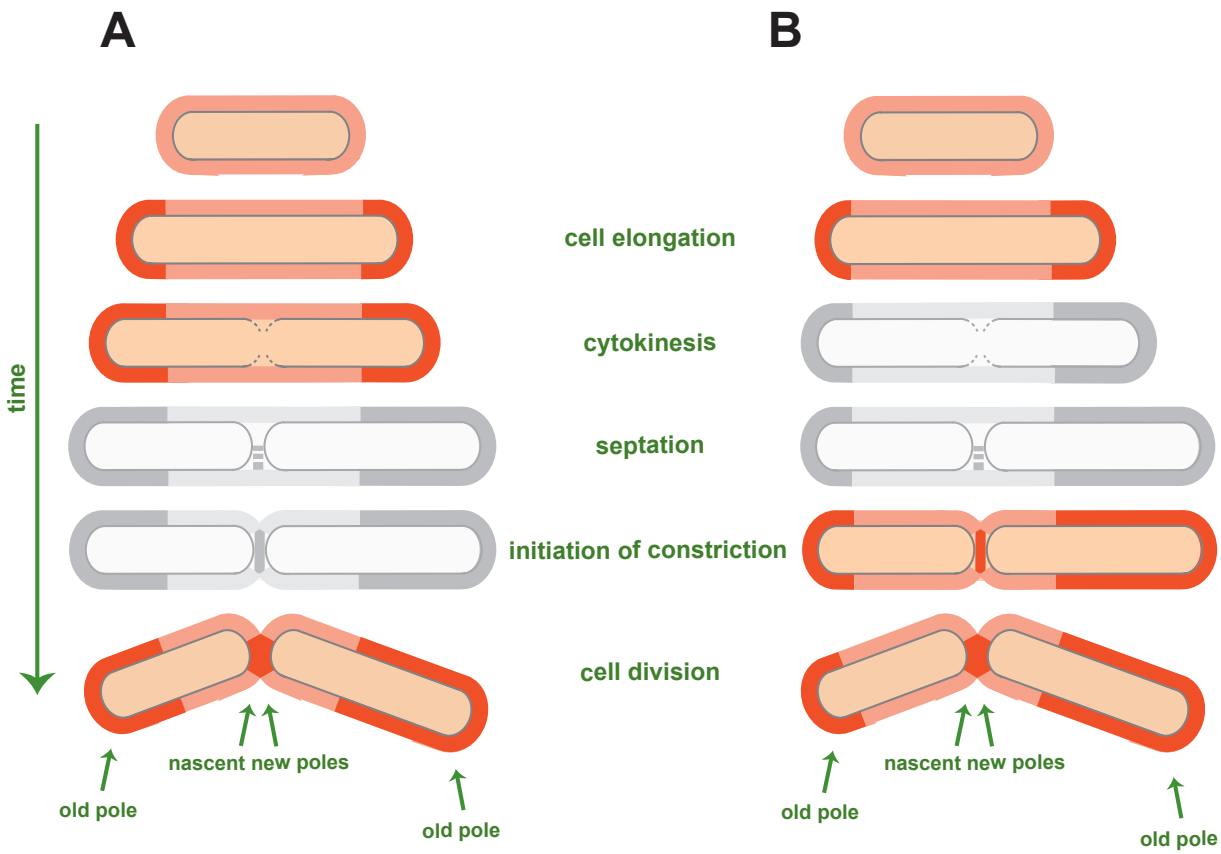

Figure 1.2. Elongation and division of mycobacteria generates asymmetric daughter cells. Mycobacterial cells elongate by incorporating cell wall material (dark orange or grey) at their cell poles and all mother cells contain an old pole (which was inherited from the previous cell division) and a new pole (which was synthesized during the previous cell division). The process of cell division can be subdivided into several stages, including synthesis of the plasma membrane (thin grey line) roughly at mid-cell during cytokinesis, synthesis of a peptidoglycan septum at mid-cell (which is known as septation), constriction of the cell wall and hydrolysis of the septum as the two cells physically separate. Two models have been described to explain how daughter cells of different sizes are generated and the models differ in terms of their definitions of cell division. **(A)** In the first model [13], in which cytokinesis is used to define cell division, growth at both cell poles is symmetric until cytokinesis. From cytokinesis until the cells physically separate, growth occurs predominantly at the old pole, which generates two daughter cells of unequal sizes. In this model, septation and the initiation of constriction were not specifically measured (cells shown in grey). **(B)** In the second model [10], in which the initiation of constriction is used to define cell division, the poles elongate at different rates throughout the cell cycle, with the old pole elongating faster than the new pole at all stages of the process. This model did not specifically measure cytokinesis or septation (cells shown in grey). Despite discrepancies in the timing of asymmetric growth, both models demonstrate that mycobacterial growth generates daughter cells of unequal sizes.

cell constriction [10], which indicates the beginning of physical separation. Using physical separation as the read-out for cell division, the authors found that cells elongate preferentially at the old pole throughout the entire cell cycle (which the authors term unipolar growth) and this was also observed in *M.*

tuberculosis [10]. Subsequent studies, which have also used the physical separation of daughter cells to define cell division, have also shown that polar growth occurs predominantly at the old pole throughout the cell cycle [11,12]. Whether polar elongation is symmetric or asymmetric depends, in part, on whether cell division is defined as cytokinesis [13] or the physical separation of cells [10]. The use of a fluorescent tagged allele of Wag31 may also mask fully wildtype elongation, as recently reported [19]. However, irrespective of the methods used, both models are in agreement that the cell cycle produces daughter cells of different sizes, which elongate at different rates.

Daughter cells that inherit the old pole are larger than their siblings that inherit the new pole and they also elongate faster after the cells separate [10,13]. Hence, cell size, cell age and the nature of the cell poles (old versus new, which correlates with cell size) determine the elongation rate (referred to as velocity in Ref. 13) of newly divided cells. Thus, although daughter cells are genetically identical cells, they are phenotypically different. This is in marked contrast to *E. coli* [10,12], and even *Corynebacterium glutamicum*, which also displays polar growth but produces daughter cells of a similar size and with similar elongation rates [11]. Asymmetric growth of mycobacteria leads to intrinsic heterogeneity in the population, which can have important consequences. For example, large and small daughter cells within microcolonies have been reported to differ in their susceptibility to antibiotics, such that large cells (that have inherited the old pole) are more sensitive to cell wall synthesis inhibitors than their smaller sibling cells [10]. However, this has been challenged by studies in which antibiotic sensitivity was tested across populations instead of within microcolonies [13,20]. Furthermore, asymmetric growth disturbs the distribution of cell wall components, with one daughter cell inheriting mostly newly synthesized cell wall (Figure 1.2). The production of phenotypically distinct daughter cells may confer an advantage when the population is challenged with the variable environments encountered in the host and it could also contribute to the heterogeneous bacterial population that is observed in patients with TB, including cells that are recalcitrant to antibiotics.

Peptidoglycan synthesis

Polar growth requires the synthesis of new cell wall material, which is particularly complicated for mycobacteria as they must simultaneously synthesize PG, arabinogalactan (AG), and mycolic acids (MA) (Figure 1.3). Although the arabinogalactan and mycolic acid biosynthetic machineries have been characterized, here we focus on peptidoglycan synthesis as more is known about how PG synthesis and remodelling contribute to cell proliferation. For both elongation and division, PG precursor subunits (which are known as Lipid II) [18] are shuttled from the cytosol to the periplasm by MviN, a transmembrane protein that links precursor synthesis to cell wall incorporation. MviN activity is promoted by FhaA (which contains a forkhead associated (FHA) domain) that recognizes phosphorylated threonines and binds to a phosphorylated domain of MviN [21]. FhaA localizes to the poles and septa [21], the sites where active cell wall synthesis occurs, so it may be involved in localizing MviN. After transport to the cell exterior, Lipid II is covalently inserted into the expanding cell wall (Figure 1.3).

The elongation complex

Penicillin binding proteins (PBPs) and PG hydrolases coordinate PG synthesis and hydrolysis, respectively, and are therefore key players in PG remodelling that require stringent regulation. A macromolecular machine, known as the elongation complex, regulates peptidoglycan remodelling during cell elongation, and comprises proteins with scaffolding, hydrolytic and synthetic roles [18] (Figure 2.2A). To ensure that elongation is directed to the cell poles, cytoplasmic proteins anchor the elongation complex at these sites. In actinobacteria, the coiled-coil protein DivIVA is used as an anchor [22,23], rather than cytoskeletal-like proteins, which are used to guide cell wall synthesis in other bacteria [18]. In *B. subtilis* DivIVA recognizes membrane curvature [22], which ensures its localization to the poles; recent data indicates the recognition of membrane curvature also targets Wag31, the mycobacterial DivIVA homologue, to the pole [19].

It is likely that Wag31 anchors the nascent elongation complex at the pole and functions as a base for the recruitment of the remaining components of the complex [19]. As proper Wag31 localization at the

Figure 1.3. Protein machineries direct cell growth and division.
Large macromolecular complexes comprised of PG synthases (pink), PG hydrolases (green), structural proteins (yellow) and regulatory factors (blue) coordinate cell elongation and cell division. **(A)** The multi-protein elongation complex drives polar elongation and is anchored at the poles by Wag31, which is stabilized by CwsA. The PG synthase PonA1 incorporates new PG subunits into the spaces created by the hydrolases. PonA2 and the nonclassical transpeptidases LdtA and/or LdtB might coordinate PG synthesis with PonA1, which would generate the two different types of crosslinks (4→3 and 3→3) that are observed in mycobacterial PG. Protein cofactors may coordinate this different activity or activate the PG synthases **(B)** Another large macromolecular machine, the divisome, is responsible for cell division. Septation is initiated by polymerization of FtsZ and subcellular placement of the Z-ring is regulated by several factors (purple), including ClpX, ChiZ and Rv3660c, as well as phosphorylation of FtsZ by PknA. FhaB stabilizes the Z-ring and then the structural proteins FtsW, FtsQ, CrgA and CwsA assemble to form the divisome. The PG synthases PBPB, PBPA, and PonA1 synthesize the septum and the hydrolases RipA and RpfB (and possibly other hydrolases) cleave the septum to separate the daughter cells. Septal hydrolysis might also be facilitated by FtsEX, but this remains to be confirmed.

Figure 1.3 (Continued)

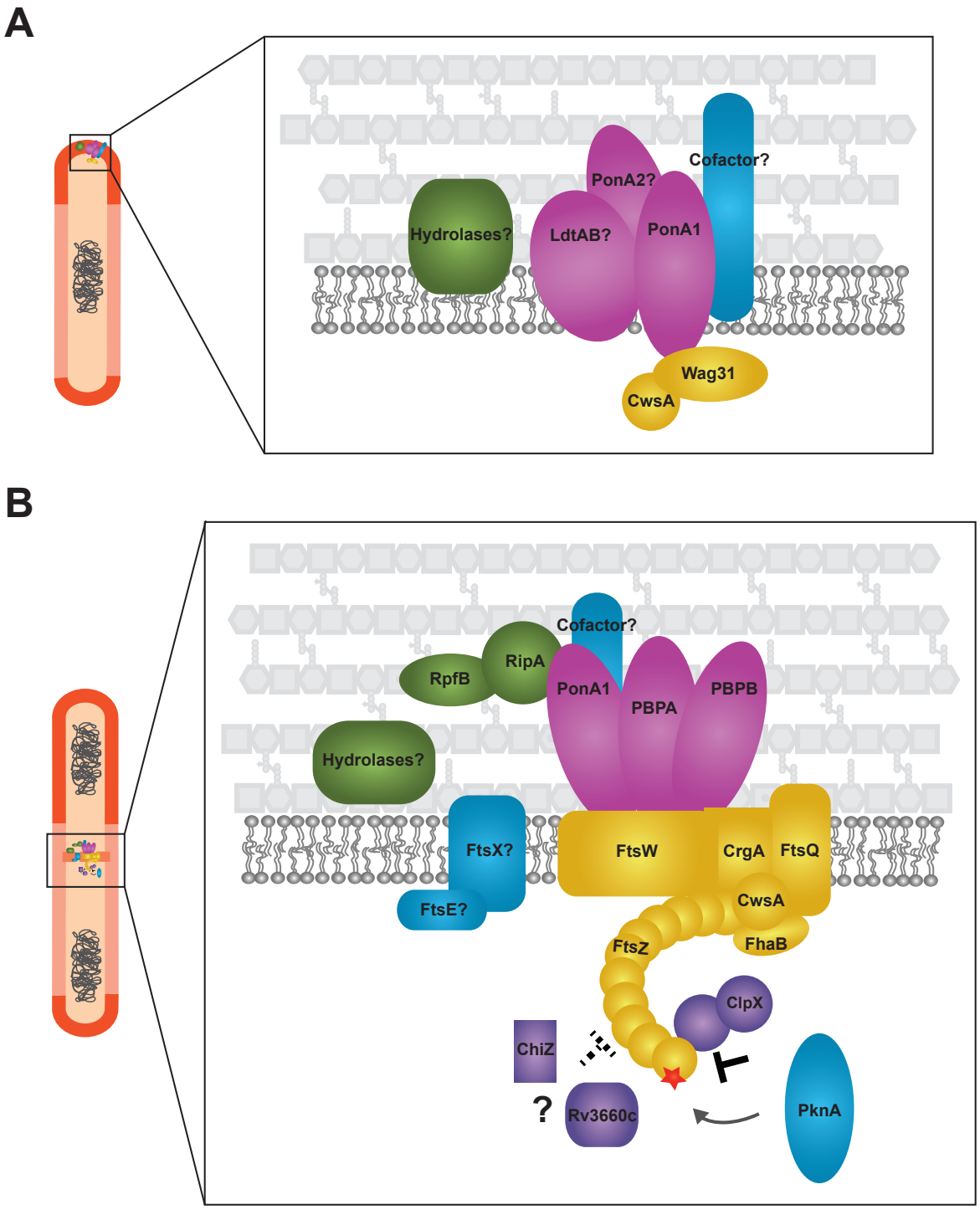

pole [24,25] requires interaction with cell wall synthesis protein A (CwsA) [26], CwsA may recruit or stabilize Wag31 at the pole (Figure 1.3A). Indeed, overexpression of CwsA increases polar localization of Wag31 in *M. smegmatis* [27] whereas deletion of *cwsA* decreases Wag31 polar localization [26]. Expression of a phosphomimetic version of Wag31 stimulates the enzymatic activity of MurG and MraY [25] (which are involved in Lipid II synthesis), suggesting that Wag31 may interact with Lipid II synthases and link Lipid II biosynthesis to cell wall incorporation. This hypothesis is supported by the close proximity of *wag31* to the Lipid II biosynthetic cluster (a 6kb distance) in the mycobacterial genome. After the establishment of the Wag31 anchor, it is likely that peptidoglycan remodelling enzymes are then recruited. Wag31 might interact directly with transmembrane PG synthases, such as PonA1, which would ensure that cell wall synthesis is connected to cytoplasmic cues, and genetic evidence indicates that such interactions exist. For example, Wag31 is required for shape maintenance and peptidoglycan incorporation at the pole [19,24,25,28] and its depletion produces round cells that have growth defects [24], and Wag31 overexpression produces branching [28]. These phenotypes are consistent with PonA1 depletion [29] and overexpression (Kieser, KJ and Rubin, EJ, unpublished data), respectively.

M. tuberculosis PonA1 and PonA2 are predicted to be essential for growth during infection [30]. PonA1 localizes to the poles and division septum in *M. smegmatis* [29], which suggests that it may synchronize the elongation and division complexes. Indeed, PonA1 interacts with the hydrolase RipA, which localizes to the septum and is required for cell division [29]. Mycobacterial elongation does not seem to require monofunctional PBPA [31], the putative homologue of PBP2, which is required for cell elongation in *E. coli* [18]. Deletion of *pbpA* in *M. smegmatis* produces cells that are viable but form filaments [31], suggesting that PBPA has a role in division instead of elongation in mycobacteria. Because mycobacterial PG is heavily 3→3 crosslinked (Figure 1.1), noncanonical transpeptidases (such as LdtA and/or LdtB) might be recruited to the elongation complex to substitute for PBPA. Recent evidence has shown that the absence of LdtA and LdtB leads to the production of bulging, short cells, which suggests a defect in cell elongation [32]. The coordination of 4→3 and 3→3 crosslinking during elongation may be facilitated by cofactors that modulate the activity of PG synthases [18] (Figure 1.3A).

Mycobacterial cell division

Following elongation, mycobacteria divide at roughly mid-cell to form two daughter cells and a large multi-protein complex, known as the divisome, coordinates this step. Crosstalk between components of the elongation complex and the divisome probably triggers peptidoglycan synthesis to move from the poles to mid-cell [33]. The divisome contains cytoskeletal-like proteins, structural factors, and PG synthases and hydrolases [18,23] (Figure 1.3B) that coordinate both the synthesis and then the splitting of the septum during cell division.

Asymmetric septation

Septal site selection contributes to the inherent phenotypic heterogeneity of mycobacterial cells. Unlike other species, such as *E. coli* or *C. glutamicum,* several studies have revealed that septa are placed over a surprisingly wide zone within the cell body of *Mycobacterium bovis BCG*, *Mycobacterium marinum* and *M. smegmatis* [11,12]. What are the functional consequences of promiscuous septal placement? Irregular septation enhances the asymmetric size of daughter cells and results in the differential distribution of proteins and small molecules to daughter cells, which further increases population heterogeneity [34].

Formation of the Z-ring

In almost all bacteria, septation is initiated by polymerization of the self-activating GTPase FtsZ into a ring-like structure, known as the Z-ring [35]. The Z-ring determines the site of septation and provides the energy for membrane constriction [36], in addition to serving as the scaffold for downstream peptidoglycan remodelling enzymes [18]. As the Z-ring determines the site of eventual cell division, its proper placement is paramount. Mycobacteria regulate Z-ring formation at multiple levels by modulating FtsZ polymerization and guiding Z-ring localization. The MinD homologue Rv3660c is a putative regulator of Z-ring formation and its overexpression reduces *ftsZ* expression and inhibits septum formation, resulting in highly elongated cells [37]. Unlike other bacteria, mycobacterial FtsZ is phosphorylated through the action of PknA, a serine-threonine protein kinase (STPK), which reduces GTP hydrolysis by FtsZ and hence its polymerization *in vitro* is inhibited [38]; both activities are required for constriction of the Z-ring to promote division [36]. Expression of mycobacterial PknA in *E. coli*, results in phosphorylation

of *E. coli* FtsZ and the production of elongated cells [38], which suggests that FtsZ phosphorylation perturbs polymerization and dysregulates septum formation in the cell. ClpX, an integral member of the ClpXP protease, regulates FtsZ polymerization through a direct interaction with FtsZ and overexpression of ClpX decreases the production of Z-rings, resulting in elongated cells [39]. A similar phenotype has been observed on overexpression of ChiZ, a lysin motif (LysM) domain containing protein [40]. As overexpression of any of these factors individually does not abolish Z-ring formation, this suggests that these systems function in parallel to coordinate Z-ring formation.

The divisome

After the Z-ring forms at approximately mid-cell, other proteins assemble to form the divisome. In addition to FtsZ, the structural elements of the divisome are FhaB, FtsW, FtsQ, CrgA and CwsA (Figure 1.3B). The small FtsZ-interacting protein FhaB (also known as FipA) forms a bridge between FtsZ and FtsQ and its deletion increases cell length [41], which suggests that FhaB is crucial for mediating interactions between FtsZ and FtsQ to ensure proper Z-ring formation. The FtsZ-FhaB-FtsQ ternary complex has been shown to be required for Z-ring formation under oxidative stress, and consequently loss of FhaB inhibits bacterial replication in macrophages [41]. FtsZ also interacts with the cytoplasmic tail of FtsW, which is unique to mycobacteria [42]. PBPB (a homologue of *E. coli* PBP3) joins the complex by interacting with the extracytoplasmic loops of FtsW [42] and the FtsZ-FtsW-PBPB complex links cytoplasmic structural cues (polymerization of the Z-ring) to septum synthesis [42]. FtsQ associates with the actinomycete-specific cell division protein, CrgA [43], which in turn interacts with FtsZ, PBPA and PBPB, thereby stabilizing the whole complex. CrgA localizes to the divisome after FtsZ and has a role in recruiting PBPB. Depletion of CrgA results in elongated cells, which is probably due to the inability to recruit PBPB to the divisome [43]. Furthermore, CrgA interacts with the elongation complex protein CwsA [26], and this interaction might coordinate elongation and division during the cell cycle to ensure that septum formation occurs post-elongation.

These structural components stabilize the divisome and promote the synthesis of a septum. Three PG synthases, PBPA, PBPB, and PonA1, synthesize the septal peptidoglycan. PonA1 is the sole bifunctional

PG synthase known to localize to the septum [29]. As described above, PBPA functions predominantly in septation [31] and the other monofunctional transpeptidase, PBPB, is required for septal synthesis and growth *in vitro* [44]. Chemical inhibition of PBPB produces branched cells [45]. Continued cell elongation can occur even with abnormal septation, which suggests that elongation and division are discrete, but interconnected, processes. PBPB also interacts with the polar anchor protein Wag31 [46], likely when the division septum is transitioning to a pole. This physical crosstalk with the elongation complex may allow elongation to occur even when PBPB's synthesis of septal PG is chemically dysregulated. The Wag31-PBPB interaction is particularly important for survival during oxidative stress [46], and similarly to the CrgA-CwsA interaction, it might have a role in relaying information between the elongation and division machineries. Recent evidence suggests that Wag31 localizes to the division site after formation of the septum, and its concentration increases as division commences [13]. This would enable Wag31 to form an anchor at the nascent cell pole immediately after cell division to facilitate recruitment of the elongation complex for the next division cycle.

Cell division

After completion of septum synthesis, it is then cleaved to physically separate daughter cells. Peptidoglycan contains a variety of chemical bonds that require cleavage by distinct enzymes [18]. In other bacterial systems, multiple PG hydrolases, which display functional redundancy, participate in cell division [18]. By contrast, mycobacteria have at least one essential PG hydrolase, RipA [47], and its depletion results in the generation of cell chains that fail to grow [47]. RipA interacts with another PG hydrolase known as resuscitation promoting factor (Rpf) B [48], and *in vitro* analysis has demonstrated that these two PG hydrolases synergistically cleave peptidoglycan [47]. This synergy is counteracted by the PG synthase PonA1, probably owing to competition with RpfB for binding to RipA [29]. The balance between PonA1-RipA and RipA-RpfB interactions may be used as a mechanism to ensure that synthesis of the septum precedes its hydrolysis. Septal hydrolysis in other species, such as *E. coli*, requires amidases and FtsE and FtsX [18] but the activity of mycobacterial amidases and other hydrolases in septation is poorly understood [49,50]. Recent evidence suggests that FtsX regulates the hydrolytic activity of RipC [51], although the role of RipC in mycobacterial cell division remains unclear. At the

completion of cytokinesis, mycobacteria exhibit a “v-snapping” phenotype [23] (Figure 1.2). This may result from asymmetric splitting of the septum or from uneven shearing of the arabinogalactan and mycolic acid layers on the cell surface [23].

Does dissolution of the septum affect cell shape? Although cell length is heterogeneous in mycobacteria, cell width seems to be uniform. This may be due to the retention of unsalvageable peptidoglycan in the polar cap. RipA, homologues of which are not essential in other bacterial species, generates peptide fragments [47] that cannot be used in future crosslinking reactions, which inhibits the incorporation of new PG monomers. Thus, insertion of nascent material might be restricted to the sub-polar region [19] because of the static polar cap, resulting in cells of uniform width.

Regulation of growth and division

Mycobacteria encode a plethora of regulatory pathways to control cell wall synthesis, cell growth and division, and the enzymes and processes involved represent another source of heterogeneity [52].

Transcriptional regulation

Cell wall biosynthesis can be modulated at the level of gene expression. The three transcription factors, EmbR, MabR, and FasR regulate expression of the cell wall synthases EmbA, EmbB, and the FASI and FASII complexes [53-55]. The transcriptional activator EmbR binds to the promoter of the *embCAB* operon, which encodes arabinosyltransferases in *M. tuberculosis*, to increase arabinogalactan synthesis [53] (Figure 1.4A). The FHA domain of EmbR is phosphorylated by the serine/threonine kinase PknH, which promotes EmbR binding to the *embCAB* promoter, and this is further enhanced in macrophages as PknH expression is known to increase [53]. This increase in arabinogalactan synthesis may facilitate adaptation to the stresses encountered inside macrophages.

Large and complex lipids such as the immunomodulatory mycolic acids are energetically expensive to produce, and the cell has evolved to tightly regulate their synthesis. The transcription factors MabR and FasR, both of which are required for cell proliferation, regulate mycolic acid synthesis [54,55]. MabR

binds to the promoter of the FASII locus and negatively regulates expression of *fabD*, *acpM*, *kasA* and *kasB*, thereby decreasing MA production [54]. MabR overexpression also decreases *fas* expression, suggesting that feedback between the FASI and FASII complexes (Figure 1.1) regulates transcript levels [54]. Mycolic acid production is also positively regulated through the activity of FasR, which binds to conserved sites in the *fas* promoter [55]. Depletion of FasR results in decreased expression of *fas* and reduction in mycolic acid synthesis in *M. smegmatis* [55]. The opposing regulation carried out by MabR and FasR enables fine-tuning of mycolic acid production.

Two component systems (TCSs) are also involved in regulating gene expression. Mycobacteria encode twelve TCSs that function analogously to the STPK system. The TCS response regulator MtrA is required for growth of *M. tuberculosis* [56], and deletion of its cognate sensor kinase MtrB in *M. smegmatis* causes cells to swell and form chains [57], indicating that this TCS is essential for the maintenance of cell shape and division. MtrA binds to the promoters of several cell division factors, including the mycolic acid transferases FbpA, FbpB, and FbpC[56], and the divisome-specific PG hydrolase RipA [57]. Phosphorylation of MtrA negatively regulates *fbpB* expression [56]. By contrast, MtrA positively regulates *fbpA* expression irrespective of its phosphorylation status [56]. *mtrA* is upregulated by low pH [58], which suggests that MtrA can regulate cell cycle progression and production of mycolic acids in response to pH changes in the macrophage.

Post-translational modifications

Mycobacteria have a surprisingly large complement of eukaryotic-like STPKs that regulate important steps in cell morphogenesis [59,60]. As mycobacteria lack canonical regulatory systems for the coordination of cell division, the large complement of STPKs and TCSs may substitute for such systems. Phosphorylation modulates growth through two main mechanisms: by directly controlling protein activity or by stimulating and balancing protein-protein interactions between cell envelope biogenesis [61-63], elongation [21] and divisome proteins [41,60]. The two kinases, PknA and PknB, are essential for growth *in vitro* [59]; overexpression of either PknA or PknB produces bulging cells that have reduced growth rates, whereas depletion of either kinase generates elongated, narrow cells [59].

Figure 1.4. Regulatory mechanisms controlling synthesis of the mycobacterial cell wall.
Mycobacteria use several mechanisms to regulate cell wall synthesis and cell division. **(A)** At the transcriptional level, the transcription factor EmbR activates expression of *embCAB*, which encodes EmbA and EmbB, arabinosyltransferases involved in AG synthesis, and increase AG production by binding to the *embCAB* promoter. Phosphorylation of EmbR by the kinase PknH stimulates promoter binding, leading to an increase in AG synthesis. **(B)** Post-translational modifications of cell wall precursor synthases, such as phosphorylation of FabH, also occurs. FabH shuttles mycolic acids from FASI to FASII for acyl chain extension, but its activity is inhibited by PknF-mediated phosphorylation, thereby decreasing mycolic acid production. **(C)** Mycobacteria encode a unique pupylation system that targets proteins for proteasomal degradation, including those involved in cell wall synthesis. For example, the response regulator MtrA is pupylated by PafA, which promotes its proteasomal degradation. This relieves MtrA repression of *fbpB*, which encodes mycolic acid transferase complex member FbpB, expression, increasing mycolic acid cell wall incorporation.

Figure 1.4 (Continued)

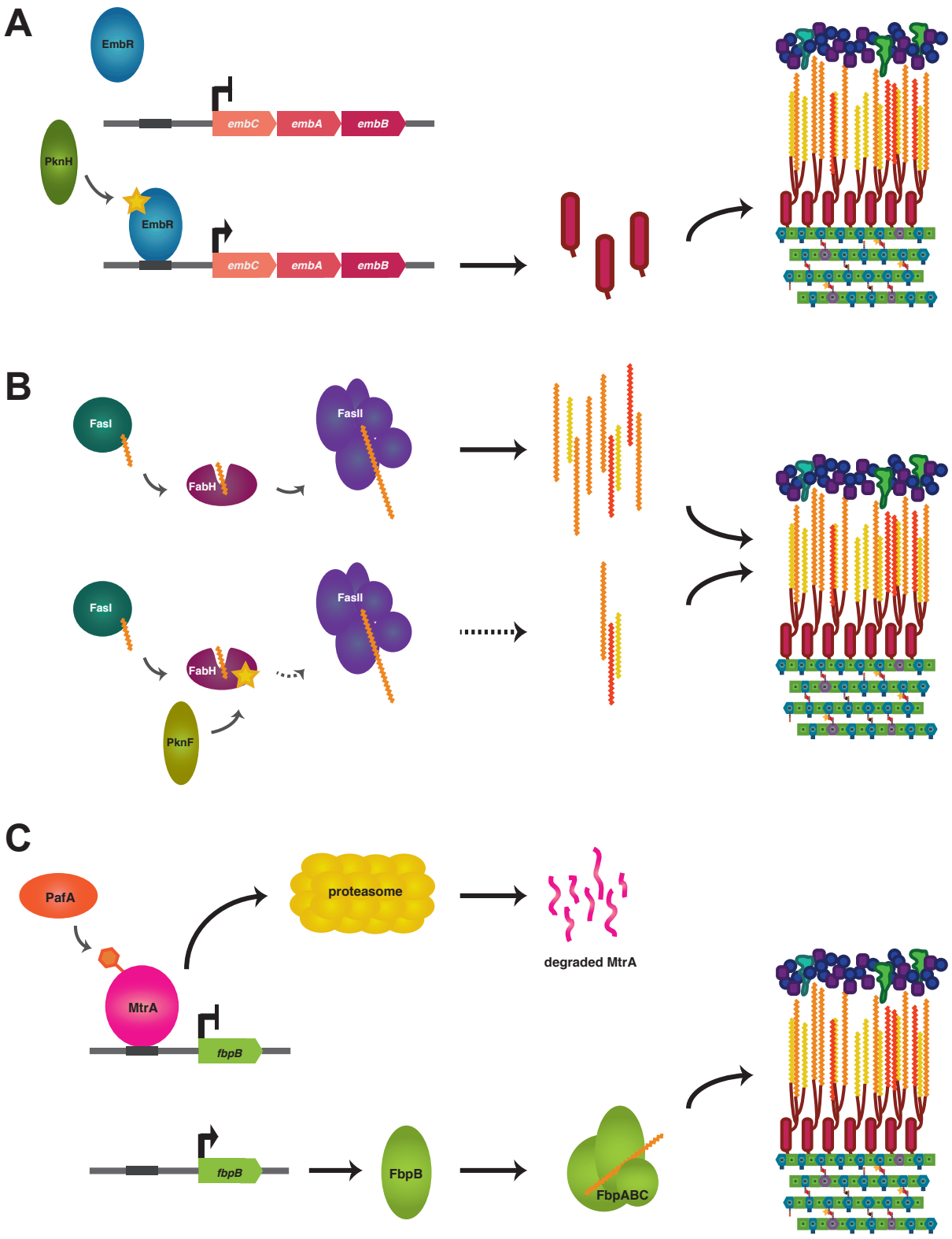

Assembly and disassembly of the divisome is regulated, in part, by phosphorylation. Phosphorylation of FtsZ by PknA reduces its polymerization *in vitro* and probably promotes its interaction with FhaB, which contains an FHA domain, that is required for FtsZ interaction [41]. Because FhaB interacts with other divisome components, its interaction with FtsZ might stabilize the interactions between the Z-ring and the rest of the divisome complex. FhaB is also phosphorylated by PknA, which is necessary for FtsZ-FhaB-FtsQ ternary complex formation [41]. In addition, FtsQ is phosphorylated [60] but whether this is required for interactions with FhaB or CrgA remains unexplored. FtsZ, FhaB, and FtsQ are key structural components of the divisome, and the high degree of phosphorylation may regulate formation of the divisome in response to environmental cues.

Synthesis of all components of the cell wall is affected by phosphorylation. The transmembrane protein MviN, which likely shuttles Lipid II precursors across the periplasm, is phosphorylated by PknB and this recruits its essential interacting partner, FhaA [21]. Phosphorylation of Wag31 by PknA is required for correct polar localization and PG biosynthesis [25]. Hyper-phosphorylation of Wag31 can stimulate Lipid II synthesis [25] and probably PG incorporation**.** The PG synthase PonA1 is also phosphorylated [60]. As PonA1 functions as part of both the elongation complex and the divisome [29], its phosphorylation status may direct PonA1 to the distinct complexes.

Arabinogalactan and mycolic acid synthesis are also subject to phosphorylative control. As described above, EmbR is phosphorylated by PknH [53] which results in the stimulation of arabinogalactan synthesis. Several factors involved in MA precursor synthesis are phosphorylated, including FabD, FabH, MabA, KasAB, InhA, Pks13, and PcaA [61,63,64]. Phosphorylation of KasB [64] and MabA [62] leads to an increase in their activity and increased production of mycolic acids. Phosphorylation of FabH**,** which shuttles mycolic acid precursors from FASI to FASII synthase, decreases its catalytic activity [64], which probably decreases mycolic acid production (Figure 1.4B).

Protein processing and degradation

Several studies have shown that proteolytic processing of cell division proteins is required for normal mycobacterial growth [46,65-67]. The essential hydrolase RipA requires cleavage for full catalytic activity to separate daughter cells [65,66]. The essential septal synthase PBPB also undergoes cleavage by the metalloprotease Rv2869 during oxidative stress [46], which may decrease cell division during unfavorable conditions.

In addition to processing, cell division proteins are subject to degradative control. Mycobacteria encode a system analogous to eukaryotic ubiquitylation, which is termed pupylation [67,68]. Conjugation of the prokaryotic ubiquitin-like protein (Pup) by PafA to target proteins results in their proteasomal degradation, and in addition, Pup can also be removed by the depupylase Dop (which is functionally analogous to de-ubiquitylases) [69], providing another layer of regulation**.** Several factors that are involved in cell wall assembly are pupylation targets, including MurA, KasB, and MtrA [68]. MtrA is targeted for proteasomal degradation [68], and its directed turnover may regulate cell wall assembly and cell division. For example, MtrA's degradation could relieve repression of *fbpB*, a member of the mycolic acid transferase complex (Figure 1.4C). However, not all pupylated proteins are targeted to the proteasome [68] and it remains to be determined what effect, if any, this modification has on the function of MurA and KasB, for example, and the processes they control.

Cell wall remodelling and asymmetric growth *in vivo*

Cell wall plasticity facilitates bacterial survival

Cell envelope biogenesis and cell division are tightly regulated, and the many levels of regulation provide ample opportunity for stochastic phenotypic differences to arise between individual cells. Such differences are likely to amplify the heterogeneity that is produced by asymmetric cell elongation and division. Moreover, re-structuring of the cell wall is a major mechanism that *M. tuberculosis* uses to adapt to the changing host environment [14-17] and to subvert host defences during infection [70]. In addition, the cell wall is a major target for antibiotics and mutations in components of the cell wall synthesis machinery lead

to clinical drug resistance [71], which highlights the importance of this structure as an interface with the host and as a clinical drug target.

The three major cell wall components exist as irregular structures. Peptidoglycan and arabinogalactan are extensively modified with glycolyl, amide, succinyl, and galactosamine residues [72-74] and PG contains unusual linkages between monomers [72,75] (Figure 1.1). The three forms of mycolic acids (α-meroacids, methoxy-meroacids, and keto-meroacids) are synthesized with different acyl chain lengths and saturation and are also modified by cyclopropanation, all of which vary from molecule to molecule [76,77] (Figure 1.1). The combination of these alterations induces physicochemical changes in the cell wall, which have been found in bacteria that are grown *in vivo*, suggesting that they are part of an adaptive response for the generation of a heterogeneous bacterial population. A potential consequence of this population diversity is that a subpopulation of bacteria are equipped to survive when faced with the dynamic stresses encountered *in vivo*, such as the immune response and antibiotics.

Several studies have shown that the composition of the cell wall changes during infection (Figure 1.5). Bacilli isolated from chronically infected patients are no longer acid-fast, which suggests that gross structural and/or compositional changes occur during extended periods of *in vivo* growth [14]. Cells isolated from infected guinea pigs display differences in mycolate composition compared to cells grown *in vitro* [15]. Transcriptional analysis of bacteria isolated from diverse regions of the lung has revealed substantial changes in the expression of cell wall biosynthetic genes and membrane proteins compared to *in vitro* cultures [16], including the upregulation of lipid synthesis genes. For example, *pcaA*, *desA1* and *desA3*, which are involved in mycolic acid processing, are upregulated and are required for virulence *in vivo* [78]. Furthermore, the length and abundance of the cell wall lipids phthiocerol dimycocerosate (PDIM) and sulfolipid-1 (SL-1) increase during growth of *M. tuberculosis in vivo* [17]. Upregulation of lipid biosynthesis could confer multiple benefits to the bacterium: a thicker cell wall restricts the transit of toxic molecules (such as antibiotics) across the cell membrane, mycolic acids can manipulate the immune system [79] and absorb oxidative radicals [80] and lipids function as a sink for toxic byproducts from

cholesterol catabolism during growth in macrophages [81,82], which is required for bacterial survival in a murine model of TB [83].

Mycobacterial peptidoglycan is also extensively modified to interact with and adapt to host conditions (Figure 1.5). The noncanonical transpeptidases LdtA and LdtB catalyze the predominant 3→3 peptide crosslink in PG. LdtB expression peaks during late log phase and late stationary phase, whereas LdtA expression increases during late stationary phase only [84]. LdtB mutants are unable to persist and decline in number over the course of infection [84]. These data indicate that heavily 3→3 crosslinked peptidoglycan is necessary for maintenance of the infection and resisting immune clearance. LdtB mutants are also more susceptible to amoxicillin [84], suggesting that these unique crosslinks may have a clinically relevant role in resisting antibiotic stress.

In addition to unconventional crosslinks, transcriptomic analysis of *M. tuberculosis* isolated from granulomas has shown that several steps of peptidoglycan biosynthesis are upregulated *in vivo*, including genes responsible for precursor production (such as *murE* and *ddl*) and remodelling (such as *Rv1730c* and *rpfA*) [16]. In addition, PonA1 is required for *M. tuberculosis* survival during hypoxia [85] and PonA2 is required during infection [86] and to support growth of *M. smegmatis* in reduced replication states [87,88]. Furthermore, PG editing by low molecular weight PBPs, such as DacB1 and DacB2, which hydrolyze the terminal D-alanine residues from N-acetyl muramic acid (NAM) subunits, is required for survival in the host as DacB1 is predicted to be essential for infection of nonhuman primates [89]. DacB1 remodelling of PG may maintain the 3→3 crosslinks critical for persisting *in vivo*, as removal of the terminal D-alanines inhibits 4→3 crosslinking. These data correlate with genetic evidence that demonstrates additional cell wall assembly enzymes become essential in host-like conditions [30,44,90-92]. Taken together, these data suggest that cells must undergo peptidoglycan remodelling to adapt to a variety of stresses, many of which mirror conditions that might be encountered in the host during latent or active infection.

The wide range of microenvironments imposed by the host induce a variety of metabolic

Figure 1.5. Cell wall remodelling may promote survival during infection.
During growth *in vivo,* substantial changes occur in the cell wall of *M. tuberculosis*. Active proliferation during infection and the utilization of host carbon sources during growth in macrophages leads to an increase in the production of mycolic acids and cell wall lipids such as PDIM, which may promote survival in the host environment. In addition, during growth *in vivo*, peptidoglycan is remodelled and the crucial 3→3 crosslinks that promote chronic infection and antibiotic resistance are maintained. During slow growth and in nonreplicative states, the cell wall becomes thicker, probably due to an increase in the synthesis of multiple cell wall layers. During slow growth and nonreplicative states, as well as in hypoxic environments, *M. tuberculosis* downregulates the abundance of immunostimulatory mycolic acids to potentially avoid immune recognition and crosslinking of PG may increase to promote cell wall rigidity and bacterial survival under stress. These cell wall changes, combined with the inherent plasticity of cell wall synthesis, generate a population of unique single cells that may have variable fitness during infection.

Figure 1.5 (Continued)

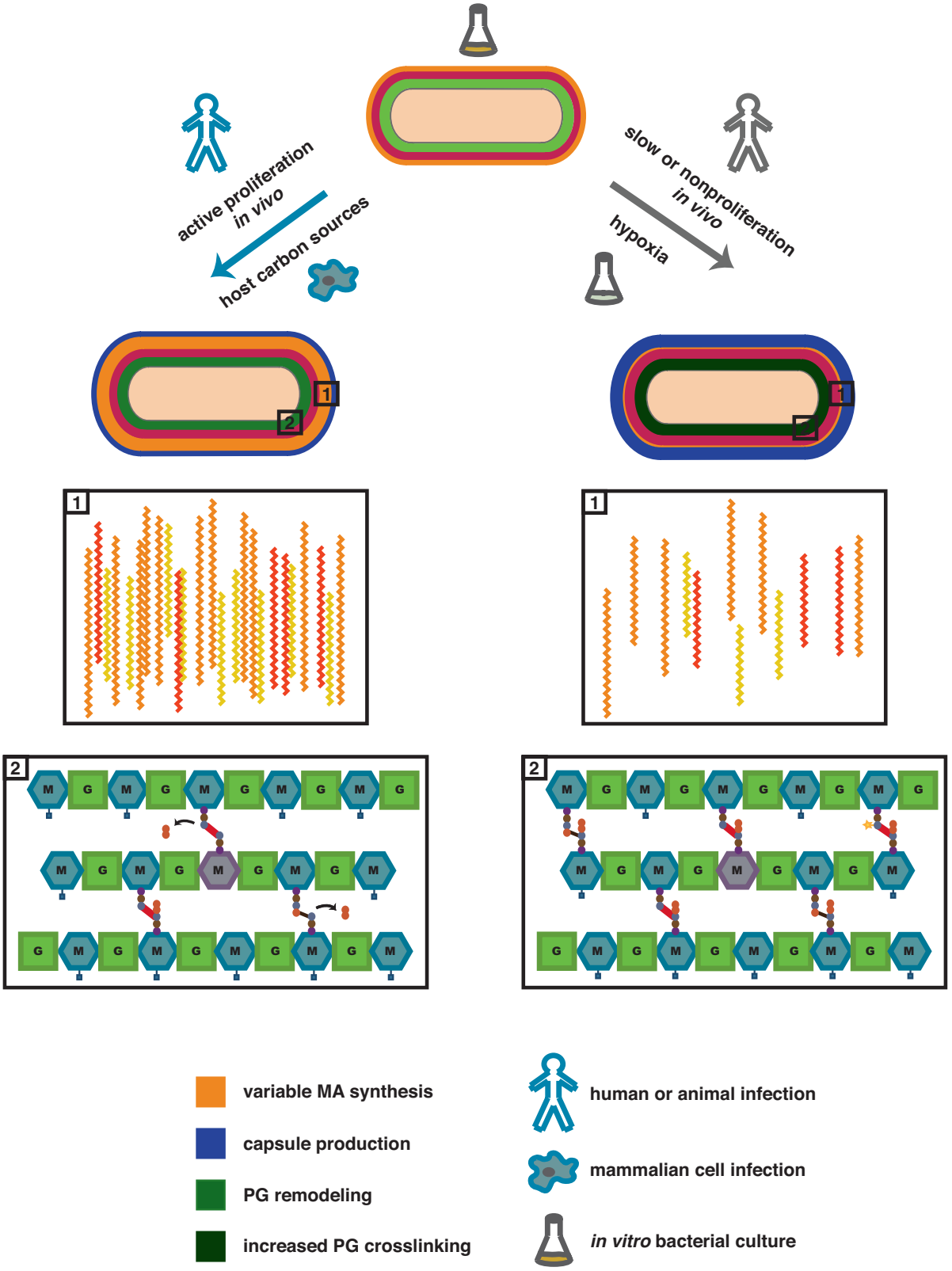

changes [81,82,93] that, combined with stochastic variation in cell wall composition, such as variable peptidoglycan modifications, and asymmetric cell division, could result in a substantially heterogeneous bacterial population. Changes in metabolism and growth rate [93,96] have consequences for the cell wall. For example, mutation of cell wall genes generate low fitness mutants under slow growth rates in a carbon-limited chemostat, which suggests that PG synthesis, mycolic acid synthesis and synthesis of the cell surface lipid PDIM [97] are all required under these conditions. These cell wall synthetic requirements probably result in gross changes in the cell wall, such as the thickening observed by electron microscopy in low oxygen environments [98]. Many of these changes might be closely linked to overall lipid metabolism, as the lipid-rich cell wall obtains its precursors from normal metabolism [17,81,82]. If lipid production decreases, which occurs during hypoxia [99], the lipid composition of the cell wall changes (Figure 1.5). As many of these lipids are pro-inflammatory molecules [78,79], changes in their abundance will also affect interactions between the pathogen and the host. Indeed, deletion of *kasB*, a component of the mycolic acid synthase complex FASII, in a clinical strain of *M. tuberculosis* attenuates virulence [100]. Immunocompetent mice infected with a *ΔkasB* mutant seem to remain healthy for up to 600 days post-infection, whereas mice infected with wild-type or a *kasB* complemented strain succumb to infection within 356 days. The persistence of *ΔkasB* bacteria is probably due to their shortened and altered mycolic acid chains [100], which are predicted to reduce immunogenicity.

Asymmetric growth may enhance population heterogeneity

Asymmetric growth and the resulting heterogeneity in cell size may have a role in the lifecycle of *M. tuberculosis* within the human host, including its ability to actively grow in the range of host microenvironments as well as to persist in a quiescent state [5].

Several studies have modelled how asymmetric growth and division influence cell fate during antibiotic therapy *in vitro* [10,20]. For instance, as mentioned above, analysis of microcolonies suggests that cells, which have inherited the old pole, are more recalcitrant to cell wall inhibitors than sibling cells that have inherited the new pole [10]. In addition to the heterogeneity that accompanies cell growth and division, recent work suggests that stochastic changes in *katG*, which produces the catalase-peroxidase KatG that

is required to activate isoniazid, gene expression are responsible for mycobacterial survival during isoniazid treatment [20]. It has been shown that individual *M. smegmatis* cells vary in their susceptibility to isoniazid, which is independent of the genetic background and cell age [20]. Unlike *E. coli*, these stochastic processes are also independent of growth rate and cell size [101]. Variation in gene expression is also likely to influence cellular responses other than antibiotic resistance, which would also contribute to the ability to adapt to different conditions – an essential requirement for persisting in hypoxic conditions *in vivo* [93] as well as for antibiotic tolerance [102-104]. Deterministic and stochastic means of tolerance to antibiotics, combined with the diversity in cell size and cell wall composition, could contribute to the notoriously long course of antibiotic therapy that is required to treat *M. tuberculosis* infections.

Outlook

The mycobacterial cell wall is a complex structure and the mechanisms required for its biogenesis, including regulation, reflect this complexity. Regulation of cell wall synthesis occurs at the level of transcription and post-translational mechanisms, including proteolytic processing, pupylation and widespread phosphorylation. This enables mycobacteria to manipulate the composition of the cell wall in response to changing environmental conditions in the host. Thus, it seems reasonable to propose that dynamic remodelling of the cell wall [14-17] and the unusual mechanism of asymmetric elongation and division [10-13], are major contributors to the ability of the bacterium to evade immunity and persist within the host.

The findings presented in this Review offer insight into how cell-to-cell heterogeneity can arise in the population. The mechanisms controlling asymmetric growth and its regulation remain to be elucidated, but it is likely that interplay between the elongation and division machineries is important. Finally, population diversity is further enhanced by stochastic changes in gene expression, which lead to variation in growth, particularly on exposure to antibiotics [20].

Biochemical and genetic techniques have made substantial headway in elucidating the details of cell wall synthesis during growth *in vitro*. However, several hurdles remain. Studying the mechanistic basis and

the importance of heterogeneity in individual bacteria will require more advanced single cell techniques, such as microfluidics, an area that is just emerging. Similarly, progress in our understanding of bacterial adaptation during infection is required; although *in vitro* models and animal models can replicate some aspects of infection, their correlation with *in vivo* infection of the human host remains largely unknown. Thus, we still require technical breakthroughs to gain a more complete picture of the mycobacterial cell wall, as well as cell growth and division in the most important environment – us.

Acknowledgements

The authors thank S. Dove, C. Sassetti and S. Fortune for discussion of the ideas presented in this review and to C. Boutte, M. Chao and N. Peters for critical reading of the manuscript. The authors are grateful to J. McKinney and anonymous referees for excellent suggestions and improvements. The authors also thank A. Goranov for discussion of cell growth models. Support was provided by the National Institutes of Health (NIH U01-GM094568 to EJR) and the National Science Foundation (NSF Graduate Research Fellowship DGE-1144152 to KJK).

Section 1.3 References

1. World Health Organization. Global tuberculosis report 2013. (2013).
2. Das, B. *et al.* CD271+ Bone Marrow Mesenchymal Stem Cells May Provide a Niche for Dormant Mycobacterium tuberculosis. *Sci Transl Med* 5, 170ra13–170ra13 (2013).
3. Ernst, J. D. The immunological life cycle of tuberculosis. *Nat Rev Immunol* 12, 581–591 (2012).
4. Philips, J. A. & Ernst, J. D. Tuberculosis Pathogenesis and Immunity. *Annu. Rev. Pathol. Mech. Dis.* 7, 353–384 (2012).
5. Barry, C. E., III *et al.* The spectrum of latent tuberculosis: rethinking the biology and intervention strategies. *Nat Rev Micro* 7, 845–855 (2009).
6. Davis, J. M. & Ramakrishnan, L. The Role of the Granuloma in Expansion and Dissemination of Early Tuberculous Infection. *Cell* 136, 37–49 (2009).
7. Lin, P. L. *et al.* Sterilization of granulomas is common in active and latent tuberculosis despite within-host variability in bacterial killing. *Nat Med* 20, 75–79 (2014).

8. Via, L. E. *et al.* Tuberculous granulomas are hypoxic in guinea pigs, rabbits, and nonhuman primates. *Infect Immun* 76, 2333–2340 (2008).

9. Mattila, J. T. *et al.* Microenvironments in Tuberculous Granulomas Are Delineated by Distinct Populations of Macrophage Subsets and Expression of Nitric Oxide Synthase and Arginase Isoforms. *J Immunol* 191, 773–784 (2013).

10. Aldridge, B. B. *et al.* Asymmetry and Aging of Mycobacterial Cells Lead to Variable Growth and Antibiotic Susceptibility. *Science* 335, 100–104 (2012).

11. Joyce, G. *et al.* Cell Division Site Placement and Asymmetric Growth in Mycobacteria. *PLoS ONE* 7, e44582 (2012).

12. Singh, B. *et al.* Asymmetric growth and division in Mycobacterium spp.: compensatory mechanisms for non-medial septa. *Mol Microbiol* 88, 64–76 (2013).

13. Santi, I., Dhar, N., Bousbaine, D., Wakamoto, Y. & McKinney, J. D. Single-cell dynamics of the chromosome replication and cell division cycles in mycobacteria. *Nat Commun* 4, 1–10 (2013).

14. Seiler, P. *et al.* Cell-wall alterations as an attribute of Mycobacterium tuberculosis in latent infection. *J INFECT DIS* 188, 1326–1331 (2003).

15. Bhamidi, S. *et al.* A bioanalytical method to determine the cell wall composition of Mycobacterium tuberculosis grown in vivo. *Anal Biochem* 421, 240–249 (2012).

16. Rachman, H. *et al.* Unique Transcriptome Signature of Mycobacterium tuberculosis in Pulmonary Tuberculosis. *Infect Immun* 74, 1233–1242 (2006).

17. Jain, M. *et al.* Lipidomics reveals control of Mycobacterium tuberculosis virulence lipids via metabolic coupling. *Proc Natl Acad Sci USA* 104, 5133–5138 (2007).

18. Typas, A., Banzhaf, M., Gross, C. A. & Vollmer, W. From the regulation of peptidoglycan synthesis to bacterial growth and morphology. *Nat Rev Micro* 10, 123–136 (2012).

19. Meniche, X. *et al.* Sub-polar addition of new cell wall is directed by DivIVA in mycobacteria. *Proc Natl Acad Sci USA*, in press, (2014).

20. Wakamoto, Y. *et al.* Dynamic Persistence of Antibiotic-Stressed Mycobacteria. *Science* 339, 91–95 (2013).

21. Gee, C. L. *et al.* A Phosphorylated Pseudokinase Complex Controls Cell Wall Synthesis in Mycobacteria. *Sci Signal* 5, ra7–ra7 (2012).

22. Flärdh, K. Cell polarity and the control of apical growth in Streptomyces. *Curr Opin Microbiol* 13, 758–765 (2010).

23. Hett, E. C. & Rubin, E. J. Bacterial growth and cell division: a mycobacterial perspective. *Microbiol Mol Biol Rev* 72, 126–156 (2008).

24. Kang, C.-M., Nyayapathy, S., Lee, J.-Y., Suh, J.-W. & Husson, R. N. Wag31, a homologue of the cell division protein DivIVA, regulates growth, morphology and polar cell wall synthesis in mycobacteria. *Microbiology* 154, 725–735 (2008).

25. Jani, C. *et al.* Regulation of polar peptidoglycan biosynthesis by Wag31 phosphorylation in mycobacteria. *BMC Microbiol* 10, 327 (2010).

26. Plocinski, P. *et al.* Mycobacterium tuberculosis CwsA Interacts with CrgA and Wag31, and the CrgA-CwsA Complex Is Involved in Peptidoglycan Synthesis and Cell Shape Determination. *J Bacteriol* 194, 6398–6409 (2012).

27. Plocinski, P. *et al.* Mycobacterium tuberculosis CwsA overproduction modulates cell division and cell wall synthesis. *Tuberculosis* 93, S21–S27 (2013).

28. Nguyen, L. *et al.* Antigen 84, an effector of pleiomorphism in Mycobacterium smegmatis. *J Bacteriol* 189, 7896–7910 (2007).

29. Hett, E. C., Chao, M. C. & Rubin, E. J. Interaction and Modulation of Two Antagonistic Cell Wall Enzymes of Mycobacteria. *PLoS Pathog* 6, e1001020 (2010).

30. Zhang, Y. J. *et al.* Tryptophan Biosynthesis Protects Mycobacteria from CD4 T-Cell-Mediated Killing. *Cell* 155, 1296–1308 (2013).

31. Dasgupta, A., Datta, P., Kundu, M. & Basu, J. The serine/threonine kinase PknB of Mycobacterium tuberculosis phosphorylates PBPA, a penicillin-binding protein required for cell division. *Microbiology* 152, 493–504 (2006).

32. Schoonmaker, M. K., Bishai, W. R. & Lamichhane, G. Nonclassical transpeptidases of Mycobacterium tuberculosis alter cell size, morphology, cytosolic matrix, protein localization, virulence and resistance to β-lactams. *J Bacteriol* 196, 1394–1402 (2014).

33. van der Ploeg, R. *et al.* Colocalization and interaction between elongasome and divisome during a preparative cell division phase in Escherichia coli. *Mol Microbiol* 87, 1074–1087 (2013).

34. Kysela, D. T., Brown, P. J. B., Huang, K. C. & Brun, Y. V. Biological Consequences and Advantages of Asymmetric Bacterial Growth. *Annu. Rev. Microbiol.* 67, 417–435 (2013).

35. Adams, D. W. & Errington, J. Bacterial cell division: assembly, maintenance and disassembly of the Z ring. *Nat Rev Micro* 7, 642–653 (2009).

36. Li, Y. *et al.* FtsZ Protofilaments Use a Hinge-Opening Mechanism for Constrictive Force Generation. *Science* 341, 392–395 (2013).

37. England, K., Crew, R. & Slayden, R. Mycobacterium tuberculosis septum site determining protein, Ssd encoded by rv3660c, promotes filamentation and elicits an alternative metabolic and dormancy stress response. *BMC Microbiol* 11, 79 (2011).

38. Thakur, M. & Chakraborti, P. K. GTPase activity of mycobacterial FtsZ is impaired due to its transphosphorylation by the eukaryotic-type Ser/Thr kinase, PknA. *J Biol Chem* 281, 40107–40113 (2006).

39. Dziedzic, R. *et al.* Mycobacterium tuberculosis ClpX interacts with FtsZ and interferes with FtsZ assembly. *PLoS ONE* 5, e11058 (2010).

40. Chauhan, A. *et al.* Interference of Mycobacterium tuberculosis cell division by Rv2719c, a cell wall hydrolase. *Mol Microbiol* 62, 132–147 (2006).

41. Sureka, K. *et al.* Novel role of phosphorylation-dependent interaction between FtsZ and FipA in mycobacterial cell division. *PLoS ONE* 5, e8590 (2010).

42. Datta, P. *et al.* Interaction between FtsW and penicillin-binding protein 3 (PBP3) directs PBP3 to mid-cell, controls cell septation and mediates the formation of a trimeric complex involving FtsZ,

FtsW and PBP3 in mycobacteria. *Mol Microbiol* 62, 1655–1673 (2006).

43. Plocinski, P. *et al.* Characterization of CrgA, a new partner of the Mycobacterium tuberculosis peptidoglycan polymerization complexes. *J Bacteriol* 193, 3246–3256 (2011).

44. Zhang, Y. J. *et al.* Global Assessment of Genomic Regions Required for Growth in Mycobacterium tuberculosis. *PLoS Pathog* 8, e1002946 (2012).

45. Slayden, R. A. & Belisle, J. T. Morphological features and signature gene response elicited by inactivation of FtsI in Mycobacterium tuberculosis. *J Antimicrob Chemoth* 63, 451–457 (2009).

46. Mukherjee, P. *et al.* Novel role of Wag31 in protection of mycobacteria under oxidative stress. *Mol Microbiol* 73, 103–119 (2009).

47. Hett, E. C., Chao, M. C., Deng, L. L. & Rubin, E. J. A Mycobacterial Enzyme Essential for Cell Division Synergizes with Resuscitation-Promoting Factor. *PLoS Pathog* 4, e1000001 (2008).

48. Hett, E. C. *et al.* A partner for the resuscitation-promoting factors of Mycobacterium tuberculosis. *Mol Microbiol* 66, 658–668 (2007).

49. Deng, L. L. *et al.* Identification of a novel peptidoglycan hydrolase CwlM in Mycobacterium tuberculosis. *Biochim Biophys Acta* 1747, 57–66 (2005).

50. Machowski, E. E., Senzani, S., Ealand, C. & Kana, B. D. Comparative genomics for mycobacterial peptidoglycan remodelling enzymes reveals extensive genetic multiplicity. *BMC Microbiol* 14, 75 (2014).

51. Mavrici, D. *et al.* Mycobacterium tuberculosis FtsX extracellular domain activates the peptidoglycan hydrolase, RipC. *Proc Natl Acad Sci USA* pii. 201321812 (2014).

52. Avery, S. V. Microbial cell individuality and the underlying sources of heterogeneity. *Nat Rev Micro* 4, 577–587 (2006).

53. Sharma, K. *et al.* Transcriptional Control of the Mycobacterial embCAB Operon by PknH through a Regulatory Protein, EmbR, In Vivo. *J Bacteriol* 188, 2936–2944 (2006).

54. Salzman, V. *et al.* Transcriptional regulation of lipid homeostasis in mycobacteria. *Mol Microbiol* 78, 64–77 (2010).

55. Mondino, S., Gago, G. & Gramajo, H. Transcriptional regulation of fatty acid biosynthesis in mycobacteria. *Mol Microbiol* 89, 372–387 (2013).

56. Rajagopalan, M. *et al.* Mycobacterium tuberculosis Origin of Replication and the Promoter for Immunodominant Secreted Antigen 85B Are the Targets of MtrA, the Essential Response Regulator. *J Biol Chem* 285, 15816–15827 (2010).

57. Plocinska, R. *et al.* Septal Localization of the Mycobacterium tuberculosis MtrB Sensor Kinase Promotes MtrA Regulon Expression. *J Biol Chem* 287, 23887–23899 (2012).

58. Rohde, K. H., Abramovitch, R. B. & Russell, D. G. Mycobacterium tuberculosis Invasion of Macrophages: Linking Bacterial Gene Expression to Environmental Cues. *Cell Host Microbe* 2, 352–364 (2007).

59. Kang, C.-M. *et al.* The Mycobacterium tuberculosis serine/threonine kinases PknA and PknB: substrate identification and regulation of cell shape. *Genes Dev* 19, 1692–1704 (2005).

60. Prisic, S. *et al.* Extensive phosphorylation with overlapping specificity by Mycobacterium tuberculosis serine/threonine protein kinases. *Proc Natl Acad Sci USA* 107, 7521–7526 (2010).

61. Molle, V. *et al.* Phosphorylation of InhA inhibits mycolic acid biosynthesis and growth of Mycobacterium tuberculosis. *Mol Microbiol* 78, 1591–1605 (2010).

62. Veyron-Churlet, R., Zanella-Cleon, I., Cohen-Gonsaud, M., Molle, V. & Kremer, L. Phosphorylation of the Mycobacterium Tuberculosis β-Ketoacyl-Acyl Carrier Protein Reductase MabA Regulates Mycolic Acid Biosynthesis. *J Biol Chem* 285, 12714–12725 (2010).

63. Corrales, R. M. *et al.* Phosphorylation of Mycobacterial PcaA Inhibits Mycolic Acid Cyclopropanation: Consequences for Intracellular Survival and Phagosome Maturation Block. *J Biol Chem* 287, 26187–26199 (2012).

64. Molle, V. & Kremer, L. Division and cell envelope regulation by Ser/Thr phosphorylation: Mycobacterium shows the way. *Mol Microbiol* 75, 1064–1077 (2010).

65. Chao, M. C. *et al.* Protein Complexes and Proteolytic Activation of the Cell Wall Hydrolase RipA Regulate Septal Resolution in Mycobacteria. *PLoS Pathog* 9, e1003197 (2013).

66. Ruggiero, A. *et al.* Structure and functional regulation of RipA, a mycobacterial enzyme essential for daughter cell separation. *Structure* 18, 1184–1190 (2010).

67. Pearce, M. J., Mintseris, J., Ferryera, J., Gygi, S. P. & Darwin, K. H. Ubiquitin-Like Protein Involved in the Proteasome Pathway of Mycobacterium Tuberculosis. *Science* 322, 1101–1104 (2008).

68. Festa, R. A. *et al.* Prokayrotic Ubiquitin-Like Protein (Pup) Proteome of Mycobacterium tuberculosis. *PLoS ONE* 5, e8589 (2010).

69. Burns, K. E. *et al.* "Depupylation“" of Prokaryotic Ubiquitin-like Protein from Mycobacterial Proteasome Substrates. *Mol Cell* 39, 821–827 (2010).

70. Cambier, C. J. *et al.* Mycobacteria manipulate macrophage recruitment through coordinated use of membrane lipids. *Nature* 505, 218–222 (2014).

71. Farhat, M. R. *et al.* Genomic analysis identifies targets of convergent positive selection in drug-resistant Mycobacterium tuberculosis. *Nat Genet* 45, 1183–1189 (2013).

72. Kumar, P. *et al.* Meropenem inhibits D,D-carboxypeptidase activity in Mycobacterium tuberculosis. *Mol Microbiol* 86, 367–381 (2012).

73. Mahapatra, S., Scherman, H., Brennan, P. J. & Crick, D. C. N Glycolylation of the nucleotide precursors of peptidoglycan biosynthesis of Mycobacterium spp. is altered by drug treatment. *J Bacteriol* 187, 2341–2347 (2005).

74. Skovierova, H. *et al.* Biosynthetic Origin of the Galactosamine Substituent of Arabinogalactan in Mycobacterium tuberculosis. *J Biol Chem* 285, 41348–41355 (2010).

75. Lavollay, M. *et al.* The Peptidoglycan of Stationary-Phase Mycobacterium tuberculosis Predominantly Contains Cross-Links Generated by L,D-Transpeptidation. *J Bacteriol* 190, 4360–4366 (2008).

76. Barry, C. E., Crick, D. C. & McNeil, M. R. Targeting the formation of the cell wall core of M. tuberculosis. *Infect Disord Drug Targets* 7, 182–202 (2007).

77. Takayama, K., Wang, C. & Besra, G. S. Pathway to Synthesis and Processing of Mycolic Acids in Mycobacterium tuberculosis. *Clin Microbiol Rev* 18, 81–101 (2005).

78. Barkan, D., Hedhli, D., Yan, H. G., Huygen, K. & Glickman, M. S. Mycobacterium tuberculosis Lacking All Mycolic Acid Cyclopropanation Is Viable but Highly Attenuated and Hyperinflammatory in Mice. *Infect Immun* 80, 1958–1968 (2012).

79. Vander Beken, S. *et al.* Molecular structure of the Mycobacterium tuberculosis virulence factor, mycolic acid, determines the elicited inflammatory pattern. *Eur. J. Immunol.* 41, 450–460 (2010).

80. Dubnau, E. *et al.* Oxygenated mycolic acids are necessary for virulence of Mycobacterium tuberculosis in mice. *Mol Microbiol* 36, 630–637 (2000).

81. Griffin, J. E. *et al.* Cholesterol Catabolism by Mycobacterium tuberculosis Requires Transcriptional and Metabolic Adaptations. *Chem Biol* 19, 218–227 (2012).

82. Lee, W., VanderVen, B. C., Fahey, R. J. & Russell, D. G. Intracellular Mycobacterium tuberculosis Exploits Host-derived Fatty Acids to Limit Metabolic Stress. *J Biol Chem* 288, 6788–6800 (2013).

83. Pandey, A. K. & Sassetti, C. M. Mycobacterial persistence requires the utilization of host cholesterol. *Proc Natl Acad Sci USA* 105, 4376–4380 (2008).

84. Gupta, R. *et al.* The Mycobacterium tuberculosis protein LdtMt2 is a nonclassical transpeptidase required for virulence and resistance to amoxicillin. *Nat Med* 16, 466–469 (2010).

85. Saxena, A., Srivastava, V., Srivastava, R. & Srivastava, B. S. Identification of genes of Mycobacterium tuberculosis upregulated during anaerobic persistence by fluorescence and kanamycin resistance selection. *Tuberculosis* 88, 518–525 (2008).

86. Vandal, O. H. *et al.* Acid-Susceptible Mutants of Mycobacterium tuberculosis Share Hypersusceptibility to Cell Wall and Oxidative Stress and to the Host Environment. *J Bacteriol* 191, 625–631 (2009).

87. Patru, M.-M., & Pavelka, M. S. A Role for the Class A Penicillin-Binding Protein PonA2 in the Survival of Mycobacterium smegmatis under Conditions of Nonreplication. *J Bacteriol* 192, 3043–3054 (2010).

88. Keer, J., Smeulders, M. J., Gray, K. M. & Williams, H. D. Mutants of Mycobacterium smegmatis impaired in stationary-phase survival. *Microbiology* 146, 2209–2217 (2000).

89. Dutta, N. K. *et al.* Genetic Requirements for the Survival of Tubercle Bacilli in Primates. *J INFECT DIS* 201, 1743–1752 (2010).

90. Griffin, J. E. *et al.* High-Resolution Phenotypic Profiling Defines Genes Essential for Mycobacterial Growth and Cholesterol Catabolism. *PLoS Pathog* 7, e1002251 (2011).

91. Rengarajan, J., Bloom, B. R. & Rubin, E. J. Genome-wide requirements for Mycobacterium tuberculosis adaptation and survival in macrophages. *Proc Natl Acad Sci USA* 102, 8327–8332 (2005).

92. Sassetti, C. M. & Rubin, E. J. Genetic requirements for mycobacterial survival during infection. *Proc Natl Acad Sci USA* 100, 12989–12994 (2003).

93. Eoh, H. & Rhee, K. Y. Multifunctional essentiality of succinate metabolism in adaptation to hypoxia in Mycobacterium tuberculosis. *Proc Natl Acad Sci USA* 110, 6554–6559 (2013).

94. Gill, W. P. *et al.* A replication clock for Mycobacterium tuberculosis. *Nat Med* 15, 211–214 (2009).

95. Ford, C. B. *et al.* Use of whole genome sequencing to estimate the mutation rate of Mycobacterium tuberculosis during latent infection. *Nat Genet* 43, 482–486 (2011).

96. Chao, M. C. & Rubin, E. J. Letting Sleeping dos Lie: Does Dormancy Play a Role in Tuberculosis? *Annu. Rev. Microbiol.* 64, 293–311 (2010).

97. Beste, D. J. V. *et al.* The Genetic Requirements for Fast and Slow Growth in Mycobacteria. *PLoS ONE* 4, e5349 (2009).

98. Cunningham, A. F. & Spreadbury, C. L. Mycobacterial stationary phase induced by low oxygen tension: cell wall thickening and localization of the 16-kilodalton α-crystallin homolog. *J Bacteriol* 180, 801–808 (1998).

99. Galagan, J. E. *et al.* The Mycobacterium tuberculosis regulatory network and hypoxia. *Nature* 499, 178–183 (2013).

100. Bhatt, A. *et al.* Deletion of kasB in Mycobacterium tuberculosis causes loss of acid-fastness and subclinical latent tuberculosis in immunocompetent mice. *Proc Natl Acad Sci USA* 104, 5157–5162 (2007).

101. Balaban, N. Q. Bacterial Persistence as a Phenotypic Switch. *Science* 305, 1622–1625 (2004).

102. Lenaerts, A. J. *et al.* Location of Persisting Mycobacteria in a Guinea Pig Model of Tuberculosis Revealed by R207910. *Antimicrob Agents Ch* 51, 3338–3345 (2007).

103. Baek, S.-H., Li, A. H. & Sassetti, C. M. Metabolic regulation of mycobacterial growth and antibiotic sensitivity. *PLoS Biol* 9, e1001065 (2011).

104. Ojha, A. K. *et al.* Growth of Mycobacterium tuberculosis biofilms containing free mycolic acids and harbouring drug-tolerant bacteria. *Mol Microbiol* 69, 164–174 (2008).

105. Kaur, D., Guerin, M. E., Skovierová, H., Brennan, P. J. & Jackson, M. Chapter 2: Biogenesis of the cell wall and other glycoconjugates of Mycobacterium tuberculosis. *Adv Appl Microbiol* 69, 23–78 (2009).

106. Bansal-Mutalik, R. & Nikaido, H. Mycobacterial outer membrane is a lipid bilayer and the inner membrane is unusually rich in diacyl phosphatidylinositol dimannosides. *Proc Natl Acad Sci USA* 111, 4958–4963 (2014).

107. Sani, M. *et al.* Direct visualization by cryo-EM of the mycobacterial capsular layer: a labile structure containing ESX-1-secreted proteins. *PLoS Pathog* 6, e1000794 (2010).

108. Zumla, A., Nahid, P. & Cole, S. T. Advances in the development of new tuberculosis drugs and treatment regimens. *Nat Rev Drug Discov* 12, 388–404 (2013).

109. Hancock, I. C., Carman, S., Besra, G. S., Brennan, P. J. & Waite, E. Ligation of arabinogalactan to peptidoglycan in the cell wall of Mycobacterium smegmatis requires concomitant synthesis of the two wall polymers. *Microbiology* 148, 3059–3067 (2002).

110. Raymond, J. B., Mahapatra, S., Crick, D. C. & Pavelka, M. S. Identification of the namH gene, encoding the hydroxylase responsible for the N-glycolylation of the mycobacterial peptidoglycan. *J Biol Chem* 280, 326–333 (2005).

111. Mahapatra, S. *et al.* Mycobacterial lipid II is composed of a complex mixture of modified muramyl and peptide moieties linked to decaprenyl phosphate. *J Bacteriol* 187, 2747–2757 (2005).

112. Girardin, S. E. *et al.* Peptidoglycan molecular requirements allowing detection by Nod1 and Nod2. *J Biol Chem* 278, 41702–41708 (2003).

113. Coulombe, F. *et al.* Increased NOD2-mediated recognition of N-glycolyl muramyl dipeptide. *J Exp Med* 206, 1709–1716 (2009).

114. Hansen, J. M. *et al.* N-glycolylated peptidoglycan contributes to the immunogenicity but not pathogenicity of Mycobacterium tuberculosis. *J INFECT DIS* 209, 1045–1054 (2014).

115. Makarov, V. *et al.* Benzothiazinones Kill Mycobacterium tuberculosis by Blocking Arabinan Synthesis. *Science* 324, 801–804 (2009).

116. Crick, D. C., Mahapatra, S. & Brennan, P. J. Biosynthesis of the arabinogalactan-peptidoglycan complex of Mycobacterium tuberculosis. *Glycobiology* 11, 107R–118R (2001).

117. Skovierova, H. *et al.* AftD, a novel essential arabinofuranosyltransferase from mycobacteria. *Glycobiology* 19, 1235–1247 (2009).

118. Layre, E. *et al.* A Comparative Lipidomics Platform for Chemotaxonomic Analysis of Mycobacterium tuberculosis. *Chem Biol* 18, 1537–1549 (2011).

119. Sacco, E. *et al.* The missing piece of the type II fatty acid synthase system from Mycobacterium tuberculosis. *Proc Natl Acad Sci USA* 104, 14628–14633 (2007).

120. Lea-Smith, D. J. *et al.* The Reductase That Catalyzes Mycolic Motif Synthesis Is Required for Efficient Attachment of Mycolic Acids to Arabinogalactan. *J Biol Chem* 282, 11000–11008 (2007).

121. Leger, M. *et al.* The Dual Function of the Mycobacterium tuberculosis FadD32 Required for Mycolic Acid Biosynthesis. *Chem Biol* 16, 510–519 (2009).

122. Grzegorzewicz, A. E. *et al.* Inhibition of mycolic acid transport across the Mycobacterium tuberculosis plasma membrane. *Nat Chem Biol* 8, 334–341 (2012).

123. Pacheco, S. A., Hsu, F. F., Powers, K. M. & Purdy, G. E. MmpL11 Protein Transports Mycolic Acid-containing Lipids to the Mycobacterial Cell Wall and Contributes to Biofilm Formation in Mycobacterium smegmatis. *J Biol Chem* 288, 24213–24222 (2013).

124. Varela, C. *et al.* MmpL Genes Are Associated with Mycolic Acid Metabolism in Mycobacteria and Corynebacteria. *Chem Biol* 19, 498–506 (2012).

125. Carel, C. *et al.* Mycobacterium tuberculosis Proteins Involved in Mycolic Acid Synthesis and Transport Localize Dynamically to the Old Growing Pole and Septum. *PLoS ONE* 9, e97148 (2014).

126. Scheffers, D.-J. & Pinho, M. G. Bacterial cell wall synthesis: new insights from localization studies. *Microbiol Mol Biol Rev* 69, 585–607 (2005).

127. Singh, S. K., SaiSree, L., Amrutha, R. N. & Reddy, M. Three redundant murein endopeptidases catalyse an essential cleavage step in peptidoglycan synthesis of Escherichia coliK12. *Mol Microbiol* 86, 1036–1051 (2012).

128. Meisner, J. *et al.* FtsEX is required for CwlO peptidoglycan hydrolase activity during cell wall elongation in Bacillus subtilis. *Mol Microbiol* 89, 1069–1083 (2013).

129. Kawai, Y., Daniel, R. A. & Errington, J. Regulation of cell wall morphogenesis in Bacillus subtilis by recruitment of PBP1 to the MreB helix. *Mol Microbiol* 71, 1131–1144 (2009).

130. Garner, E. C. *et al.* Coupled, Circumferential Motions of the Cell Wall Synthesis Machinery and MreB Filaments in B. subtilis. *Science* 333, 222–225 (2011).

131. Fenton, A. K. & Gerdes, K. Direct interaction of FtsZ and MreB is required for septum synthesis and cell division in Escherichia coli. *EMBO J* 32, 1953–1965 (2013).

132. Errington, J., Daniel, R. A. & Scheffers, D. J. Cytokinesis in Bacteria. *Microbiol Mol Biol Rev* 67, 52–65 (2003).

133. Smith, T. J., Blackman, S. A. & Foster, S. J. Autolysins of Bacillus subtilis: multiple enzymes with multiple functions. *Microbiol* 146, 249–262 (2000).

134. de Boer, P. A. J. Advances in understanding E. coli cell fission. *Curr Opin Microbiol* 13, 730–737 (2010).

135. Durand-Heredia, J., Rivkin, E., Fan, G., Morales, J. & Janakiraman, A. Identification of ZapD as a Cell Division Factor That Promotes the Assembly of FtsZ in Escherichia coli. *J Bacteriol* 194, 3189–3198 (2012).

Chapter 2

Protein complexes and proteolysis of the cell wall hydrolase RipA govern septal resolution in mycobacteria

Section 2.1: Overview and Attributions

Overview

This chapter is comprised of a manuscript that was published in PLoS Pathogens in February 2013 as well as additional unpublished work (Figures 2.9 and 2.10).

Attributions

For the published manuscript, I performed the experiments in Figures 2.1B,C; 2.3C; 2.4; 2.5B; 2.6B; and 2.7D,E. Michael Chao performed the remaining experiments except for those in Figure 2.7B,C which were performed by Shoko Minami. Michael Chao and I composed and edited the manuscript. I also generated the strains and performed the experiments in the unpublished data section (Figures 2.9 and 2.10).

Section 2.2 Protein complexes and proteolytic activation of the cell wall hydrolase RipA regulate septal resolution in mycobacteria

Michael C. Chao[1]*, Karen J. Kieser[1]*, Shoko Minami[1], Daniela Mavrici[2], Bree B. Aldridge[1], Sarah M. Fortune[1], Tom Alber[2], and Eric J. Rubin[1‡]

[1]Department of Immunology and Infectious Diseases, Harvard School of Public Health, Boston, MA 02115, USA.

[2] Department of Molecular and Cell Biology, QB3 Institute, University of California, Berkeley, CA 94720, USA.

* Authors contributed equally

‡ Corresponding Author: erubin@hsph.harvard.edu

‡ **Corresponding Author Present Address:**

Harvard Institutes of Medicine, Room 1007A

4 Blackfan Circle

Boston, MA 02115

(617) 432-3337

Abstract

Peptidoglycan hydrolases are a double-edged sword. They are required for normal cell division, but when dysregulated can become autolysins lethal to bacteria. How bacteria ensure that peptidoglycan hydrolases function only in the correct spatial and temporal context remains largely unknown. Here, we demonstrate that dysregulation converts the essential mycobacterial peptidoglycan hydrolase RipA to an autolysin that compromises cellular structural integrity. We find that mycobacteria control RipA activity through two interconnected levels of regulation *in vivo*—protein interactions coordinate PG hydrolysis, while proteolysis is necessary for RipA enzymatic activity. Dysregulation of RipA protein complexes by treatment with a peptidoglycan synthase inhibitor leads to excessive RipA activity and impairment of correct morphology. Furthermore, expression of a RipA dominant negative mutant or of differentially processed RipA homologues reveals that RipA is produced as a zymogen, requiring proteolytic processing for activity. The amount of RipA processing differs between fast-growing and slow-growing mycobacteria and correlates with the requirement for peptidoglycan hydrolase activity in these species. Together, the complex picture of RipA regulation is a part of a growing paradigm for careful control of cell wall hydrolysis by bacteria during growth, and may represent a novel target for chemotherapy development.

Introduction

Mycobacterium tuberculosis is the causative agent of tuberculosis and accounts for up to 10 million symptomatic infections a year [1]. The spread of multi-, extensively- and now totally- drug resistant strains [2] has created a pressing need to understand essential mycobacterial processes in an effort to define

novel targets for chemotherapy. One highly essential bacterial process is peptidoglycan (PG) synthesis and remodeling, which is critical for providing structural integrity in nearly all bacteria. PG forms a continuous macromolecular mesh that is part of the bacterial cell wall and is required for correct cellular morphology and opposition to osmotic forces. Despite extensive biochemical and genetic characterization of the enzymes responsible for the synthesis and degradation of PG (reviewed in [3,4]), the mechanism by which these enzymes coordinate their activities remains poorly defined. It is clear, however, that dysregulation of this homeostatic balance frequently has lethal effects on the bacterium—inactivation of peptidoglycan synthases, either through the use of penicillin derivatives or overexpression of dominant negative forms of PG synthetic enzymes, induces lysis of cells [5,6]. In many cases, this lethality can be suppressed by inactivation of several peptidoglycan hydrolases [5,7], suggesting that PG hydrolase autolysin activity is restrained by functional interactions with PG synthases. This idea is consistent with a 'make-then-break' approach to cell wall synthesis where new PG subunits are first incorporated before the existing sacculus is cleaved to allow expansion [8]. One example of this is the formation of the septal PG—cells ensure that the septal PG is formed before PG hydrolases cleave apart the daughter cells.

Recent work suggests that the activity of PG synthetic and hydrolytic enzymes is regulated by the formation of protein complexes. In *E. coli*, the PG amidases AmiA, AmiB and AmiC can interact with non-enzymatic partners that upregulate septal peptidoglycan hydrolysis [9]. Conversely, the major bifunctional PG synthases, PBP1A and PBP1B in *E. coli* interact with and rely on essential lipoprotein partners for function [10]. In addition to interactions with non-enzymatic partners, several affinity chromatography and genetic studies have identified interactions between PG modulating enzymes themselves [11]. While the exact interactions may be species-specific, in general, PG synthases can associate with both other PG synthases and with PG hydrolases. Likewise, PG hydrolases can form predicted hydrolytic complexes with other autolysins [11,12,13]. These results suggest a general paradigm where PG modulating enzymes of both similar and opposing functions assemble as multi-protein complexes that spatially and temporally coordinate PG synthesis and hydrolysis during bacterial growth and division. An immediate challenge is to translate the many identified interactions into functional *in vivo* effects on the growth and division of bacteria.

Previously, we have studied regulation of the essential *M. tuberculosis* PG hydrolase, RipA (Rv1477). RipA belongs to the NLPC/p60 family, and has been characterized as a D,L D-glutamate-diaminopimelic acid (DAP) endopeptidase that cleaves within the pentapeptide bridges of the PG sacculus, thereby removing cell wall crosslinks [14]. The RipA homologue in Listeria (P60) and in *Mycobacterium marinum* (IipA) can be deleted, but this causes septal resolution defects [15,16]. In contrast, RipA is essential in *M. tuberculosis* [17], and depletion of RipA produces a chaining phenotype in *M. smegmatis*, which causes severe growth inhibition [18]. This is unlike the case in *E. coli*, where extensive chaining and growth inhibition requires inactivation of several PG hydrolases [19].

In this work, we interrogate the mechanism by which RipA activity is regulated *in vivo* during vegetative growth. We report that RipA requires careful control to support growth and division without compromising the cell's structural integrity—RipA becomes a lethal autolysin when its activity is dysregulated. Under physiological conditions, RipA relies on protein interactions to correctly control its degradative capacity. These interactions are also necessary for proteolytic cleavage of RipA to produce active enzyme. RipA cleavage and activation is more robust in *M. smegmatis* than in the pathogenic *M. tuberculosis* or *M. bovis* BCG, which may be a reflection of the different PG hydrolysis requirements between fast and slow growing mycobacteria. However, bypassing RipA cleavage by overexpressing fully active truncated enzyme compromises the structural integrity of both *M. smegmatis* and *M. tuberculosis*, suggesting that RipA cleavage may be rate-limited in order to synchronize PG hydrolysis with the growth rate of the bacterium. These results suggest a model in which RipA is regulated by several interconnected post-transcriptional mechanisms—proteolytic processing produces active enzyme, while protein-protein interactions upstream and downstream of cleavage ensure RipA functions correctly at the septum.

Results

Dysregulated RipA functions as a lethal autolysin

When RipA is depleted, daughter cells are unable to separate and instead, grow as chains (Figure 2.1A). While cells require peptidoglycan hydrolysis to accomplish cell separation, excessive cell wall degradation

can compromise structural integrity and lead to lysis. We hypothesized that RipA sits in this precarious situation, where the cell cannot tolerate either too little or too much RipA activity.

We investigated whether excessive RipA activity is toxic to mycobacteria by inducing *M. smegmatis* RipA ($RipA_{Sm}$) from a tetracycline-inducible episomal plasmid in *M. smegmatis.* Unlike the chaining phenotype we have previously observed with RipA depletion, RipA overexpression caused the rod-shaped cells to become spherical and lyse, (Figure 2.1A,D). This is dependent on catalytic activity, as overexpression of a catalytic mutant, $RipA_{Sm}$ C408A, does not display this phenotype (Figure 2.1A,D). The spherical phenotype of $RipA_{Sm}$ overexpression led to a severe growth defect by optical density (Figure 2.1B) and over one hundred fold killing, as determined by CFU enumeration (Figure 2.1C). Thus, excessive RipA activity in the cell is highly lethal.

RipA depletion protects against PBP inhibition

To determine whether a more physiological level of RipA could be converted to a lethal autolysin, we dysregulated RipA activity through the use of the beta-lactam antibiotic meropenem. Beta-lactam antibiotics block PG precursor incorporation, which causes excessive PG hydrolase activity and cell lysis [7]. While *M. tuberculosis* is relatively resistant to most beta-lactams, recent work has shown that meropenem is more resistant to the endogenous mycobaterial beta-lactamase, and is highly effective at killing *M. tuberculosis*, especially in combination with the beta-lactamase inhibitor clavulanate [20]. Meropenem targets PBP2 and PBP3 in *E. coli*, as well as L,D transpeptidases in *M. tuberculosis* [21,22]. Since RipA is known to interact with the PG synthase PBP1, which is required for normal vegetative growth [23] and morphology in mycobacteria [24] (depletion of the protein leads to rounded cells), we asked whether meropenem treatment can dysregulate RipA and convert the enzyme into a lethal autolysin.

We first treated *M. smegmatis* with 10 μg/mL meropenem and assessed morphological changes over time by microscopy. Treated cells filament and swell at the poles and septa, which are the sites of mycobacterial PG incorporation (Figure 2.2A, arrows). This morphological toxicity correlated with a

Figure 2.1. Dysregulation of RipA in *M. smegmatis* causes growth attenuation.
(A) Micrographs of RipA dysregulated strains after 24 hours of depletion or induction. RipA depletion was achieved by placing *ripA* under the control of an anhydrotetracycline (aTc) inducible promoter [18]. Depletion occurred over 24 hours by growing this strain in the absence of aTc. Alternately, wildtype RipA ($RipA_{Sm}$) or catalytically inactive ($RipA_{Sm}$ C408A) *M. smegmatis* RipA was overexpressed in wildtype cells. In the C408A overexpression strain, both chaining (white arrows) and bulging (red arrows) cells were observed. Membranes were stained with TMA-DPH. Scale bar represents 2 μm. **(B)** *M. smegmatis* strains overexpressing wildtype ($RipA_{Sm}$) and catalytically inactive (C408A) RipA were induced with aTc and growth assessed by OD_{600} over time. **(C)** *M. smegmatis* was induced with aTc to overexpress either wildtype $RipA_{Sm}$ or inactive $RipA_{Sm}$ C408A. Colony forming units (CFUs) were enumerated at the indicated time course by serial dilution and plating onto inducer-free agar. **(D)** Time-lapse microscopy was used to visualize *M. smegmatis* grown on an agar pad with aTc to overexpress wildtype $RipA_{Sm}$ (left panels) or catalytically inactive $RipA_{Sm}$ C408A (right panels). A transcriptional cytosolic GFP reporter was used to visualize RipA induction as well as determine cytokinesis and cell lysis. Presented here are frames from agar pads at four time points post-induction, showing individual cells before and after cell lysis, as detected by loss of GFP signal (arrows). Scale bar represents 2 μm.

Figure 2.1 (Continued)

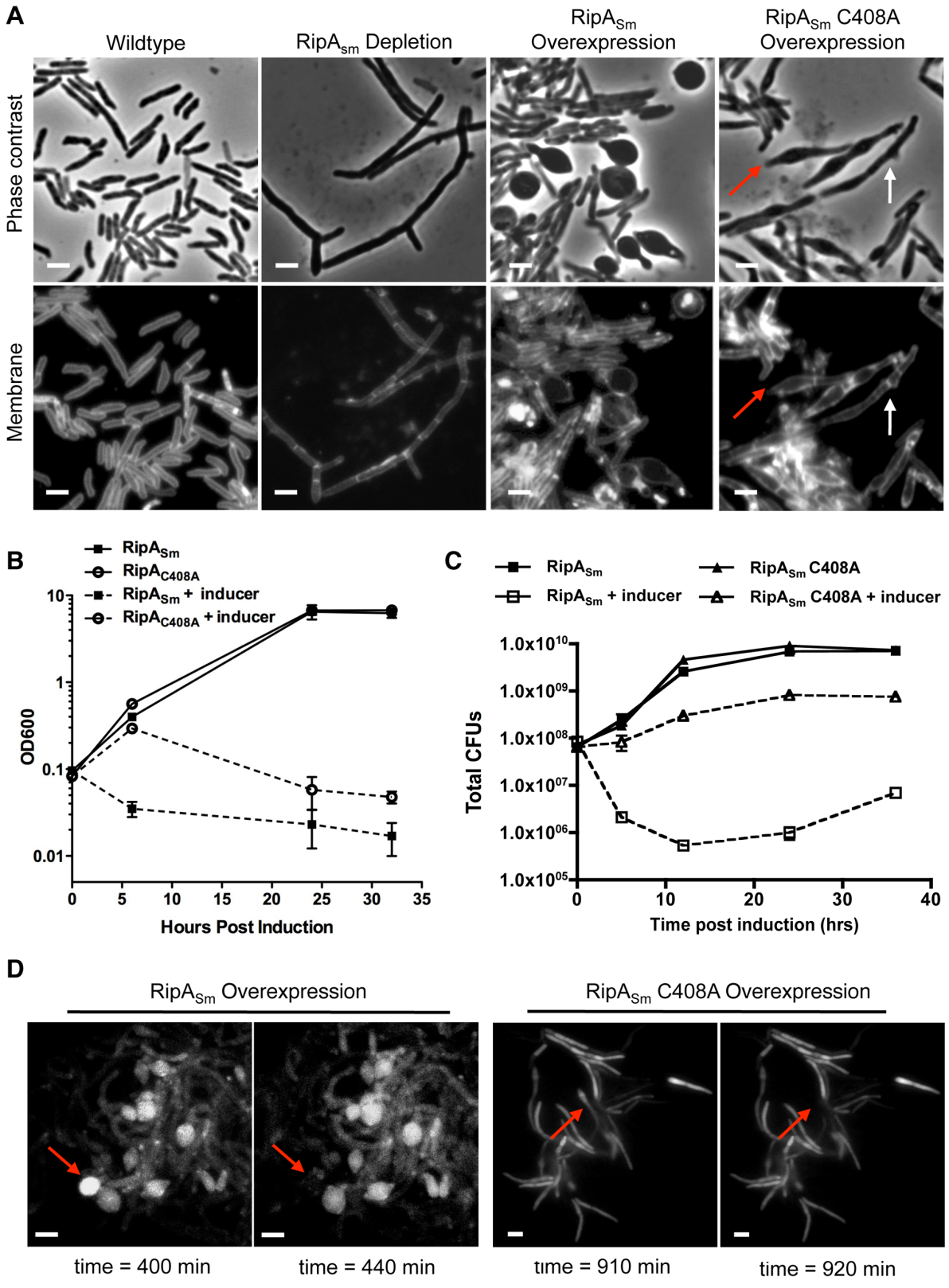

Figure 2.2. RipA depletion protects cells from meropenem-induced lysis.
(A) A RipA conditional depletion strain of *M. smegmatis* was grown in the presence of inducer (RipA replete conditions) and 10 μg/mL of meropenem. Cells were imaged for morphological changes at various time points after meropenem addition. During meropenem treatment, septal and polar bulging were observed (arrows). Cell membranes were stained with FM4-64. Scale bar represents 2 μm. **(B)** Lysis of *M. smegmatis* cells from (A) was also characterized by OD_{600} at various times post meropenem treatment. **(C)** The RipA conditional depletion strain of *M. smegmatis* was grown with anhydrotetracylcine (aTc) inducer (RipA replete) or pre-depleted (RipA deplete) in the absence of aTc for 6 hours. These cells were then treated with 10μg/mL of meropenem for 6 hours, washed, serially diluted and plated for CFU enumeration. (**, the difference between survival in RipA replete cells and RipA depleted cells in the presence of meropenem was significant with a p-value = 0.0006). **(D)** Cells post meropenem treatment in (C) were imaged by fluorescence microscopy to determine morphological changes. The plasma membrane was visualized with FM4-64. Scale bar represents 2 μm.

Figure 2.2 (Continued)

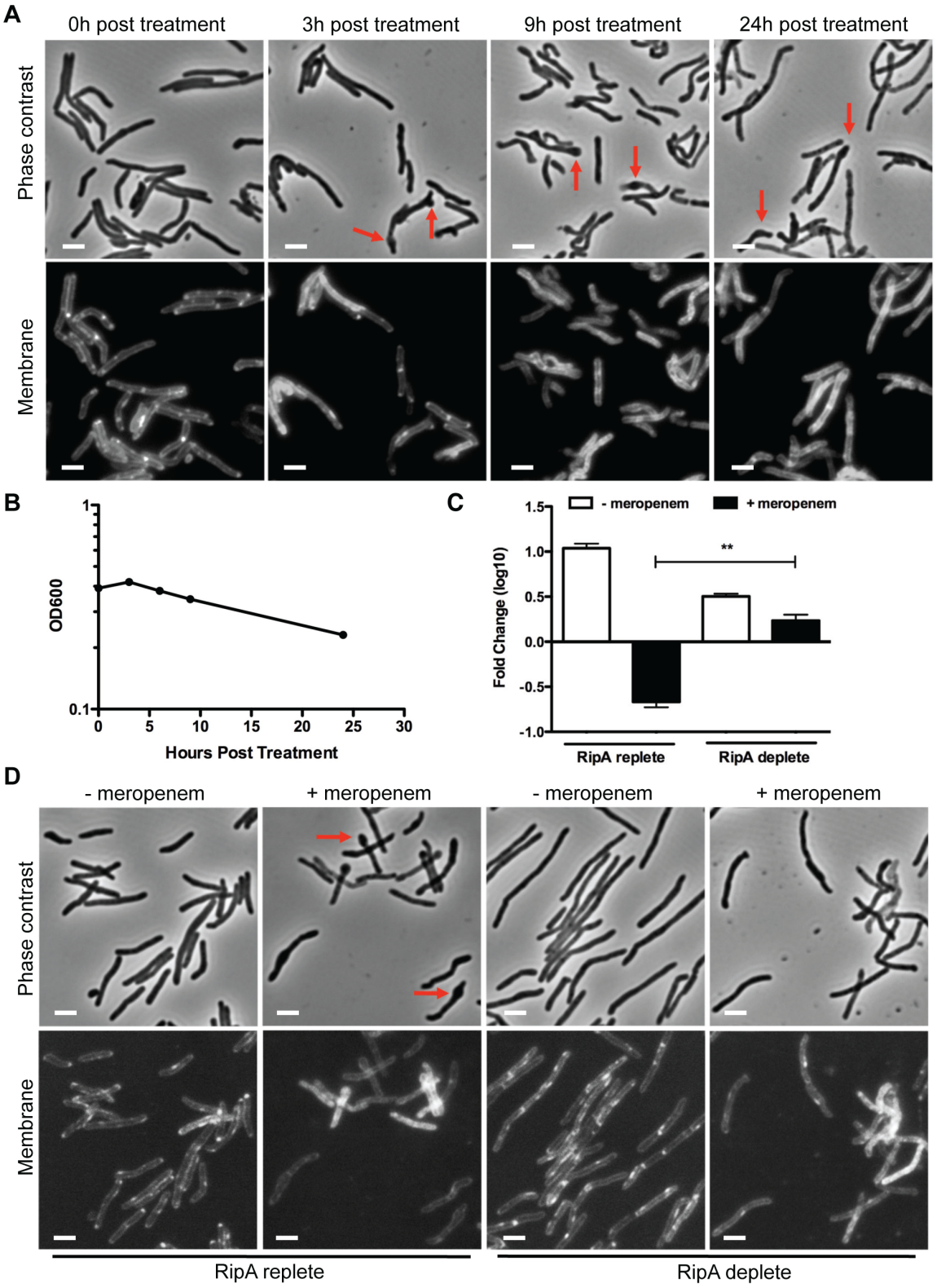

decrease in optical density over time, which suggested lysis (Figure 2.2B). This was borne out by CFU analysis, which showed that 80% of treated cells were killed within 6 hours of meropenem treatment (Figure 2.2C, bar 2).

The bulging at sites of PG incorporation after meropenem treatment suggested an excess of PG hydrolase activity. Since RipA localizes both to poles and septa, we hypothesized that RipA may play a role in killing meropenem treated cells. To test this idea, we depleted *M. smegmatis* of RipA before meropenem treatment and then assessed survival with meropenem treatment by CFU enumeration. We found that unlike RipA replete cells (Figure 2.2C, bar 2), meropenem did not kill RipA depleted cells (Figure 2.2C, bar 4). Furthermore, while RipA replete cells bulged under meropenem treatment as expected (Figure 2.2D, arrows), the RipA depleted cells appeared refractory to swelling (Figure 2.2D). As a control, cells were treated with SDS (which causes non-specific cell wall and membrane stress), as well as streptomycin, which targets protein synthesis. These control cells showed no survival or morphological differences between RipA replete and depleted cells (data not shown), demonstrating RipA specifically interacts with meropenem-affected pathways. Given that RipA enzymatic activity is modulated through protein-protein interactions with different PG synthetic and hydrolytic partners [18,24], the meropenem data suggest that RipA is held in check in complexes by an interacting protein, such as PBP1. Furthermore, although there are many hydrolases that could contribute to cell death when PG synthesis is blocked, we found that at least for the synthases blocked by the clinically relevant beta-lactam antibiotic meropenem, RipA is quantitatively the single most important hydrolase.

RipA post-transcriptional processes are required for septal resolution

Our results demonstrate that RipA dysregulation is highly detrimental to the cell. Thus, mycobacteria must control the activity of RipA during growth—there must be enough PG hydrolase activity around to support growth and division, but not an excessive amount so as to compromise structural integrity. One way this control may be regulated is at the transcriptional level.

We assessed whether the cell downregulates RipA expression using quantitative PCR. Since RipA is required for septation, which does not occur in non-replicative conditions, we compared RipA expression between exponential and stationary phases. We found that RipA remained expressed from exponential phase through the transition into stationary phase (data not shown), suggesting there may be post-transcriptional mechanisms responsible for restraining RipA activity when it is not needed. Thus, we investigated whether achieving tight control of RipA activity may rely on post-transcriptional processes.

We hypothesized that removal of wildtype RipA from its endogenous niche *in vivo* would inhibit correct septal resolution and therefore phenocopy RipA depletion. If RipA requires downstream interactions for activity, e.g. with members of septal complexes or with post-translational enzymatic regulatory proteins, then we should be able to create a dominant negative RipA mutant, where the critical catalytic cysteine [25] is mutated to a nonfunctional alanine. Overexpression of the $RipA_{Sm}$ C408A catalytic mutant should result in competition between nonfunctional RipA and endogenous RipA for required post-translational activation processes. If RipA requires these interactions to function, then we would observe chaining. Indeed, when we induced $RipA_{Sm}$ C408A, cells grew as short chains (Figure 2.1A, white arrows), suggesting that RipA interactions are necessary for correct septal PG hydrolysis.

While overexpression of the $RipA_{Sm}$ C408A mutant produced a severe growth defect (Figure 2.1B,C), it was not accompanied by the widespread lysis that was observed upon wildtype $RipA_{Sm}$ overexpression (Figure 2.1C). The apparent drop in optical density upon longer induction of the $RipA_{Sm}$ C408A strain (Figure 1B) was due to clumping of the culture, which though affecting optical density, did not lead to a drop in CFU, indicating growth inhibition rather than lysis (Figure 2.1C). However, we did observe occasional lysis of the $RipA_{Sm}$ C408A strain in addition to the dominant negative chaining phenotype. Some cells within a chain produced a slight bulging phenotype, which is indicative of an increase in PG hydrolytic activity (Figure 2.1A, red arrows). These bulging cells, like in RipA dysregulated cells, can go on to lyse (Figure 2.1D), though this does not lead to detectable cell death by CFU enumeration (Figure 2.1C). It is possible that displacement of endogenous wildtype RipA from complexes at the septum leads

to activity at ectopic sites in a subset of cells. Alternatively, RipA overexpression could stimulate other endogenous PG hydrolases.

RipA is proteolytically processed in vivo

When we used a RipA polyclonal antibody that recognizes a C-terminal epitope, we observed truncated RipA species from mycobacteria by Western blotting. When we overexpressed $RipA_{Sm}$, we found several bands smaller than the predicted full length protein (Figure 2.3A, lane 3). Likewise, we saw these truncated bands when we overexpressed $RipA_{Sm}$ C408A in *M. smegmatis* (Figure 2.3A, brackets). These products were not due to non-specific cytoplasmic degradation of overexpressed RipA, as we fractionated $RipA_{Sm}$ C408A overexpressing cells and found that RipA processed species were enriched in the cell wall fraction (data not shown). The efficiency of fractionating mycobacteria was confirmed by Western blotting against RpoB (cytosolic) and mycobacterial antigen 85 (cell wall) markers. Thus, these results suggest that RipA undergoes physiological post-translational processing in the periplasmic or cell wall compartment.

To further demonstrate that RipA processing is physiological and not an artifact of overexpression, we used Western blotting to estimate the size of RipA in wildtype *M. smegmatis* whole cell lysates. In mid-exponential phase cells, RipA formed a smear of ~30 kDa (Figure 2.3A, lane 2, red arrow) with no detectable full length protein present. This signal was specific for RipA, as cells depleted for RipA (Figure 2.3A, lane 1) had decreased signal compared to wildtype cells (Figure 2.3A, lane 2) when equal amounts of total protein were analyzed (Figure 2.3B). Furthermore, processed endogenous RipA partitioned to the cell wall compartment (data not shown). The smear of processed RipA suggests there are multiple processing sites. This may represent multiple cleavage products or further modifications to the protein. A recent crystal structure of RipA suggests a protease labile loop exists between the N inhibitory and C terminal PG hydrolase domains; this loop is hypothesized to be the site of cleavage *in vivo*, which is required for RipA enzymatic activation [25]. We mutated candidate residues in the loop in an attempt to identify cleavage sites but were unsuccessful in blocking RipA processing.

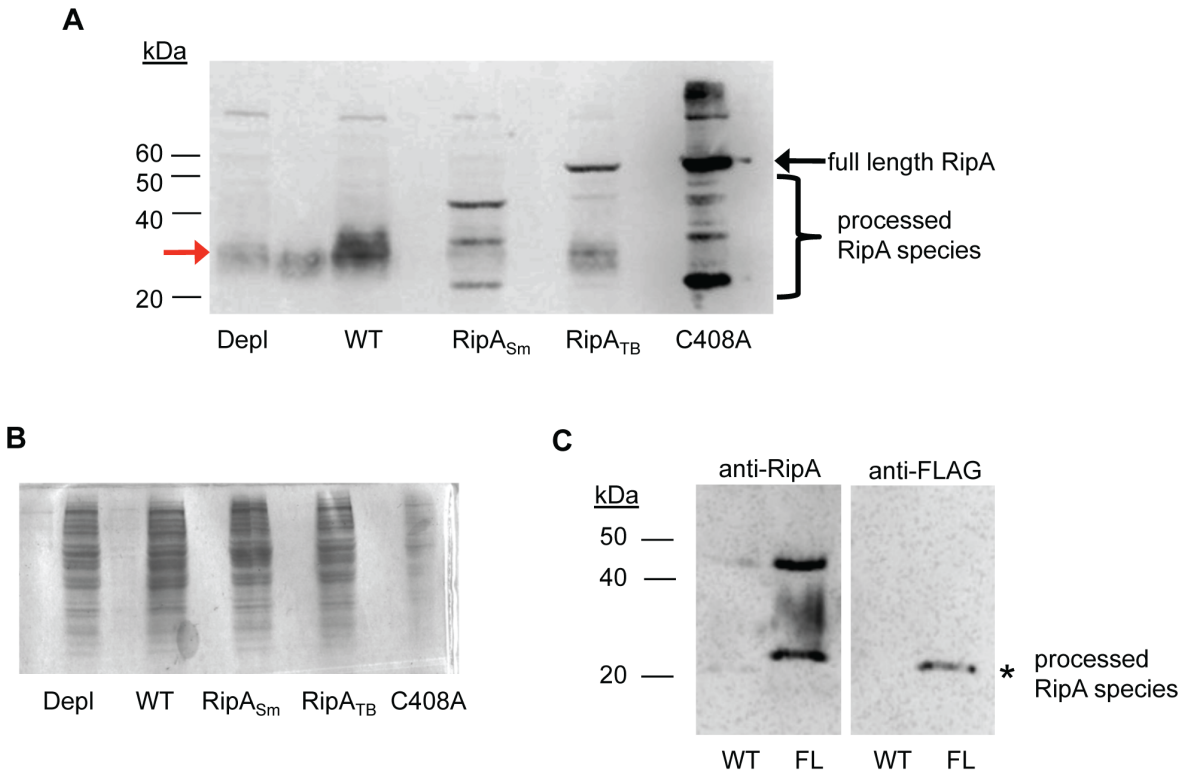

Figure 2.3. RipA$_{Sm}$ but not RipA$_{TB}$ is proteolytically processed in *M. smegmatis*.
(A) Whole cell lysates were made from cells depleted for RipA (DepI), wildtype *M. smegmatis* (WT), and cells overexpressing either wildtype RipA$_{Sm}$ (RipA$_{Sm}$), RipA$_{TB}$ (RipA$_{TB}$), or catalytically inactive RipA$_{Sm}$ C408A (C408A). The lysates were probed with anti-RipA polyclonal antibody. Full length RipA (arrow), and proteolytically cleaved endogenous RipA (red arrow) and recombinant species (brackets) were detected. **(B)** Coomassie stain of RipA-expressing *M. smegmatis* cells showing total protein loaded. Lanes are identical to (A). As RipA$_{Sm}$ C408A induction is particularly strong, this sample was deliberately underloaded to prevent its signal in (A) from overwhelming detection of less abundant species. **(C)** Western blots with anti-RipA (left panel) and anti-FLAG antibodies (right panel). Culture filtrates were collected from wildtype *M. smegmatis* (WT) and cells in which chromosomal RipA was C-terminally fused to a FLAG epitope (FL). A truncated RipA species that is shifted by the FLAG tag was observed (asterisk).

Truncated RipA species were found associated with the cell wall compartment and in culture filtrates. In the culture filtrate, a RipA fragment appeared as a single band at approximately 25 kDa (Figure 2.3C, asterisk). We demonstrated this signal was specific by C-terminally tagging endogenous RipA on the chromosome of *M. smegmatis* with a FLAG epitope. This 25 kDa species exhibited altered mobility due to the epitope and could be detected by both anti-RipA (Figure 2.3C, left panel) and anti-FLAG antibodies

(Figure 2.3C, right panels). These results indicate that RipA exists physiologically in a smaller form than the predicted full length protein.

RipA requires processing for activity

The observation of RipA cleavage suggested this process could be required for the protein's function *in vivo*. To test whether RipA processing is correlated with division, we titrated overexpression of $RipA_{Sm}$ C408A and quantified the amount of induction needed to mediate chaining. We found that low level overexpression with 30 ng/mL inducer was sufficient to cause chaining (Figure 2.4A) without saturating the processing machinery, since these cells did not accumulate full length RipA (Figure 2.4B). Instead, mildly overexpressed RipA was processed down to two sets of smaller species at around 23 kDa and 12 kDa (Figure 2.4B). We also saw a dose-dependent saturation of the endogenous processing capacity, with high induction leading to accumulation of full length RipA (Figure 2.4B), as well as loss of processed endogenous RipA (data not shown). When we quantified recombinant protein levels by comparing densitometry with endogenous RipA protein (Figure 2.4C), we found that even mild $RipA_{Sm}$ C408A overexpression at 30ng/mL of inducer (processed recombinant protein is approximately 10% of endogenous wild type RipA levels) was sufficient to cause chaining and cellular toxicity (Figure 2.4A). Together with qPCR data showing that $RipA_{Sm}$ C408A induction does not affect endogenous RipA transcription (data not shown), these data suggest direct competition between the $RipA_{sm}$ C408A mutant and endogenous RipA for processing machinery, and that the processed, not full length, form of RipA is required for division.

However, though correlated with function, the processed species we observed could be the product of an inactivating event. To test this, we took advantage of the observation that the *M. tuberculosis* homologue of RipA ($RipA_{TB}$) functions differently in *M. smegmatis* than its native counterpart, despite having the same general domain architecture. In contrast to $RipA_{Sm}$, which is toxic when overexpressed, overexpression of $RipA_{TB}$ in *M. smegmatis*, surprisingly caused no toxicity or cell morphological differences (Figure 2.5A,B), despite similar protein levels (Figure 2.3A). We examined whether $RipA_{Sm}$ toxicity was correlated with its processing by performing Western blot analysis on $RipA_{TB}$ overexpressing

M. smegmatis. In contrast to overexpression of $RipA_{Sm}$, when wildtype $RipA_{TB}$ is overexpressed we observed only a single full length band at 55 kDa (Figure 2.3A, right arrow). The absence of processing correlates with the lack of detectable $RipA_{TB}$ toxicity in *M. smegmatis*. Thus, we hypothesize that proteolytic cleavage is required for activating RipA *in vivo*.

However, it could be formally possible that $RipA_{TB}$ cannot recognize *M. smegmatis* peptidoglycan or is not intrinsically active enough in *M. smegmatis* to cause morphological defects. To test if $RipA_{TB}$ can be enzymatically functional in *M. smegmatis*, we deleted the predicted N-terminal inhibitory segment by fusing the truncated active domain of $RipA_{TB}$ to the RipA secretion signal peptide ($RipA_{TB}$-AD). As a control, we also produced a construct in which the *M. smegmatis* RipA active domain ($RipA_{Sm}$-AD) can be secreted. None of the strains produced growth defects when uninduced (data not shown). As expected $RipA_{Sm}$-AD, like full length $RipA_{Sm}$, was fully functional when induced and disrupted cell wall integrity, leading to bulging of the cells and a concomitant growth defect (Figure 2.6A,B). When $RipA_{TB}$-AD was secreted, we found that it was also functional and behaved in the same way as $RipA_{Sm}$-AD (Figure 2.6A,B). Thus, the catalytic domain of $RipA_{TB}$ can be active in *M. smegmatis,* but full length $RipA_{TB}$ is not toxic because it does not undergo efficient processing in *M. smegmatis*.

RipA processing in M. tuberculosis requires additional steps

Given the potentially toxic nature of hyperactive RipA we hypothesized that RipA processing and activation may be less robust in slow-growing mycobacteria in order to match their much slower rate of growth and consequent lower requirement for peptidoglycan hydrolysis. To investigate this model, we first determined whether RipA is processed in *M. tuberculosis* by overexpressing $RipA_{TB}$. By Western blot analysis, we found multiple immunoreactive smaller species of $RipA_{TB}$, suggesting processing in *M. tuberculosis* (Figure 2.7D, brackets). However, the induction of $RipA_{TB}$ in *M. tuberculosis* did not produce morphological changes or growth defects, even after five days of induction (Figure 2.7A,B). This overexpression produced about 3 fold more protein (most of which is in the processed form) than endogenous full length RipA (Figure 2.7E), which is similar to the amount of overexpression needed to observe cell chaining in *M. smegmatis* with the $RipA_{Sm}$ C408A allele (Figure 2.4C). The lack of

Figure 2.4. Proteolyzed $RipA_{Sm}$ C408A overexpression correlates with morphological toxicity. **(A)** Micrographs of *M. smegmatis* grown in various concentrations of inducer to overexpress $RipA_{Sm}$ C408A-FLAG. Scale bar represents 2 μm. **(B)** Total cell lysates from *M. smegmatis* overexpressing $RIpA_{Sm}$ C408A-FLAG under various inducer concentrations were probed with anti-FLAG antibody. Both full length (arrow) and processed $RipA_{Sm}$ C408A species (brackets) were detected, including two major processed species: a band at 25 kDa and a doublet around 12 kDa. **(C)** Samples from (B) were probed with anti-RipA antibody and densitometry analysis performed. The levels of full length (black), processed (red) and total (blue) recombinant $RipA_{Sm}$ C408A proteins were compared to endogenous RipA levels. The fold overexpression of $RipA_{Sm}$ C408A relative to endogenous RipA was graphed as a function of inducer concentration.

Figure 2.4 (Continued)

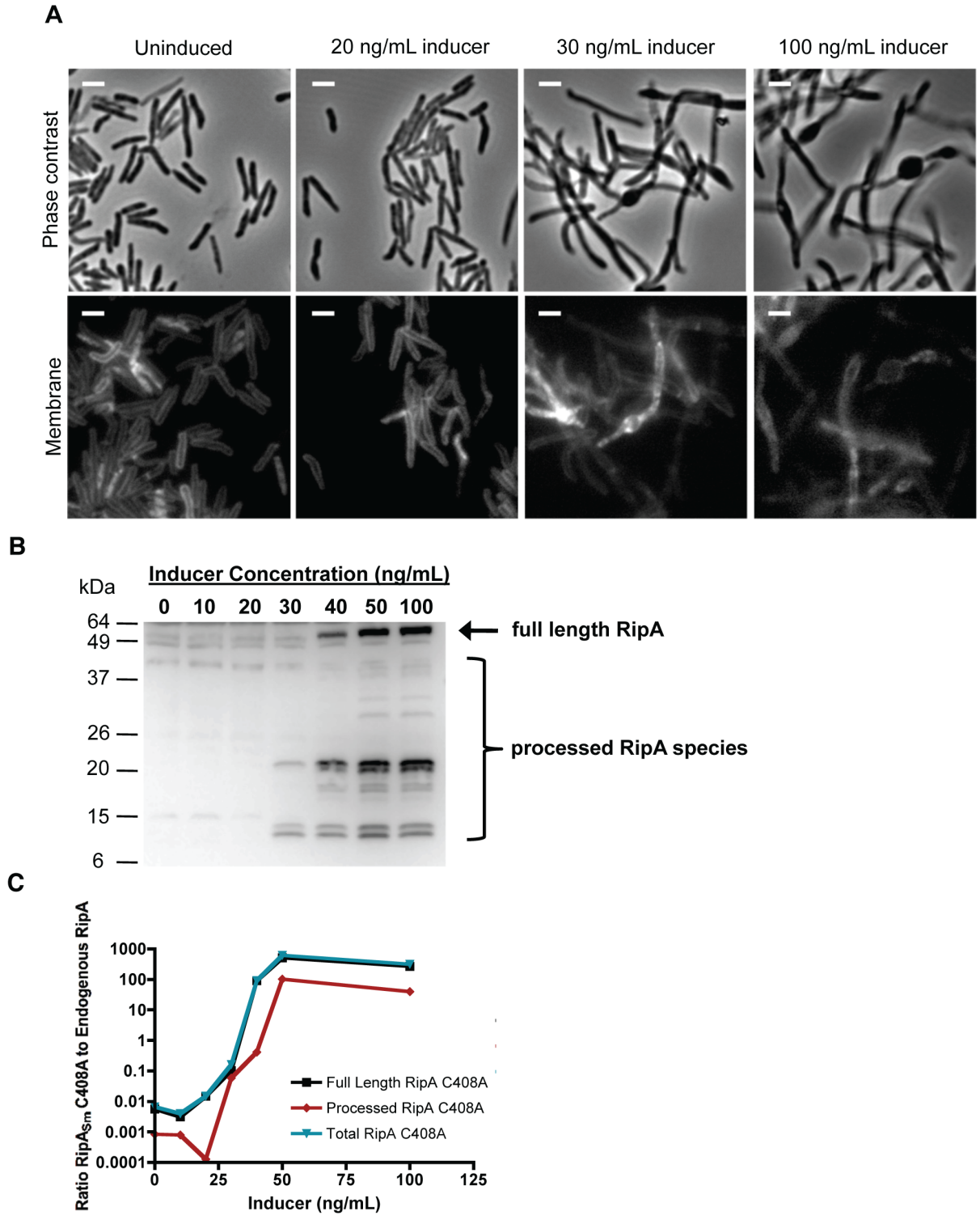

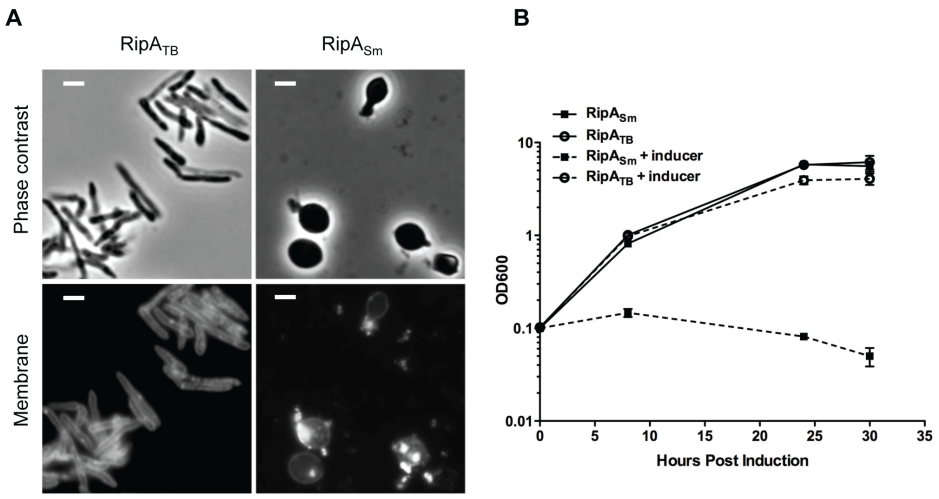

Figure 2.5. RipA is differentially active in a species-specific manner.
(A) Fluorescence micrographs of *M. smegmatis* strains induced with aTc to overexpress *M. tuberculosis* RipA (RipA$_{TB}$) or *M. smegmatis* RipA (RipA$_{Sm}$). Membranes were stained with TMA-DPH. Scale bar represents 2 µm. **(B)** *M. smegmatis* strains in (A) were induced with aTc to overexpress RipA$_{TB}$ and RipA$_{Sm}$ constructs. Growth of these strains was monitored over time by OD_{600}.

morphological changes in *M. tuberculosis* is also in contrast with the marked lethality of RipA$_{Sm}$ overexpression in *M. smegmatis* (Figure 2.1).

One explanation for this dichotomy may be that the slow growth of *M. tuberculosis* might mask morphological or growth defects caused by RipA overexpression. To test this possibility, we bypassed RipA processing by secreting truncated RipA$_{TB}$-AD in *M. tuberculosis*. Induction of RipA$_{TB}$-AD produced a severe growth defect in *M. tuberculosis* (Figure 2.7C), and concomitant cell rounding (Figure 2.7A) similar to that seen when RipA$_{Sm}$ was overexpressed in *M. smegmatis*. These results show that unchecked RipA activity is toxic even to slow-growing mycobacteria. Since full length RipA$_{TB}$ induction does not produce this toxicity, *M. tuberculosis* may have intrinsically less robust RipA processing than in *M. smegmatis*. Indeed, in *M. tuberculosis,* we observed a band of 55kDa on Western blots probed with anti-RipA antisera. This band is the same size as full length RipA$_{TB}$ and appears in both uninduced and induced samples (Figure 2.7D, arrow). As this form was not detected in wildtype *M. smegmatis* lysates (Figure 2.3A), it may represent endogenous, unprocessed full length RipA. The same full length band was also observed in *M. bovis* BCG cell lysates. These data, along with the active domain overexpression analysis,

support the idea that slow-growing mycobacteria process RipA less efficiently in order to keep this potentially lethal activity in check.

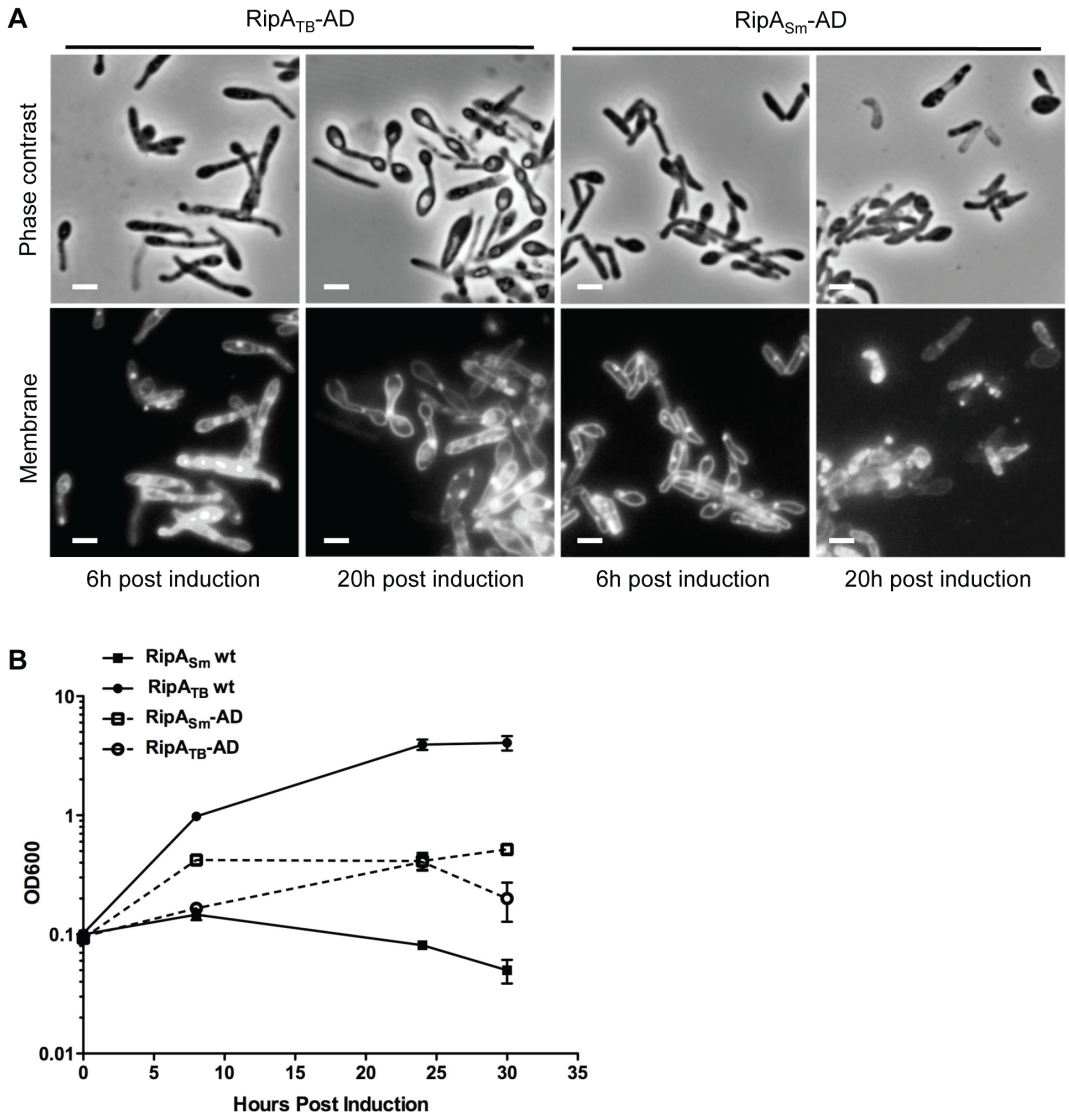

Figure 2.6. Truncation causes RipA$_{TB}$ to become active in *M. smegmatis*.
(A) *M. tuberculosis* and *M. smegmatis* RipA were truncated to the active endopeptidase domain (AD) and fused to the RipA secretion signal to generate RipA$_{TB}$-AD and RipA$_{Sm}$-AD. Micrographs of *M. smegmatis* overexpressing RipA$_{TB}$-AD or RipA$_{Sm}$-AD were taken at 6 and 20 hours post induction with aTc. Membranes were visualized by FM4-64 staining. Scale bar represents 2 μm. **(B)** *M. smegmatis* strains were constructed to overexpress full length RipA$_{TB}$ and RipA$_{Sm}$ and truncated RipA$_{TB}$-AD, RipA$_{Sm}$-AD constructs under the control of aTc. Growth of these strains in the presence of inducer was assessed over time by OD$_{600}$.

Discussion

Bacteria rely on peptidoglycan (PG) for shape and structure. The prevailing view of PG remodeling requires the concerted action of synthetic enzymes ligating new subunits into the existing PG lattice followed by hydrolysis of the PG sacculus by autolysins to allow cellular expansion or division. This process is accomplished through the action of large holoenzyme complexes in the periplasm consisting of both PG synthetic and hydrolytic enzymes. Disruption of PG synthesis in these complexes can dysregulate cognate PG hydrolases, which can then become autolysins that lyse the cell [26]. Thus, the coordination and regulation of PG hydrolases is a critical process for survival of the bacterium.

Here we find that RipA in *M. tuberculosis* and *M. smegmatis* can behave as an autolysin, resulting in the formation of spherical cells and lysis when overexpressed or dysregulated. Overexpression of a RipA dominant negative mutant not only causes loss of septal resolution and chaining but also leads to uncontrolled activity of endogenous PG hydrolases and lysis in a subset of cells. Thus, RipA requires downstream interactions to govern its correct function during septal resolution, as well as prevent lethal ectopic hydrolase activity. The relatively low amount of dominant negative RipA (about 10% of endogenous RipA) required for chaining suggests that the cell has finely tuned the amount of active RipA in the cell to near the level required for division; even loss of 10% of these active RipA species (which is manifest in a partial loss of endogenous RipA processing (Figure S7A) leads to a block in septal resolution. While it is clear that $RipA_{Sm}$ C408A overexpression can interfere with endogenous RipA activation, given its known interactions with two other PG remodeling enzymes that localize to the septum—RpfB and PBP1 [18,24,27]—it is possible the dominant negative mutant also incorporates into and inhibits functional PG remodeling complexes. A combination of these two activities may contribute to the $RipA_{Sm}$ C408A mutant's potency at inducing chaining at relatively low levels of induction.

Supporting the presence of regulatory RipA septal complexes, we showed chemical inhibition of peptidoglycan incorporating PBPs (of which the RipA binding partner PBP1 is a member) results in cell rounding and lysis. Loss of PG synthetic activity within a PG remodeling complex may allow cognate PG

Figure 2.7. Processed RipA is toxic to *M. tuberculosis*.
(A) Full length $RipA_{TB}$ and truncated $RipA_{TB}$-AD was overexpressed in *M. tuberculosis* for several days with addition of aTc. Cells were analyzed by microscopy for changes in morphology. Membranes were stained with FM4-64. Scale bar represents 2 μm. **(B)** Growth of *M. tuberculosis* induced with aTc and overexpressing full length $RipA_{TB}$ was measured by OD_{600}. **(C)** Growth of *M. tuberculosis* induced with aTc and overexpressing truncated $RipA_{TB}$-AD was measured by OD_{600}. **(D)** *M. tuberculosis* RipA ($RipA_{TB}$) was overexpressed in *M. tuberculosis* by induction (lane 2) with aTc for 48 hours. $RipA_{TB}$ was then detected by anti-RipA Western blot analysis. Uninduced lysates were used a control (lane 1). Full length RipA (arrow) and processed forms (brackets) were detected. **(E)** Total overexpressed protein was quantified from (D) by performing densitometry analysis on bands apparent in the induced strain that are absent from the uninduced control. Fold change in total $RipA_{TB}$ overexpression relative to endogenous full length RipA signal was graphed.

Figure 2.7 (Continued)

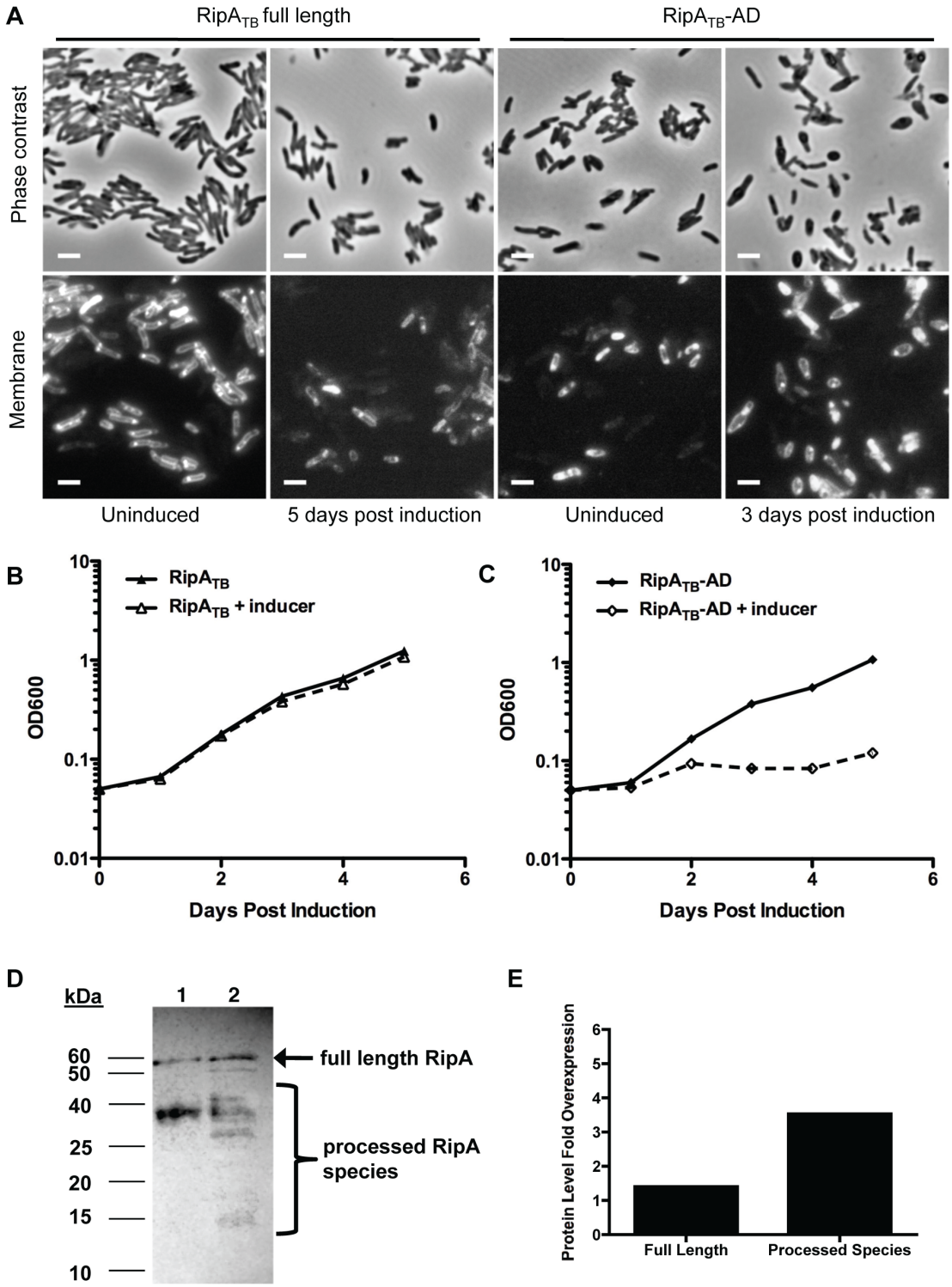

hydrolases (such as RipA) to become hyperactive and lyse the cell. We found that RipA depleted cells were specifically protected against meropenem-induced killing, but remained sensitive to other unrelated stresses. The depletion of the RipA likely affects the expression of RipB, which resides downstream in the same operon and has the same *in vitro* enzymatic specificity as RipA [14]. However, RipB is not essential for growth [28], and we have previously shown that RipA appears to be more phenotypically active than RipB *in vivo*. RipA, but not RipB, can complement the growth inhibition and cell chaining defects observed in the *ripAB* depletion strain [18]. While we cannot discount the possibility that RipB contributes to meropenem-mediated killing, it seems more likely that RipA is the main enzyme responsible for this lethal phenotype. Together, our data suggests that meropenem-induced killing is RipA dependent. However, we do observe a slight but significant difference in growth between RipA depleted cells in the presence and absence of meropenem (Figure 2.2C, lanes 2 and 4) that suggests there may also be some RipA independent growth inhibition (but not lysis) due to meropenem treatment. This may reflect the fact that meropenem can target several transpeptidases [21,22]. Despite this, since RipA appears to mediate meropenem's bactericidal capacity, and thus appears to be a more attractive target for drug development—we would expect that a chemical activator of RipA might act synergistically with meropenem treatment. From these data alone, it may be possible that a RipA inhibitor would be contraindicated in combination with meropenem, as it would antagonize the effect of PBP blockade, but we have previously observed that RipA depletion can sensitize cells to carbenicllin, a β-lactam antibiotic that also targets various transpeptidases [18]. In previous assays, in contrast to meropenem, carbenicillin sensitization required long term RipA depletion—it had no bactericidal effect on cells depleted for RipA in the same time scale as our meropenem studies. These data suggest that extended treatment with a RipA inhibitor may weaken cells enough to cause sensitivity to PBP inhibitors to which the cell was previously resistant. It would be interesting to determine whether RipA blockade can, in fact, synergize with existing PG targeting antibiotics *in vivo*.

Because of the threat of lethal autolysin activity, cells can control PG hydrolases through several, interconnected regulatory mechanisms. RipA is no exception, as we have found that in addition to protein interactions that modulate its function, RipA requires proteolytic activation. RipA exists primarily as

smaller processed forms in *M. smegmatis*. Recent work with RipA *in vitro* has mapped a protease labile loop between a putative N terminal blocking domain and the C terminal p60 PG hydrolase domain [25]. The size of our truncated RipA species could contain the predicted size of the p60 domain itself after cleavage within this loop, but we were unable to determine the exact cleavage site(s) for RipA proteolytic activation *in vivo* using site directed mutagenesis—mutation of two pairs of highly scissile aspartate-proline peptide bonds [29] at DP301 and DP315 to alanines had no effect on the ability of RipA to be cleaved in *M. smegmatis* (data not shown). This is consistent with the activation of Auto amidase in *Listeria monocytogenes*, which is also produced as a zymogen and becomes active only after proteolytic processing and removal of an N terminal inhibitory domain [30]. For Auto it was not possible to isolate single amino acid substitutions that abolish processing; instead, only deletion of the loop prevented proteolytic cleavage [30], which suggests that the activation loop is intrinsically labile and might be cleaved by many different proteases. Like Auto amidase, RipA's labile loop can be cleaved by many proteases *in vitro* [25], and thus may be a target of several proteases *in vivo*. This may explain why we see a smear of RipA truncated species in wildtype mycobacteria, as opposed to a single truncated band.

Given the work of Ruggiero et al [25], it was likely that RipA is produced as a zymogen *in vivo*, like Auto amindase. However, another recent report suggested a different effect of the N terminal domain in blocking RipA enzymatic activity [14,25]. While both studies agreed that the N terminal domain appears to partially block the C terminal endopeptidase active site, the authors reached opposite conclusions as to whether the N terminus is inhibitory. Ruggiero et al [25] found that truncated RipA containing only the C terminal p60 domain was able to cleave purified PG, while full length RipA had minimal activity [25]. In contrast, Böth et al [14] showed that full length RipA was capable of degrading small synthetic PG fragments, and truncation of the N terminus produced no increase in enzymatic activity. However, in the latter work, the authors did not perform enzymatic digests using full length RipA on purified PG, as performed by Ruggiero et al. It is possible that the reported differences between these studies reflects the ability of small PG fragments to enter the RipA active site, despite partial occlusion by the N terminal domain, while access of larger substrates such as crosslinked and polymerized PG is blocked. Our results favor the zymogen model, as we have found that processing of the N terminal domain is required

for full RipA enzymatic activation *in vivo*. Likewise, the lack of processing of $RipA_{TB}$ in *M. smegmatis* likely accounts for the absence of its toxicity upon overexpression. While it is possible that full length RipA could serve some degradation function on smaller substrates *in vivo*, our results suggest that its main peptidoglycan remodeling activity requires removal of the N terminus, which contains a functional inhibitory domain.

Furthermore, using the less efficiently processed $RipA_{TB}$ homologue, we showed that protein interactions are not only necessary for regulating functional septal complexes but also promote RipA proteolytic activation. Full length $RipA_{Sm}$ is toxic when overexpressed in *M. smegmatis*, but full length $RipA_{TB}$ does not produce the same phenotype. However, when we bypassed processing and expressed the truncated $RipA_{TB}$ active domain in *M. smegmatis*, we observed a full gain of toxicity. These results suggest that the interactions between $RipA_{Sm}$ and the cellular factors necessary for processing do not occur with the $RipA_{TB}$ homologue. Since septation is a highly conserved process, these data may not indicate different binding partners in slow and fast growing mycobacteria but rather that the *M. smegmatis* and *M. tuberculosis* binding partners have evolved together and may have higher affinities for one another.

Together, our work demonstrates that RipA regulation occurs at multiple levels post-transcriptionally. We did not see any transcriptional downregulation in cells transitioning into non-replicating conditions (data not shown). In fact, there was a significant increase in RipA transcription during the transition to stationary phase, but the functional consequence of this observation remains unknown. Furthermore, while overexpression of the dominant negative $RipA_{Sm}$ C408A allele modulates processing of endogenous RipA, this is due to competition for processing and not transcriptional feedback, even at high induction conditions (data not shown). This lack of transcriptional modulation is consistent with the observation that *ripA* expression has only limited variation across dozens of published experimental conditions (summarized on TBDB [31]), including general and antibiotic stresses. The only conditions under which *ripA* expression have been found to change are under non-replication conditions and, recently, when cells are blocked in cell division [32]. In the latter work, Plocinska *et al* found that *ripA* can be regulated by the MtrAB two component system. Specifically, inhibiting septum formation prevents MtrB, which localizes at

the septum, from activating the MtrA response regulator, leading to *ripA* downregulation. The authors proposed an interesting model in which *ripA* transcription could be upregulated by MtrB when it assembles at the division site; however, it remains unclear whether MtrAB regulation of *ripA* transcription occurs during normal growth or, instead, represents a stress response when cell division is inhibited. While the question of *ripA* transcriptional regulation during vegetative growth remains to be tested, our work suggests that post-translational mechanisms like processing may represent a key way of controlling RipA hydrolytic activity during growth. Therefore, we propose that protein-protein interactions help establish RipA function at the septum, where it is then aided in becoming proteolytically cleaved in the periplasm (Figure 2.8). After enzymatic activation, functional RipA can rely on both upstream and downstream protein interactions to help place it in the correct context during cell division—inhibition of cognate PG synthases can lead to dysregulated cell wall hydrolysis. The benefit of having multiple levels of RipA regulation is that the cell can exert a tighter control over RipA's activation and potential autolysin activity.

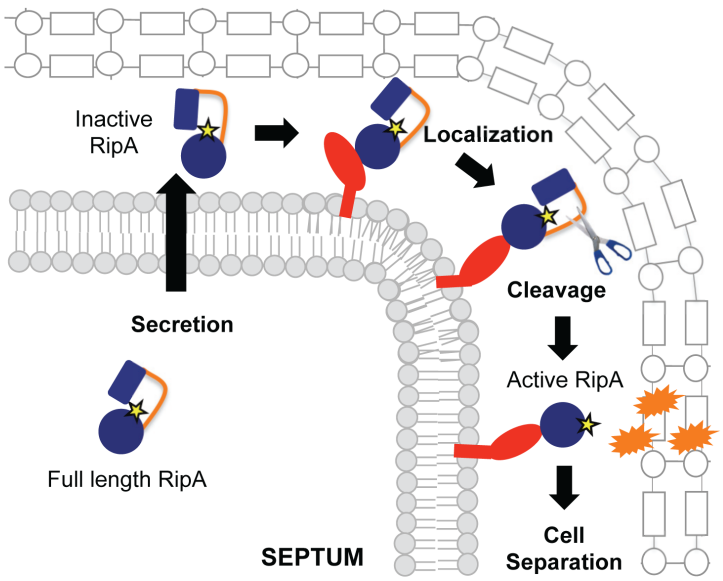

Figure 2.8. Model for RipA activation through proteolytic processing and protein interactions
RipA is produced as a full length zymogen with an N-terminal secretion signal. Once in the periplasm, RipA can bind to its interaction partners, leading to recruitment of proteases that cleave the extended loop between an N-terminal blocking domain and the C-terminal peptidoglycan hydrolase domain. The cleaved RipA C-terminal domain is now active and functions by cleaving the septal peptidoglycan, splitting the daughter cells, perhaps in conjunction with other hydrolases.

We found that RipA in *M. tuberculosis* is subject to less proteolytic activation than in *M. smegmatis*. The slow-growing mycobacteria like *M. tuberculosis* and *M. bovis* BCG might well have slower rates of PG hydrolysis and, consequently, reduced RipA activity. Indeed, we find significant amounts of full length $RipA_{TB}$ in slow-growing mycobacterial lysates, a form not present in *M. smegmatis* lysates. Furthermore, while expression of the active domain of $RipA_{TB}$ leads to severe growth inhibition with concomitant bulging, overexpression of full length $RipA_{TB}$ has no such effect in *M. tuberculosis*, suggesting that slow-growing mycobacteria proteolytically activate less RipA than their fast-growing counterparts. The mechanism behind this additional control over RipA activation is not known, but may be at the level of expression or functional kinetics of the protease(s) responsible for RipA cleavage. In fact, there is an additional stretch of amino acids in $RipA_{Sm}$ compared to $RipA_{TB}$, which sits at the beginning of the N terminal inhibitory domain. Ultimately, an integrated mechanism for controlling PG hydrolases may represent a broad paradigm among cell wall degrading proteins. Multiple levels of regulation might be required to synchronize their activity to the cellular requirement while avoiding overactivity and toxicity. In support of this, expression of a dominant negative RipA allele at 10% of the endogenous RipA levels leads to abnormal chaining. Thus, *M. smegmatis* appears to carefully titrate the amount of processed RipA to nearly the minimum levels it requires for division,

Finally, beyond division mechanics, post-translational PG hydrolase regulation has the added benefit of inducing changes quickly in response to changing environmental conditions, especially in times of low transcription such as non-replicative conditions [33,34]. The byproducts of PG hydrolysis can act as sensors for the bacterial environment, whether *in vitro* or within a host. For example, in *B. subtilis*, muropeptides have been found to be sufficient to induce spore resuscitation [35,36] while in *M. tuberculosis*, RpfB, a lysozyme that is known to be a RipA interacting partner [27], is required for regrowth from both *in vitro* and *in vivo* non-replication states [37,38]. The exact mechanism behind mycobacterial resuscitation remains unclear, but muropeptide-based signaling could play a major role. In fact, we found processed RipA species in the culture filtrates and recent work by Mir et al demonstrated that the addition of muropeptides to dormant *M. tuberculosis* facilitated resuscitation, possibly through the binding and

signaling of the essential mycobacterial integral membrane kinase, PknB [39]. Thus, soluble PG remodeling proteins might play a role in fostering communication across a bacterial population.

In summary, this work has further defined two connected, but distinct, mechanisms to regulate the activity of RipA, a potential autolysin that is essential for septal resolution in mycobacteria. The complexity of this regulation, which involves protein interactions as well as proteolytic activation, underscores the importance of carefully coordinating cell wall hydrolysis during growth and division. By dissecting the molecular regulation of PG hydrolases, we gain fundamental insight into how the bacterial cell wall is dynamically maintained and also open up avenues for novel chemotherapeutics, especially against major human pathogens such as *M. tuberculosis*.

Materials and Methods

Strains and Culture Conditions

E. coli XL-1 Blue (Stratagene, Santa Clara, CA) were grown at 37C in LB broth or agar and used for cloning. Selection was performed using kanamycin (50 mg/mL), hygromycin (100 mg/mL), ampcillin (100 mg/mL) or zeocin (25 mg/mL) when appropriate. *Mycobacterium smegmatis* mc^2155 was grown at 37 °C, unless otherwise indicated, in Middlebrook 7H9 broth supplemented with ADC (albumin-dextrose-catalase) and 0.05% Tween80. Selection of *M. smegmatis* was achieved by supplementation of kanamycin (25 mg/mL), hygromycin (50 mg/mL) or zeocin (25 mg/mL). *M. tuberculosis* H37Rv and *M. bovis* BCG were grown in liquid Middlebrook 7H9 broth and plated on Middlebrook 7H10 agar supplemented with OADC (oleic acid-albumin-dextrose-catalase) (BD Biosciences, Franklin Lakes, NJ). *M. smegmatis* in which the RipA endogenous promoter has been replaced by a tetracycline induclble promoter was previously constructed and characterized in [18].

Recombinant DNA Constructs

Mtb RipA (Rv1477) and Msmeg RipA (MSMEG_3145) mutants were constructed through PCR stitching using the following primers:

Mtb C383A RipA Forward (CCGTCGGCTTCGACGCCTCAGGCCTGGTGTTG)

Mtb C383A Reverse (CAACACCAGGCCTGAGGCGTCGAAGCCGACGG)

Msmeg RipA C408A Forward (ACCGTCGGCTTCGACgcCTCGGGTCTGATG)

Msmeg C408A Reverse (CATCAGACCCGAGgcGTCGAAGCCGACGGT).

Msmeg RipA DP301AA DP315AA double point mutants were constructed by PCR stitching using the following primers:

Msmeg RipA DP315AA Forward

(GCGATCCCGAGCGCGTTCGTCAGCGGTGcCgCCATCGCGATCATCAAC)

Msmeg RipA DP300AA Reverse

(GAACGCGCTCGGGATCGCAGGCAGGGTCgCGgCCCACACGGCCCAGTT)

Secreted, RipA catalytic domain constructs were made using the *M. smegmatis* RipA secretion signal amino acids 1-51—Reverse primer: GAACCTgatatcGACGAGCGTGGCGAG. The $RipA_{TB}$ active domain contained amino acids 332-472, while $RipA_{Sm}$ active domain contained amino acids 357 to 494.

Tetracycline inducible strains were created by cloning RipA genes into the Tet On plasmid, pSE100. For time-lapse microscopy, green fluorescenct protein was cloned downstream $RipA_{Sm}$ C408A to create a transcriptional reporter. GFP was also cloned downstream in frame with $RipA_{Sm}$ to create a translational fusion. These inducible plasmids were then transformed into mycobacteria in which the plasmid pMC1s, which encodes the *tetR* gene, had already been integrated at the L5 site.

Protein Expression

Recombinant gene products were expressed using a published anhydrotetracycline inducible system [40]. Anhydrotetracycline induction was performed with 100 ng/mL of anhydrotetracycline unless otherwise indicated.

Meropenem Treatment and CFU Enumeration

M. smegmatis with chromosomal *ripA* under the control of a tetracycline inducible promoter was grown in 7H9 ADC in the presence of 100 ng/mL anhydrotetracycline (aTc) to an OD of 0.2. The culture was split, and the RipA sample was treated with 10 mg/mL of meropenem (Sigma) for 6 hours. For the RipA depleted cells, the culture was pelleted at 5000 rpm for 10 minutes and resuspended in 7H9 ADC without aTc. These cells were grown for 6 hours at 37 °C to deplete for RipA. Once depletion was confirmed by microscopic examination of the culture for chaining, 10 mg/mL meropenem was added and the culture was incubated at 37 °C for 6 hours. After 6 hours of meropenem treatment, both RipA replete and depleted cultures were serially diluted and plated onto LB supplemented with hygromycin, kanamycin and 100 ng/mL aTc. Plates were incubated for 3 days at 37 °C and colonies were counted. As a control, RipA replete and depleted cells were also treated with 0.08% SDS, 0.08 µg/mL streptomycin (Sigma) or 500 µg/mL carbenicillin (Sigma).

Protein Fractionation and Preparation

Cell free culture supernatants were precipitated with 10% TCA (tricholoroacetic acid) overnight at 4 °C. Precipitates were pelleted at 15,000xg for 15 minutes at 4 °C and washed once with ice cold acetone. The acetone wash was decanted, and the pellet was air dried at room temperature. Precipitated protein was resuspended in reducing SDS loading buffer at 65 °C, for 10 minutes.

M. smegmatis was fractionated by French press three times. Unbroken cells and insoluble material were pelleted at 1000xg for 10 minutes. The supernatant was collected and insoluble cell wall material pelleted at 27,000xg at 4 °C for 40 minutes. The remaining supernatant was centrifuged at 100,000xg for 1 hour at 4 °C to isolate the membrane fraction. The supernatant contained the soluble cytosolic fraction.

Immunoblotting and Densitometry Analyses

Rabbit polyclonal antibody was made from and affinity purified using a peptide derived from the Msmeg RipA epitope: NAGRKIPSSQMRRG (Genscript, Piscataway, NJ). Anti-RipA antibody was diluted to 1mg/mL and used at a dilution of 1:1000. Anti-FLAG antibody (Sigma, St. Louis, MO) was used according to manufacturer's instructions. Protein samples were mixed with 4x Laemmli SDS PAGE buffer

(Boston BioProducts, Inc, Boston MA) and boiled for 5 minutes. *M. bovis* BCG and *M. tuberculosis* protein samples were boiled for 20 minutes. Proteins were separated on 12% Tris-glycine polyacrylamide gels, transferred to PVDF membrane (Pall Corp, Pensacola, FL), probed with anti-sera and developed with SuperSignal chemiluminescent reagent (Thermo, Pittsburg, PA). Densitometry on Western blot signal was performed using Multiguage software (Fujifilm).

Microscopy and Imaging

For TMA-DPH (Invitrogen, Carlsbad, CA) staining, bacteria were centrifuged and media removed. pPellets were resuspended in 50 mM TMA-DPH in PBS and incubated in the dark for 10 minutes. Cells were also stained in FM4-64Fx (Invitrogen) at a concentration of 5 mg/mL in PBS for 10 minutes, and then fixed and stored in 4% paraformaldehyde. Samples were imaged using a Nikon TE-200E microscope with a 100x (NA1.4) objective and captured with an Orca-II ER cooled CCD camera (Hamamatsu, Japan). Shutter and image acquisition were controlled using Metamorph Software (Molecular Devices). Final images were prepared using Adobe Photoshop 7.0.

Time Lapse Microscopy

Four Gene Frames (Fisher Scientific) were stacked onto a glass slide and filled with Middlebrook 7H9 in low melting point agar, supplemented with 50 mg/mL of hygromycin and 100 ng/mL aTc. A glass coverslip was flattened atop the agar to create a smooth surface and then removed after the agar set. The agar pad was sliced into eighths and seven of the pieces were removed to provide an air reservoir. Onto the remaining pad, exponential phase *M. smegmatis* was pipetted and allowed to adsorb until the surface of the pad appeared dry. Finally, a glass coverslip was applied and the slide was imaged on the microscope in an environmental chamber warmed to 37 °C (Applied Precision, Inc.).

Time-lapse images were acquired using a DeltaVision epifluorescence microscope with an automated stage enclosed with a 100x oil objective (Plan APO NA1.40). Cells were imaged every 10 minutes for up to 18 hours using brightfield and fluorescence illumination (461-489 nm; Applied Precision, Inc.) and images recorded with a CoolSnap HQ2 camera (Photometric). Focus was maintained using the software-

based autofocus (Applied Precision, Inc).

Real Time PCR

M. smegmatis samples were collected at the indicated growth phases (log, OD_{600}=0.5; early stationary, OD_{600}=2; Stationary, 24 hours of OD_{600} > 7) and stored in RNA Protect Bacteria Reagent (Qiagen, Valencia, CA) at -80 °C. The pellets were then mechanically disrupted by beadbeatting for three 1-minute cycles, and RNA isolated using the RNeasy Mini Kit (Qiagen), with one additional DNAse treatment (Qiagen) on the column before elution and a second DNAse digestion with Turbo DNase according to manufacturer's instructions (Ambion, Foster City, CA). Reverse transcription was carried out using the High Capacity cDNA Reverse Transcription kit (Applied Biosystem, Foster City, CA). Quantitative PCR reactions were set up in Power SyBr green PCR master mix (Applied Biosystems) and run and analyzed on a Step One Plus real time system (Applied Biosystems).

ripA expression was measured using the following primers: 5' CAGATCGGTGTGCCCTACTC; 5' GGCGAACATGTAGAGCATCAG; or against the 3' UTR region: 5' GCTCGAGGCCCCTTACAC; 5' GGAGCGCAAAGTAATCCCATCAG

ripA expression was normalized to *sigA* levels, which utilized the following primers: 5' AAGACACCGACCTGGAACTC; 5'AGCTTCTTCTTCCTCGTCCTC.

Acknowledgements

We would like to thank Kristi Guinn and Babak Javid for their review of the manuscript, as well as members of the Rubin and Fortune labs for their insights into the project. We are grateful to the Goldberg lab for the gift of ClpP antibody. We would also like to acknowledge funding support for this work from the Burroughs Wellcome Fund and NIH Grant U01-GM094568. Karen J. Kieser is supported by National Science Foundation Graduate Research Fellowship DGE-1144152.

Section 2.3 The role of RipA's N- and C-termini in modulating RipA activity

RipA's N-terminal domains of unknown function

The N-terminal region of RipA that is proteolyzed contains two domains of unknown function that exist mainly in mycobacteria [25]. The second of these two domains was found to block the active site of RipA [25]. We hypothesized that the N-terminus formed important protein-protein interactions (that may or may not impact RipA's rate of proteolysis). Overexpression of just the N-terminus could deplete RipA from its endogenous complexes critical for cell division. To test this hypothesis, I generated a construct to overexpress the N-terminal region of *M. smegmatis* RipA tagged to RFP and overexpressed this RipA truncation in *M. smegmatis* cells. Upon treatment with the small molecule inducer anhydrotetracycline, I found that cells were markedly inhibited for growth and exhibited polar bulges (Figure 2.9A,B). These data suggest that RipA's N-terminus did not form protein-protein interactions at the level sufficient to deplete RipA from its normal protein complexes, as the cells did not chain (the RipA depletion phenotype). While the precise role of RipA's N-terminal domains of unknown function remains obscure, overexpression of this region of the protein is highly toxic to cells.

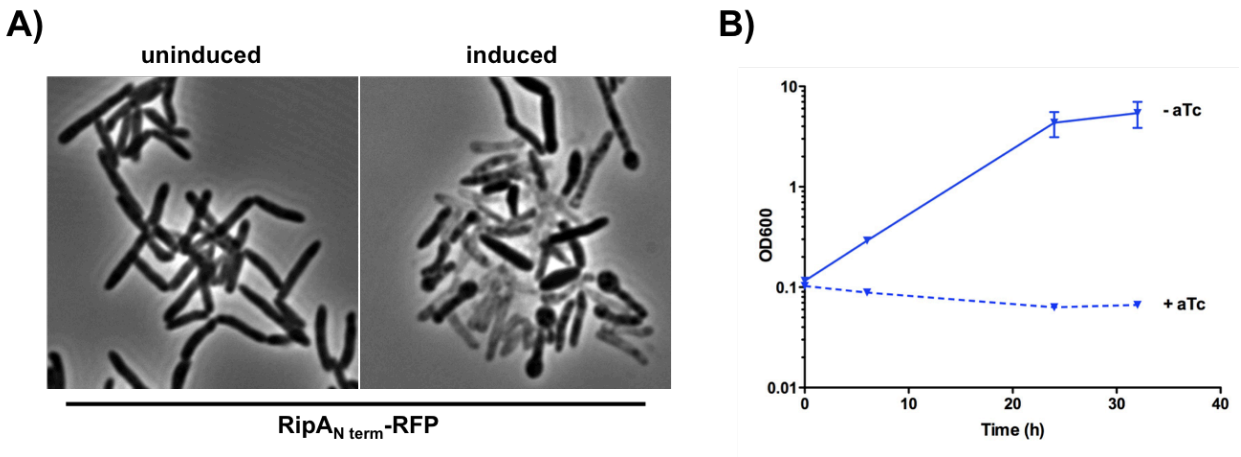

Figure 2.9 Overexpression of RipA's N-terminus induces cell death
(A) Overexpression of RipA's N-terminus tagged with RFP in *M. smegmatis* cells with the addition of the small molecule anhydrotetracycline (aTc). Cells were analyzed for cell shape changes with light microscopy. **(B)** Overexpression of the N-terminal region of RipA inhibits cell proliferation in *M. smegmatis*. Population doubling was measured by OD_{600} at the timepoints indicated.

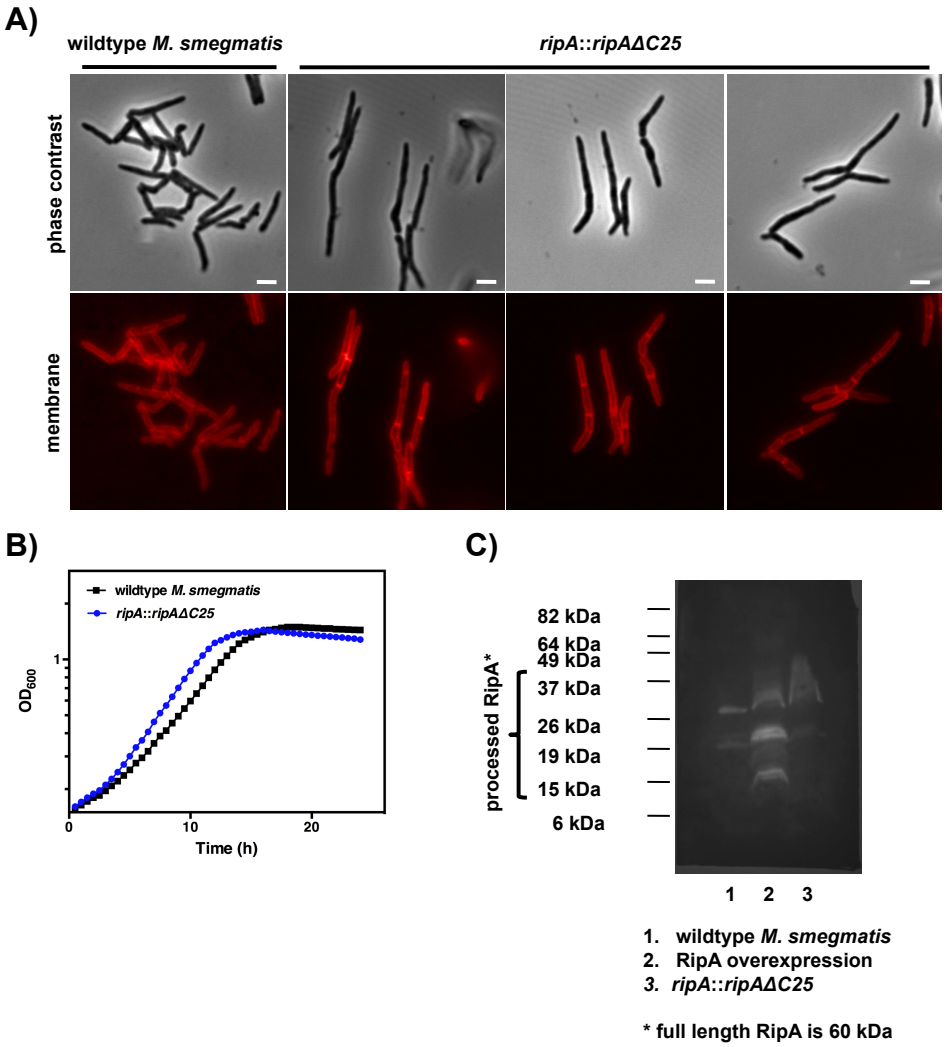

Figure 2.10 RipA's C-terminus is required for normal septal resolution
(A) Wildtype *M. smemgatis* cells and *M. smegmatis* cells that lack RipA's C-terminal 25 amino acids were imaged by light microscopy. Membranes were visualized with FM4-64. Scale bar represents 2μm. **(B)** Population doubling rates of the RipA truncation and wildtype *M. smegmatis* cells were measured by OD_{600} every 30 minutes. **(C)** Western blot analysis of RipA proteolysis of wildtype *M. smegmatis*, cells that overexpress RipA, and the truncation of RipA's last 25 amino acids. RipA bands were visualized with a RipA antibody.

The C-terminal interaction domain of RipA is required for normal activity

Previous studies from the lab demonstrated that the C-terminal 25 amino acids of RipA were critical for interacting with both RpfB as well as PonA1. These two RipA-interacting partners have opposing

enzymatic activity – RpfB is a PG hydrolase whereas PonA1 is a PG synthase. Furthermore, it was shown that PonA1 modulated the *in vitro* synergistic hydrolysis of PG carried out by RpfB and RipA. These findings produced an interesting model wherein PonA1 was critical for the survival of mycobacterial cells because it governed the lytic activity of RipA. This could be particularly important in *M. smegmatis*, where RipA proteolysis appears to occur at a different rate than in *M. tuberculosis*.

Furthermore, PonA1 is required for the viability of *M. smegmatis* in culture whereas it is predicted to be dispensable for growth of *M. tuberculosis* in culture. This differential essentiality could correlate with the differential rate of RipA activation in these species. To test these hypotheses, I attempted to generate a deletion of endogenous RipA's C-terminal 25 amino acids. I successfully isolated this RipA truncation, which demonstrated that the RipA-PonA1 interaction is not required for the survival of *M. smegmatis*. There must be additional reasons for the essentiality of *ponA1* in this species. Loss of the PonA1 and RpfB interaction surface did appear to alter RipA activity – the RipA truncation cells form short chains (Figure 2.10A), indicating that RipA is not fully capable of hydrolyzing the septal PG joining the daughter cells. However, these truncation cells appear to double at rates highly similar to wildtype *M. smegmatis* (Figure 2.10B), which may be due to the levels of RipA proteolysis that are near to wildtype levels (Figure 2.10C).

Section 2.4 References

1. WHO (2010) Global Tuberculosis Control 2010. Geneva: WHO Press.

2. Udwadia ZF, Amale RA, Ajbani KK, Rodrigues C (2012) Totally drug-resistant tuberculosis in India. Clin Infect Dis 54: 579-581.

3. Sauvage E, Kerff F, Terrak M, Ayala JA, Charlier P (2008) The penicillin-binding proteins: structure and role in peptidoglycan biosynthesis. FEMS Microbiol Rev 32: 234-258.

4. Vollmer W, Joris B, Charlier P, Foster S (2008) Bacterial peptidoglycan (murein) hydrolases. FEMS Microbiol Rev 32: 259-286.

5. Meisel U, Höltje J-V, Vollmer W (2003) Overproduction of Inactive Variants of the Murein Synthase PBP1B Causes Lysis in Escherichia coli. J Bacteriol 185: 5342-5348.

6. Legaree BA, Adams CB, Clarke AJ (2007) Overproduction of Penicillin-Binding Protein 2 and Its Inactive Variants Causes Morphological Changes and Lysis in Escherichia coli. J Bacteriol 189: 4975-4983.

7. Heidrich C, Ursinus A, Berger J, Schwarz H, Holtje J-V (2002) Effects of Multiple Deletions of Murein Hydrolases on Viability, Septum Cleavage, and Sensitivity to Large Toxic Molecules in Escherichia coli. J Bacteriol 184: 6093-6099.

8. den Blaauwen T, de Pedro MA, Nguyen-Distèche M, Ayala JA (2008) Morphogenesis of rod-shaped sacculi. FEMS Microbiol Rev 32: 321-344.

9. Uehara T, Parzych KR, Dinh T, Bernhardt TG (2010) Daughter cell separation is controlled by cytokinetic ring-activated cell wall hydrolysis. EMBO J 29: 1412-1422.

10. Paradis-Bleau C, Markovski M, Uehara T, Lupoli TJ, Walker S, et al. (2010) Lipoprotein cofactors located in the outer membrane activate bacterial cell wall polymerases. Cell 143: 1110-1120.

11. Vollmer W, von Rechenberg M, Höltje J-V (1999) Demonstration of Molecular Interactions between the Murein Polymerase PBP1B, the Lytic Transglycosylase MltA, and the Scaffolding Protein MipA of Escherichia coli. Journal of Biological Chemistry 274: 6726-6734.

12. Romeis T, Höltje JV (1994) Specific interaction of penicillin-binding proteins 3 and 7/8 with soluble lytic transglycosylase in Escherichia coli. J Biol Chem 269: 21603-21607.

13. Bertsche U, Kast T, Wolf B, Fraipont C, Aarsman ME, et al. (2006) Interaction between two murein (peptidoglycan) synthases, PBP3 and PBP1B, in Escherichia coli. Mol Microbiol 61: 675-690.

14. Böth D, Schneider G, Schnell R (2011) Peptidoglycan remodeling in Mycobacterium tuberculosis: comparison of structures and catalytic activities of RipA and RipB. J Mol Biol 413: 247-260.

15. Pilgrim S, Kolb-Maurer A, Gentschev I, Goebel W, Kuhn M (2003) Deletion of the Gene Encoding p60 in Listeria monocytogenes Leads to Abnormal Cell Division and Loss of Actin-Based Motility. Infect Immun 71: 3473-3484.

16. Gao L-Y, Pak M, Kish R, Kajihara K, Brown EJ (2006) A mycobacterial operon essential for virulence in vivo and invasion and intracellular persistence in macrophages. Infect Immun 74: 1757-1767.

17. Sassetti CM, Boyd DH, Rubin EJ (2003) Genes required for mycobacterial growth defined by high density mutagenesis. Molecular Microbiology 48: 77-84.

18. Hett EC, Chao MC, Deng LL, Rubin EJ (2008) A mycobacterial enzyme essential for cell division synergizes with resuscitation-promoting factor. PLoS Pathog 4: e1000001.

19. Heidrich C, Templin MF, Ursinus A, Merdanovic M, Berger J, et al. (2001) Involvement of N-acetylmuramyl-L-alanine amidases in cell separation and antibiotic-induced autolysis of Escherichia coli. Molecular Microbiology 41: 167-178.

20. Hugonnet J-E, Tremblay LW, Boshoff HI, Barry CE, Blanchard JS (2009) Meropenem-Clavulanate Is Effective Against Extensively Drug-Resistant Mycobacterium tuberculosis. Science 323: 1215-1218.

21. Gupta R, Lavollay M, Mainardi J-L, Arthur M, Bishai WR, et al. (2010) The Mycobacterium tuberculosis protein LdtMt2 is a nonclassical transpeptidase required for virulence and resistance to amoxicillin. Nat Med 16: 466-469.

22. Sumita Y, Fakasawa M (1995) Potent activity of meropenem against Escherichia coli arising from its simultaneous binding to penicillin-binding proteins 2 and 3. Journal of Antimicrobial Chemotherapy 36: 53-64.

23. Billman-Jacobe H, Haites RE, Coppel RL (1999) Characterization of a Mycobacterium smegmatis Mutant Lacking Penicillin Binding Protein 1. Antimicrob Agents Chemother 43: 3011-3013.

24. Hett EC, Chao MC, Rubin EJ (2010) Interaction and modulation of two antagonistic cell wall enzymes of mycobacteria. PLoS Pathog 6: e1001020.

25. Ruggiero A, Marasco D, Squeglia F, Soldini S, Pedone E, et al. (2010) Structure and Functional Regulation of RipA, a Mycobacterial Enzyme Essential for Daughter Cell Separation. Structure 18: 1184-1190.

26. Slayden RA, Belisle JT (2009) Morphological features and signature gene response elicited by inactivation of FtsI in Mycobacterium tuberculosis. Journal of Antimicrobial Chemotherapy 63: 451-457.

27. Hett EC, Chao MC, Steyn AJ, Fortune SM, Deng LL, et al. (2007) A partner for the resuscitation-promoting factors of Mycobacterium tuberculosis. Molecular Microbiology 66: 658-668.

28. Zhang YJ, Ioerger TR, Huttenhower C, Long JE, Sassetti CM, et al. (2012) Global assessment of genomic regions required for growth in Mycobacterium tuberculosis. PLoS Pathog 8: e1002946.

29. Breci LA, Tabb DL, Yates JR, 3rd, Wysocki VH (2003) Cleavage N-terminal to proline: analysis of a database of peptide tandem mass spectra. Anal Chem 75: 1963-1971.

30. Bublitz M, Polle L, Holland C, Heinz DW, Nimtz M, et al. (2009) Structural basis for autoinhibition and activation of Auto, a virulence-associated peptidoglycan hydrolase of Listeria monocytogenes. Molecular Microbiology 71: 1509-1522.

31. Reddy TB, Riley R, Wymore F, Montgomery P, DeCaprio D, et al. (2009) TB database: an integrated platform for tuberculosis research. Nucleic Acids Res 37: D499-508.

32. Plocinska R, Purushotham G, Sarva K, Vadrevu IS, Pandeeti EV, et al. (2012) Septal localization of the Mycobacterium tuberculosis MtrB sensor kinase promotes MtrA regulon expression. J Biol Chem 287: 23887-23899.

33. Segev E, Smith Y, Ben-Yehuda S (2012) RNA dynamics in aging bacterial spores. Cell 148: 139-149.

34. Voskuil MI, Visconti KC, Schoolnik GK (2004) Mycobacterium tuberculosis gene expression during adaptation to stationary phase and low-oxygen dormancy. Tuberculosis (Edinb) 84: 218-227.

35. Shah IM, Dworkin J (2010) Induction and regulation of a secreted peptidoglycan hydrolase by a membrane Ser/Thr kinase that detects muropeptides. Molecular Microbiology 75: 1232-1243.

36. Shah IM, Laaberki M-H, Popham DL, Dworkin J (2008) A Eukaryotic-like Ser/Thr Kinase Signals Bacteria to Exit Dormancy in Response to Peptidoglycan Fragments. Cell 135: 486-496.

37. Downing KJ, Mischenko VV, Shleeva MO, Young DI, Young M, et al. (2005) Mutants of Mycobacterium tuberculosis lacking three of the five rpf-like genes are defective for growth in vivo and for resuscitation in vitro. Infection and Immunity 73: 3038 - 3043.

38. Biketov S, Potapov V, Ganina E, Downing K, Kana B, et al. (2007) The role of resuscitation promoting factors in pathogenesis and reactivation of Mycobacterium tuberculosis during intra-peritoneal infection in mice. BMC Infectious Diseases 7: 146-153.

39. Mir M, Asong J, Li X, Cardot J, Boons GJ, et al. (2011) The extracytoplasmic domain of the Mycobacterium tuberculosis Ser/Thr kinase PknB binds specific muropeptides and is required for PknB localization. PLoS Pathog 7: e1002182.

40. Ehrt S, Guo XV, Hickey CM, Ryou M, Monteleone M, et al. (2005) Controlling gene expression in mycobacteria with anhydrotetracycline and Tet repressor. Nucleic Acids Res 33: e21.

Chapter 3

The peptidoglycan synthase PonA1 governs cell elongation in mycobacteria

Section 3.1 Overview and Attributions

Overview

This chapter is composed of a manuscript that I wrote and to which Eric and Cara Boutte contributed editorial input. Others provided feedback on the data and manuscript (see Acknowledgements). All supplementary data for the chapter are in Appendix 2. The manuscript is currently under review at PLoS Pathogens.

Attributions

I performed the experiments and analyzed the data in Figures 3.1; 3.2; 3.3; 3.4; 3.5B,C,D; and Table 3.1 (see Attributions in Appendix 2 for further information on the Supplementary Data for this chapter). I made all the strains for the experiments except for the *E. coli* overexpression vectors for wildtype and TG-PonA1, which were made by Michael Chao. Cara Boutte made the *E. coli* expression strains for the phospho-profiling experiments. Christina Baer and Cara Boutte purified the *Mtb* kinases for the phosphorylation experiments. Amy Barczak performed the lipidomic analysis and analyzed the data in Figure S3. Xavier Meniche performed the mass spec and analyzed the data in Figure S7D. Jemila Caplan Kester made the microfluidic devices I used for timelapse microscopy experiments shown in Figures 3.5 and S8. Hesper Rego helped set up the experiment in her CellASIC microfluidic device that is displayed in Figure S5. Noman Siddiqi and Shoko Wakabayashi performed the aerosol infection shown in Figure 3.1, and Shoko Wakabayashi helped with the mouse harvests for the same experiment.

Section 3.2 Phosphorylation of the peptidoglycan synthase PonA1 governs the rate of polar elongation in mycobacteria

Karen J. Kieser[1], Cara C. Boutte[1*], Jemila C. Kester[1*], Christina E. Baer[2], Amy K. Barczak[3], Xavier Meniche[2], Michael C. Chao[1], E. Hesper Rego[1], Christopher M. Sassetti[2], Sarah M. Fortune[1], Eric J. Rubin[1,4‡]

[1] Department of Immunology and Infectious Disease, Harvard T.H. Chan School of Public Health, Boston, MA USA 02115

[2] Department of Microbiology and Physiological Systems and Howard Hughes Medical Institute, University of Massachusetts Medical School, Worcester, MA 01605

[3] Division of Infectious Disease, Massachusetts General Hospital, Boston, MA 02114

[4] Department of Microbiology and Immunobiology, Harvard Medical School, Boston, MA USA 02115

* authors contributed equally

‡ Corresponding Author: erubin@hsph.harvard.edu

‡ Corresponding Author Present Address:

Harvard Institutes of Medicine, Room 1007A

4 Blackfan Circle

Boston, MA 02115

(617) 432-3337

Abstract

Cell growth and division are required for the progression of bacterial infections. Most rod-shaped bacteria grow by inserting new cell wall along their mid-section. However, mycobacteria, including the human pathogen *Mycobacterium tuberculosis*, produce new cell wall material at their poles. How mycobacteria

control this different mode of growth is incompletely understood. Here we find that PonA1, a penicillin binding protein (PBP) capable of transglycosylation and transpeptidation of cell wall peptidoglycan (PG), is a major governor of polar growth in mycobacteria. PonA1 is required for growth of *Mycobacterium smegmatis* and is critical for *M. tuberculosis* during infection. In both cases, PonA1's catalytic activities are both required for normal cell length, though loss of transglycosylase activity has a more pronounced effect than transpeptidation. Mutations that alter the amount or the activity of PonA1 result in abnormal formation of cell poles and changes in cell length. Moreover, altered PonA1 activity results in dramatic differences in antibiotic susceptibility, suggesting that a balance between the two enzymatic activities of PonA1 is critical for survival. We also find that phosphorylation of a cytoplasmic region of PonA1 is required for normal activity. Mutations in a critical phosphorylated residue affect transglycosylase activity and result in abnormal rates of cell elongation. Together, our data indicate that PonA1 is a central determinant of polar growth in mycobacteria, and its governance of cell elongation is required for robust cell fitness during both host-induced and antibiotic stress.

Introduction

Mycobacterium tuberculosis, the causative agent of tuberculosis (TB), remains a significant threat to human health. The World Health Organization estimates that 1.5 million individuals die of TB every year, and that roughly 2 billion people are latently infected with *M. tuberculosis* (*Mtb*) [1]. Despite the substantial global burden of TB, little is known about the bacterium's basic physiological pathways, including cell growth and division.

Two processes govern cell growth: elongation of the cell and then division of that cell into two daughter cells. Cell division involves the synthesis and then splitting of a peptidoglycan layer (a macromolecule composed of disaccharides crosslinked by short peptides), called the septum, which occurs roughly at mid-cell. Bacteria elongate by incorporating new cell wall material into their existing cell wall, which is often a layer or layers of complex saccharides that surrounds the cell's plasma membrane. Many rod-

shaped bacteria grow by elongating their mid-section; however, mycobacteria have a different body plan and elongate by incorporating new cell wall precursors at the cell poles [2,3].

Cell growth and division rely on the synthesis of new cell wall. The bacterial cell wall is required for cell survival and determines bacterial shape. Peptidoglycan (PG) is a major component of bacterial envelopes and is central to the integrity of the cell wall. PG is remodeled in response to stress and undergoes rounds of synthesis and hydrolysis every cell cycle to promote cell elongation and division [2,3]. Although coordination of PG synthesis has been extensively studied in other bacterial species, this process, particularly during elongation, remains relatively unexplored in mycobacteria.

One key enzyme that plays a central role in elongation and septation is PonA1, which localizes to the cell pole and septum, where it interacts with the essential PG hydrolase RipA [4,5]. Our previous work suggested that PonA1 was essential in *Mycobacterium smegmatis* (*Msm*) [4], indicating that we could use *Msm* as a convenient tool to define cellular activity specific to PonA1. Studying PonA1 enables us to determine how the cell governs one of the most critical steps in PG synthesis – elongation of the cell pole.

PonA1 is a penicillin binding protein (PBP), a member of a family of proteins that promotes cell growth and division through the synthesis of PG [2,3]. PonA1 has two catalytic domains that carry out the two extracellular necessary reactions for peptidoglycan synthesis: transglycosylation (TG) and transpeptidation (TP). TG reactions link the repeating disaccharide units that form the glycan backbone of peptidoglycan. Pentapeptide tails descend from the glycan chains and are crosslinked by TP reactions [2,3]. In addition to its two catalytic domains, PonA1 contains a long unconserved cytoplasmic tail. The cytoplasmic tail is phosphorylated [6], an unusual modification for PBPs that may play a role in PonA1's cellular function.

Here we provide evidence that PonA1 is required for cell proliferation in *Msm* and is necessary for normal survival of *Mtb* during infection. It plays multiple roles in determining cell length and defining new growth. PonA1 is an early polar localizing factor that can nucleate elongation complexes to construct new cell

poles, whose elongation rates are modulated by PonA1's phosphorylation. Changes in PonA1 activity impact cell shape and growth, likely through insults to the cell wall peptidoglycan, that ultimately results in reduced cell fitness during infection and stress. Collectively, our data suggest that cell elongation in mycobacteria requires PonA1, whose catalytic and regulatory activities modulate the function of cell growth complexes.

Results

Normal growth of *M. smegmatis* and *M. tuberculosis* requires PonA1

Transcriptional depletion of *ponA1* (MSMEG_6900, Entrez Gene ID 4536904) was previously shown to severely impact proliferation of *Msm* and induces the formation of lemon-shaped or ballooning cells, suggesting that PonA1 plays a critical role in cell growth in mycobacteria [4]. To determine whether PonA1 is essential for growth of *Msm*, we used an allelic replacement system [7] that allows exchange of PonA1 alleles on the bacterial chromosome (Figure 3.1A). We generated two exchange vectors, one encoding wildtype *ponA1* and a negative control vector lacking *ponA1*. Exchanging wildtype *ponA1* with a similar wildtype *ponA1* fully restored bacterial growth; however, exchange of *ponA1* with the negative control vector abolished bacterial growth (Figure 3.1A). The few remaining colonies on the negative control plate were confirmed *ponA1*$^{+}$ by PCR (seven colonies from approximately $4x10^{8}$ transformed cells). These data show that growth of *Msm* requires *ponA1*. However, transposon mutagenesis data from *M. tuberculosis* H37Rv (*Mtb*) suggested that *ponA1* (Rv0050, Entrez Gene ID 887065) could be disrupted without compromising proliferation of *Mtb* in culture [8], but that such a disruption would impact survival in a mouse model of TB [9]. We therefore tested whether *ponA1* could be deleted from the *Mtb* genome by recombineering (see Materials and Methods for details). We successfully isolated a *ΔponA1 Mtb* mutant and confirmed that *ΔponA1 Mtb* cells grew similarly to wildtype *Mtb* under standard laboratory culture conditions (S1A,B Figure in Appendix 2). However, *ΔponA1 Mtb* cells replicated less robustly than wildtype *Mtb* in the lungs of C57Bl6 mice at 15 and 42 days post infection (dpi) and were moderately impaired in dissemination to the spleen at 42 dpi (Figure 3.1B), indicating that loss of PonA1 impacted *Mtb* fitness during infection. Together, these data show that PonA1 is necessary for normal growth of *Msm* in culture and promotes normal fitness of *Mtb* during infection.

PonA1's synthesis of glycan chains is essential for *M. smegmatis* viability and for normal cell length of *M. tuberculosis*

PonA1's essentiality in *Msm* is unusual, since PBPs in many bacterial species, including *Escherichia coli* [10], *Bacillus subtilis* [11], *Vibrio cholerae* [12], and even the highly related, polar growing actinomycete *Corynebacterium glutamicum* [13] have largely redundant roles. The *Msm* genome encodes two other bifunctional PBPs, PonA2 and PonA3, with presumably similar catalytic activities [14], whereas *Mtb* encodes just PonA1 and PonA2 [15]. To identify which function of PonA1 was essential in *Msm*, we produced a panel of PonA1 mutants with varying catalytic functionality (S2A Figure) for use in the allelic exchange system shown in Figure 3.1A. Mutations in homologous active site residues eliminated catalytic activity in *in vitro* assays for *E. coli* PBP1a [16] and PBP1b [17]. In *E. coli*, genetic ablation of TP activity did not alter TG activity [16,17], whereas elimination of TG activity also abolished the enzyme's TP activity *in vitro*, presumably because the substrate for the TP reaction was not produced [16,17]. However, whether loss of TP activity also abolishes TG activity in the cell remains unclear.

To test whether TG, TP or both activities were required to sustain growth, we transformed *Msm* with the exchange vectors and tested for appropriate chromosomal integration by antibiotic selection (see Materials and Methods). We found that only a $PonA1_{TP-}$ allele (predicted to lack TP activity) was capable of rescuing bacterial growth while $PonA1_{TG-}$ and $PonA1_{TG-TP-}$ alleles (which lack either TG or both activities) failed to rescue bacterial survival (Figure 3.2A). These data suggest that PonA1's polymerization of glycan strands is required in *Msm*, but that its crosslinking of PG is dispensable. This is consistent with a previous report of an *Msm* mutant with a transposon insertion in *ponA1* that generates a truncated protein that includes the TG domain but lacks the TP domain [18]. This mutant is likely still capable of transglycosylation, as the TG domain still exists, but loss of penicillin binding confirmed that its transpeptidation functionality was ablated [18].

In *Mtb*, PonA1's synthesis of glycan chains is required for normal bacterial growth. *Mtb* cells that expressed a $PonA1_{TG-}$ allele exhibited moderately impaired viability and dissemination during infection,

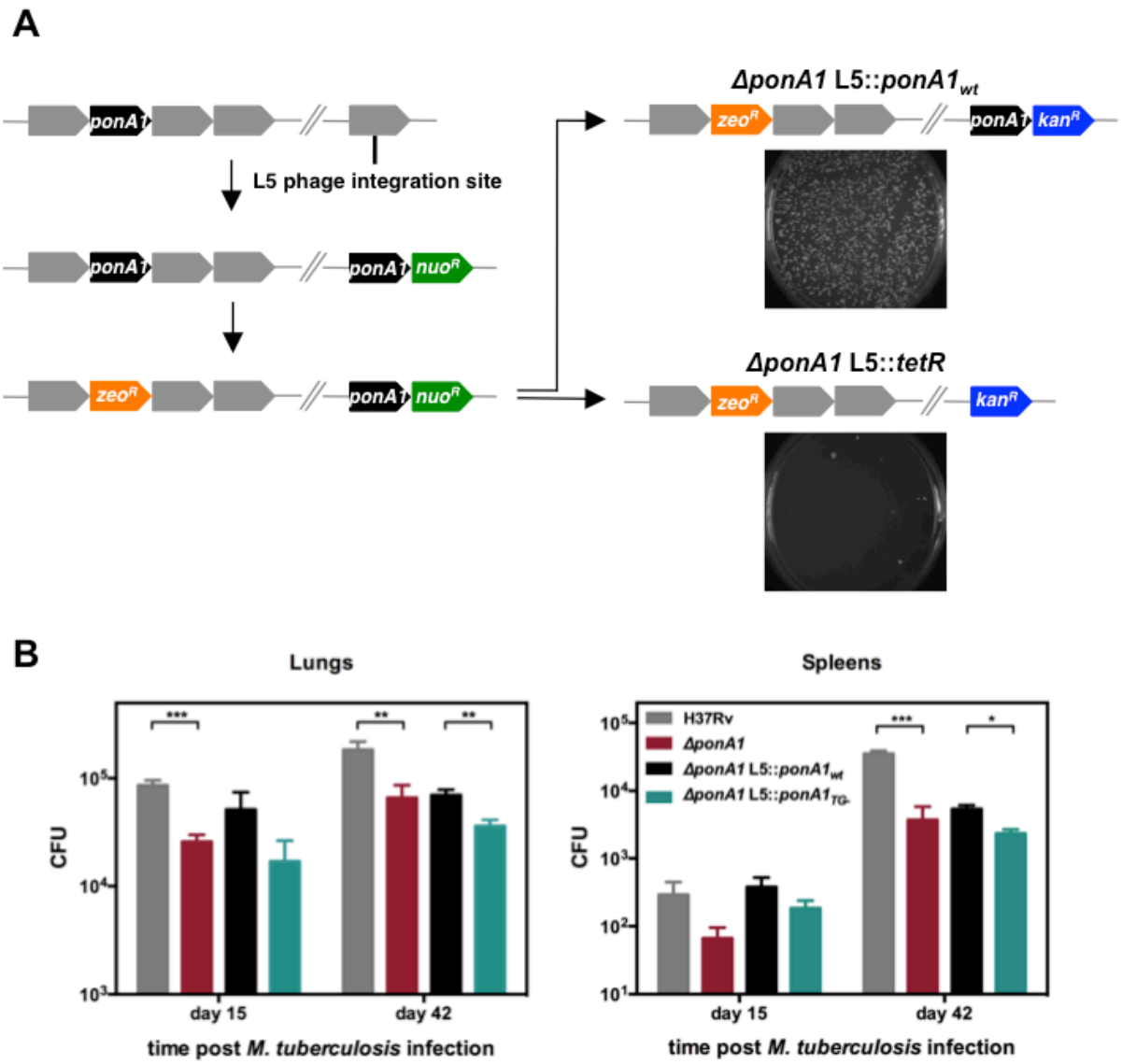

Figure 3.1. PonA1 is essential in *M. smegmatis* and required for normal growth of *M. tuberculosis*. **(A)** An allelic exchange system in *M. smegmatis* provides an efficient method to test the importance of PonA1 for bacterial survival. **(B)** C57Bl6 mice were aerosol infected with H37Rv wildtype, *ΔponA1*, *ΔponA1*::*ponA1*$_{wt}$, and *ΔponA1*::*ponA1*$_{TG-}$ (an allele of PonA1 with a catalytic active site mutation in the transglycosylase (TG) domain), and CFU were enumerated were from lung and spleen homogenates at 15 and 42 days post infection (dpi). Statistical significance was calculated by a one-tailed t-test (lungs at 15 dpi, H37Rv compared to *ΔponA1* *** indicates p-value = 0.0005; lungs 42 dpi, H37Rv compared to *ΔponA1* ** indicates p-value = 0.0089, and *ΔponA1*::*ponA1*$_{wt}$ compared to *ΔponA1*::*ponA1*$_{TG-}$ ** indicates p-value = 0.0042. Spleens at 42 dpi, H37Rv compared to *ΔponA1* *** indicates p-value = 0.0001, and *ΔponA1*::*ponA1*$_{wt}$ compared to *ΔponA1*::*ponA1*$_{TG-}$ * indicates p-value = 0.0122).

similar to *ΔponA1* cells, when compared to isogenic wildtype (Figure 3.1B). This fitness defect could be associated with abnormal cell length, as *ΔponA1* and *ΔponA1* L5::*ponA1*$_{TG-}$ cells are shorter than their isogenic wildtypes by 14% and 21%, respectively (Figure 3.2B) but showed no gross cell shape changes or substantial population doubling defects (S1A,B,C Figure). The *ΔponA1* L5::*ponA1*$_{TG-}$ cells also produced somewhat less phthiocerol dimycocerosate (PDIM) (S3 Figure), a cell wall lipid that is important for robust growth during infection. Lower PDIM production by this strain may contribute to the decreased fitness of these cells in the host, although we do not suspect that low PDIM is related to TG- PonA1 as low PDIM production has been described in unrelated genetic mutants [19]. Furthermore, *ΔponA1 Mtb* cells exhibit a cell length defect but produce PDIM at levels similar to or slightly above wildtype H37Rv, suggesting that PDIM loss is not necessarily correlated with decreased cell length. The change in cell length observed with *ΔponA1* and *ΔponA1* L5::*ponA1*$_{TG-}$ cells suggests that PonA1's polymerization of glycan chains is required for normal cell length in *Mtb*. Altered peptidoglycan structure in these shorter cells likely underlies their decreased ability to resist host-induced stresses.

Correct cell length depends on PonA1's crosslinking of peptidoglycan

The differential essentiality of PonA1's TG and TP activities in the cell suggested that they could be uncoupled. Uncoupling of the TG and TP activities for PonA1 may be unusual. *in vitro* studies have shown that in other bifunctional PBPs, the TP domain crosslinks the nascent glycan strands produced by the *cis*-TG domain, and it cannot function in the absence of TG activity [16,17,20]. Accordingly, we hypothesized that uncoupling of PonA1's catalytic activities could impact cell elongation and/or division, resulting in altered cell morphology. We imaged *Msm* cells that expressed PonA1$_{wt}$ or PonA1$_{TP-}$ and quantified cell length. We found that PonA1$_{TP-}$ *Msm* were 24% shorter on average than isogenic wildtype (Figure 3.2C,D) and had impaired population doubling (S2B,C Figure) although similar levels of protein were expressed (S2D Figure). These data suggest that PonA1's crosslinking of PG is required for normal cell length, and that the balance of PonA1 catalytic activities could have a role in controlling cell length and withstanding stress. Impaired PonA1 crosslinking in *Mtb* decreased cell length as well. Cells that expressed a PonA1$_{TP-}$ or PonA1$_{TG-TP-}$ allele were 11% or 6% shorter on average, respectively, than isogenic wildtype (Figure 3.2B). These data indicate that while PonA1's TG activity is critical for cell

Figure 3.2. PonA1's glycan synthesis is required in *M. smegmatis* and catalytic activity promotes normal cell elongation. (A) Allelic exchange (see Figure 3.1A) with vectors encoding alleles of PonA1 with varying catalytic activities (TG-, transglycosylase mutant; TP-, transpeptidase mutant; TG-TP-, transglycosylase and transpeptidase double mutant) in *M. smegmatis*. **(B)** *M. tuberculosis* strains were grown in culture and total cell length was measured: H37Rv wildtype (234 cells), *ΔponA1* (241 cells; approximate p-value < 0.0001 by the Kolmogorov-Smirnov test), *ΔponA1 L5*::$ponA1_{wt}$ (212 cells), *ΔponA1 L5*::$ponA1_{TG-}$ (220 cells; approximate p-value < 0.0001 by the Kolmogorov-Smirnov test), *ΔponA1 L5*::$ponA1_{TP-}$ (227 cells; approximate p-value < 0.0001 by the Kolmogorov-Smirnov test), and *ΔponA1 L5*::$ponA1_{TG-TP-}$ (209 cells; approximate p-value < 0.0001 by the Kolmogorov-Smirnov test). **(C)** *Msm* cells that express $PonA1_{TP-}$ were assessed for morphological changes via light microscopy. Scale bar, 2 μm. **(D)** Cell length was measured for *ΔponA1 L5*::$ponA1_{TP-}$ cells (229 cells) and compared to wildtype *M. smegmatis* cell length (wt Msm, 251 cells; approximate p-value < 0.0001 by the Kolmogorov-Smirnov test) or isogenic wildtype cell length (*ΔponA1 L5*::$ponA1_{wt}$, 247 cells; approximate p-value < 0.0001 by the Kolmogorov-Smirnov test).

Figure 3.2 (Continued)

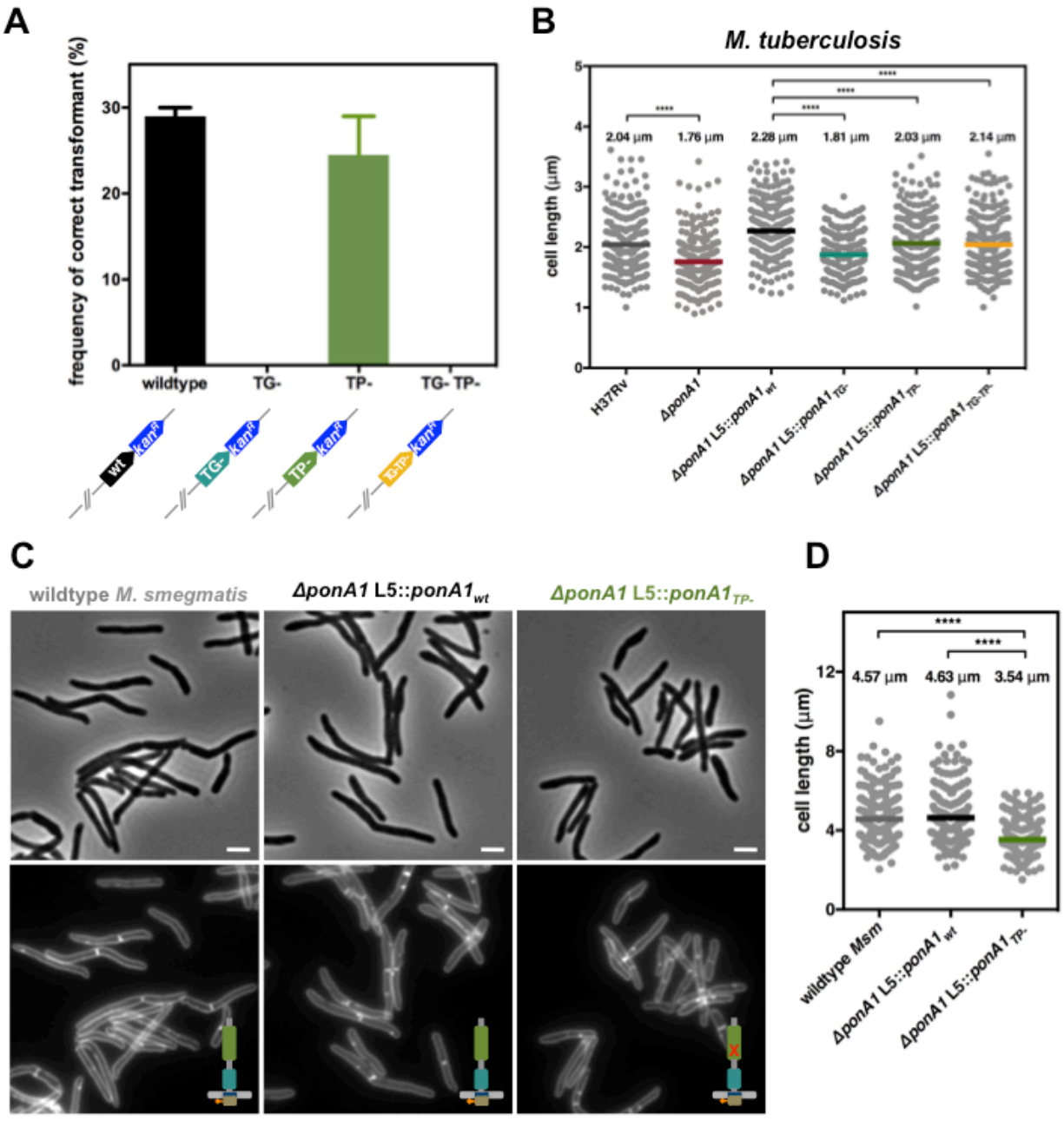

viability and normal cell length (Figure 3.1B and Figure 3.2), its TP activity also has a role in maintaining correct cell length in *Mtb*, although these mutations do not significantly alter population doubling rates (S1B,C,D Figure).

PonA1's transpeptidase domain is dispensable for cell survival

As PonA1's TG activity was necessary for the viability of *Msm*, we hypothesized that the TG domain as the sole periplasmic domain would be sufficient to rescue bacterial growth. Furthermore, our previous work indicated that PonA1 dampened the hydrolytic activity of the RipA-RpfB complex *in vitro* [4], suggesting that PonA1's modulation of RipA's lytic activity could also contribute to the requirement of PonA1 in *Msm*. PonA1's TP domain mediates the interaction with RipA [4]. To test whether *Msm* could survive with only PonA1's TG domain in the periplasm, we generated a truncation mutant of PonA1 that eliminated the TP domain ($PonA1_{1\text{-}360}$) (S2A Figure). We tested whether this truncation could complement loss of PonA1 via allelic exchange (Figure 3.1A). We found that $PonA1_{1\text{-}360}$ could support bacterial survival and growth. However, cells that expressed $PonA1_{1\text{-}360}$ exhibited cell shape defects (Figure 3.3A) and were 38% shorter than isogenic wildtype cells (Figure 3.3B). These morphological changes translated to diminished population growth rates (S2E,F Figure); however, these phenotypic differences were not due to difference in protein expression of the truncated PonA1 allele (S2G Figure). In sum, these data suggest that PonA1's TG activity is necessary and that the TG domain is the critical periplasmic domain required for the survival of *Msm*. PonA1 modulation of RipA activity may be an important cellular role for PonA1, but it is not absolutely required for viability of *Msm*, which has other means of controlling RipA lytic activity [5].

Linear polar elongation requires balanced PonA1 activity

Our data together suggest that PonA1 is critical for robust growth and that its catalytic activity is required for normal cell length. Do these critical catalytic activities lead to a dominant negative phenotype such that replacing wildtype PonA1 in cell growth complexes induces cellular toxicity? We tested this hypothesis by overproducing PonA1 in *Msm*. The overproduction of the $PonA1_{TG\text{-}TP\text{-}}$ double mutant induced the formation of ectopic cell poles (Figure 3.4A) and severely inhibited population growth rates

(Figure 3.4B), as did the single catalytic mutants. However, we observed the same phenotypes with overproduction of wildtype PonA1 (Figure 3.4A,B). This is in contrast to overproduction of the PonA1 homologue PBP1b in *E. coli*, which exhibits a dominant negative phenotype when overexpressed; namely, catalytically inactive PBP1b, but not wildtype PBP1b, inhibited growth and induced cell lysis [21]. These data suggest the cellular activity of PonA1 is different than its PBP1b homologue in *E. coli*. The growth inhibition with PonA1 overproduction in *Msm* correlated with the observation that the wildtype *ponA1* complement in *Mtb* (*ΔponA1* L5::$PonA1_{wt}$), which is driven by a strong promoter, did not fully complement wildtype growth at later time points in both lungs and spleens (Figure 3.1B). These data suggest that overproduction of PonA1 in *Mtb* also impacted cell fitness. Collectively, these results indicate that the cell must tightly regulate PonA1 levels and activity to maintain robust cell growth.

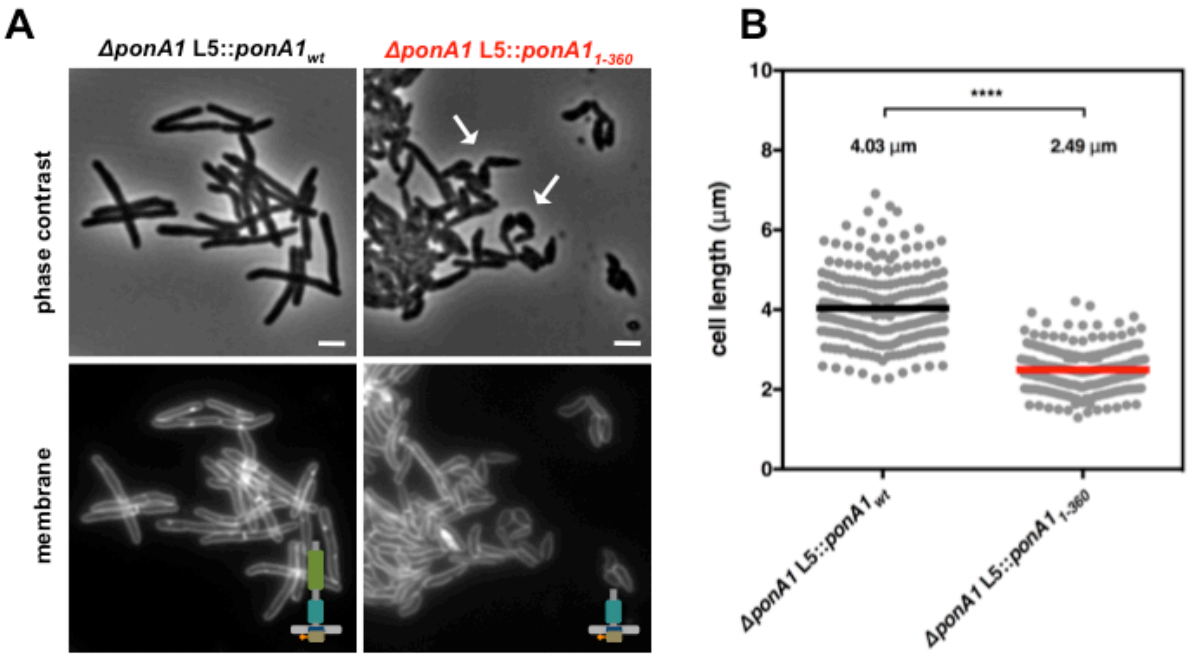

Figure 3.3. PonA1's periplasmic domains modulate cell shape in mycobacteria. (A) Wildtype PonA1 was replaced with a PonA1 truncation containing the cytoplasmic tail and TG domain ($PonA1_{1-360}$) via allelic exchange. Cells were analyzed via light microscopy. Scale bar, 2 μm. **(B)** Cell length of $PonA1_{1-360}$ cells (266 cells) was quantitated and compared to cell length of isogenic wildtype (251 cells; approximate p-value < 0.0001 by the Kolmogorov-Smirnov test). These measurements were taken on a different day than Figure 3.2C,D, hence the slight difference in isogenic wildtype cell length.

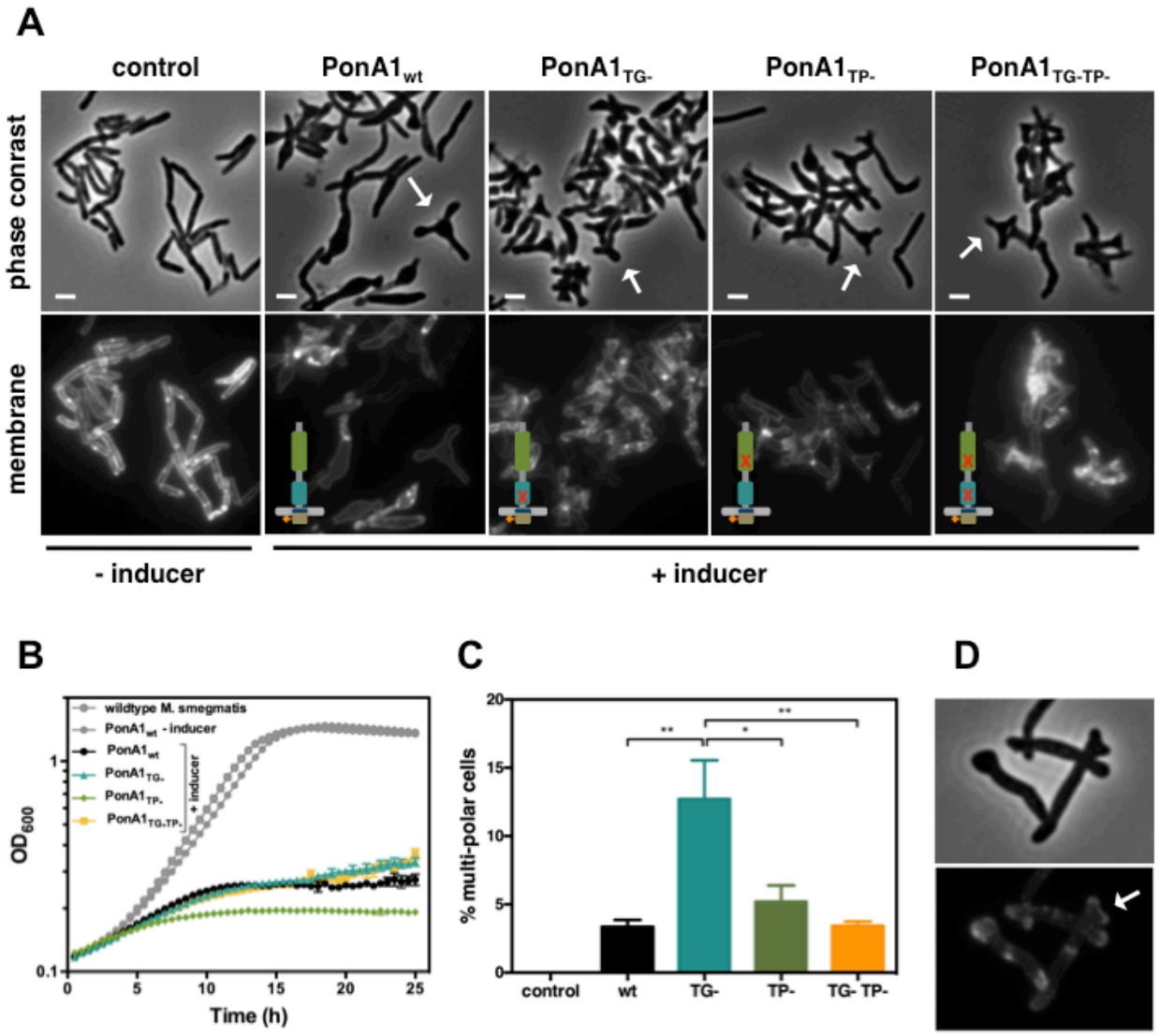

Figure 3.4. Excess PonA1 induces ectopic polar growth in *M. smegmatis*.
(A) PonA1 was overexpressed in *Msm* cells, and cells were visualized with light microscopy. Scale bar, 2 μm. **(B)** Population growth was determined for the overexpression strains (black, teal, green, and gold lines), uninduced wildtype overexpression strain (gray unfilled circle), and widltype *M. smegmatis* (gray filled circle) by taking OD_{600} measurements every 30 minutes. **(C)** The frequency of multi-poled cells was quantitated by counting appropriately misshapen cells in light microscopy images (statistical significance was assessed by one-way analysis of variance with Bonferroni's multiple comparison test, and multiplicity adjusted p-values are reported. $PonA1_{wt}$ compared to $PonA1_{TG-}$, p-value = 0.0039; $PonA1_{TG-}$ compared to $PonA1_{TP-}$, p-value = 0.0225; $PonA1_{TG-}$ compared to $PonA1_{TG-TP-}$, p-value = 0.0042). **(D)** The localization pattern of PonA1-RFP was assessed by fluorescence microscopy.

Although PonA1's enzymatic activity is not required for ectopic pole formation in *Msm*, it influenced the frequency of ectopic poles. Cells that overproduced $PonA1_{TG-}$ induced the formation of multi-poled cells at a higher frequency than other alleles of PonA1 (Figure 3.4C). Taken together, these results suggest that some balance between TG and TP activities is required to induce pole formation. However, no enzymatic activity is required for this phenomenon, suggesting another role for PonA1, perhaps as a scaffold or recruitment factor within protein complexes that promote cell pole growth.

Previous work showed that ectopically-produced PonA1-RFP localized to the pole and septum [4]. A chromosomally RFP-tagged *ponA1* also exhibits polar and mid-cell localization (S3D Figure). To determine whether PonA1 localized at the ectopic growth pole, we imaged *Msm* cells that overproduced PonA1-RFP. We observed that PonA1-RFP localized to each ectopic tip of the growing pole (Figure 3.4D). Furthermore, PonA1 localized to the pole prior to its degeneration into ectopic poles (S5A Figure, follow pole with white arrow), suggesting that PonA1 is an early localizing factor that promotes elongation of the cell pole. Ectopic polar growth occurred predominantly from one pole and not both poles (Figure 3.4A, S4 and S5 Figures), which correlated with the expected pattern of asymmetric polar elongation [22,23], and cells that did not overexpress PonA1 did not exhibit ectopic polar growth (Figure 3.4A, S5B Figure). Occasional cells with bulges or ectopic poles exhibited no RFP signal at those foci. PonA1's localization to the pole prior to the generation of ectopic poles indicates that PonA1 is intimately involved in not just elongating the pole, but in formation of the cell pole itself, potentially through interaction with DivIVA, which is required for pole formation in mycobacteria [23]. Furthermore, overexpression of PonA1 did not induce misplaced septa, suggesting that the majority of PonA1 is targeted to the cell pole during normal growth.

Ectopic polar growth upon overproduction of PonA1 in *Msm* is distinct from that observed in *E. coli*, where ectopic branches appeared when combinations of PBP1a and several low molecular weight PBPs were jointly deleted [24,25]. These data suggest that PonA1's role in mycobacterial growth is distinct from the homologous bifunctional PBPs in *E. coli*. This phenotype may be due to the fundamentally different way that mycobacteria elongate – from the cell pole and not along the lateral body as in *E. coli*.

Mycobacteria control cell elongation through post-translational modification of PonA1

One method the cell may use to regulate PonA1 activity is through post-translational modification. *Mtb* PonA1's cytoplasmic tail was recently identified as a substrate for the serine-threonine protein kinase PknB [6]. Prisic *et al* suggested the H37Rv genome had a misannotated start site for *rv0050*, which was corroborated by another report that identified an alternative protein translation start site in the 5' UTR of *ponA1* [26]. We have used a construct beginning 426 nucleotides upstream of the annotated start site, which captures the phosphorylation site, reported translational start site, and yields a predicted transmembrane domain [27] (S6A Figure), a necessary feature of all PBPs [28]. We accordingly aligned the mc^2155 genome for *Msm* PonA1; the start site was shifted 126 nucleotides upstream, which aligned well with -426 *Mtb* PonA1 (S6A,B Figure). Furthermore, the -426 *Mtb* PonA1 complemented growth of *Msm* lacking endogenous PonA1, which demonstrated that the -426 *Mtb* PonA1 allele was functional (S6A,B Figure). The -426 *Mtb* PonA1 protein was also produced at equivalent levels to *Msm* PonA1 (S6C Figure). To test whether -426 *Mtb* PonA1 was phosphorylated, we purified from *E. coli* the cytoplasmic domain tagged to MBP along with his-MBP-tagged kinase domains of all the functional serine-threonine kinases of *Mtb*. Phospho-transfer profiling of MBP-*Mtb* $PonA1_{cyto}$ with the kinases revealed that PknB efficiently phosphorylated -426 *Mtb* PonA1 *in vitro* (Figure 3.5A). The specificity of the phosphorylation on MBP-*Mtb* $PonA1_{cyto}$'s T34 residue (S6B Figure) was verified by mass spectrometric analysis (S7D Figure).

Because PknB's phosphorylation of other targets modulates key steps in cell growth and division [2], we hypothesized that PonA1's phosphorylation might play a role in regulating cell elongation or division. We tested this hypothesis by constructing two different alleles of *Msm* PonA1, one in which phosphorylation is blocked by substitution of an alanine residue for the targeted threonine (T50A) and another where an aspartate substitution might mimic the effects of phosphorylation (T50D) and confirmed these isoforms were stable (S6C Figure). We swapped these for the native allele and measured *Msm* cell length. Cells that expressed the T50A allele were longer than isogenic wildtype, whereas cells that expressed the T50D allele were shorter than isogenic wildtype (Figure 3.5B). Because the observed changes in cell length did not alter gross optical density measurements of these cell populations (S8A Figure), we used

Figure 3.5. Phosphorylation regulates the rate of cell elongation. (A) Phospho-transfer profiling assays were performed with the kinase domains of the major serine-threonine protein kinases of *M. tuberculosis* (*Mtb* Pkn) to assess phosphorylation of *Mtb* MBP-PonA1$_{cyto}$. **(B)** Cell length of *M. smegmatis* cells that express a T50A allele of *ponA1* (134 cells; approximate p-value = 0.0145 by the Kolmogorov-Smirnov test) was compared to isogenic wildtype cells (219 cells). Length of cells that express a T50D allele (139 cells) was compared to isogenic wildtype (approximate p-value = 0.0082 by the Kolmogorov-Smirnov test). **(C)** Cells that expressed a T50A (127 cells) or *Δ*cyto allele (202 cells) in addition to isogenic wildtype cells (174 cells) were stained with a cell surface dye and visualized by timelapse microscopy. Elongation rate was quantitated and compared to isogenic wildtype (T50A cells, approximate p-value = 0.0002 by the Kolmogorov-Smirnov test; *Δ*cyto, approximate p-value < 0.0001 by the Kolmogorov-Smirnov test). **(D)** Total cell length was measured of *M. tuberculosis* cells that expressed a T34A allele (211 cells; approximate p-value = 0.0066 by the Kolmogorov-Smirnov test) or a T34D allele (207 cells; approximate p-value < 0.0001 by the Kolmogorov-Smirnov test) and compared to isogenic wildtype (202 cells). **(E)** *Msm* cells that encode a T50A,TP- allele were visualized by light microscopy. Multiple septa are highlighted with white arrows.

Figure 3.5 (Continued)

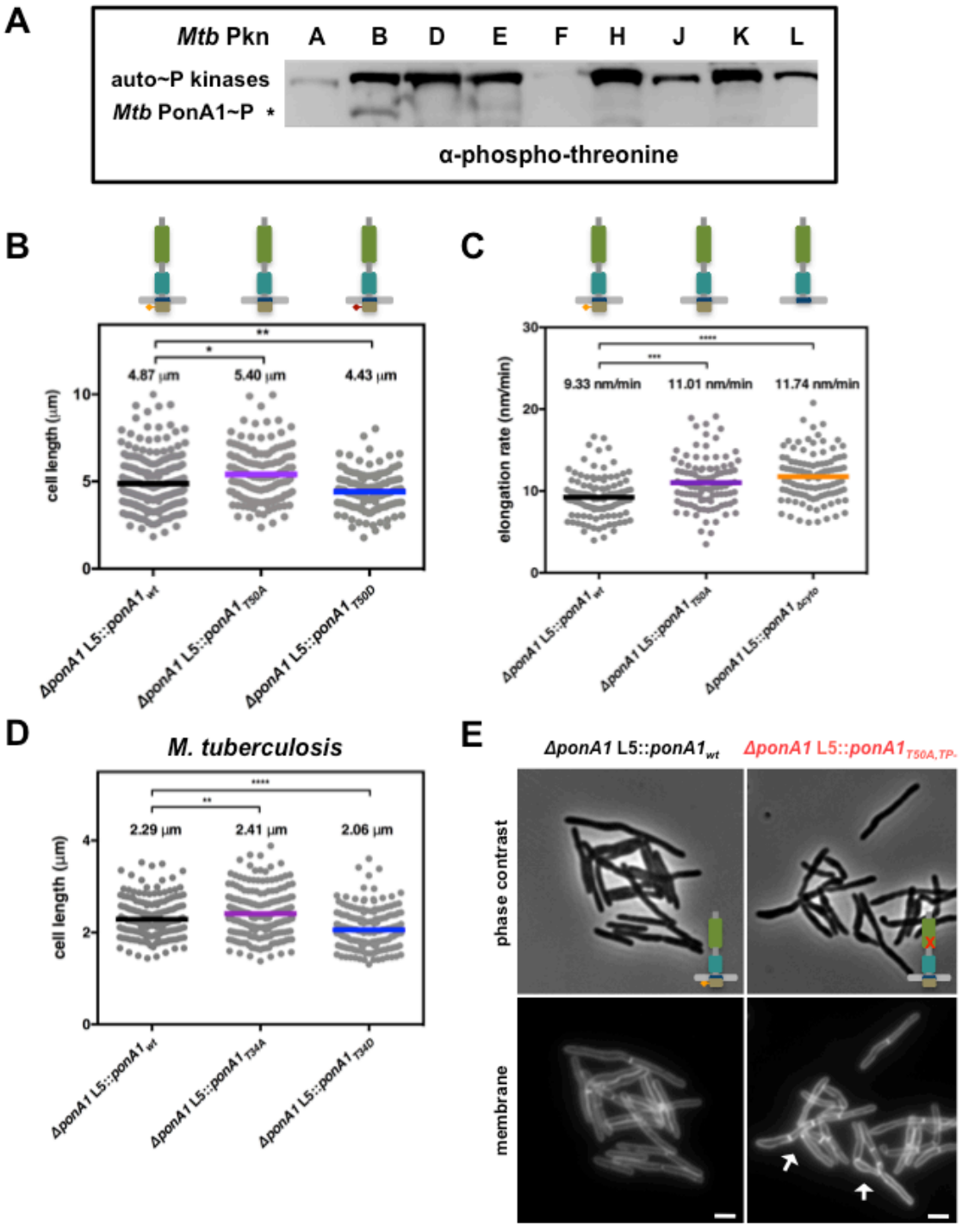

timelapse microscopy to measure single cell elongation and division events. Cells were labeled with a green fluorescent amine-reactive dye that stains the cell surface and does not diffuse over time. This allows the visualization of new cell growth (S8B Figure) [22,29]. After labeling, cells were imaged in custom microfluidic devices, and cell elongation and cell division events were quantified over time (S8B Figure; see Materials and Methods for details). *Msm* cells that expressed PonA1$_{T50A}$ allele elongated 15% faster than isogenic wildtype (Figure 3.5C). This faster elongation rate correlated with increased cell length at division (S8C Figure), and did not alter generation time at the single cell level (S8D Figure). Timelapse microscopy analysis did not show substantial growth differences between the PonA1$_{T50D}$ mutant and isogenic wildtype cells.Truncation of the cytoplasmic tail of PonA1 (PonA1$_{\Delta cyto}$), which generated a stable protein (S6C Figure), phenocopied the increased elongation rate (Figure 3.5C), supporting the role of PonA1's cytoplasmic domain, and likely its phosphorylation, in downregulating cell elongation. Cells that expressed PonA1$_{T50A}$ or PonA1$_{\Delta cyto}$ elongated predominantly from the old pole (S8E Figure) instead of the new pole (S8F Figure), in agreement with the expected growth pattern for mycobacteria [22,23]. These data indicate that loss of PonA1's phosphorylation does not alter the subcellular localization of elongation complexes or PonA1's localization in the elongation complex itself. Thus, it appears that PonA1's cytoplasmic domain is not critical for localizing PonA1 in the elongation complex or for interactions with other factors in that complex, but instead likely interacts with cytoplasmic factors that are involved in modulating the activity of the elongation complex. For example, it could mediate interaction with DivIVA, a key determinant of polar growth in mycobacteria [23].

PonA1's phosphorylation plays a similar role in *Mtb*. We measured the length of cells that expressed a T34A allele or a T34D allele. We found that the T34A mutant increased cell length by 5% compared to isogenic wildtype, while *Mtb* that encoded the T34D allele were 11% shorter than isogenic wildtype (Figure 3.5D). These data correlate with the observation in *Msm*. Furthermore, expression of T34A *Mtb* PonA1 in *Msm* increased cell length of *Msm* while expression of T34D *Mtb* PonA1 decreased *Msm* cell length. Collectively, these data suggest that PonA1's phosphorylation reduces elongation in both *Mtb* and *Msm* and provides the cell with a facile method to modulate cell length, an important response to certain stress conditions, including in-host survival [30].

Because PonA1's phosphorylation was not essential for protein function, but did modulate cell elongation rate, we hypothesized that PonA1's phosphorylation regulated its enzymatic activity. To test this, we generated a double mutant in which the phosphorylation and transpeptidase active sites were ablated. *Msm* cells that expressed this double PonA1 mutant ($PonA1_{T50A,TP-}$) were defective for normal cell separation. Cells formed short chains with cells of mixed length containing several septa (Figure 3.5E). This is distinct from the short cell phenotype of TP- cells (Figure 3.2C,D) and the elongated cell phenotype of T50A cells (Figure 3.5B), neither of which form short chains. Additionally, the *Msm* $PonA1_{T50A,TP-}$ cells had diminished growth rates compared to either of the single mutants or isogenic wildtype (S9A,B Figure), although similar protein levels were produced (S9C Figure). These data suggest that the peptidoglycan synthesized by this PonA1 mutant diminishes efficient cleavage. This could indicate that PonA1's phosphorylation regulates its TG activity – the remaining enzymatic activity in this mutant – and that the observed division defects result from imbalanced synthesis of peptidoglycan.

Altering PonA1 activity changes antibiotic susceptibility

Because changes to PonA1's phosphorylation status or synthetic ability altered cell shape and viability, we investigated whether these mutations would impact cell physiology under stress conditions, particularly antibiotic treatment. We previously demonstrated that single nucleotide polymorphisms in *ponA1* identified in clinical isolates alter *Mtb*'s fitness during rifampicin treatment [31]. We tested if altered *Mtb* PonA1 enzymatic or regulatory activity would also impact cell fitness in the presence of rifampicin. Indeed, *Mtb* cells that expressed $PonA1_{TG-}$ or $PonA1_{T34D}$ were 5 and 4 fold more tolerant to rifampicin treatment than isogenic wildtype, respectively (S10A Figure). In contrast, the inactivation of PonA1's TP activity or blockade of phosphorylation did not alter cell survival in the presence of rifampicin (S10A Figure). In sum, these data suggest that altering PonA1 catalytic and regulatory activity changes cell fitness when exposed to the clinically relevant antibiotic rifampicin, although the mechanism remains unclear.

We also hypothesized that changes in PonA1 activity would alter susceptibility to cell wall stress, including antibiotics that target PG synthesis. Genetically ablating *Mtb* PonA1's TP activity or its

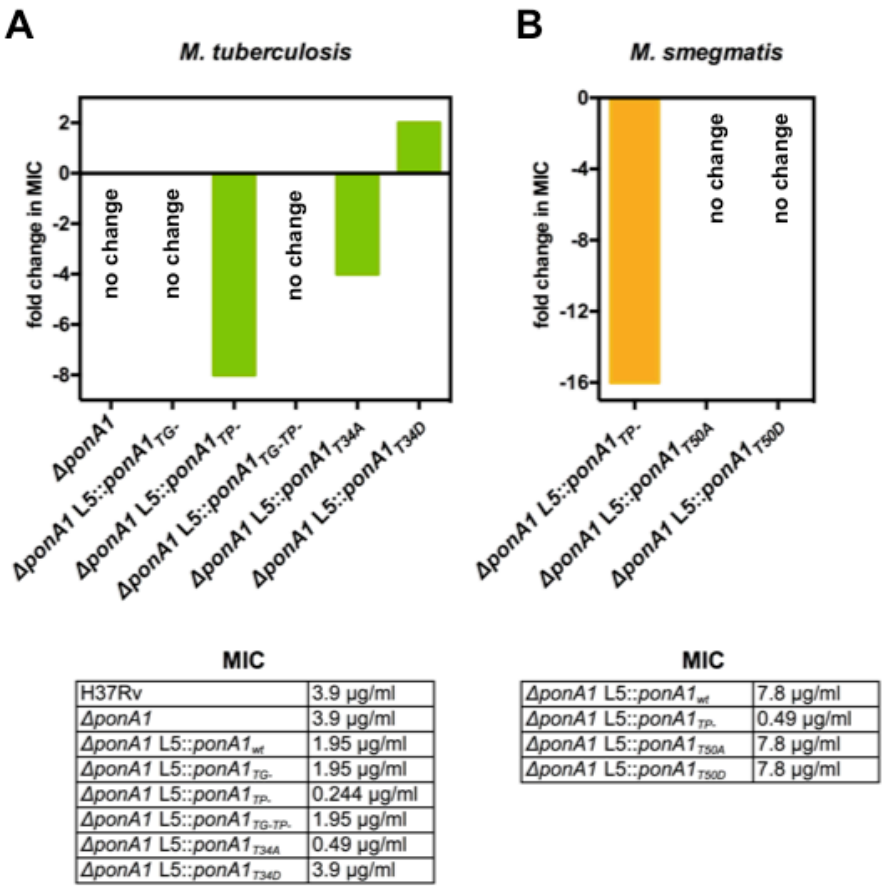

MIC	
H37Rv	3.9 µg/ml
ΔponA1	3.9 µg/ml
ΔponA1 L5::*ponA1*$_{wt}$	1.95 µg/ml
ΔponA1 L5::*ponA1*$_{TG-}$	1.95 µg/ml
ΔponA1 L5::*ponA1*$_{TP-}$	0.244 µg/ml
ΔponA1 L5::*ponA1*$_{TG-TP-}$	1.95 µg/ml
ΔponA1 L5::*ponA1*$_{T34A}$	0.49 µg/ml
ΔponA1 L5::*ponA1*$_{T34D}$	3.9 µg/ml

MIC	
ΔponA1 L5::*ponA1*$_{wt}$	7.8 µg/ml
ΔponA1 L5::*ponA1*$_{TP-}$	0.49 µg/ml
ΔponA1 L5::*ponA1*$_{T50A}$	7.8 µg/ml
ΔponA1 L5::*ponA1*$_{T50D}$	7.8 µg/ml

Figure 3.6 PonA1's TP activity is required for normal teicoplanin tolerance. (A) The minimum inhibitory concentration of teicoplanin for *Mtb* wildtype or *ponA1* mutant strains. The fold change in MIC for *Mtb ΔponA1* was calculated by comparison with H37Rv. The fold change in MIC for all other *Mtb* strains was calculated by comparison with isogenic wildtype (*Mtb ΔponA1* L5::*ponA1*$_{wt}$). **(B)** The minimum inhibitory concentration of teicoplanin for *Msm ponA1* mutant strains. The fold change in MIC was calculated by comparison with isogenic wildtype (*Msm ΔponA1* L5::*ponA1*$_{wt}$).

phosphorylation site decreased by 8- or 4-fold, respectively, the minimum inhibitory concentration (MIC) of teicoplanin, a glycopeptide that inhibits PG crosslinking [32] (Figure 3.6). The increased sensitivity to teicoplanin suggests that imbalanced peptidoglycan synthesis occurred in TP- as well as T34A cells, indicating that phosphorylation may regulate PonA1's TG activity (the remaining catalytic activity of the TP- mutant). A shifted teicoplanin MIC was also observed in *Msm* where the TP- allele exhibits a 16-fold change in MIC (Figure 3.6), although the *Msm* T50A allele did not phenocopy the shifted teicoplanin MIC. However, *Msm* cells that expressed PonA1$_{T50A}$ alleles were more susceptible to a range of meropenem concentrations (S10B Figure), supporting the idea that balanced PonA1 activity is required for

architecturally sound peptidoglycan to resist stress. We also tested whether inhibiting glycan synthesis would impact cellular fitness of PonA1 mutants, but observed minimal efficacy of the small molecule inhibitor moenomycin A (S10C Figure).

Our data suggested that PonA1 activity modulated cell fitness in the presence of drugs. We tested whether changes to PonA1 activity would alter cell fitness under other chemical stresses that target the cell wall. Upon treatment with SDS, *Msm* cells that expressed PonA1$_{TP-}$ and PonA1$_{T50A}$ exhibited a modest decrease in survival (S11A,B Figure). D-amino acids have also been shown to modulate cell wall homeostasis [34], and we tested the fitness of PonA1$_{TP-}$ cells in the presence of D-Met. *Msm* PonA1$_{TP-}$ cells grew less robustly and did not reach the same optical density at stationary phase as compared to isogenic wildtype cells (S11C,D Figure). Furthermore, PonA1$_{TP-}$ cells exhibited aberrant cell shape in deep stationary phase. After four days of growth in culture, *Msm* PonA1$_{TP-}$ cells became wider and shorter compared to isogenic wildtype (S11E Figure, white arrows). These data together indicate that normal PonA1 catalytic and regulatory activity is required for the synthesis of structurally robust peptidoglycan to ensure cellular survival in the face of multiple stresses.

Discussion

The paradigms of cell growth and division in rod-shaped bacteria are based on organisms that grow fundamentally differently than mycobacteria. Consequently, our understanding of mycobacterial growth – and the cell's ability to repress growth – remains elementary. We have addressed this knowledge gap by investigating how a key cell wall synthase, PonA1, promotes and regulates cell growth in mycobacteria.

PonA1 is non-redundant during cell growth

We found that PonA1 is essential in *Msm* and required for normal proliferation in the lung as well as dissemination outside of the lung during an *Mtb* infection (Figure 3.1). These data suggest that the major PBPs in mycobacteria do not have truly redundant functions. This is similar to *E. coli* where distinct complexes employ PBP1a or PBP1b in *E. coli* [3], as well as recent work in *V. cholerae* [12] and *Listeria*

monocytogenes [35] that show PBP1a and PBP1b have specialized biological roles during infection. Furthermore, this implies a revision of the classic understanding of the PBPs as redundant factors. Imperfect redundancy during stress could be exploited to identify unique physiological roles for the PBPs in a variety of bacterial species.

The differential essentiality of PonA1 in *Msm* and *Mtb* for growth in culture is somewhat surprising, but does suggest a difference in expression or functionality of other PBPs, such as the highly homologous protein PonA2, in these species. The role for bifunctional PBPs in *Mtb* cell elongation is probably jointly fulfilled by PonA1 and PonA2, whereas *Msm* has evolved to solely depend on PonA1. Even though PonA1 exhibits different essentiality in *Mtb* and *Msm*, the role of PonA1 is likely highly similar in the two species. We found that *Mtb* PonA1 complements survival of *Msm* depleted of endogenous PonA1 (S7 Figure), and the two proteins are 70% identical at the sequence level (S6 Figure). Furthermore, our data suggest that the physiological role of PonA1 in both *Msm* and *Mtb* is very analogous.

Governance of cell length and shape

Our data suggest that PonA1's polymerization of glycan strands plays a key role in determining cell length (Figure 3.2, Figure 3.7A). Indeed, overproduction of TG-inactive PonA1 in *Msm* yields cells 38% shorter when compared to isogenic wildtype (Figure 3.4A and S4A,B Figures). These cells' length defect is not solely due to their higher frequency of ectopic pole formation, as even cells without ectopic poles are noticeably shorter than isogenic wildtype (S4A Figure). Balanced PonA1 catalytic activity, however, is required for normal cell length. Whereas TG seems to play a large role in modulating cell length, PonA1's TP activity is also required for normal cell length (Figure 3.2). This supports the model wherein efficient PG synthesis occurs when one enzyme is catalytically capable of both synthesizing and crosslinking nascent glycan strands [3]. The linking of PonA1's activities provides tight control over cell length and the protection of cell integrity and growth.

We found that PonA1-specific PG crosslinking is not required in mycobacteria, although it does promote normal cell length. This suggests that other factors either can compensate for lack of PonA1 crosslinking

when absent or that PonA1 normally functions in the elongation complex with another crosslinking enzyme [2], as is true for other bacterial species [3,20]. Because mycobacterial peptidoglycan is estimated to contain predominantly 3–3 crosslinks [36,37], formed by L,D-transpeptidases, these 'non-classical' 3–3 crosslinking enzymes may be active in the elongation complex under wildtype conditions. Indeed, deletion of LdtB in *Mtb* results in shorter cells [38].

Linear cell growth

We found that PonA1 catalytic activity is required for normal cell length and that PonA1 is an early acting factor that promotes extension of the cell pole. Overproduction of PonA1-RFP localizes to the cell pole when the cell is still rod-shaped (S5 Figure). These cells then generate an ectopic pole, which is also marked by PonA1-RFP. We also see the formation of ectopic poles when PonA1-FLAG is overproduced (Figure 3.4, S4 Figure), suggesting that this observation is not an artifact of the fusion partner. Combined with the fact that enzymatically inactive PonA1 induces ectopic pole formation, these data suggest that PonA1 is important for nucleating elongation complexes, and that PonA1 is a major factor that promotes pole elongation in mycobacteria. Because overproduction of enzymatically inactive PonA1 still results in ectopic pole formation, it is clear that other factors are involved in physically synthesizing new cell wall at these foci. This could be endogenous PonA1, but other factors are also likely involved in elongation. Identification of PonA1's interacting partners would illuminate the composition of the elongation complex in mycobacteria and provide further understanding of how cell length and cell shape maintenance are controlled. For example, it would be of great interest to determine whether PonA1 and DivIVA interact, even transiently, in the elongation complex. DivIVA is required for the rod-shape of mycobacteria [23] but has no enzymatic activity. It must coordinate cell growth with the enzymes that synthesize new cell wall [23]. PonA1, as a key factor that promotes cell elongation, may be one such factor that DivIVA helps position or facilitate its activity at the pole.

Even at hyper-physiological levels, PonA1 is properly recruited to the cell pole, as PonA1-RFP localizes at the pole before it degenerates into ectopic poles (S5 Figure). Furthermore, ectopic poles are not produced along the cell body. This suggests that the machinery that recruits PonA1 to the cell pole is not

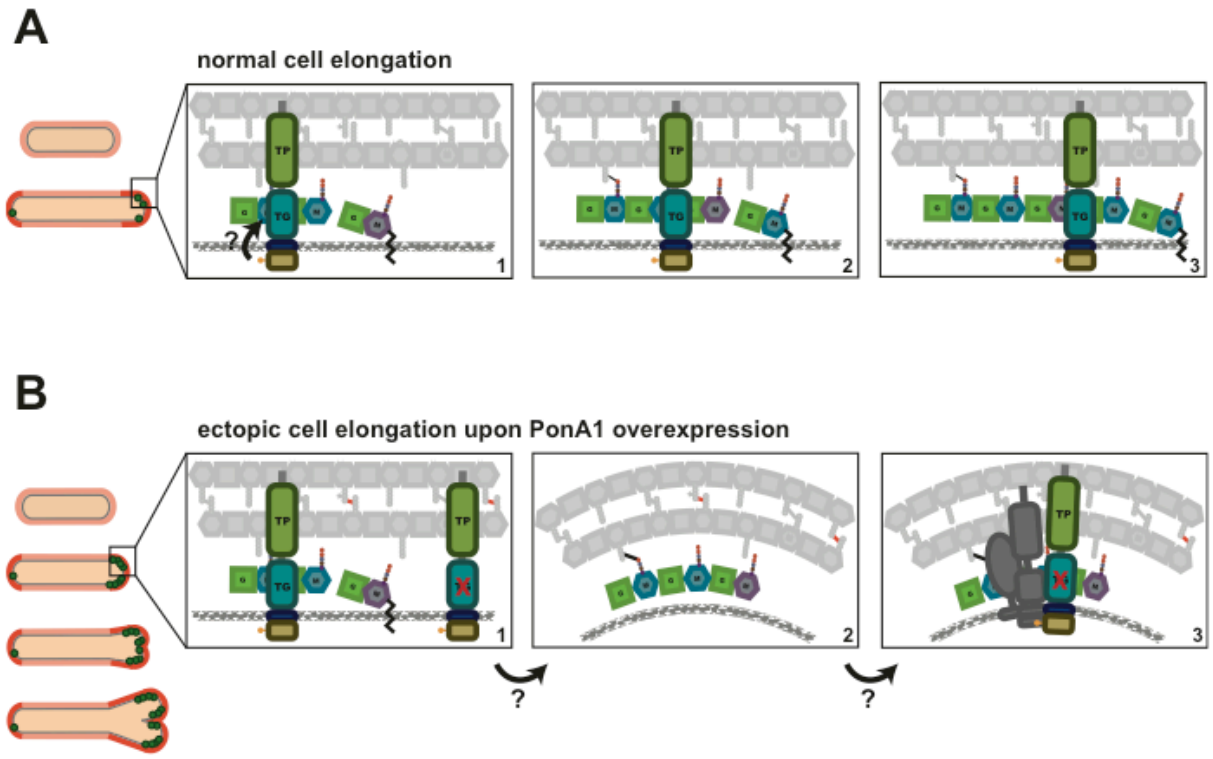

Figure 3.7. A model for how PonA1 promotes cell elongation in mycobacteria. (A) We propose a model wherein PonA1 localizes early to the growth tip and promotes pole elongation through PG synthesis. PonA1 may recruit other factors to form the elongation complex or they are recruited independently of PonA1 (factors not shown). Together with these factors, polar elongation proceeds (orange cells). PonA1 furthers cell elongation through its synthesis of PG. PonA1's synthesis of glycan strands (colored subunits, panels 1-3) and its crosslinking of those glycan strands (black lines, panels 2-3) promote normal cell length. These catalytic activities are potentially modulated through PonA1's phosphorylation (arrow), which acts to regulate the rate of cell elongation. **(B)** Excess PonA1 stimulates ectopic cell elongation (orange cells). The frequency of ectopic pole formation increases with imbalanced PG crosslinking and may result from changes in local peptidoglycan architecture (panels 1-2, factors removed from panel 2 for clarity). These architectural changes may act like a sink that 'recruits' additional protein-interactors of PonA1 or additional elongation complex components to spur cell elongation at ectopic sites (panel 3, dark gray factors).

saturated even at increased levels of PonA1 nor is PonA1's recruitment mechanism rate-limiting for elongation under physiological levels of PonA1. Additionally, the ectopic growth pole normally forms at one cell pole, although occasional cells with both cell ends sporting ectopic growth poles have been observed; however, these cells tend to have multiple septa (S4C Figure, white arrows). These data support a model of mycobacterial elongation where the cell poles are asymmetrically active, at least for a time [2,22,29].

Interestingly, the frequency of ectopic poles correlates with specific imbalanced PonA1 activity. The development of ectopic poles was highest with a PonA1 isoform that can crosslink PG but cannot polymerize glycan strands. Although we have not shown that loss of PonA1 TG activity does not also abolish PonA1 TP activity in the cell (as has been shown for *E. coli* enzymes *in vitro*), the fact that the TG-TP- double mutant did not yield a similar level of ectopic poles, suggests the TG- allele possesses different cellular activity and may not be a completely inactive enzyme. It could possess some level of imbalanced PG crosslinking. These data suggest that imbalanced crosslinking might contort local PG architecture, which may change the curvature of the membrane enough to misdirect elongation complexes to those foci (Figure 3.7B). Alternatively, PonA1 may nucleate elongation complexes at these contorted foci to then extend a functional growth pole. Although these ectopic poles elongate over time, they eventually block cell growth. These data suggest that PonA1's coordination of polar growth must be tightly regulated to maintain linearity of the bacterial cell. This may be accomplished through proper protein-protein interactions and regulation of PonA1 activity.

Phosphorylation regulates elongation rate

We found that cell growth is regulated through PonA1's phosphorylation. Phosphorylation of PBPs is unusual, and only mycobacteria have so far been reported to phosphorylate their PBPs [6], suggesting that phosphorylation could regulate the activity of these proteins in mycobacteria. We found that the absence of PonA1's phosphorylation increased the rate of single cell elongation (Figure 3.5), suggesting that PonA1's phosphorylation normally dampens cell elongation in both *Msm* and *Mtb*. Cells of both species that harbor PonA1 alleles that cannot be phosphorylated (*Msm* T50A and *Mtb* T34A) are longer, suggesting that phosphorylation negatively regulates cell elongation (Figure 3.5). PonA1's phosphorylation is consistent with PknB's phosphorylation of other members of the PG biosynthetic pathway [39,40]. In fact, PknB regulates PG synthesis at each key point of the pathway: precursor synthesis (GlmU) [40], export (MviN) [39] and polymerization (PonA1). Interestingly, PknB's phosphorylation of these three distinct factors is inhibitory, providing consistent regulation of PG biogenesis at multiple steps. It would be of interest to determine if PonA1 phosphorylation correlates with stages of the cell cycle; PonA1 may be phosphorylated as the cells begin the switch from elongation to

septation, where cells need to slow down elongation. Alternatively, PonA1's phosphorylation status may cycle with rounds of peptidoglycan synthesis during growth. Further work is required to test these models in addition to determining if PonA1's phosphorylation impacts *Mtb* fitness during growth during infection.

How PonA1's phosphorylation specifically regulates cell elongation is unknown, although our data suggest that it could act to regulate its TG activity. In the absence of PonA1 phosphorylation, its TG functionality could be hyperactive. This could lead to increased cell length observed with T50A cells (Figure 3.5) and correlates with the shortness of *Mtb* cells expressing TG- (Figure 3.1) or overexpressing TG- *Msm* cells (Figure 3.4, S4 Figure). Additionally, when the T50A mutation is combined with TP-, *Msm* cells exhibit substantial defects in division (Figure 3.5), which could be a result of hyper-active glycan chain synthesis without corresponding crosslinking by PonA1's *cis*-TP domain, altering the normal cellular response to PG synthesis. Differences in antibiotic susceptibility correlate between PonA1's phosphorylation and TG activity as well. In *Mtb*, $PonA1_{T34D}$ and $PonA1_{TG-}$ cells exhibit the same rifampicin tolerance (S10A Figure), whereas T34A and TP- have the same teicoplanin profile (Table 1). In sum, these data suggest a model wherein PonA1's phosphorylation regulates its TG activity (Figure 3.7A). How this could be achieved remains unclear, although it is possible that conformational changes occur upon phosphorylation. Alternatively, PonA1 phosphorylation may impact the stability of the elongation complex or of PonA1's retention in the elongation complex, which could underlie the changes in cell length observed when cells express phosphorylation mutants. In any case, this is an unusual example of cytoplasmic regulation of periplasmic protein activity, though, given the number of phosphorylated proteins found in mycobacteria, this might be a common theme in these organisms.

Altering PonA1 activity changes antibiotic susceptibility

Changes to PonA1 regulatory or enzymatic activity are required for robust growth during antibiotic treatment, suggesting that PonA1 mediates tolerance to drugs that target penicillin binding proteins or PG synthesis. We found a marked enhanced susceptibility of *Mtb* and *Msm* TP- cells to teicoplanin. Enhanced sensitivity of PonA1 TP- cells may reflect an increased cellular toxicity from imbalanced peptidoglycan synthesis. Recent work suggested that beta-lactams are particularly effective because they

not only target TP domains of penicillin binding proteins but they also block crosslinking of nascent glycan strands, leading to an accumulation of uncrosslinked or improperly crosslinked strands that are then degraded, causing a futile cycle of synthesis and degradation that consumes resources [33]. Teicoplanin treated PonA1 TP- cells may be experiencing this cellular toxicity. Because the TP- allele is likely still capable of transglycosylation, it can synthesize nascent glycan strands that will then be blocked from crosslinking when cells are treated with a crosslinking inhibitor. This could lead to an accumulation of uncrosslinked glycan strands and induce cellular toxicity, resulting in the increased teicoplanin sensitivity these cells exhibit. Because the T34A allele demonstrates a similar shifted MIC, it suggests that glycan strand synthesis is also altered in this mutant. Loss of phosphorylation may lead to enhanced TG activity, with a consequent imbalance of crosslinking of the new glycan chains when cells are treated with teicoplanin. Furthermore, the endogenous mycobacterial beta-lactamase is ineffective with drugs like teicoplanin, increasing their potential usefulness. These data suggest that transpeptidation inhibitors, such as teicoplanin, could be a fruitful avenue for TB drug development.

Materials and Methods

Bacterial strains and culture conditions

M. smegmatis mc^2155 was cultured in Middlebrook 7H9 salts (Becto-Dickinson) supplemented with ADC (5 g/L albumin, 2 g/L dextrose, 3 g/L catalase), 0.25% glyercol, and 0.05% Tween-80 or plated on LB agar. *M. tuberculosis* H37Rv was cultured in Middlebrook 7H9 salts supplemented with OADC (oleic acid, albumin, dextrose, catalase [BD Biosciences, Franklin Lakes, NJ]), 0.25% glycerol, and 0.05% Tween-80 or plated on 7H10 agar. Selection was performed at 50 μg/ml hygromycin, 25 μg/ml kanamycin, 20 μg/ml zeocin or 20 μg/ml nourseothricin for both liquid and solid media. *E. coli* XL-1 Blue (Stratagene, Santa Clara, CA) or Top10 (Invitrogen, Carlsbad, CA) were used for cloning and were cultured in LB broth or agar. Selection for *E. coli* occurred at 100 μg/ml hygromycin, 50 μg/ml kanamycin, 20 μg/ml zeocin or 50 μg/ml nourseothricin for both liquid and solid media. All strains were grown at 37°C. The generation of single copy PonA1 mutant strains is described further below. To generate multicopy PonA1 strains,

alleles of *ponA1* were subcloned into an anhydrotetracycline inducible pMS2 derivative plasmid [41]. These plasmids were transformed into an *M. smegmatis* mc^2155 strain with the pMC1s plasmid [41], encoding the *tetR* repressor, integrated at the L5 phage integration site.

Recombinant DNA constructs

M. smegmatis PonA1 (MSMEG_6900) and *M. tuberculosis* PonA1 (Rv0050) catalytic mutants were generated using site directed mutagenesis and PCR stitching. *M. smegmatis* PonA1 truncation mutants were generated by PCR. The double T50A,TP- Msm PonA1 construct was generated via PCR stitching. For all Mtb PonA1 constructs, the -426 start site was used. All constructs used in this study were cloned under the strong promoter pUV15 modified to contain TetR operator sites [41] (although no TetR is encoded in the cells' genomes so expression of *ponA1* is constitutive). All PCR reactions were performed with KOD Xtreme™ Hot Start DNA polymerase (EMD Millipore, Billerica, MA). All *M. smegmatis* and *M. tuberculosis* PonA1 constructs listed above were cloned as translational fusions with either the FLAG epitope or monomeric red fluorescent protein (RFP). The FLAG epitope and RFP do not obstruct PonA1 function, as both tags recombineered onto the C-terminus of *ponA1* on the chromosome complement *Msm* survival.

Deletion of ponA1 in *M. tuberculosis*

A *ponA1* (Rv0050) knockout construct was generated by PCR and subcloning. Because *ponA1* exists in an operon, the 5' and 3' 25 nucleotides of *ponA1* were preserved in the knockout construct. The 500 nucleotides upstream of *ponA1* were PCR amplified with a 3' *NdeI* restriction endonuclease site. The 500 nucleotides downstream of *ponA1* were PCR amplified with a 5' *PvuI* restriction endonuclease site. A hygromycin resistance cassette flanked by loxP sites was amplified with a 5' *NdeI* site and a 3' *PvuI* site. These three fragments were subcloned by digesting with *NdeI* and/or *PvuI*. The final ligated product was PCR amplified and used to replace *ponA1* in the *Mtb* H37Rv genome via recombineering [42]. Cells were plated on 7H10 plates with 50 μg/ml hygromycin. After incubation at 37°C for three weeks, colonies were inoculated into 2 ml of selective 7H9. Cell lysates were generated and screened by PCR for correct

recombinants. One out of 11 colonies was positive for recombination; loss of *ponA1* from the genome was verified by PCR and whole genome sequencing.

Ethics Statement

The Institutional Animal Care and Use Committee of Harvard University approved and monitored all protocols, personnel, and animal use. The animal facilities are AAALAC accredited, and work was performed under the NIH Office of Laboratory Animal Welfare (OLAW) permit number A-3431-01.

Mouse infections

Six week old wildtype female C57Bl6 mice (Jackson Laboratories, Bar Harbor, ME) were aerosol infected with low doses of *M. tuberculosis* H37Rv wildtype, H37Rv *ΔponA1::Hyg*, H37Rv *ΔponA1::Hyg* L5::$ponA1_{wt}$, and H37Rv *ΔponA1::Hyg* L5::$ponA1_{TG-}$. Strains were confirmed as PDIM positive by mass spectrometry prior to infection using established protocols [43]. Fifteen mice were infected per strain, and five mice were sacrificed at 1 day, 15 days, and 42 days post infection, respectively. To minimize suffering, animals were first put to sleep with isoflurane before sacrifice. Lungs and spleens were homogenized and serially diluted on selective 7H10 plates (for the genetically modified strains) or 7H10 plates lacking antibiotics (for H37Rv wildtype) for CFU enumeration.

Allelic exchange in *M. smegmatis*

A marked copy of PonA1 was first integrated in the chromosome at the L5 phage integration site. The endogenous locus of PonA1 was then replaced with a different antibiotic cassette via recombineering. This dual marked strain was then transformed with an L5-integrating vector that is marked with a third antibiotic cassette. This second integration event replaces the original integrated allele, and selection for the third antibiotic recovers cells with the desired allele (Figure 3.1A). Exchange at the L5 site is imperfect and to confirm desired transformants, cells are patched onto plates containing the first L5 integrant marker or the second L5 integrant marker. Cells that are mono-resistant to the second L5 integrant antibiotic are counted as correct transformants; frequencies of correct transformation are calculated by comparison to wildtype *ponA1* control transformations.

Timelapse microscopy and data analysis

For the data in Figure 3.5 and S8 Figure, vegetatively growing *M. smegmatis* cells were washed twice in 1X PBS with 0.1% Tween 20, stained with 50 µg/ml Alexa488 (Invitrogen), and filtered twice through a 10 µm filter to obtain single cells. Cells were inserted into custom microfluidic devices (see Reference [22]) and imaged at 37°C with constant flow of selective 7H9. Cells were imaged with a DeltaVision PersonalDV microscope using the 60x objective (Plan APO NA1.42) every 10 minutes for a minimum of 18 hours. Images were captured with a CoolSnap HQ2 camera (Photometric). Cell elongation and division events were annotated using ImageJ (National Institutes of Health) with the ObjectJ plugin (Norbert Vischer and Stelian Nastase, University of Amsterdam, http://simon.bio.uva.nl/objectj/index.html). Cell elongation was measured as new unstained cell wall material; cell division was defined as the first frame when physical invagination of the cell wall was visible. A custom Python script was used to analyze the annotations.

For the data in S4 Figure, *M. smegmatis* cells were imaged using a CellASIC® microfluidic system (EMD Millipore, Billerica, MA). Vegetatively growing cells were cultured for four hours ± 100 ng/mL anhydrotetracycline (aTc) inducer to overexpress $PonA1_{TG}$-RFP prior to growth in the CellASIC® chambers. Cells were imaged every 15 minutes for 17 hours with constant flow of selective 7H9 ± 100 ng/mL aTc. Images were captured by a Nikon Eclipse TI microscope using the 60x objective, which is maintained at 37°C with an objective heater. Images were captured with a CoolSNAP SQ2 camera. The image montage in S4 Figure was compiled with FIJI [44].

Light microscopy and image analysis

For imaging, cells were washed once in 1x PBS and resuspended in 1X PBS ± 2.5 µg/ml FM4-64Fx (Invitrogen) to visualize the plasma membrane. After resuspension, cells were incubated in the dark for 10 minutes prior to imaging. For *M. tuberculosis*, cells were first fixed overnight in 1% formalin in the biosafety level 3 facility before removal and consequent imaging. Cells were imaged on a Nikon TE-200E microscope using the 100x (NA1.40) objective. Images were captured with an Orca-II ER cooled CCD camera (Hamamatsu, Japan). Exposure and image acquisition were controlled with Metamorph Software

(Molecular Devices). Final images were prepared in Adobe Photoshop CS3. To quantitate cell length, the fluorescent images of cells stained with FM4-64Fx were used. Cell length was calculated using ImageJ software (National Institutes of Health) and converted to microns using the appropriate pixel to micron conversion. Length was measured from cell pole to the opposite cell pole or from cell pole to septum, if present. Cell synchronization is not yet possible for mycobacteria; hence, cell lengths were measured for unsynchronized populations. To quantitate the frequency of multi-poled cells, cells were both imaged and scored blind to eliminate potential bias. The figure shows data from five combined experiments. 2652 cells were imaged and counted for $PonA1_{wt}$, 2910 cells for $PonA1_{TG-}$ cells, 2054 for $PonA1_{TP-}$ cells, and 2379 for $PonA1_{TG-TP-}$ cells. The control represents data collected from uninduced cells. Overexpression of PonA1 was induced with 100 ng/mL aTc.

***in vitro* kinase assays and detection of PonA1's phosphorylation site**

N-terminally his-MBP-tagged kinase domains of the nine canonical serine-threonine protein kinases from *Mtb* were expressed and purified from *E. coli* using a nickel column and then an S75 size exclusion column, in kinase buffer (50 mM Tris pH7.5, 150 mM NaCl, 20% glycerol). His-MBP-PonA1 (cytoplasmic domain) was expressed and purified from *E. coli* using Ni-NTA beads (Novagen) according to the protocol recommended by the manufacturer. Protein levels were measured by A280, and kinase reactions were started by mixing 1 µg of kinase, 10 µg of his-MBP-PonA1(cyto), 1mM $MnCl_2$ and 1mM ATP. Reactions were incubated at room temperature for 1 hour and stopped by addition of Laemmli buffer. Samples were heated, separated by SDS-PAGE, and detected by western blot using α-phospho-threonine antibody (Cell Signaling Technology). Kinase reactions for mass spectrometry were performed the same way, using only his-MBP-PknB and his-MBP-PonA1(cyto). The his-MBP-PonA1 protein band was cut out of the polyacrylamide gel and in-gel trypsin digested. Samples were analyzed by liquid chromatography (LC)/MS/MS with an Agilent 6520 Accurate-Mass Quadrupole Time-of-Flight instrument. Peptides were separated on a POROSHELL 300SB-C18 (2.1 × 75 mm, 5 µm) at a 0.5 mL/min flow rate, by using a linear gradient of increasing acetonitrile in water. Spectrum Mill software (Agilent) was used to identify peptides.

Antibiotic treatment and determination of bacterial cell fitness

The antibacterial effects of teicoplanin (Sigma Aldrich, St. Louis, MO) and moenomycin A (Sigma Aldrich, St. Louis, MO) were determined by culturing exponentially growing *M. tuberculosis* or *M. smegmatis* cells in complete 7H9 in non-treated 96 well plates (Genesee Scientific, San Diego, CA) in the presence of serially diluted drug, in duplicate. Plates also contained duplicate untreated wells as controls. *M. tuberculosis* was grown to OD_{600} of 0.5 before culturing ± drug at a calculated starting OD_{600} of 0.006 for six days at 37°C with shaking. *M. smegmatis* was grown to OD_{600} of 0.5 before culturing ± drug at a calculated starting OD_{600} of 0.05 for 16 hours at 37°C with shaking. Bacterial growth was evaluated by adding 0.002% resazurin (Alamar Blue, Sigma Aldrich, St. Louis, MO) to each well. *M. tuberculosis* plates were incubated with resazurin for 18-24 hours. *M. smegmatis* plates were incubated with resazurin for 3-5 hours. Wells were scored as blue or purple indicating metabolically inactive cells and pink as metabolically active cells. The inhibitory effects of meropenem (Sigma Aldrich, St. Louis, MO) were determined by growing *M. smegmatis* to an OD_{600} of 0.5 before culturing ± drug at a calculated starting OD_{600} of 0.1. Cells were grown in complete 7H9 in 96 well honeycomb plates (Growth Curves USA, Piscataway, NJ) ± drug, in triplicate, at 37°C with shaking in a Bioscreen growth curve machine (Growth Curves USA, Piscataway, NJ). Optical density was measured by absorbance at 600nm every 30 minutes for 48 hours. The inhibitory effects of rifampicin (Sigma Aldrich, St. Louis, MO) were determined by growing *M. tuberculosis* to an OD_{600} of 0.5 before culturing ± drug at a calculated starting OD_{600} of 0.1. Cells were grown in complete 7H9 in 24 well untreated plates ± drug, in triplicate, at 37°C with shaking. Optical density was measured after six days, and growth was normalized to untreated control wells.

Optical density measurements

Population growth curves for *M. smegmatis* strains were performed in 96 well honeycomb plates (Growth Curves USA, Piscataway, NJ), in triplicate, at 37°C with shaking in a Bioscreen growth curve machine (Growth Curves USA, Piscataway, NJ). Cells were grown to an OD_{600} of 0.5 before beginning the growth curve at a calculated starting OD_{600} of 0.1. Cells were grown in complete 7H9 with the appropriate antibiotic selection. Optical density was measured by absorbance at 600nm every 30 minutes for 48 hours. Error bars are often too small to see. Population growth curves for *M. tuberculosis* strains were

performed in 30 ml inkwells (Corning Life Sciences, Corning, NY), in triplicate, at 37°C with shaking. Cells were grown to an OD_{600} of 0.5 before beginning the growth curve at a calculated starting OD_{600} of 0.1. Cells were grown in complete 7H9 with the appropriate antibiotic selection. Optical density was measured daily by absorbance at 600nm.

Immunoblotting

Cells were pelleted, washed once in 1X PBS, and lysed by bead-beating. 6X Laemmli buffer was added to the whole cell lysate and then boiled for 10 minutes. Proteins were separated on a 12-14% Tris-Glycine SDS PAGE gels (BioRad, Hercules, CA), transferred to PVDF membrane (Pall Corp, Pensacola, FL), incubated with anti-FLAG antibodies (Sigma Aldrich, St. Louis, MO) at 1:15,000 dilution, washed thrice in 1X PBST, and incubated with a 1:1000 dilution of a secondary antibody conjugated to HRP (Pierce, Rockford, IL). Membranes were incubated with SuperSignal chemiluminescent reagent (Thermo Fisher Scientific, Rockford, IL) for 5 minutes in the dark and imaged on a FluorChem8900 (AlphaInnotech, Santa Clara, CA).

Data representation and statistical analysis

Prism 6.0 software (GraphPad Software, La Jolla, CA) was used to graph and analyze numerical data. Statistical tests in the Prism software were used to calculate significance of measurements as described in the Figure Legends. The doubling times in S2 Figure and S9 Figure were generated by fitting an exponential growth function (in Prism) to all datapoints between 5 and 13 hours of OD_{600} measurements.

Acknowledgements

We thank Thomas Bernhardt, Simon Dove, Tobias Dörr, and Nick Peters for helpful discussions and thoughtful review of the data. We thank Matthew Waldor for generous access to the Bioscreen machine, and Bree Aldridge for help with image annotation. We are grateful to Noman Siddiqi, Shoko Wakabayashi, Jessica Pinkham, and Larry Pipkin for excellent technical support at the Harvard T.H. Chan School of Public Health Biosafety Level 3 Facility.

Section 3.3 References

1. World Health Organization. Global tuberculosis report 2014. World Health Organization; 2014.

2. Kieser KJ, Rubin EJ. How sisters grow apart: mycobacterial growth and division. Nat Rev Micro. 2014;12:550–62.

3. Typas A, Banzhaf M, Gross CA, Vollmer W. From the regulation of peptidoglycan synthesis to bacterial growth and morphology. Nat Rev Micro.; 2012;10:123–36.

4. Hett EC, Chao MC, Rubin EJ. Interaction and Modulation of Two Antagonistic Cell Wall Enzymes of Mycobacteria. PLoS Pathog. 2010;6:e1001020.

5. Chao MC, Kieser KJ, Minami S, Mavrici D, Aldridge BB, Fortune SM, Alber T, Rubin EJ. Protein Complexes and Proteolytic Activation of the Cell Wall Hydrolase RipA Regulate Septal Resolution in Mycobacteria. PLoS Pathog. 2013;9:e1003197.

6. Prisic S, Dankwa S, Schwartz D, Chou MF, Locasale JW, Kang C-M, et al. Extensive phosphorylation with overlapping specificity by Mycobacterium tuberculosis serine/threonine protein kinases. Proc Natl Acad Sci USA. 2010;107:7521–6.

7. Pashley CA, Parish T. Efficient switching of mycobacteriophage L5-based integrating plasmids in Mycobacterium tuberculosis. FEMS Microbiol Lett. 2003;229:211–5.

8. Zhang YJ, Ioerger TR, Huttenhower C, Long JE, Sassetti CM, Sacchettini JC, Rubin EJ. Global Assessment of Genomic Regions Required for Growth in Mycobacterium tuberculosis. PLoS Pathog. 2012;8:e1002946.

9. Zhang YJ, Reddy MC, Ioerger TR, Rothchild AC, Dartois V, Schuster BM, et al. Tryptophan Biosynthesis Protects Mycobacteria from CD4 T-Cell-Mediated Killing. Cell.; 2013;155:1296–308.

10. Paradis-Bleau C, Markovski M, Uehara T, Lupoli TJ, Walker S, Kahne DE, et al. Lipoprotein Cofactors Located in the Outer Membrane Activate Bacterial Cell Wall Polymerases. Cell. 2013;143:1110–20.

11. McPherson DC, Popham DL. Peptidoglycan synthesis in the absence of class A penicillin-binding proteins in Bacillus subtilis. J Bacteriol. 2003;185:1423–31.

12. Dörr T, Möll A, Chao MC, Cava F, Lam H, Davis BM, et al. Differential requirement for PBP1a and PBP1b in in vivo and in vitro fitness of Vibrio cholerae. Infection and Immunity. 2014;82:2115–24.

13. Valbuena N, Letek M, Ordóñez E, Ayala JA, Daniel RA, Gil JA, et al. Characterization of HMW-PBPs from the rod-shaped actinomycete Corynebacterium glutamicum: peptidoglycan synthesis in cells lacking actin-like cytoskeletal structures. Mol Microbiol. 2007;66:643–57.

14. Patru M-M, Pavelka MS. A Role for the Class A Penicillin-Binding Protein PonA2 in the Survival of Mycobacterium smegmatis under Conditions of Nonreplication. J Bacteriol. 2010;192:3043–54.

15. Cole ST, Brosch R, Parkhill J, Garnier T, Churcher C, Harris D, et al. Deciphering the biology of Mycobacterium tuberculosis from the complete genome sequence. Nature. 1998;393:537–44.

16. Born P, Breukink E, Vollmer W. In vitro synthesis of cross-linked murein and its attachment to sacculi by PBP1A from Escherichia coli. J Biol Chem. 2006;281:26985–93.

17. Terrak M, Ghosh TK, van Heijenoort J, Van Beeumen J, Lampilas M, Aszodi J, et al. The catalytic, glycosyl transferase and acyl transferase modules of the cell wall peptidoglycan-polymerizing penicillin-binding protein 1b of Escherichia coli. Mol Microbiol. 1999;34:350–64.

18. Billman-Jacobe H, Haites RE, Coppel RL. Characterization of a Mycobacterium smegmatis mutant lacking penicillin binding protein 1. Antimicrob Agents Ch. 1999;43:3011–3.

19. Domenech P, Reed MB. Rapid and spontaneous loss of phthiocerol dimycocerosate (PDIM) from Mycobacterium tuberculosis grown in vitro: implications for virulence studies. Microbiology. 2009;155:3532–43.

20. Banzhaf M, van den Berg van Saparoea B, Terrak M, Fraipont C, Egan A, Philippe J, et al. Cooperativity of peptidoglycan synthases active in bacterial cell elongation. Mol Microbiol. 2012;85:179–94.

21. Meisel U, Holtje J-V, Vollmer W. Overproduction of Inactive Variants of the Murein Synthase PBP1B Causes Lysis in Escherichia coli. J Bacteriol. 2003;185:5342–8.

22. Aldridge BB, Fernandez-Suarez M, Heller D, Ambravaneswaran V, Irimia D, Toner M, Fortune SM. Asymmetry and Aging of Mycobacterial Cells Lead to Variable Growth and Antibiotic Susceptibility. Science. 2012;335:100–4.

23. Meniche X, Otten R, Siegrist MS, Baer CE, Murphy KC, Bertozzi CR, Sassetti CM. Subpolar addition of new cell wall is directed by DivIVA in mycobacteria. Proc Natl Acad Sci USA. 2014;111:E3243–51.

24. Nelson DE, Young KD. Penicillin binding protein 5 affects cell diameter, contour, and morphology of Escherichia coli. J Bacteriol. 2000;182:1714–21.

25. De Pedro MA, Young KD, Höltje J-V, Schwarz H. Branching of Escherichia coli cells arises from multiple sites of inert peptidoglycan. J Bacteriol. 2003;185:1147–52.

26. Schubert OT, Mouritsen J, Ludwig C, Röst HL, Rosenberger G, Arthur PK, et al. The Mtb Proteome Library: A Resource of Assays to Quantify the Complete Proteome of Mycobacterium tuberculosis. Cell Host Microbe.; 2013;13:602–12.

27. Krogh A, Larsson B, Heijne von G, Sonnhammer ELL. Predicting transmembrane protein topology with a hidden markov model: application to complete genomes. J Mol Biol. 2001;305:567–80.

28. Sauvage E, Kerff F, Terrak M, Ayala JA, Charlier P. The penicillin-binding proteins: structure and role in peptidoglycan biosynthesis. FEMS Microbiol Rev. 2008;32:234–58.

29. Santi I, Dhar N, Bousbaine D, Wakamoto Y, McKinney JD. Single-cell dynamics of the chromosome replication and cell division cycles in mycobacteria. Nat Commun.; 2013;4:1–10.

30. Chauhan A, Madiraju MVVS, Fol M, Lofton H, Maloney E, Reynolds R, Rajagopalan M. Mycobacterium tuberculosis Cells Growing in Macrophages Are Filamentous and Deficient in FtsZ Rings. J Bacteriol. 2006;188:1856–65.

31. Farhat MR, Shapiro BJ, Kieser KJ, Sultana R, Jacobson KR, Victor TC, et al. Genomic analysis identifies targets of convergent positive selection in drug-resistant Mycobacterium tuberculosis. Nat Genet.; 2013;45:1183–9.

32. Binda E, Marinelli F, Marcone G. Old and New Glycopeptide Antibiotics: Action and Resistance. Antibiotics. 2014;3:572–94.

33. Cho H, Uehara T, Bernhardt TG. Beta-Lactam Antibiotics Inducea Lethal Malfunctioning of the Bacterial Cell Wall Synthesis Machinery. Cell.; 2014;159:1300–11.

34. Lam H, Oh D-C, Cava F, Takacs CN, Clardy J, De Pedro MA, et al. D-amino acids govern stationary phase cell wall remodeling in bacteria. Science. 2009;325:1552–5.

35. Rismondo J, Möller L, Aldridge C, Gray J, Vollmer W, Halbedel S. Discrete and overlapping functions of peptidoglycan synthases in growth, cell division and virulence of Listeria monocytogenes. Mol Microbiol. 2015;95:332-51.

36. Lavollay M, Arthur M, Fourgeaud M, Dubost L, Marie A, Veziris N, et al. The Peptidoglycan of Stationary-Phase Mycobacterium tuberculosis Predominantly Contains Cross-Links Generated by L,D-Transpeptidation. J Bacteriol. 2008;190:4360–6.

37. Kumar P, Arora K, Lloyd JR, Lee IY, Nair V, Fischer E, et al. Meropenem inhibits D,D-carboxypeptidase activity in Mycobacterium tuberculosis. Mol Microbiol. 2012;86:367–81.

38. Schoonmaker MK, Bishai WR, Lamichhane G. Nonclassical transpeptidases of Mycobacterium tuberculosis alter cell size, morphology, cytosolic matrix, protein localization, virulence and resistance to β-lactams. J Bacteriol. 2014;196:1394–402.

39. Gee CL, Papavinasasundaram KG, Blair SR, Baer CE, Falick AM, King DS, et al. A Phosphorylated Pseudokinase Complex Controls Cell Wall Synthesis in Mycobacteria. Sci Signal. 2012;5:ra7–ra7.

40. Parikh A, Verma SK, Khan S, Prakash B, Nandicoori VK. PknB-Mediated Phosphorylation of a Novel Substrate, N-Acetylglucosamine-1-Phosphate Uridyltransferase, Modulates Its Acetyltransferase Activity. J Mol Biol.; 2009;386:451–64.

41. Ehrt S, Guo XV, Hickey CM, Ryou M, Monteleone M, Riley LW, et al. Controlling gene expression in mycobacteria with anhydrotetracycline and Tet repressor. Nucleic Acids Res. 2005;33:e21.

42. Van Kessel JC, Hatfull GF. Recombineering in Mycobacterium tuberculosis. Nat Meth. 2007;4:147–52.

43. Layre E, Sweet L, Hong S, Madigan CA, Desjardins D, Young DC, et al. A comparative lipidomics platform for chemotaxonomic analysis of Mycobacterium tuberculosis. Chem Biol. 2011; 18: 1537–49.

44. Schindelin J, Arganda-Carreras I, Frise E, Kaynig V, Longair M, Pietzsch T, Preibisch S, et al. Fiji: an open-source platform for biological-image analysis. Nat Meth.; 2012;9:676–82.

Chapter 4

Mapping cell wall synthesis pathways in *Mycobacterium tuberculosis*

Section 4.1 Overview and Attributions

Overview

This chapter is comprised of a manuscript that I wrote, and Eric contributed helpful editorial input. We will submit this manuscript soon.

Attributions

I generated all the *M. tuberculosis* mutant and knockout strains. I generated the *ΔponA1* transposon genomic library, which Tom Ioerger sequenced. I developed a pipeline in the lab, with invaluable help from Michael Chao, Kasia (Catherine) Baranowski, and the Microbiology and Immunobiology Department's IT team, to go from raw sequencing data to genome-mapped sequence reads. Kasia Baranowski generated the *ΔponA2* and *ΔldtB* transposon mutant libraries, and we analyzed the data together. Jarukit Long and Christopher Sassetti provided wildtype transposon library data (I mapped the raw sequencing data). I performed all experiments and analyses in Figures 4.4, 4.5, 4.6, 4.7, and 4.8. Others offered key help at certain experimental junctures (see Acknowledgements).

Section 4.2 *Mycobacterium tuberculosis* requires correlated 4-3 and 3-3 peptidoglycan crosslinking for robust growth

Karen J. Kieser[1], Catherine Baranowski[1], Michael C. Chao[2], Jarukit E. Long[3], Christopher M. Sassetti[3,4], James C. Sacchettini[5], Thomas R. Ioerger[6], Matthew K. Waldor[2,4], Eric J. Rubin[1,7‡]

[1] Department of Immunology and Infectious Disease, Harvard T.H. Chan School of Public Health, Boston, MA USA 02115

[2] Division of Infectious Diseases, Brigham & Women's Hospital and Department of Microbiology and Immunobiology, Harvard Medical School, Boston, MA, USA 02115

[3] Department of Microbiology and Physiological Systems, University of Massachusetts Medical School, Worcester, MA, USA 01605

[4] Howard Hughes Medical Institute, Chevy Chase, MD, USA 20815

[5] Department of Biochemistry and Biophysics and Department of Chemistry, Texas A&M University, College Station, TX, USA 77843

[6] Department of Computer Science, Texas A&M University, College Station, TX, USA 77843

[7] Department of Microbiology and Immunobiology, Harvard Medical School, Boston, MA, USA 02115

[‡] Corresponding Author: erubin@hsph.harvard.edu

[‡] Corresponding Author Present Address:

Harvard Institutes of Medicine, Room 1007A

4 Blackfan Circle

Boston, MA 02115

Phone: 617-432-3335

Abstract

Successful synthesis of the major bacterial cell wall macromolecule peptidoglycan (PG) is an essential process for all walled bacteria. PG, composed of saccharide strands crosslinked by peptides, is one of the most elemental components of a bacterial cell. While PG metabolism has been extensively studied in model organisms, it remains poorly understand in mycobacteria, a group that includes the important human pathogens *Mycobacterium tuberculosis* (*Mtb*) and *Mycobacterium leprae*. In an effort to understand how *Mtb* coordinates its peptidoglycan synthesis, we focused on the key PG synthases PonA1, PonA2, and LdtB. In *Mycobacterium smegmatis*, a saprophytic mycobacterium, PonA1, but not PonA2, is required for bacterial growth in culture. However, *Mtb* controls its PG biogenesis differently

because PonA1 and PonA2 are both dispensable for growth in culture. 3–3 PG crosslinks, such as those synthesized by LdtB, are the predominant crosslink in mycobacterial PG, suggesting these enzymes are active throughout the cell cycle. These 3–3 transpeptidases can be inhibited by cabapenems, but little is known about their cellular roles and regulation to facilitate drug optimization. We hypothesized that unique genetic interactions among these key biosynthetic proteins would help define mycobacterial PG metabolism. To identify these interactions, we performed whole genome transposon mutagenesis screens in *ΔponA1*, *ΔponA2*, and *ΔldtB Mtb* cells and found distinct factors that were required to sustain bacterial growth in the absence of each of these enzymes. We show that either PonA1 or PonA2 is required for growth of *Mtb* and that each of them correlate 4–3 and 3–3 crosslinking with LdtB. Our data also suggest *Mtb* coordinates synthesis of its different cell envelope layers, likely using PonA1 and its genetic interacting partners to do so. This work improves our understanding of how *Mtb* builds its cell wall and its role in ensuring robust bacterial fitness.

Introduction

Mycobacterium tuberculosis (*Mtb*) is the etiologic agent of tuberculosis (TB), which remains one of world's greatest health burdens. The World Health Organization estimates that one third of the world's population harbor *Mtb* and that 1.5 million individuals died of TB last year [1]. Mtb's success as a pathogen is due in part to its cell wall, which is notorious for its complexity and has been implicated in antibiotic resistance [2]. The cell wall is a critical interface for host-pathogen interactions, and pressure from the host environment induces architectural changes that may promote *Mtb*'s survival in the host [2]. As a key interaction surface between host and pathogen, understanding the synthesis and biochemistry of the cell wall could facilitate our understanding of how the cell wall promotes *Mtb*'s survival during infection.

An essential component of bacterial cell walls, including *Mtb*'s, is peptidoglycan (PG), a complex macromolecule that provides structural support and resistance to turgor pressure [3]. Aberrations to peptidoglycan can be lethal to the bacterial cell [4–6]. Hence, its synthesis and proper maintenance are critical to bacterial survival. Peptidoglycan consists of long glycan chains, composed of two different

saccharides, which are crosslinked via pentapeptide tails that descend from the glycan chains. These peptide tails can be joined with two different linkages: a 4–3 crosslink (joining the fourth and third amino acid of the respective peptide tails) or a 3–3 crosslink (joining the third amino acids on neighboring peptide tails), which is the predominant form of peptidoglycan crosslinks in mycobacteria [7,8].

Due to its fundamental importance to bacteria, the synthesis and structure of peptidoglycan has been examined for decades, predominantly in organisms like *Escherichia coli* or *Bacillus subtilis*. However, less is known about the synthesis of this major cell wall macromolecule in pathogenic organisms, including *Mtb* [2]. We previously showed that a major mycobacterial peptidoglycan synthase, PonA1 (capable of polymerizing both the glycan strands as well as the 4–4 crosslinks between strands), was required for growth of the saprophytic *Mycobacterium smegmatis* (*Msm*) in culture [4] (Chapter 3) but that PonA1 was dispensable for growth of *Mtb* in culture, but was required for normal fitness of *Mtb* during infection (Chapter 3). These data suggested that different methods of controlling PG biogenesis existed in *Mtb* compared to *Msm*, and this paradigm likely extends to the multiple layers of *Mtb*'s cell envelope.

Furthermore, the unusual prevalence of 3–3 peptide linkages in mycobacterial PG shows that the construction of PG is different in mycobacteria than many other rod-shaped organisms. Because different enzymes synthesize the 4–3 and 3–3 crosslinks, the composition of the cell wall synthase machinery is likely different in mycobacteria than the "classic" cell wall synthesis complexes found in other organisms [2]. The wide prevalence of 3–3 crosslinks in mycobacterial PG throughout different growth stages [8] suggests that these enzymes are active during normal growth, however little is known about their cellular roles or regulation during growth and peptidoglycan biogenesis. Of the five encoded 3–3 transpeptidases in *Mtb* [9], most studies have focused on LdtB, as it mediates tolerance to transpeptidation inhibitors [9–11], is required for normal virulence in a mouse model of TB [10], and is important for normal cell shape [11]. The cellular role of the remaining 3–3 transpeptidases remains unclear [12], although LdtA also appears required for normal cell shape [11].

The 3–3 transpeptidases accept different substrates [12] and have different active sites and domain structure [12–15] than the classical 4–3 transpeptidases. Consequently, their antibiotic susceptibility differs [16]. The classic antibiotic penicillin targets 4–3 transpeptidases (the "penicillin binding proteins"), but 3–3 transpeptidases have less affinity for penicillin and related small molecules. Penicillin insensitivity is aggravated in *Mtb* because of endogenous beta-lactamases [17,18], which hydrolyze the core beta-lactam ring of penicillin. However, 3–3 transpeptidases are susceptible to carbapenems [12,19-21], including meropenem and imipenem, which are more resistant to BlaC hydrolysis than penicillins [19]. Recent studies have shown that *Mtb* grown in culture is susceptible to carbapenems, including extensively drug resistant *Mtb* [19], which is on the rise [1]. However, the efficacy of these drugs is limited for TB disease in mice and humans [22,23], necessitating further optimization. To that end, we need a better understanding of the activity of these 3–3 transpeptidases during growth and cell wall biogenesis.

To investigate how *Mtb* governs cell wall biogenesis, we used major 4–3 and 3–3 transpeptidases as probes of peptidoglycan synthesis. We performed genome-wide screens in *Mtb* cells that lack either the bifunctional PG synthase PonA1, its homologue PonA2, or the 3–3 transpeptidase LdtB. We identified discrete genetic interacting factors for these enzymes, suggesting that these synthases have distinct cellular roles in assembling *Mtb*'s peptidoglycan. Furthermore, we find that *Mtb* cannot survive if both *ponA1* and *ponA2* are disrupted, indicating that these enzymes play a critical, and complementary, role in PG biogenesis. We further provide evidence that synthesis of 4–3 and 3–3 crosslinks is correlated in *Mtb*. PonA1 and LdtB are both important for normal growth, while loss of PonA2 and LdtB is lethal to bacterial cells. In sum, our findings provide an understanding of how *Mtb* governs biogenesis of its complex peptidoglycan and how its coordinated synthesis by 4–3 and 3–3 transpeptidases promotes robust bacterial growth.

Results

Whole genome mutagenesis identifies PonA1's PG biogenesis partners in *M. tuberculosis*

Unlike *Msm*, PonA1 is not required for proliferation of *Mtb* during growth in culture, but is required for normal bacterial growth during infection [4] (Chapter 3). These data suggest that *Mtb* has fundamentally different ways of controlling its cell wall biogenesis than does *Msm*. To uncover the factors responsible for the differential control of PG biogenesis in *Mtb*, we undertook an unbiased whole genome screen in *ΔponA1 Mtb* cells. We mutagenized *ΔponA1 Mtb* cells with a transposon that inserts at TA dinucleotides throughout the genome. We then used highthroughput sequencing to map the genomic location of the transposon insertions [24] (see Materials and Methods for details) (Figure 4.1). Analysis of the transposon insertion profiles [25] between wildtype and *ΔponA1 Mtb* revealed ten factors predicted to be required in cells that lack PonA1 (Figure 4.2A, "essential" factors). Most of these factors are associated with or predicted to be involved with cell wall synthesis. For example, factors involved in peptidoglycan (*rv3682*), arabinogalactan (*rv0806*) or mycolic acid (*rv0642*) synthesis in addition to cell wall precursor production (*rv1086*) were predicted as required in *ΔponA1* cells (Figure 4.2A). These data suggest that the cell requires either PonA1 or PonA2 for peptidoglycan synthesis, analogous to the situation in *E. coli* [26]. These data also indicate that the cell may use PonA1 and its genetic interacting factors, like *rv0806*, to coordinate synthesis of the multiple layers of the mycobacterial cell wall.

This unbiased screening approach also eight identified factors whose transposon disruption in *ΔponA1* cells appeared beneficial to the cell. Their transposon insertion rate was higher in *ΔponA1* cells than wildtype cells (Figure 4.2A, "enriched"). For example, the transcription factor EspR had higher levels of transposon insertions in cells that lack *ponA1* compared to wildtype *Mtb*. This could indicate that EspR regulates *ponA1* transcription and that cells without *ponA1* can afford to lose *espR* function at a higher rate than wildtype cells.

Identification of PonA2's PG synthesis partners in *M. tuberculosis*

The homologous bifunctional PBPs in *E.coli*, PBP1a and PBP1b, seem to function in different subcellular complexes [3] and have been shown to have discrete interaction partners [27,28]. We hypothesized that PonA1 and PonA2 would also have discrete interacting factors. Indeed, our previous work showed that PonA1 localizes to two distinct subcellular compartments, the septum and the cell pole, where it likely has

Figure 4.1. Schematic of experimental determination of genetic and chemical interactions in *M. tuberculosis*. Transposon mutagenesis is a powerful method to identify interactions between specific genes in a bacterial genome. Transposons are introduced into the *Mtb* genome via phage. The genomic location of the transposon insertion is determined via highthroughput sequencing and mapping of sequence reads to the genome. Genetic interactions can be identified by a differential transposon insertion profile in a gene (e.g. *gene B*) in wildtype cells versus mutant cells (e.g. *ΔgeneD::*Abx^R). The loss of *geneB* and *geneD*, either through transposon disruption or directed knockout, is lethal to cells whereas cells survive the single gene mutations. Genetic interactions can be confirmed in two different ways, either by the complementary reverse whole genome screen or by targeted knockouts. Cellular assays, for example with drug inhibition of a pathway of interest (here, cell wall synthesis), can determine the relative contribution of genetic interacting factors to the cell pathway being targeted. Abx^R, antibiotic resistance cassette.

Figure 4.1 (Continued)

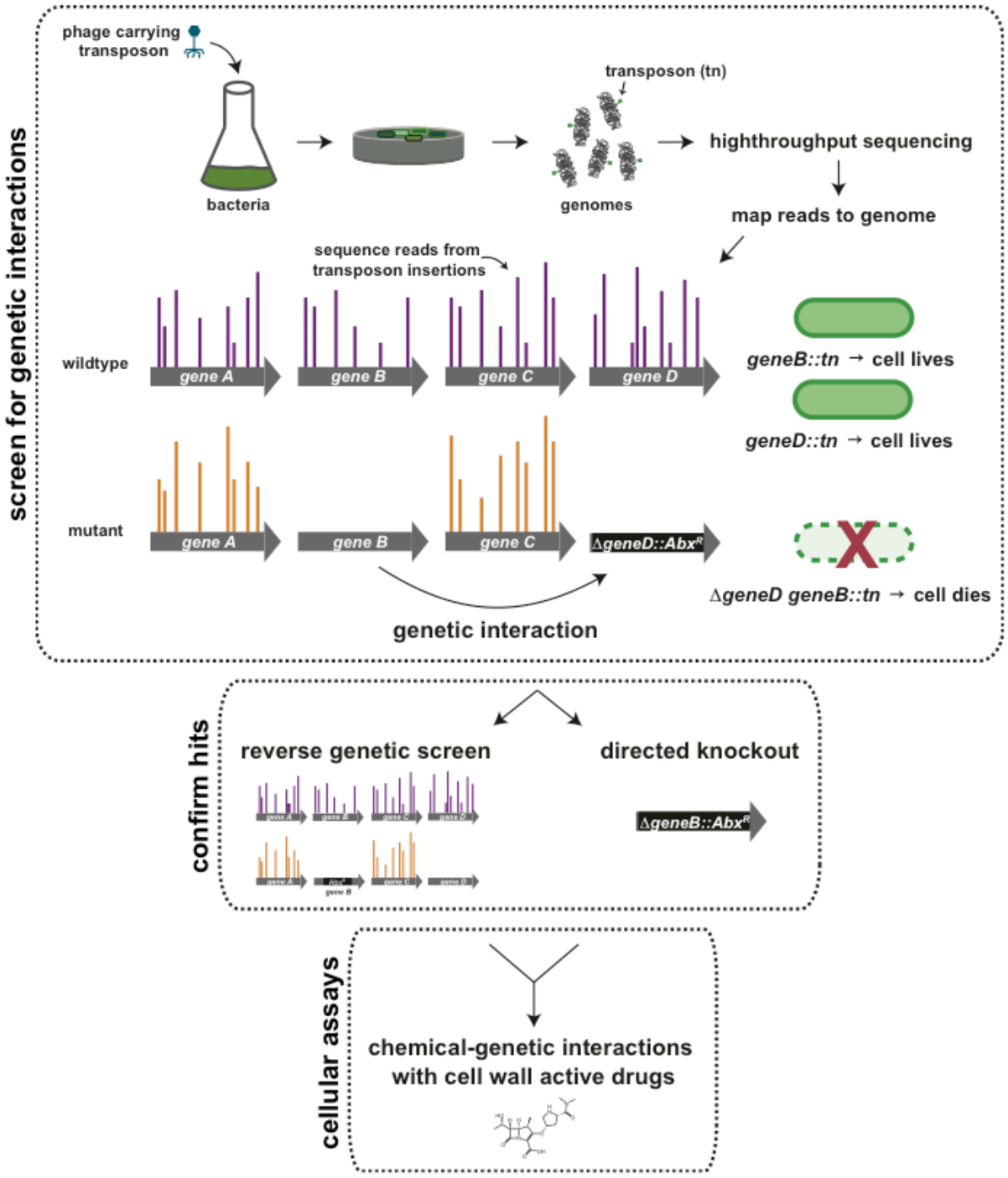

A

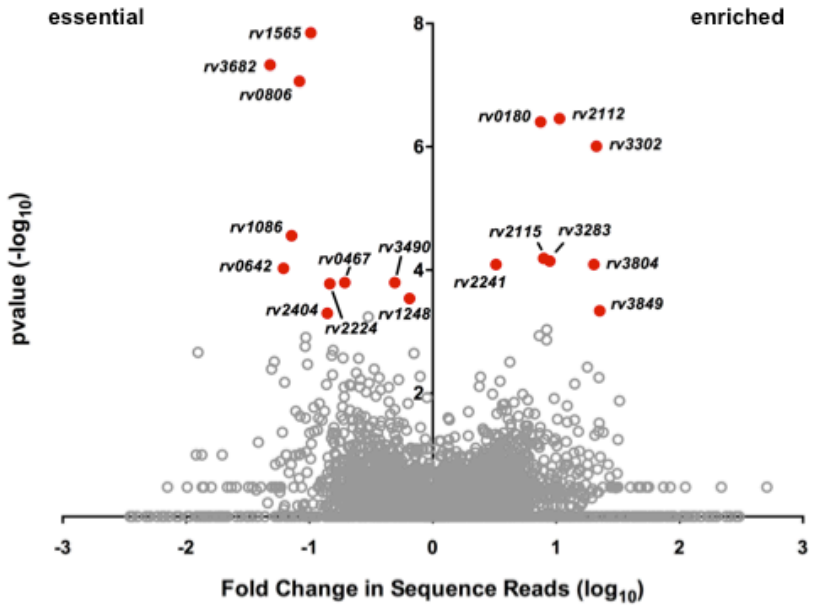

B

	Cellular Pathway	Name	Locus	p-value	Fold Change
essential loss kills *ΔponA1* cells	cell wall/membrane	Rv1565	*rv1565*	1.4E-08	9.8
	cell wall/membrane	PonA2	*rv3682*	4.7E-08	20.8
	cell wall/membrane	CpsY	*rv0806*	8.6E-08	12.0
	cell wall/membrane	Rv1086	*rv1086*	2.8E-05	13.9
	cell wall/membrane	MmaA4	*rv0642*	9.4E-05	16.2
	cell wall/membrane	OtsA	*rv3490*	1.6E-04	2.0
	cell wall/membrane	CaeA	*rv2224*	1.7E-04	6.8
	metabolism	Icl	*rv0467*	1.6E-04	5.2
	metabolism	Rv1248	*rv1248*	2.9E-04	1.5
	translation	LepA	*rv2404*	5.0E-04	7.2
enriched loss benefits *ΔponA1* cells	cell wall/membrane	Rv0180	*rv0180*	3.9E-07	0.1
	cell wall/membrane	FbpA	*rv3804*	8.1E-05	0.0
	pupylation	Dop	*rv2112*	3.5E-07	0.1
	pupylation	Mpa	*rv2115*	6.4E-05	0.1
	transcription factor	EspR	*rv3849*	4.6E-04	0.0
	metabolism	GlpD2	*rv3302*	9.8E-07	0.0
	metabolism	SseA	*rv3283*	7.1E-05	0.1
	metabolism	AceE	*rv2241*	8.1E-05	0.3

Figure 4.2. Quantitation of the genetic interactions of the peptidoglycan synthases PonA1. (A) PonA1's genetic interactions were determined by transposon mutagenesis and quantitated by assessing the difference in sequence reads at each locus in the genome. Loci whose sequence reads were significantly different between wildtype and *ΔponA1* cells (p-value < 0.001 by the Mann-Whitney U test, red circles) are plotted according to their p-value and fold change in sequence reads from wildtype (calculated from the geometric mean). Many loci did not have a significant change in reads between *ΔponA1* and wildtype (gray circles). **(B)** Specific quantitation values and predicted cell pathways for each significantly different locus.

different interacting partners [4] (Chapter 3). To identify PonA2's genetic interactors, we performed a similar whole genome screen as that performed in *ΔponA1* cells (Figure 4.1). We expected to identify *ponA1* in this screen, as a reverse confirmation of the genetic interaction between *ponA1* and *ponA2* from our *ΔponA1* screen (Figure 4.1). Indeed, we identified *ponA1* in the *ΔponA2* screen (Figure 4.3A), however, we identified multiple additional factors predicted to be required in *ΔponA2* cells (Figure 4.3B). These included factors that were both similar to (*rv3490* and *rv1248*) and different from the factors predicted to genetically interact with *ponA1*. Together, these data strongly suggest that PonA1 and PonA2 coordinate peptidoglycan synthesis in *Mtb*, and that the cell requires at least either *ponA1* or *ponA2* to be expressed. The lower number of factors that genetically interacted with PonA2 may indicate that PonA1 forms more interactions in the cell and/or is more active during normal growth in *Mtb*, as is true in *Msm* [29] (Chapter 3).

PonA2 is required for PG synthesis in the absence of PonA1

In addition to a reverse genetic screen, a complementary method to test the predicted essentiality of candidate factors (i.e. *ponA2*'s predicted requirement in *ΔponA1* cells) is to generate targeted knockouts (Figure 4.1). Because deletion of a candidate gene in *ΔponA1* cells would be lethal (Figure 4.1), we employed an allelic exchange strategy to test the essentiality of the screen's predictions (Figure 4.4). Our complementary genetic screens confirmed the genetic interaction between *ponA1* and *ponA2* (Figure 4.1, 4.2, 4.3). Hence, PonA2 was an excellent example to test the robustness of the allelic exchange system to demonstrate that either PonA1 or PonA2 is absolutely required for proliferation of *Mtb* as predicted (Figure 4.5A). We therefore generated a *ponA2* knockout in a strain whose only copy of *ponA1* is at the L5 phage integration site (*ΔponA1* L5::*ponA1*$_{wt}$, Figure 4.4). We also generated a *ponA2* knockout in wildtype H37Rv *Mtb* as a control. *ΔponA2* and *ΔponA1* L5::*ponA1*$_{wt}$ *ΔponA2* cells grew at rates similar to wildtype *Mtb* (Figure 4.5B) and exhibit similar rod-shaped morphology to wildtype cells (Figure 4.5C), although loss of *ponA2* does moderately impact cell width (Figure 4.5D).

We then tested whether we could remove *ponA1* from the genome of *ΔponA1* L5::*ponA1*$_{wt}$ *ΔponA2* cells using allelic exchange [30] (Figure 4.4). When we transformed these cells with a vector that encoded

A

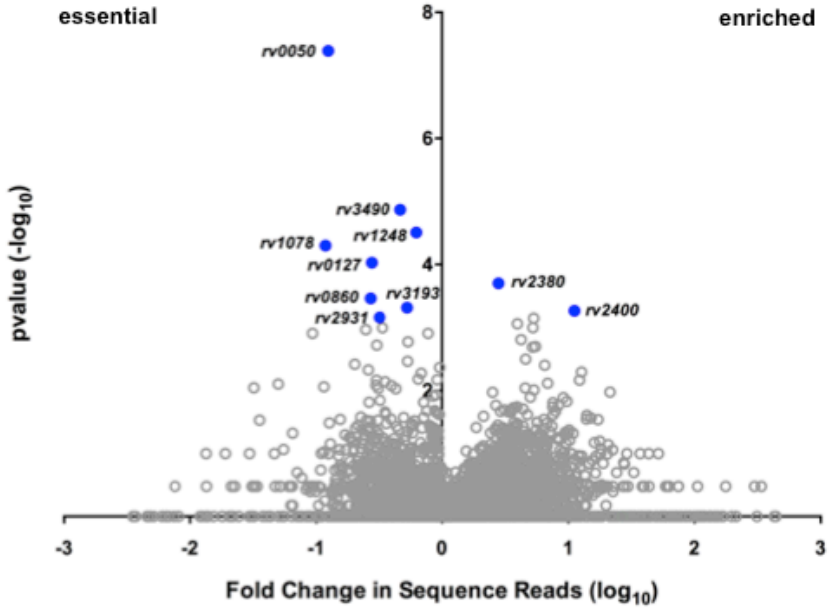

B

	Cellular Pathway	Name	Locus	p-value	Fold Change
essential loss kills ΔponA2 cells	cell wall/membrane	PonA1	*rv0050*	4.1E-08	8.0
	cell wall/membrane	OtsA	*rv3490*	1.4E-05	2.1
	cell wall/membrane	Pra	*rv1078*	5.0E-05	8.4
	cell wall/membrane	Rv3193	*rv3193*	4.8E-04	1.9
	cell wall/membrane	PpsA	*rv2931*	6.9E-04	3.1
	metabolism	Rv1248	*rv1248*	3.1E-05	1.6
	metabolism	Mak	*rv0127*	9.4E-05	3.6
	metabolism	FadB	*rv0860*	3.4E-04	3.7
enriched loss benefits ΔponA2 cells	mycobactin synthesis	MbtE	*rv2380*	2.0E-04	0.4
	cell wall/membrane	SubI	*rv2400*	5.4E-04	0.1

Figure 4.3 Quantitation of the genetic interactions of the peptidoglycan synthase PonA2. (A) PonA2's genetic interactions were determined by transposon mutagenesis and quantitated by assessing the difference in sequence reads at each locus in the genome. Loci whose sequence reads were significantly different between wildtype and *ΔponA2* cells (p-value < 0.001 by the Mann-Whitney U test, blue circles) are plotted according to their p-value and fold change in sequence reads from wildtype (calculated from the geometric mean). Gray circles denote non-significant loci. **(B)** Specific quantitation values and predicted cell pathways for each significantly different locus.

ponA1, bacterial growth was robust. However, transformation with a negative control vector that encoded the unrelated *tetR* gene blocked bacterial growth (Figure 4.5E). Similar transformations in the *ΔponA2* strain yielded robust bacterial growth (Figure 4.5E), confirming that lack of growth in the *tetR* transformed

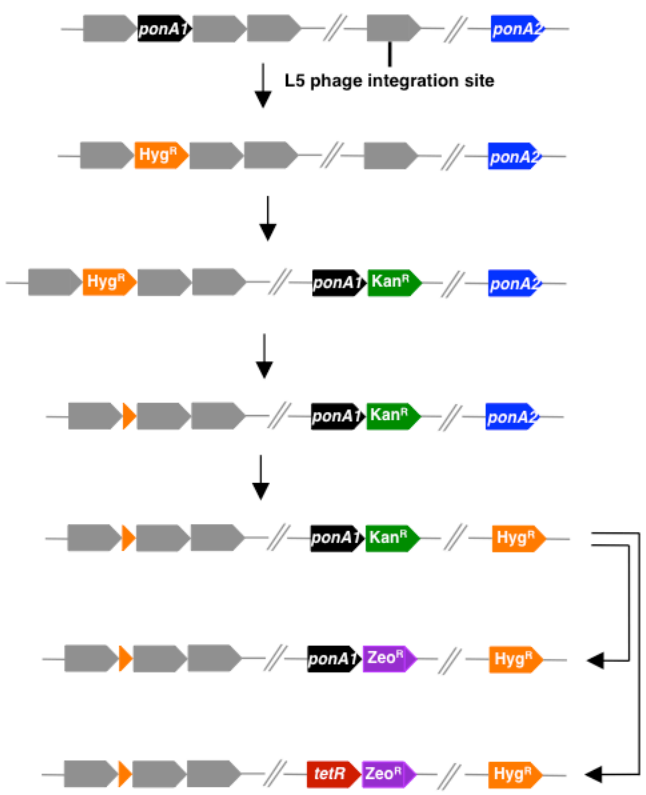

Figure 4.4. Allelic exchange system tests lethality of double mutants. The endogenous locus of *ponA1* is replaced with a hygromycin resistance cassette (Hyg^R) flanked by LoxP sites. A kanamycin (Kan^R)-marked copy of *ponA1* is integrated at the L5 phage site. The Hyg^R is removed from the chromosome by Cre recombinase. The gene of interest (*ponA2* is diagrammed here as an example) is replaced with Hyg^R. The resulting strain is transformed with a vector that integrates at the same L5 phage integration site that encodes a zeocin (Zeo^R)-marked *ponA1* or the negative control gene *tetR*. If the gene of interest is required in the absence of *ponA1*, cells wil not grow when transformed with the *tetR* vector.

ΔponA1 L5::$ponA1_{wt}$ cells was specific to the loss of *ponA1*. These data indicate that PonA2 is required in the absence of PonA1 in *Mtb* and that both enzymes have complementary roles in PG biogenesis in *Mtb*, which is distinct from the roles of these enzymes in *Msm* [4,29] (Chapter 3).

Rv1086 is required for cell wall synthesis in cells that lack PonA1

Cell wall synthesis cannot proceed without the critical lipid carrier to which cell wall precursors are attached [31]. The *Mtb* lipid carrier decaprenyl phosphate is distinct from that observed in many other rod-

Figure 4.5. The peptidoglycan synthase PonA2 functions in place of PonA1 in *ΔponA1* cells. (A) Sequence reads (gray or red vertical bars) that represent individual transposon insertions are visualized at the *rv3680-rv3683* genomic region, which spans *ponA2*, in *ΔponA1* cells (red) or wildtype cells (gray). Each possible transposon insertion site (TA dinucleotide) is depicted as short black vertical lines. Genes are displayed as gray arrows. The scale bar indicates density of sequence reads. **(B)** Population growth of wildtype H37Rv, *ΔponA2*, and *ΔponA1* L5::*ponA1*$_{wt}$ *ΔponA2* cells in standard laboratory media was measured by OD_{600} daily. **(C)** Cell morphology for cells in (B) was analyzed with light microscopy. Scale bar, 2μm. **(D)** Single cell length and width of *ΔponA2* and wildtype cells was quantitated. *ΔponA2* cells, although rod-shaped, are moderately wider than wildtype (approximate p-value < 0.0001 by the Kolmogorov-Smirnov test). **(E)** Colony forming units (CFU) were enumerated from transformation plates of an allelic exchange with either a vector that encodes *ponA1* (+*ponA1*) or a negative control vector that encodes the unrelated *tetR* (+*TetR*) in the *ΔponA1* L5::*ponA1*$_{wt}$ *ΔponA2* strain or the *ΔponA2* strain (both plates had lawn growth, and CFU counts were arbitrarily set to 6000).

Figure 4.5 (Continued)

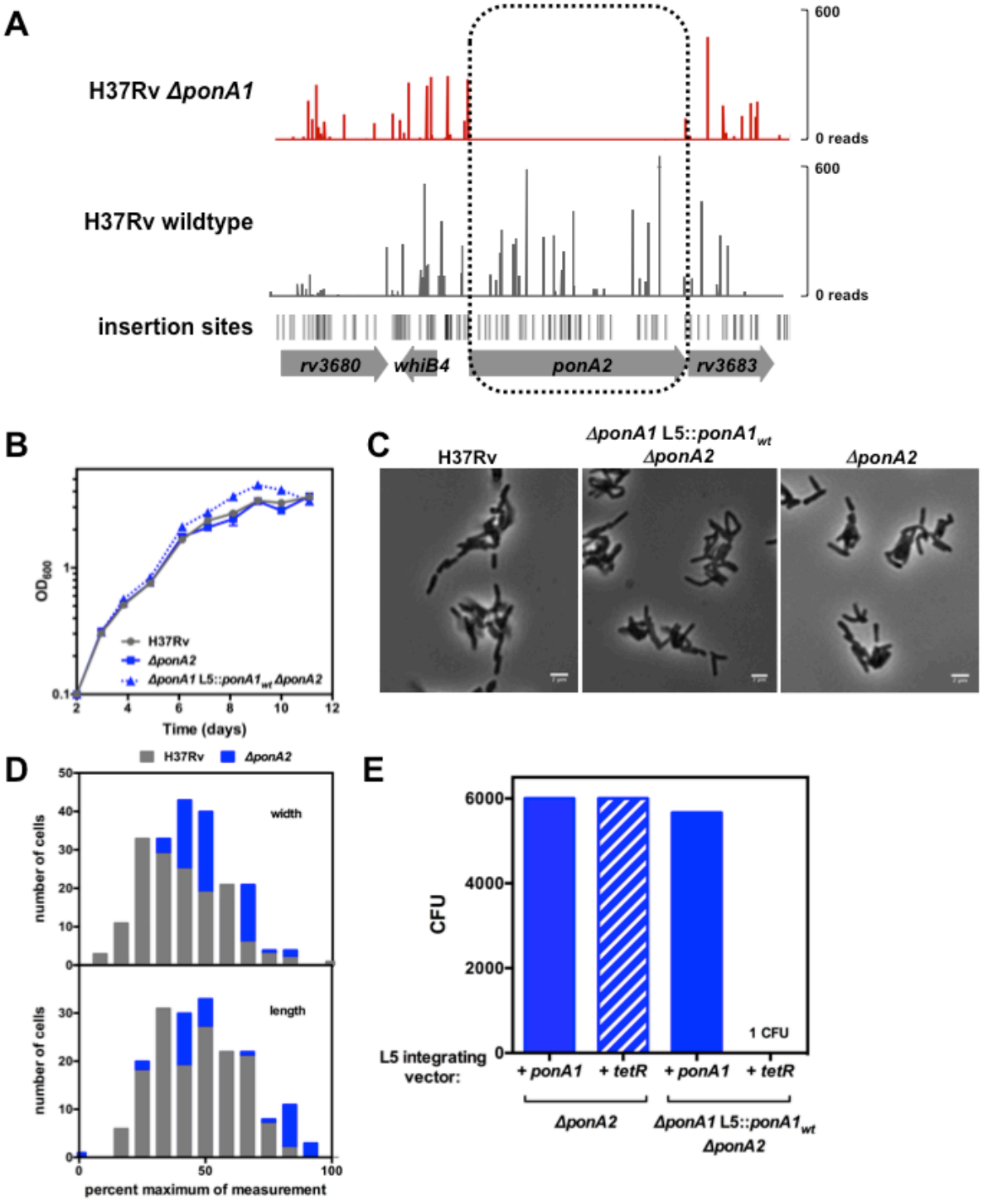

Figure 4.6. The *Z*-isoprenyl diphosphate synthase Rv1086 is required in *ΔponA1* cells. (A) Transposon insertions represented by their sequence reads (gray or red vertical bars) are visualized at the *rv1085-rv1087* genomic region, in *ΔponA1* (red) or wildtype cells (gray). Each possible transposon insertion site is depicted as short black vertical lines. Genes are displayed as gray arrows. The scale bar indicates density of sequence reads. **(B)** Population growth of wildtype, *Δrv1086*, and *ΔponA1* L5::*ponA1*$_{wt}$ *Δrv1086* cells in standard laboratory media was measured by OD_{600} daily. **(C)** Cells in (B) were imaged with light microscopy. Scale bar, 2μm. **(D)** Cell length and width of wildtype and *Δrv1086* cells were quantitated. No significant difference in either measurement was found. **(E)** Allelic exchange with a *+ponA1* or *+tetR* vector in *Δrv1086* cells or the *ΔponA1* L5::*ponA1*$_{wt}$ *Δrv1086* cells.

Figure 4.6 (Continued)

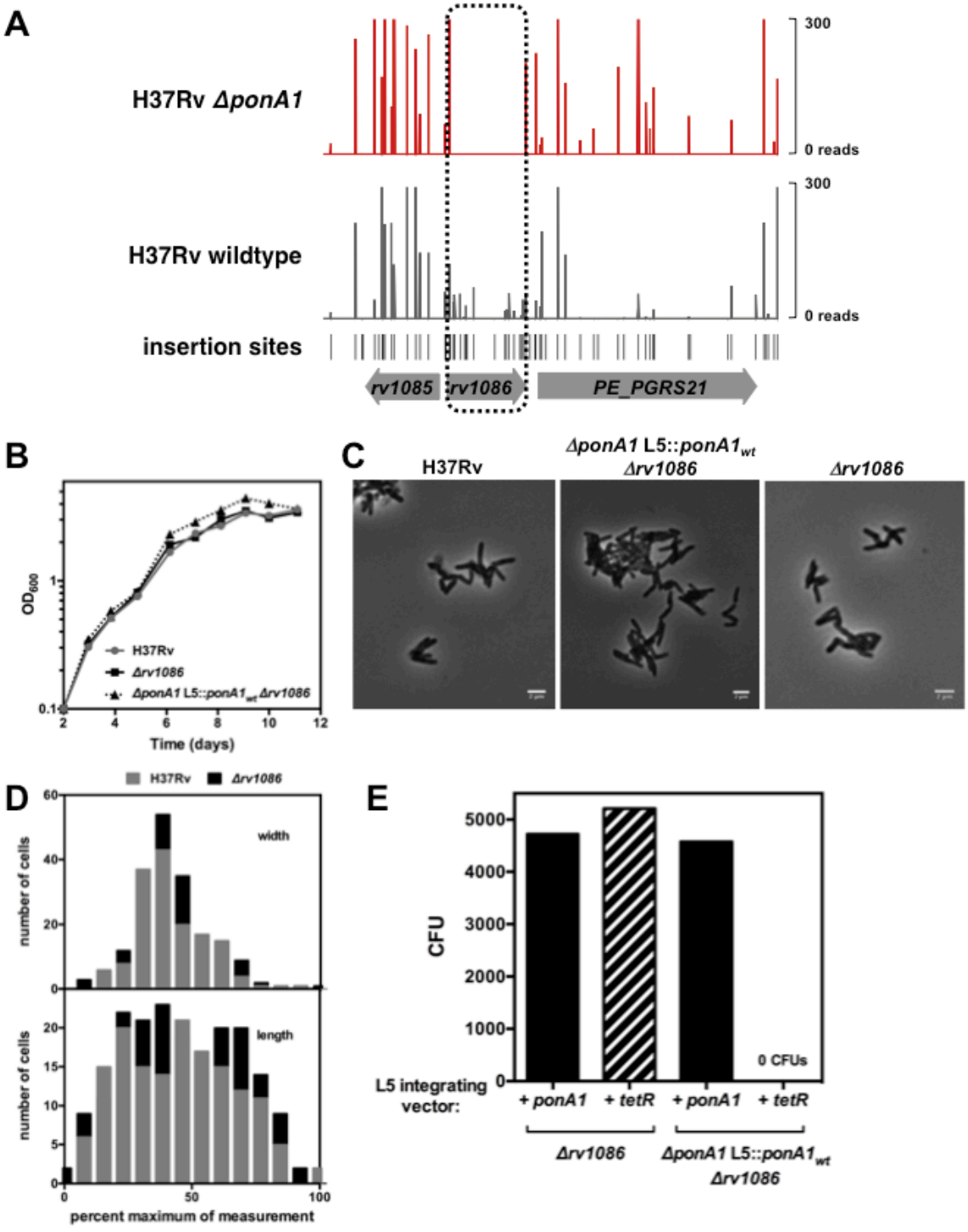

shaped organisms such as *E. coli*, which uses undecaprenyl phosphate [31]. Rv1086, a *Z*-isoprenyl diphosphate synthase carries out the first committed step in the synthesis of this lipid carrier [31-33], and our screen predicted Rv1086 was required in cells that lack PonA1 (Figure 4.2A, 4.6A). To test this prediction, we generated a knockout of *rv1086* in the *ΔponA1* L5::$ponA1_{wt}$ background as well as in wildtype *Mtb* as a control. Cells lacking *rv1086* in either background grew similarly to wildtype *Mtb* (Figure 4.6B) and exhibited similar cell shape (Figure 4.6C,D). We then tested whether we could eliminate *ponA1* from the chromosome of *ΔponA1* L5::$ponA1_{wt}$ *Δrv1086* cells by allelic exchange. Transformation of this strain with a $ponA1^{+}$ vector fully rescued bacterial growth, whereas transformation with the negative control vector completely blocked growth (Figure 4.6E). Transformation of *Δrv1086 Mtb* with either vector did not impact bacterial growth (Figure 4.6E). These data demonstrate that *rv1086* is specifically required in cells that lack *ponA1*. These results may indicate that the remaining bifunctional PG synthase in these cells, PonA2, requires a dedicated pool of precursors (perhaps because its kinetic rate of polymerization is slower than PonA1's) or that defects in cell wall synthesis result in an accumulation of lipid-linked cell wall precursors [34], to which the cell responds by necessitating lipid carrier synthesis.

Because decaprenyl phosphate forms the lipid base for both peptidoglycan and arabinogalactan precursors [35,36], we hypothesized that *Δrv1086* cells may display differential susceptibility to antibiotics known to target both of these synthetic pathways (see Figure 4.1). To test this hypothesis, we treated *Δrv1086* and wildtype *Mtb* with ethambutol, which targets AG synthesis [37], as well as teicoplanin and meropenem, which target PG synthesis [19,38]. We found that *Δrv1086* cells were 8-fold more sensitive to ethambutol and teicoplanin and 4-fold more sensitive to meropenem compared to wildtype *Mtb* (Figure 4.7), supporting its role in synthesis of the lipid carrier required for both PG and AG and that defects in lipid carrier synthesis impact multiple macromolecules of the cell wall.

CpsY is likely required for cell wall biogenesis in the absence of PonA1

CpsY has been annotated as a putative UDP-glucose-4-epimerase that may interchange glucose and galactose and other close homologues appear to not exist in the *Mtb* genome [39]. However, CpsY orthologues exist in other pathogenic mycobacteria, including *Mycobacterium leprae*, *Mycobacterium*

bovis, and *Mycobacterium marinum*, but does not exist in the nonpathogenic *Msm* (tuberculist.epfl.ch). UDP-glucose is directly utilized for the galactan moiety of arabinogalactan [36], and we chose to investigate whether CpsY is involved in cell wall synthesis. The whole genome screen predicted CpsY to be required in *ΔponA1* cells (Figure 4.2, 4.8A). We attempted to generate a *cpsY* knockout in *ΔponA1* L5::$ponA1_{wt}$ cells three times without success. However, we did delete *cpsY* from wildtype *Mtb*, suggesting that the knockout construct was correct. There may be slight differences in *ponA1* expression in the complemented mutant strain (*ΔponA1* L5::$ponA1_{wt}$) that prevented the deletion of *cpsY*. Cells that lack *cpsY* grow at rates similar to wildtype *Mtb* (Figure 4.8B) and also exhibit similar rod morphology (Figure 4.8C), although the loss of *cpsY* did moderately impact cell width (Figure 4.8D). These data suggest that *cpsY* was not required for normal bacterial growth and that its role in cell wall biogenesis likely becomes critical when cell wall synthesis has been compromised in some manner (e.g. deletion of *ponA1*).

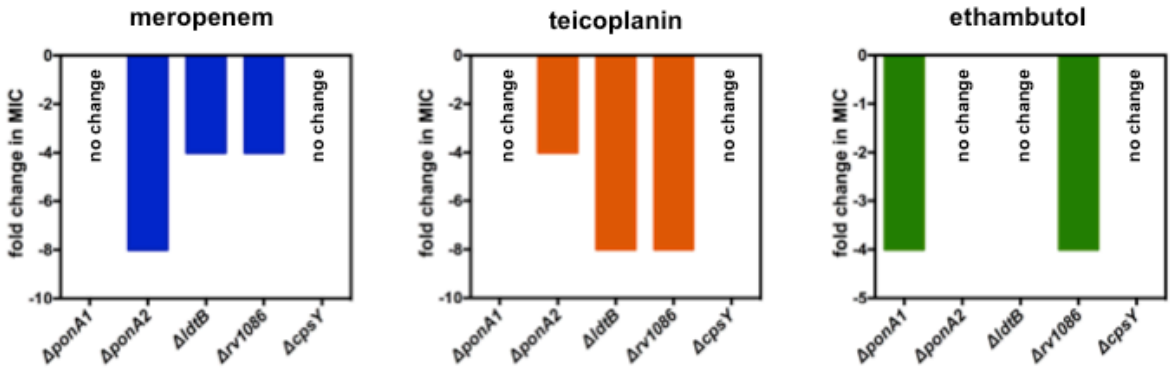

Strain	MIC
H37Rv	5 µg/ml
ΔponA1	5 µg/ml
ΔponA2	0.625 µg/ml
ΔldtB	1.25 µg/ml
Δrv1086	1.25 µg/ml
ΔcpsY	5 µg/ml

Strain	MIC
H37Rv	4 µg/ml
ΔponA1	4 µg/ml
ΔponA2	1 µg/ml
ΔldtB	0.5 µg/ml
Δrv1086	0.5 µg/ml
ΔcpsY	4 µg/ml

Strain	MIC
H37Rv	1.25 µg/ml
ΔponA1	0.3125 µg/ml
ΔponA2	1.25 µg/ml
ΔldtB	1.25 µg/ml
Δrv1086	0.3125 µg/ml
ΔcpsY	1.25 µg/ml

Figure 4.7. Cell wall active antibiotics interact differently with cell wall synthase mutants. *ΔponA1*, *ΔponA2*, *ΔldtB*, *Δrv1086*, and *ΔcpsY Mtb* cells were treated with meropenem, teicoplanin, or ethambutol. Fold change in minimum inhibitory concentration (MIC) for each drug was calculated by comparing each mutant's MIC to wildtype H37Rv's MIC for each drug.

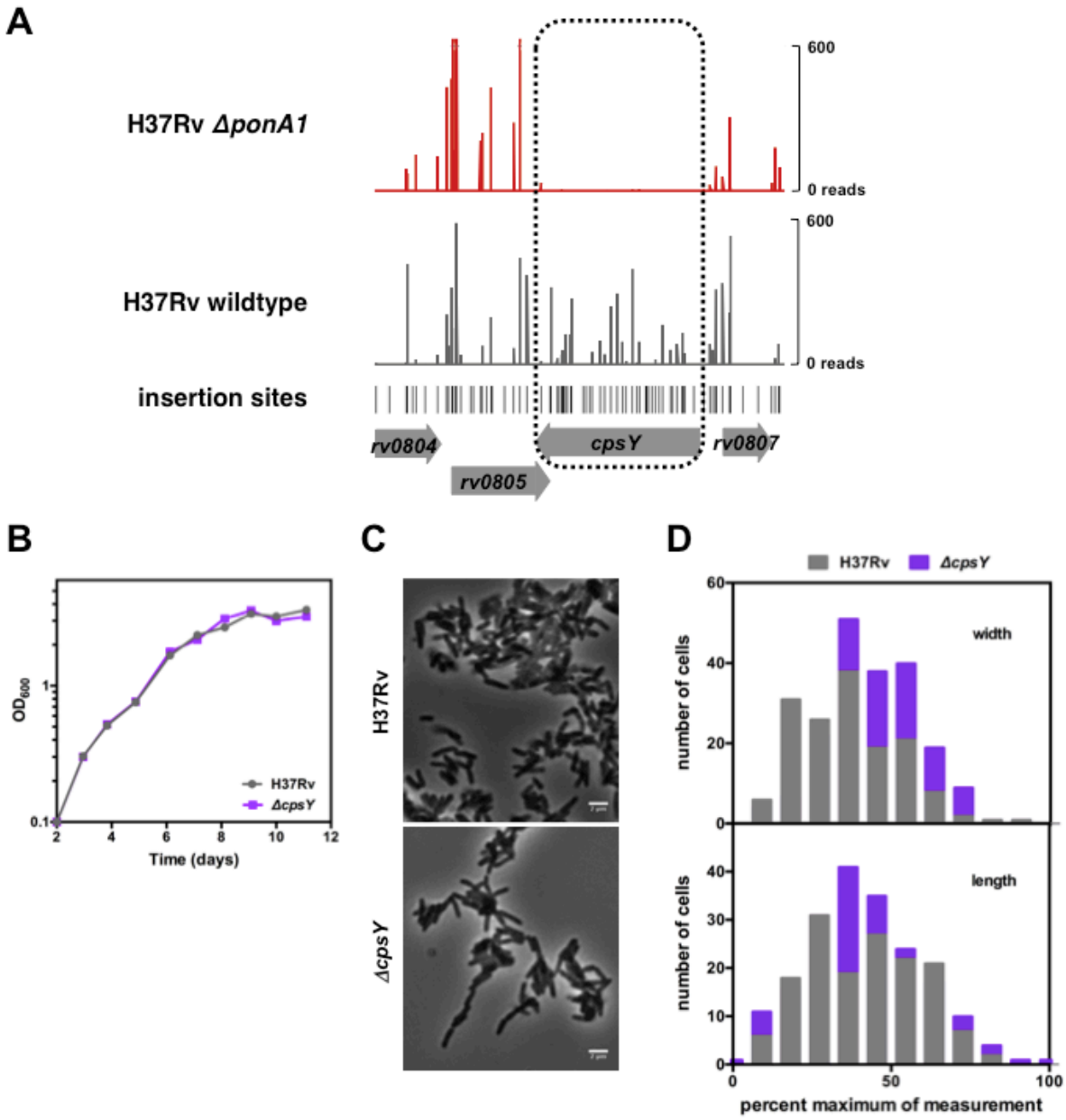

Figure 4.8. The putative UDP-galactose epimerase CpsY is likely required in *ΔponA1* cells. (A) Transposon insertions represented by their sequence reads (gray or red vertical bars) are visualized at the *rv0804-rv0807* genomic region, which spans *CpsY*, in *ΔponA1* (red) or wildtype cells (gray). Each possible transposon insertion site is depicted as short black vertical lines. Genes are displayed as gray arrows. The scale bar indicates density of sequence reads. **(B)** Population growth of wildtype and *ΔcpsY Mtb* cells in standard laboratory media was measured by OD_{600} daily. **(C)** Cells in (B) were assessed for morphology changes with light microscopy. Scale bar, 2μm. **(D)** Width and length of single cells in (B) and (C) was quantitated. Loss of *cpsY* moderately increased cell width (approximate p-value < 0.0001 by the Kolmogorov-Smirnov test).

Because of CpsY's interesting putative biochemical activity and its apparent role in pathogenic mycobacterial cell wall synthesis, we hypothesized that cells that lack *cpsY* would display differential tolerance to drugs that target cell wall biogenesis (see Figure 4.1). *ΔcpsY* cells did not show substantial changes in susceptibility to either ethambutol, teicoplanin, or meropenem (Figure 4.7), which may suggest that other enzymes compensate for CpsY activity in the presence of these drugs.

Correlated synthesis of classical and non-classical crosslinks is required for normal bacterial growth

We previously hypothesized that non-classical PG transpeptidases (that generate 3–3 peptidoglycan crosslinks instead of the 'classical' 4–3 crosslinks) may play a role in normal cell growth and could participate in the elongation complex [2]. Furthermore, because the monofunctional 4–3 transpeptidases PBPA and PBPB both localize to the septum in mycobacteria [40,41], the bifunctional enzymes PonA1 and PonA2 may be the only 4–3 crosslinking enzymes active during cell elongation. Because of this spatial separation and because mycobacterial PG contains frequent 3–3 crosslinks [7,8] we were interested in directly testing the hypothesis that a 3–3 crosslinking transpeptidase may be required in cells that lack a major bifunctional 4–3 transpeptidase. To that end, we investigated the role of LdtB (*rv2518*) in cells that lack PonA1.

To test whether LdtB was critical for cell growth in the absence of PonA1 (Figure 4.9A), we generated an *ldtB* knockout in *ΔponA1* L5::*ponA1*$_{wt}$ cells. We also deleted *ldtB* from the genome of wildtype *Mtb* as a control. Cells that lack *ldtB* grew at rates similar to wildtype, although loss of *ldtB* did diminish population growth at later growth stages. This defect was rescued in *ΔponA1* L5::*ponA1*$_{\mathrm{wt}}$ cells likely due to the strong promoter that drives *ponA1* at the L5 integration site (Figure 4.9B). *ΔldtB* cells also exhibit cell shape defects (Figure 4.9C). Loss of *ldtB* diminishes cell length, as has been previously reported [11], and substantially increases the width of the cell (Figure 4.9D). These data support a role for LdtB in maintaining proper cell shape and demonstrate that appropriate 3–3 PG crosslinking during cell growth and division is required for robust proliferation. We then tested whether we could remove *ponA1* from the *ΔponA1* L5::*ponA1*$_{wt}$ *ΔldtB* cells via allelic exchange. The cells transformed with the *ponA1*$^{+}$ vector grew

Figure 4.9. The non-classical transpeptidase LdtB is critical in *ΔponA1* cells. (A) Transposon insertions represented by their sequence reads (gray or red vertical bars) are visualized at the *rv2516-rv2520* genomic region, which spans *ldtB*, in *ΔponA1* (red) or wildtype cells (gray). Each possible transposon insertion site is depicted as short black vertical lines. Genes are displayed as gray arrows. The scale bar indicates density of sequence reads. **(B)** Population growth of wildtype, *ΔldtB*, and *ΔponA1* L5::*ponA1*$_{wt}$ *ΔldtB* cells in standard laboratory media was measured by OD_{600} daily. **(C)** Cell shape of cells in (B) was visualized with light microscopy. Scale bar, 2μm. **(D)** Single cell length and width was quantitated for wildtype and *ΔldtB* cells. Cell width of *ΔldtB* cells was significantly different (approximate p-value < 0.0001 by the Kolmogorov-Smirnov test) as was cell length (approximate p-value < 0.0001 by the Kolmogorov-Smirnov test) compared to wildtype *Mtb*. **(E)** Colony forming units (CFU) from an allelic exchange with a *+ponA1* or *+tetR* vector in the *ΔldtB* strain or the *ΔponA1* L5::*ponA1*$_{wt}$ *ΔldtB* strain were counted at 3 weeks (left panel). CFU were not visible on the *tetR* transformed *ΔponA1* L5::*ponA1*$_{wt}$ *ΔldtB* plate, which was incubated another 2 weeks (right panel, the *+ponA1* plate is shown again for comparison). Low CFU on the *ponA1* transformed *ΔldtB* strain may be due to variability in the assay or could be a function of the lower density these cells reach at later growth stages (see data in (B)).

Figure 4.9 (Continued)

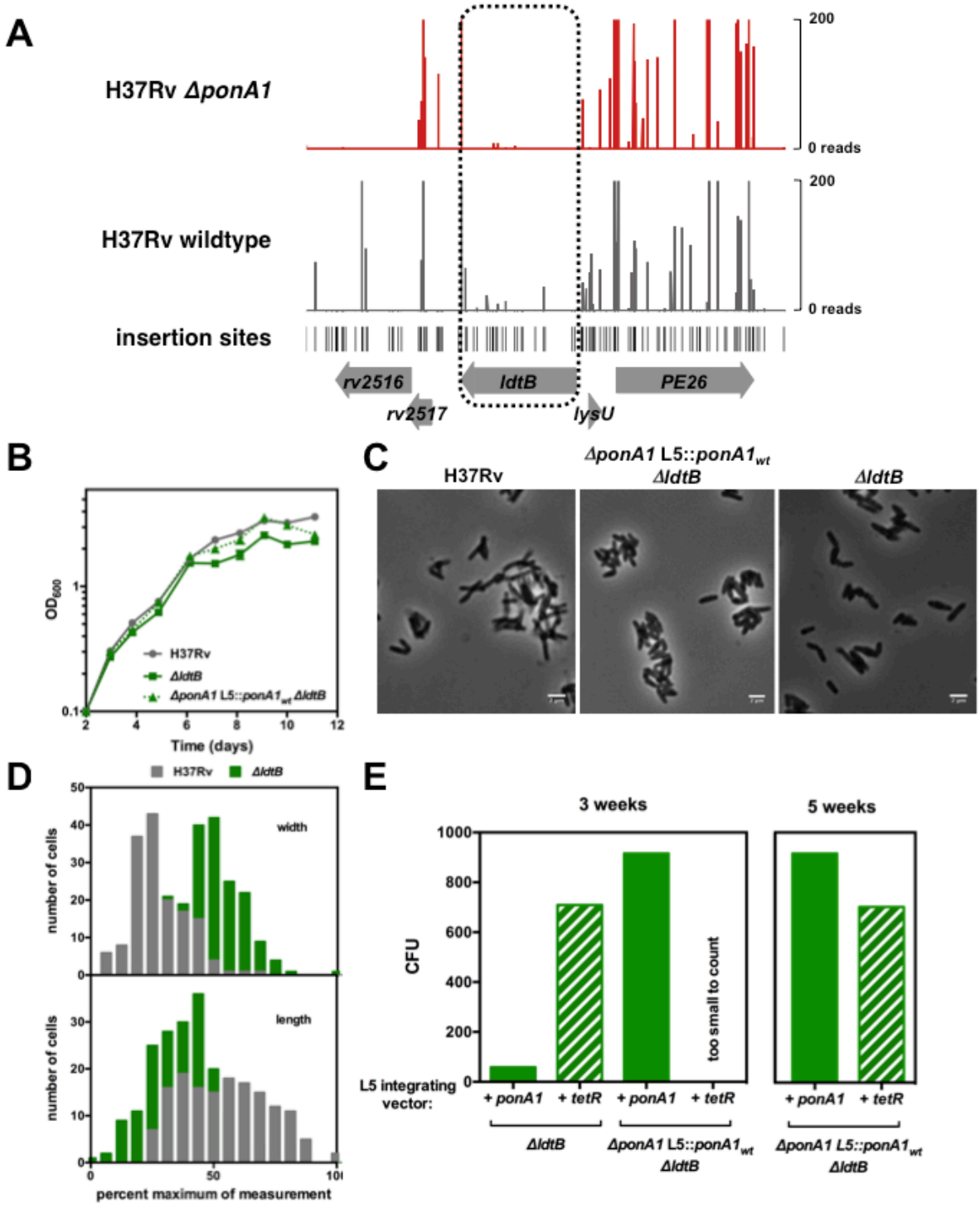

robustly after the usual 21 days (Figure 4.9E). However, the cells transformed with the negative control vector had formed barely visible colonies at 21 days. After 35 days, these *ΔponA1* L5::*tetR ΔldtB* colonies had grown to the normal size. These data show that loss of LdtB's activity in cells that have also lost PonA1 dramatically impacts cellular fitness, and that double mutants have a quantitative growth defect.

LdtB's genetic interactions

Because our data demonstrated that *Mtb* required both *ponA1* and *ldtB* for robust growth and maintenance of cell shape, we hypothesized that *ldtB* may also form similar genetic interactions with other PG synthases. To test this hypothesis, we generated a transposon mutant library in the *ΔldtB* strain and computationally assessed *ldtB*'s genetic interactions. We identified several cell wall associated genes that were predicted to be required in *ΔldtB* cells (Figure 4.10). Interestingly, *ponA2* was identified as essential in cells that lack *ldtB* (Figure 4.11A), which is phenocopied by the lack of transposon insertions in *ldtB* in cells that lack *ponA2* (Figure 4.11B). While *ponA1* was not predicted to be essential in *ΔldtB* cells (as our data also confirmed; Figure 4.9E), the magnitude of sequence reads in *ponA1* decreased (Figure 4.11C), indicating that loss of PonA1 function due to transposon disruption impacted survival of *ΔldtB* cells.

Furthermore, four factors overlap between those identified as essential in *ΔponA2* and *ΔldtB* cells, more than the overlap between *ponA1* and *ponA2* or *ponA1* and *ldtB*, strongly supporting that *ldtB* and *ponA2* function in a highly similar cellular pathway. *ΔldtB* and *ΔponA2* cells also display similar susceptibility profiles to teicoplanin, meropenem, and ethambutol, which is different than *ΔponA1* cells (Figure 4.7, Chapter 3). These data biologically support that LdtB and PonA2 function in a highly similar pathway within the cell and correlates with our biological evidence that *ponA1* and *ldtB* are together required for optimal growth. In sum, these data show that the cell requires either LdtB or one of the bifunctional peptidoglycan synthases (PonA1 or PonA2) for robust growth and may indicate that 4–3 and 3–3 crosslinking enzymes must coordinate their activity to promote bacterial survival as well as normal vegetative proliferation of *Mtb*.

A

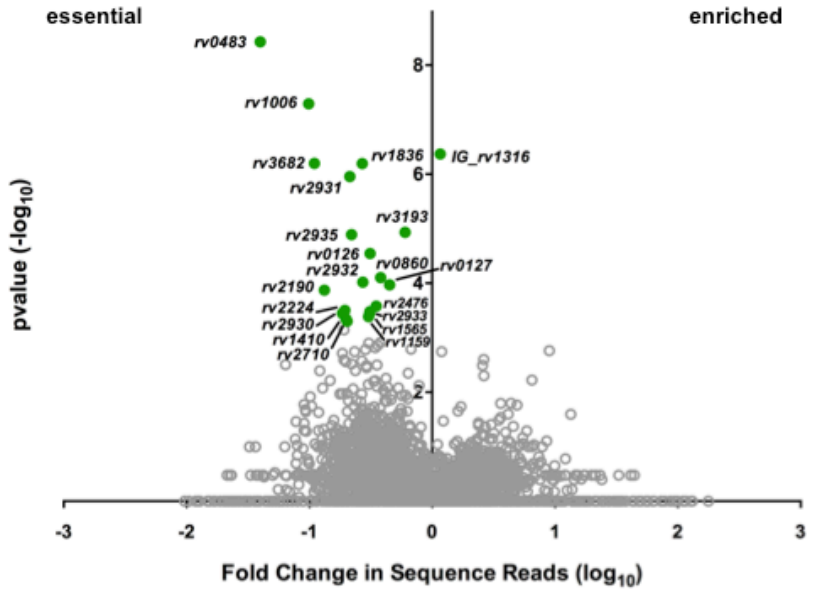

B

Cellular Pathway	Name	Locus	p-value	Fold Change
cell wall/membrane	LprQ	*rv0483*	3.7E-09	25.1
cell wall/membrane	PonA2	*rv3682*	6.3E-07	9.1
cell wall/membrane	Rv1836	*rv1836*	6.4E-07	3.7
cell wall/membrane	PpsA	*rv2931*	1.1E-06	4.7
cell wall/membrane	Rv3193	*rv3193*	1.2E-05	1.7
cell wall/membrane	PpsE	*rv2935*	1.3E-05	4.5
cell wall/membrane	TreS	*rv0126*	2.9E-05	3.2
cell wall/membrane	PpsB	*rv2932*	9.6E-05	3.7
cell wall/membrane	CaeA	*rv2224*	3.1E-04	5.1
cell wall/membrane	PpsC	*rv2933*	3.3E-04	3.2
cell wall/membrane	FadD26	*rv2930*	3.6E-04	5.4
cell wall/membrane	Rv1565	*rv1565*	3.6E-04	3.2
cell wall/membrane	Rv1410	*rv1410c*	4.5E-04	5.0
metabolism	Rv1006	*rv1006*	5.1E-08	10.1
metabolism	FadB	*rv0860*	7.9E-05	2.6
metabolism	Mak	*rv0127*	1.1E-04	2.2
metabolism	Gdh	*rv2476*	2.6E-04	2.9
metabolism	Rv1159	*rv1159*	4.1E-04	3.3
virulence/adaptation	Rv2190	*rv2190*	1.3E-04	7.6
transcription	SigB	*rv2710*	5.0E-04	4.9
metabolism	IG_Rv1316	*IG_rv1316*	4.3E-07	0.9

essential loss kills *ΔldtB* cells

enriched loss benefits *ΔldtB* cells

Figure 4.10 Quantitation of the genetic interactions of the nonclassical transpeptidases LdtB. (A) LdtB's genetic interactions were determined via whole genome transposon mutagenesis. Loci whose sequence reads were significantly different between wildtype and *ΔldtB* cells (p-value < 0.001 by the Mann-Whitney U test, green circles) are plotted according to their p-value and fold change in sequence reads from wildtype (calculated from the geometric mean). Loci without a significant change in reads are depicted as gray circles. **(B)** Specific quantitation values and predicted cell pathways for each significantly different locus.

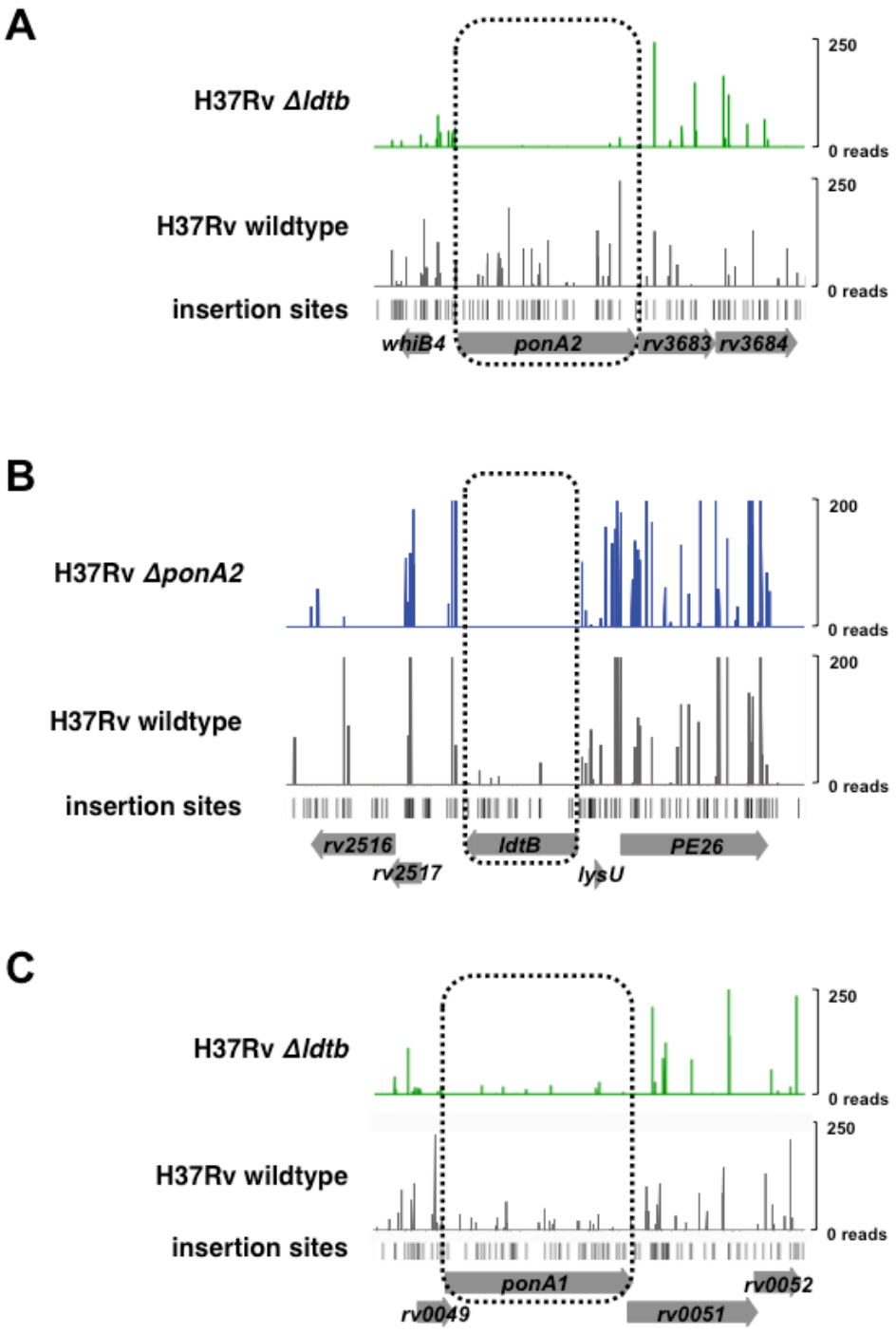

Figure 4.11. LdtB genetically interacts with PonA2. (A) Transposon insertions represented by their sequence reads (gray or green vertical bars) are visualized at the *rv3681-rv3684* genomic region, which spans *ponA2*, in *ΔldtB* (green) or wildtype cells (gray). Each possible transposon insertion site is depicted as short black vertical lines. Genes are displayed as gray arrows. The scale bar indicates density of sequence reads. **(B)** Transposon insertions represented by their sequence reads (gray or blue vertical bars) are visualized at the *rv2516-rv2519* operon, which spans *ldtb*, in *Δpona2* (blue) or wildtype cells (gray). **(C)** Transposon insertions represented by their sequence reads (gray or green vertical bars) are visualized at the *rv0049-rv0052* operon, which spans *ponA1*, in *ΔldtB* (green) or wildtype cells (gray).

Discussion

Our genetic experiments and chemical assays have elucidated cell wall synthesis networks in *Mtb*, which have highlighted unique biology between divergent peptidoglycan synthases as well as possible interactions the cell utilizes to synchronize the synthesis of its multiple cell envelope layers.

Putative EspR regulation of PonA1 activity

In addition to the cell wall synthase enzymes identified as essential in our screens, these genetic and computational methods allow the discovery of factors whose loss could be beneficial to a particular mutant. For example, disruption of EspR is better tolerated in *ΔponA1* cells than in wildtype cells (Figure 4.2A). Our previous work indicated that PonA1's intracellular activity must be tightly regulated to maintain normal bacterial growth and correct cell shape. Dysregulated PonA1 activity leads to ectopic polar growth and inhibition of bacterial proliferation (Chapter 3). EspR may be involved in maintaining normal PonA1 activity in the cell and hence is less important in the absence of PonA1. EspR is known to regulate a variety of cell wall associated factors [42]. We searched for the reported EspR consensus binding site and identified three putative EspR binding sites in the *ponA1* promoter region (using a *ponA1* start site at -426 nucleotides of the H37Rv genome annotation; see Chapter 3 for details). These three consensus sites fall at a similar upstream distance from *ponA1* as other reported EspR targets [42], supporting a putative role for EspR regulation of *ponA1* transcript (consensus site 1: ATTTGCGAC, 1430 nucleotides upstream; consensus site 2: ATTTGCTCA, 1387 nucleotides upstream; consensus site 3: CTTTGCTCC, 920 nucleotides upstream). Two additional weaker consensus binding sites also exist in the *ponA1* promoter region (weaker consensus site 1: CTTCGCCAC, 548 nucleotides upstream; weaker consensus site 2: GTTCGCGGT, 146 nucleotides upstream). Further experiments are needed to determine whether EspR indeed binds in this promoter region and influences *ponA1* transcript levels.

PonA1 and PonA2 have unique cellular roles

Although PonA1 and PonA2 are not individually required for growth of *Mtb* in culture, both of them cannot simultaneously be deleted from the cell (Figure 4.2, 4.5). Hence, *Mtb* controls its peptidoglycan synthesis differently than its saprophytic relative *Msm*, in which PonA1 is required for growth in culture. This may

relate to the different ecological niches these two organisms reside in. It seems advantageous to have two functioning enzymes that can promote essential cell wall synthesis, and the variable host environment may demand the flexibility that two separate enzymes can provide [2].

Two hypotheses can be posited for the presence of two homologous enzymes in a genome. Either a certain level of enzymatic activity is required and multiple enzymes ensure sufficient activity for cell growth or, alternatively, the two enzymes exist in distinct, but potentially overlapping, cellular pathways. Although PonA1 and PonA2 can complement each other's activity, several pieces of evidence indicate that they have distinct cellular roles, including their susceptibilities to host-like stresses or infection [29,43] (Chapter 3), as well as structural differences [44] and different impacts on cell shape (Figure 4.5, Chapter 3). These data may support a model wherein PonA1 and PonA2 exist in different subcellular complexes, as do the major bifunctional PBPs in *E. coli* [3]; perhaps PonA2 functions more in PG synthesis during cell division whereas PonA1 is required for PG synthesis during cell elongation.

The hypothesis that PonA1 and PonA2 hold distinct cellular roles is also supported by our whole genome screening data. Diverse cell wall synthase genes, such as *cpsY* and *rv1086*, become required in cells that lack PonA1, but not in cells that lack PonA2 (Figure 4.2). Indeed, few factors overlap between PonA1 and PonA2, and while our screens are not comprehensive, the saturation of our libraries (Figure 4.12A,B) indicates that we have likely identified all major candidates that genetically interact with *ponA1* and *ponA2*. The number of *ponA1* genetic interactions identified in cell wall synthesis genes suggests that cells without PonA1 have defects in several layers of the cell envelope (PG [*ponA2*], AG [*cpsY*], and MA [*mmaA4*, the mycolic acid modifying enzyme, and *fbpA*, involved in mycolic acid transport, both demonstrated altered read counts compared to wildtype], Figure 4.2). On the other hand, cells that lack PonA2 seem to exhibit fewer cell wall synthesis defects (Figure 4.3). The cell morphology phenotypes of *ΔponA1* (Chapter 3) and *ΔponA2* cells (Figure 4.5) combined with the level of cell wall synthetic genetic interactions (Figure 4.3) suggest that PonA1 may be the major cell wall synthase during active growth of *Mtb*. This may be due to differences in kinetic rates of PG polymerization between the enzymes or differential activity during different growth stages of the bacterium.

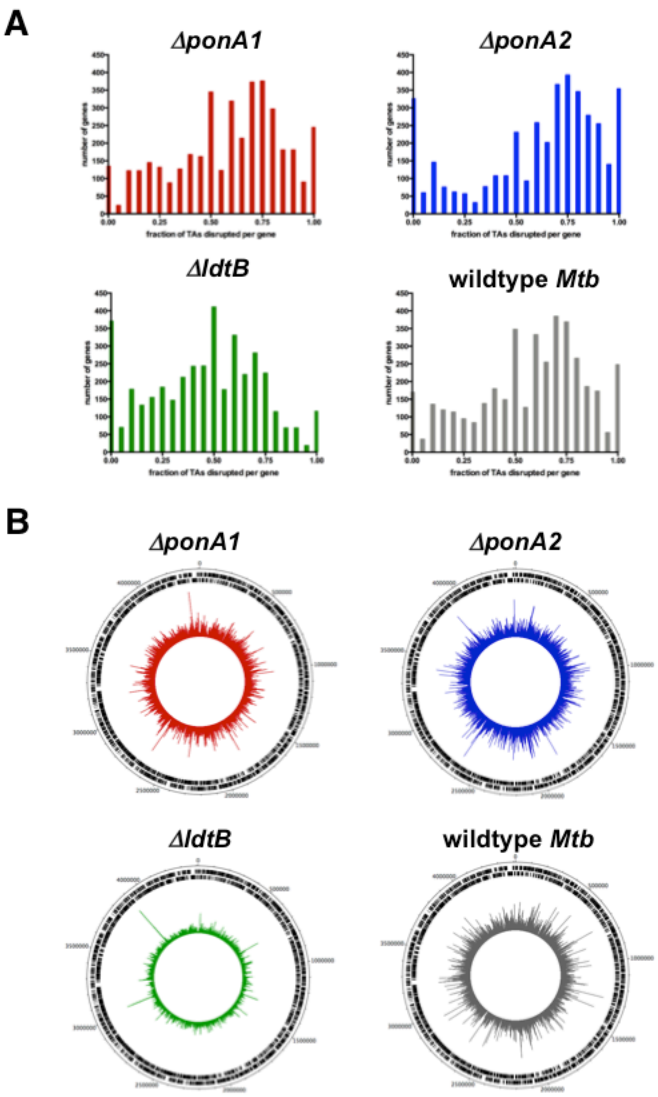

Figure 4.12. The transposon libraries are highly saturated. (A) The fraction of possible insertion sites (TA dinucleotides) that were actually disrupted by transposons was calculated per gene and plotted. These histograms can be used to estimate visually the true saturation of each library. Visual estimation of the *ΔponA1* library's saturation is circa 70%. The *ΔponA2* library is about 78% saturated. The *ΔldtB* library is circa 55% saturated, and wildtype *Mtb* is around 70% saturation. **(B)** The chromosomal distribution of sequence reads from the libraries was visualized with DNAPlotter.

Synthesis defects in distinct cell envelope macromolecules result in quantitative defects

Coordinated synthesis of the multiple *Mtb* cell envelope layers is critical for successful growth of the bacterium [45]. Our data predicted that simultaneous defects in PG and AG or MA synthesis abolish bacterial growth. The difference in sequence reads at the *cpsY* locus strongly suggests that CpsY is

required for survival of *ΔponA1* cells (Figure 4.8A). Furthermore loss of *cpsY* alters cell morphology, supporting its role in cell wall synthesis. Cells that lack PonA1 are 4-fold more susceptible to ethambutol (Figure 4.7), which indicates that an enzyme like CpsY, which becomes essential in these cells, functions in arabinogalactan synthesis. *ΔcpsY* cells do not exhibit an altered susceptibility to ethambutol (Figure 4.7), which suggests other enzymes compensate for its activity in a single mutant. These data together suggest that coordinated synthesis of arabinogalactan and peptidoglycan is required for cell survival, and that the cell may utilize CpsY and PonA1 to govern that coordination.

Lipid carrier synthesis promotes survival in cells with compromised cell envelope assembly

Our screen predicted that *rv1086*, involved in decaprenyl phosphate synthesis, was essential in *ΔponA1* cells, which we confirmed (Figure 4.6). These data indicate that cell wall synthesis that occurs in the absence of *ponA1* is divergent enough from wildtype levels that the cell attempts to promote envelope biogenesis by requiring the activity of Rv1086. Why does the cell specifically require the activity of the first dedicated enzyme in lipid carrier synthesis? One hypothesis is that the lipid carrier is being sequestered in the absence of *ponA1* due to faulty cell wall synthesis. This same lipid carrier is required for both AG and PG precursors [35,36,46] (Figure 4.13A), although for AG precursors, it is first decorated with specific moieties [36] that shunts the carrier specifically into AG synthesis. If insufficient pools of UDP-glucose exist (for example, in the absence of *cpsY*), the cell cannot continue arabinogalactan production and these lipid carriers will accumulate in the membrane (Figure 4.13A). Analogously, defects in peptidoglycan synthesis can also lead to sequestration of lipid carriers. Cells that lack PonA1 may exhibit abnormal rates of PG precursor incorporation, leading to a buildup of PG intermediates and depletion of the essential lipid carrier (Figure 4.13B). These data lead to a model wherein abnormal biogenesis of either PG or AG results in the buildup of lipid-linked precursors, similar to that observed in other organisms [34,47]. The cell attempts to overcome this limitation by requiring the activity of the first enzyme in lipid carrier synthesis (Figure 4.6).

Altogether, these data support a model wherein PonA1 and PonA2 guide cell wall synthesis with different spatial, and perhaps temporal, resolution. Their interacting partners and the rate of their respective

complex's cell wall synthesis appear different. Determining the spatiotemporal resolution of cell membrane associated proteins is technically challenging in mycobacteria, but would allow us to better understand the physiology of cell growth and cell wall synthesis in *Mtb*.

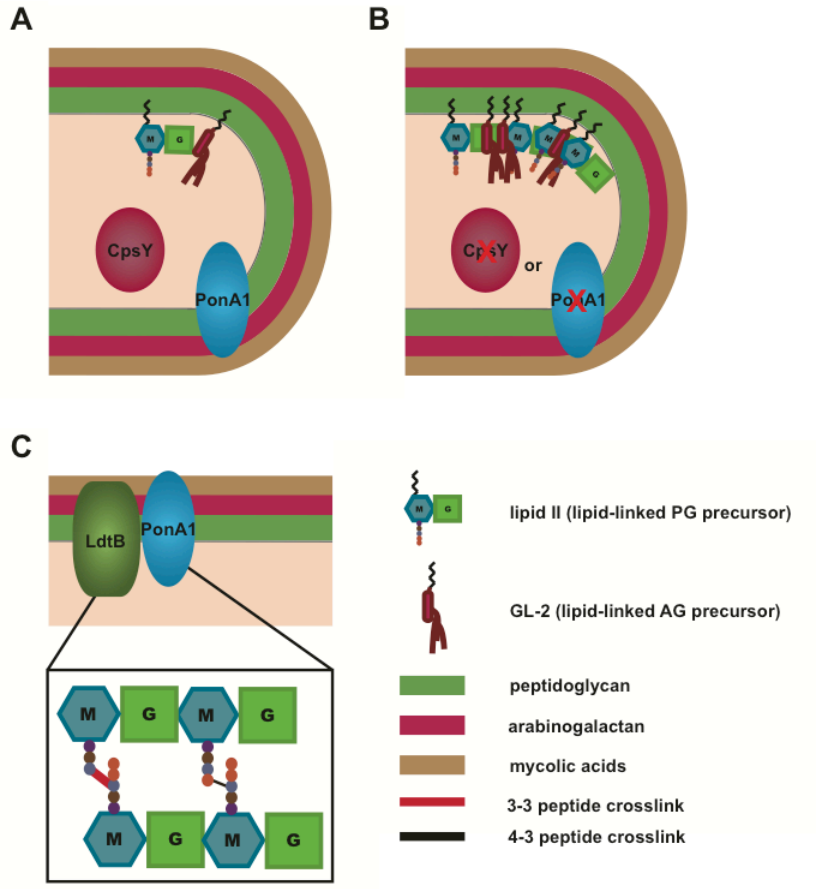

Figure 4.13. Robust cell wall synthesis requires adequate lipid carrier pools and correlation of classical and nonclassical PG transpeptidation. (A) Decaprenyl phosphate carries both peptidoglycan and arabinogalactan precursors in normal cell wall synthesis. **(B)** Changes in the activity of PonA1 or CpsY could result in the accumulation of lipid-linked precursors, damaging cell wall synthesis and cellular fitness. **(C)** Production of the critical nonclassical 3–3 peptide crosslinks, such as those synthesized by LdtB, must be correlated with the production of classical 4–3 crosslinks made by enzymes like PonA1 for robust cell growth.

Correlated synthesis of 4–3 and 3–3 crosslinking promotes bacterial growth

Because of the prevalence and importance of 3–3 crosslinks in *Mtb* biology, we previously hypothesized that 3–3 crosslinking enzymes likely play a predominant role during growth of *Mtb* [2]. Here, we tested

this hypothesis by assessing whether cell survival would be compromised in the absence of *ponA1* and *ldtB*. We demonstrated that *Mtb ΔponA1 ΔldtB* cells exhibit substantial growth defects, requiring almost twice as long to form colonies as wildtype or single mutant *Mtb* cells (Figure 4.9). These data suggest that PonA1 and LdtB correlate their PG crosslinking activity during normal growth and that their combined activity is required for normal cell fitness (Figure 4.9). These data are the first evidence that 4–3 and 3–3 transpeptidation is correlatively controlled in *Mtb*. Our genetic identification of the interaction between PonA2 and LdtB substantiates our findings – the cell clearly coordinates the 4–3 and 3–3 crosslinking of its peptidoglycan during growth. Much more remains to be discovered about how *Mtb* jointly governs these two enzymatic activities. Do Ldt enzymes exist in classical cell elongation complexes or in separate complexes? Do "classical" and "non-classical" peptidoglycan synthases interact? What are the spatiotemporal dynamics of these two distinct biochemical activities and how does the cell govern them?

The quantitative differences in the PonA1-LdtB and PonA2-LdtB interactions again suggest spatial resolution of these pathways. Investigating the spatial and temporal resolution of cell wall synthesis in *Mtb* is not only important for bacterial physiology, but could inform how cell wall active antibiotics work. These drugs interact with cell wall synthesis pathways to differing extents (Figure 4.5). Developing drugs that will target the most active cell wall synthesis pathways – and the most active enzymes in those pathways – is critical for clinical advances against tuberculosis.

Materials and Methods

Bacterial Strains and Growth Conditions

M. tuberculosis H37Rv was cultured in Middlebrook 7H9 salts supplemented with OADC (oleic acid, albumin, dextrose, catalase [BD Biosciences, Franklin Lakes, NJ]), 0.25% glycerol, and 0.05% Tween-80 or plated on 7H10 agar. Selection was performed at 50 μg/ml hygromycin, 25 μg/ml kanamycin, or 20 μg/ml zeocin for both liquid and solid media. *E. coli* Top10 (Invitrogen, Carlsbad, CA) were used for cloning and were cultured in LB broth or agar. Selection for *E. coli* occurred at 100 μg/ml hygromycin, 50

μg/ml kanamycin, or 20 μg/ml zeocin for both liquid and solid media. All strains were grown at 37°C. The construction of the *ΔponA1* and *ΔponA1* L5::*ponA1*$_{wt}$ *Mtb* strains were described in Chapter 3.

Transposon Mutagenesis

The H37Rv transposon libraries were generated using the ϕMycoMarT7 phagemid as previously described [48]. About 100,000 colonies were collected for each of the transposon libraries.

Genomic Library Construction and Highthroughput Sequencing

Genomic DNA (gDNA) was harvested from the transposon libraries as described [24]. To generate gDNA fragments amendable to highthroughput sequencing, the gDNA was sheared, end-repaired, A-tailed, and ligated to oligo adapters as described [24]. We amplified the transposon-containing gDNA through two-step PCR as described [24]. To identify the genomic position of the transposons, we subjected the amplified gDNA fragments to highthroughput sequencing using the Illumina (San Diego, CA) platform. A single replicate library was constructed for each strain and used in all downstream analyses.

Mapping and Counting Transposon Insertions

For the *ΔponA1* library, a FASTQ file was generated from the raw sequencing data using a custom Python script (all other libraries were sequenced on Illumina machines that automatically generated FASTQ files). Sequencing data were filtered for transposon-specific information and trimmed of all transposon sequence except for the TA dinucleotide insertion site using a custom Python script. Trimmed reads were then mapped to the H37Rv *Mtb* genome using Bowtie2 [49], which randomly assigns reads that map to multiple genomic sites. The *ΔponA1* library had 3.2M mapped reads with an average read count of 50. The *ΔponA2* library had 2.4M mapped reads with an average read count of 37. The *ΔldtB* library had 1.3M mapped reads with an average read count of 20. The wildtype *Mtb* library had 4.4M mapped reads with an average read count of 69.

The number of transposon insertions at each genomic TA site were counted using custom Python scripts. First, the genomic location of all TA dinucleotides are identified (the H37Rv FASTA sequence was

downloaded from NCBI). Second, the mapped transposon insertions are counted at each TA site and are associated with their appropriate genetic feature (e.g. a gene or intergenic region) (the H37Rv gene list was downloaded from the JCVI institute). Transposon insertions were visualized on DNAplotter [50] or Artemis [51] by converting the TA counts to the programs' appropriate data structure using custom Python scripts.

Assessment of Library Saturation

The complexity of the libraries was initially assessed by calculating the number of TA sites that contained a transposon insertion. The *ΔponA1* library had 54% of the genome's TA sites disrupted with a transposon. The *ΔponA2* library had 57% of the genome's TA sites disrupted. The *ΔldtB* library had 42% of the genome's TA sites disrupted. 54% of the TA sites in the wildtype library were disrupted. To gain a gene-level resolution of the transposon disruption profile, the fraction of disrupted TA sites per gene was calculated as previously described [52] using a custom Python script and Excel functions. The middle of the right-hand peak can be used to visually estimate the true saturation of the libraries (because insertions in essential genes cannot be sequenced since the bacteria are not viable, calculating the percent TA disruption is an underestimate of true saturation). The estimated true saturations of each library are reported in the legend for Figure 4.10.

Analysis of Differentially Inserted Genes

Loci that were differentially disrupted between wildtype and mutant *Mtb* cells were assessed using a published method [25]. This method uses a Mann-Whitney U-test and normalization based on simulated control libraries [25] (see Appendix C of the manual provided in Reference [7] for how to utilize resampling and the Mann-Whitney U test without using the pipeline's Hidden Markov Model (HMM). HMMs are robust for sequentially selected libraries but are a less robust statistical method for the analysis of independently generated libraries [e.g. different strain backgrounds, as performed here]). We performed 100 simulations and asked for loci that were designated statistically significantly different from wildtype (p-value < 0.001) in at least 90 of the 100 simulations. For each locus in the libraries, the geometric mean of sequence reads was calculated. The fold change (ratio) in sequence reads for each

locus was then calculated from the respective geometric mean of the locus in the mutant and wildtype libraries.

Construction of Gene Knockouts in *M. tuberculosis*

A hygromycin resistance cassette flanked with LoxP sites marked the *ponA1* deletion in the *ΔponA1* L5::*ponA1*$_{wt}$ strain. To allow further knockouts, the hygromycin cassette was removed by transforming the strain with a vector that encoded Cre recombinase and a counter-selectable sucrose-sensitive marker. After selection for the Cre vector, several clones were confirmed to be hygromycin sensitive. Those clones were then counter-selected on sucrose to remove the Cre recombinase vector. The strain is still referred to as *ΔponA1* L5::*ponA1*$_{wt}$ throughout the text. This loxed strain was then transformed with a gentamicin-resistant RecE/T plasmid for recombineering. The recombineering substrates are described further below. After recombineering, cells were plated on selective 7H10. To screen the colonies, 50 μl of log-phase cells were baked at 80°C for two hours to generate cell lysates for PCR. Positive clones were identified by multiple reactions. Clones were screened for the presence of the appropriate genomic position of the 5' and 3' recombineering construct flanks and for the absence of wildtype 5' and 3' sequence at those junctures. Clones that matched these criteria were then PCR screened for the absence of the gene of interest, to verify that a gene duplication event elsewhere in the chromosome had not occurred. Wildtype H37Rv was used as a control in all PCR reactions. PCR screening was performed with GoTaq® polymerase (Promega, Madison, WI) or KOD Xtreme^{TM} Hot Start DNA polymerase (EMD Millipore, Billerica, MA).

Recombinant DNA constructs

The *ponA2* knockout cassette was amplified from a custom designed phage [53] by PCR. The *cpsY* knockout cassette was constructed by PCR stitching 500 nucleotides of the 5' and 3' genomic sequence surrounding *cpsY* to the 5' and 3' ends of a hygromycin resistance cassette flanked by LoxP sites, respectively. The *rv1086* and *ldtB* knockout cassettes consisted of 500 nucleotides of the 5' and 3' genomic sequence surrounding *rv1086* or *ldtB* flanking a hygromycin cassette. Gen9 (Cambridge, MA) synthesized these constructs as a circular vector with *PmeI* sites at each end of the knockout cassettes.

The vector was then digested with *PmeI* (New England Biolabs, Ipswich, MA) to generate a linear product for recombineering.

ponA1 was subcloned into the L5-integrating pMC1s vector as described in Chapter 3. A zeocin resistance cassette was amplified with *SgfI* and *PflMI* enzyme sites. Subcloning with *AsiSI* (an isoschizomer of *SgfI*) and *PflMI* (New England Biolabs, Ipswich, MA) replaced the kanamycin resistance cassette on the modified *ponA1*$^{+}$ pMC1s and the original pMC1s vector (encoding *tetR*) [54] with the zeocin resistance cassette.

Allelic exchange in *M. tuberculosis*

Allelic exchange occurs via transformation of vectors at the L5 phage integration site. The *ΔponA1* L5::*ponA1*$_{wt}$ loxed strain that underwent further recombineering events to delete *ponA2*, *rv1086*, and *ldtB* as described above was used for allelic exchange. This strain's allele of *ponA1* is marked with kanamycin. Transformation of this strain with an L5-integrating vector that encodes *ponA1* or the negative control gene *tetR* marked with a zeocin antibiotic cassette and selecting for this second integration event will replace the original kanamycin-marked *ponA1* integrated allele with the desired zeocin-marked allele. After transformation, cells were recovered in non-selective 7H9 for 24 hours and then plated on selective 7H10. Colony forming units (CFU) were counted after 21 days for all plates, except for the *ΔponA1* L5::*tetR ΔldtB* cells that were counted at 35 days. Simultaneous control transformations with the same L5-integrating vectors encoding either *ponA1* or *tetR* were performed in *ΔponA2*, *Δrv1086*, *ΔcpsY* (data not shown), and *ΔldtB* cells.

Optical density measurements

Population growth curves for *Mtb* strains were performed in 30 ml inkwells (Corning Life Sciences, Corning, NY), in triplicate, at 37°C with shaking. Cells were grown to an OD_{600} of 0.5 before beginning the growth curve at a calculated starting OD_{600} of 0.1. Cells were grown in 7H9 with the appropriate antibiotic selection. Optical density was measured daily by absorbance at 600nm.

Light microscopy and image analysis

Cells were first fixed overnight in 1% formalin at 4°C in the Biosafety Level 3 facility before removal. Cells were imaged on a Nikon TE-200E microscope using the 100x (NA1.40) objective. Images were captured with an Orca-II ER cooled CCD camera (Hamamatsu, Japan). Exposure and image acquisition were controlled with Metamorph Software (Molecular Devices). Final images were prepared in FIJI [55]. Cell length was calculated using ImageJ software (National Institutes of Health) and converted to microns using the appropriate pixel to micron conversion. Length was measured from cell pole to the opposite cell pole or from cell pole to septum, if present. Cell synchronization is not yet possible for mycobacteria; hence, cell lengths were measured for unsynchronized populations.

Antibiotic treatment and determination of minimum inhibitory concentration

The antibacterial effects of meropenem, teicoplanin, and ethambutol (Sigma Aldrich, St. Louis, MO) were determined by culturing exponentially growing *M. tuberculosis* cells in complete 7H9 in non-treated 96 well plates (Genesee Scientific, San Diego, CA) in the presence of serially diluted drug, in duplicate. Plates also contained duplicate untreated wells as controls. *M. tuberculosis* was grown to OD_{600} of 0.5 before culturing ± drug at a calculated starting OD_{600} of 0.006 for six days at 37°C with shaking. Bacterial growth was evaluated by adding 0.002% resazurin (Alamar Blue, Sigma Aldrich, St. Louis, MO) to each well. Plates were incubated with resazurin for 18-24 hours. Wells were scored as blue or purple indicating metabolically inactive cells and pink as metabolically active cells.

Data representation and statistical analysis

Prism 6.0 software (GraphPad Software, La Jolla, CA) was used to graph and analyze numerical data. Statistical tests in the Prism software were used to calculate significance of measurements as reported in the figure legends.

Acknowledgements

We thank Michelle Larsen for the phage encoding the *ponA2* knockout cassette. We thank Allison Carey, E. Hesper Rego and Troy Hubbard for help with sequencing preparation. We thank Kadamba Papavinasasundaram and Kenan Murphy for the gift of the Gent^R RecE/T plasmid. We are grateful to Noman Siddiqi, Shoko Wakabayashi, Jess Pinkham, and Larry Pipkin at the Harvard T.H. Chan School of Public Health Biosafety Level 3 Facility for excellent technical support. This work was supported by the National Institutes of Health (U19 AI107774 to EJR, TRI, CMS, and JCS and U01 GM094568 to EJR), the Howard Hughes Medical Institute (to CMS and MKW), and a National Science Foundation Graduate Research Fellowship (grants DGE-1144152 and DGE0946799 to KJK).

Section 4.3 References

1. World Health Organization (2014) Global Tuberculosis Report.

2. Kieser K, Rubin E (2014) How sisters grow apart: mycobacterial growth and division. Nat Rev Microbiol 12: 550–562.

3. Typas A, Banzhaf M, Gross CA, Vollmer W (2012) From the regulation of peptidoglycan synthesis to bacterial growth and morphology. Nat Rev Microbiol 10: 123–136.

4. Hett E, Chao M, Rubin E (2010) Interaction and Modulation of Two Antagonistic Cell Wall Enzymes of Mycobacteria. PLoS Pathog 6. doi:10.1371/journal.ppat.1001020.

5. Hett E, Chao M, Deng L, Rubin E (2008) A Mycobacterial Enzyme Essential for Cell Division Synergizes with Resuscitation-Promoting Factor. PLoS Pathog 4. doi:10.1371/journal.ppat.1000001.

6. Chao M, Kieser K, Minami S, Mavrici D, Aldridge B, et al. (2013) Protein Complexes and Proteolytic Activation of the Cell Wall Hydrolase RipA Regulate Septal Resolution in Mycobacteria. PLoS Pathog 9. doi:10.1371/journal.ppat.1003197.

7. Lavollay M, Arthur M, Fourgeaud M, Dubost L, Marie A, et al. (2008) The peptidoglycan of stationary-phase Mycobacterium tuberculosis predominantly contains cross-links generated by L,D-transpeptidation. J Bacteriol 190: 4360–4366.

8. Kumar P, Arora K, Lloyd J, Lee I, Nair V, et al. (2012) Meropenem inhibits D,D-carboxypeptidase activity in Mycobacterium tuberculosis. Molecular Microbiology 86: 367–381.

9. Sanders A, Wright L, Pavelka M (2014) Genetic characterization of mycobacterial l,d-transpeptidases. Microbiology 160: 1795–1806.

10. Gupta R, Lavollay M, Mainardi J-L, Arthur M, Bishai W, et al. (2010) The Mycobacterium tuberculosis protein LdtMt2 is a nonclassical transpeptidase required for virulence and resistance to amoxicillin. Nat Med 16: 466–469.

11. Schoonmaker M, Bishai W, Lamichhane G (2014) Nonclassical Transpeptidases of Mycobacterium tuberculosis Alter Cell Size, Morphology, the Cytosolic Matrix, Protein Localization, Virulence, and Resistance to β-Lactams. J Bacteriol 196: 1394–1402.

12. Cordillot M, Dubée V, Triboulet S, Dubost L, Marie A, et al. (2013) In vitro cross-linking of Mycobacterium tuberculosis peptidoglycan by L,D-transpeptidases and inactivation of these enzymes by carbapenems. Antimicrob Agents Chemother 57: 5940–5945.

13. Böth D, Steiner E, Stadler D, Lindqvist Y, Schnell R, et al. (2013) Structure of LdtMt2, an l,d-transpeptidase from Mycobacterium tuberculosis. Acta Crystallogr D Biol Crystallogr 69: 432-441.

14. Erdemli S, Gupta R, Bishai W, Lamichhane G, Amzel L, et al. (2012) Targeting the cell wall of Mycobacterium tuberculosis: structure and mechanism of L,D-transpeptidase 2. Structure 20: 2103–2115.

15. Correale S, Ruggiero A, Capparelli R, Pedone E, Berisio R (2013) Structures of free and inhibited forms of the l,d--transpeptidase LdtMt1 from Mycobacterium tuberculosis. Acta Crystallogr D Biol Crystallogr 69: 1697–1706.

16. Mainardi J-L, Legrand R, Arthur M, Schoot B, Heijenoort J, et al. (2000) Novel Mechanism of β-Lactam Resistance Due to Bypass of DD-Transpeptidation in Enterococcus faecium. J Biol Chem 275: 16490–16496.

17. Flores A, Parsons L, Pavelka M (2005) Genetic analysis of the -lactamases of Mycobacterium tuberculosis and Mycobacterium smegmatis and susceptibility to -lactam antibiotics. Microbiology 151: 521–532.

18. Hugonnet J-E, Blanchard J (2007) Irreversible Inhibition of theMycobacterium tuberculosisβ-Lactamase by Clavulanate. Biochemistry 46: 11998-12004.

19. Hugonnet J-E, Tremblay L, Boshoff H, Barry C, Blanchard J (2009) Meropenem-clavulanate is effective against extensively drug-resistant Mycobacterium tuberculosis. Science 323: 1215–1218.

20. Kim H, Kim J, Im H, Yoon J, An D, et al. (2013) Structural basis for the inhibition of Mycobacterium tuberculosisl,d-transpeptidase by meropenem, a drug effective against extensively drug-resistant strains. Acta Crystallogr D Biol Crystallogr 69: 420-431.

21. Dubée V, Triboulet S, Mainardi J-L, Ethève-Quelquejeu M, Gutmann L, et al. (2012) Inactivation of Mycobacterium tuberculosis l,d-Transpeptidase LdtMt1 by Carbapenems and Cephalosporins. Antimicrob Agents Chemother 56: 4189–4195.

22. Veziris N, Truffot C, Mainardi J-L, Jarlier V (2011) Activity of carbapenems combined with clavulanate against murine tuberculosis. Antimicrob Agents Chemother 55: 2597–2600.

23. Chambers H, Turner J, Schecter G, Kawamura M, Hopewell P (2005) Imipenem for Treatment of Tuberculosis in Mice and Humans. Antimicrobial Agents and Chemotherapy 49: 2816-2821.

24. Long J, DeJesus M, Ward D, Baker R, Ioerger T, et al. (2015) Identifying Essential Genes in Mycobacterium tuberculosis by Global Phenotypic Profiling. Methods Mol Biol 1279: 79–95.

25. Pritchard J, Chao M, Abel S, Davis B, Baranowski C, et al. (2014) ARTIST: High-Resolution Genome-Wide Assessment of Fitness Using Transposon-Insertion Sequencing. PLoS Genet 10. doi:10.1371/journal.pgen.1004782.

26. Yousif S, Broome-Smith J, Spratt B (1985) Lysis of Escherichia coli by beta-lactam antibiotics: deletion analysis of the role of penicillin-binding proteins 1A and 1B. J Gen Microbiol 131: 2839–2845.

27. Typas A, Banzhaf M, van den Berg van Saparoea B, Verheul J, Biboy J, et al. (2010) Regulation of peptidoglycan synthesis by outer-membrane proteins. Cell 143: 1097–1109.

28. Paradis-Bleau C, Markovski M, Uehara T, Lupoli T, Walker S, et al. (2010) Lipoprotein Cofactors Located in the Outer Membrane Activate Bacterial Cell Wall Polymerases. Cell 143.
29. Patru M-M, Pavelka M (2010) A role for the class A penicillin-binding protein PonA2 in the survival of Mycobacterium smegmatis under conditions of nonreplication. J Bacteriol 192: 3043–3054.

30. Pashley C, Parish T (2003) Efficient switching of mycobacteriophage L5-based integrating plasmids in Mycobacterium tuberculosis. FEMS Microbiol Lett 229: 211–215.

31. Schulbach M, Mahapatra S, Macchia M, Barontini S, Papi C, et al. (2001) Purification, Enzymatic Characterization, and Inhibition of theZ-Farnesyl Diphosphate Synthase from Mycobacterium tuberculosis. J Biol Chem 276: 11624–11630.

32. Wang W, Dong C, McNeil M, Kaur D, Mahapatra S, et al. (2008) The structural basis of chain length control in Rv1086. J Mol Biol 381: 129–140.

33. Schulbach M, Brennan P, Crick D (2000) Identification of a short (C15) chain Z-Isoprenyl diphosphate synthase and a homologous long (C50) chain isoprenyl diphosphate synthase in Mycobacterium tuberculosis. J Biol Chem 275: 22876-22881.

34. Swoboda J, Meredith T, Campbell J, Brown S, Suzuki T, et al. (2009) Discovery of a small molecule that blocks wall teichoic acid biosynthesis in Staphylococcus aureus. ACS Chem Biol 4: 875–883.

35. Hett E, Rubin E (2008) Bacterial growth and cell division: a mycobacterial perspective. Microbiol Mol Biol Rev 72: 126–56.

36. Kaur D, Guerin ME, Skovierová H, Brennan PJ, Jackson M (2009) Chapter 2: Biogenesis of the cell wall and other glycoconjugates of Mycobacterium tuberculosis. Adv Appl Microbiol 69: 23–78.

37. Belanger A, Besra G, Ford M, Mikusová K, Belisle J, et al. (1996) The embAB genes of Mycobacterium avium encode an arabinosyl transferase involved in cell wall arabinan biosynthesis that is the target for the antimycobacterial drug ethambutol. P Natl Acad Sci USA 93: 11919–11924.

38. Dong S, Oberthür M, Losey H, Anderson J, Eggert U, et al. (2002) The Structural Basis for Induction of VanB Resistance. J Am Chem Soc 124: 90649065.

39. Cole S, Brosch R, Parkhill J, Garnier T, Churcher C, et al. (1998) Deciphering the biology of Mycobacterium tuberculosis from thecomplete genome sequence. Nature 393: 537–544.

40. Datta P, Dasgupta A, Singh A, Mukherjee P, Kundu M, et al. (2006) Interaction between FtsW and penicillin-binding protein 3 (PBP3) directs PBP3 to mid-cell, controls cell septation and mediates the formation of a trimeric complex involving FtsZ, FtsW and PBP3 in mycobacteria. Mol Microbiol 62: 1655–1673.

41. Dasgupta A, Datta P, Kundu M, Basu J (2006) The serine/threonine kinase PknB of Mycobacterium tuberculosis phosphorylates PBPA, a penicillin-binding protein required for cell division. Microbiology 152: 493–504.

42. Blasco B, Chen J, Hartkoorn R, Sala C, Uplekar S, et al. (2012) Virulence Regulator EspR of Mycobacterium tuberculosis Is a Nucleoid-Associated Protein. PLoS Pathog 8. doi:10.1371/journal.ppat.1002621.

43. Vandal O, Roberts J, Odaira T, Schnappinger D, Nathan C, et al. (2009) Acid-Susceptible Mutants of Mycobacterium tuberculosis Share Hypersusceptibility to Cell Wall and Oxidative Stress and to the Host Environment. J Bacteriol 191: 625–631.

44. Calvanese L, Falcigno L, Maglione C, Marasco D, Ruggiero A, et al. (2014) Structural and binding properties of the PASTA domain of PonA2, a key penicillin binding protein from Mycobacterium tuberculosis. Biopolymers 101: 712–719.

45. Hancock I, Carman S, Besra G, Brennan P, Waite E (2002) Ligation of arabinogalactan to peptidoglycan in the cell wall of Mycobacterium smegmatis requires concomitant synthesis of the two wall polymers. Microbiol 148: 3059–3067.

46. Bouhss A, Trunkfield A, Bugg T, Mengin-Lecreulx D (2008) The biosynthesis of peptidoglycan lipid-linked intermediates. FEMS Microbiol Rev 32: 208–233.

47. Campbell J, Singh AK, Santa Maria, Jr. JP, Kim Y, Brown S, et al. (2011) Synthetic Lethal Compound Combinations Reveal a Fundamental Connection between Wall Teichoic Acid and Peptidoglycan Biosyntheses in Staphylococcus auereus. ACS Chemical Biology 6: 106–116.

48. Sassetti C, Boyd D, Rubin E (2001) Comprehensive identification of conditionally essential genes in mycobacteria. P Natl Acad Sci USA 98: 12712–12717.

49. Langmead B, Salzberg S (2012) Fast gapped-read alignment with Bowtie 2. Nat Methods 9: 357–359.

50. Carver T, Thomson N, Bleasby A, Berriman M, Parkhill J (2009) DNAPlotter: circular and linear interactive genome visualization. Bioinformatics 25: 119–120.

51. Carver T, Harris S, Berriman M, Parkhill J, McQuillan J (2012) Artemis: an integrated platform for visualization and analysis of high-throughput sequence-based experimental data. Bioinformatics 28: 464–469.

52. Chao M, Pritchard J, Zhang Y, Rubin E, Livny J, et al. (2013) High-resolution definition of the Vibrio cholerae essential gene set with hidden Markov model–based analyses of transposon-insertion sequencing data. Nucleic Acids Res 41: 9033–9048.

53. Jain P, Hsu T, Arai M, Biermann K, Thaler D, et al. (2014) Specialized Transduction Designed for Precise High-Throughput Unmarked Deletions in Mycobacterium tuberculosis. MBio 5: e01245–14.

54. Ehrt S, Guo X, Hickey C, Ryou M, Monteleone M, et al. (2005) Controlling gene expression in mycobacteria with anhydrotetracycline and Tet repressor. Nucleic Acids Research 33: e21–e21.

55. Schindelin J, Arganda-Carreras I, Frise E, Kaynig V, Longair M, et al. (2012) Fiji: an open-source platform for biological-image analysis. Nat Methods 9: 676–682.

Chapter 5

Discussion

Section 5.1 Overview

Bacterial cells must tightly govern how cell growth and division occurs in order to ensure survival. Improperly controlled growth and division yields unviable daughter cells and the consequent diminution or even eradication of population growth. How does the cell control the complex processes – and the myriad factors that effect them – required for growth and division? One critical method is the spatiotemporal control of enzymes that carry out synthesis of the cell wall – the architectural frame that promotes cell elongation and division.

The bacterial cell wall is a complex structure often thought of as a safety net – it protects the bacterial cell from adverse exogenous agents (such as antibiotics) as well as providing resistance to interior turgor pressure. While these properties are critical, the cell wall is also the scaffold that growth and division of single cells is based upon. Cell wall synthesis physically lengthens the cell, allowing expansion of a single bacterial cell into two cells. Without new cell wall synthesis, it is impossible for bacterial cells to elongate or divide.

The physically demanding process of cell wall synthesis requires multiple discrete enzymatic activities. Our current understanding of cell wall biogenesis is that the current layers of the cell wall must remain intact, to prevent cell lysis and death, while new cell wall material is incorporated. However, to incorporate new cell wall material into the cell envelope, some level of directed hydrolysis of the existing cell wall must occur (Figure 5.1). Where this hydrolysis and new synthesis of the cell envelope occurs in the cell must be finely controlled to prevent aberrations and consequent damages to cell shape and cell fitness. My work has focused on how the cell governs these cell wall hydrolases and synthases. This chapter will focus on the biological context of my findings and discuss how my work expands our understanding of how mycobacteria spatiotemporally control cell envelope biogenesis during growth and division.

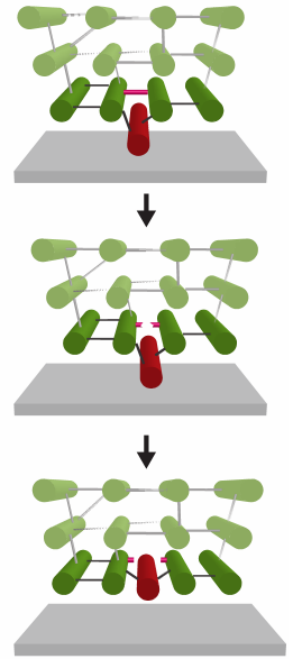

Figure 5.1 Cell wall synthesis requires local hydrolysis of the existing cell envelope. New glycan strands (red) are crosslinked to the existing peptidoglycan matrix (green). Old crosslinks (hot pink) are then hydrolyzed to allow full incorporation of the new glycan strand into the peptidoglycan layer adjacent to the cell membrane (gray). [image adapted from [1]]

Section 5.2 Results Summary and Perspectives

Spatial governance of cell wall biogenesis

Because mycobacteria incorporate new cell wall material at their cell poles, instead of along their mid-section like many rod-shaped bacteria (Chapter 1), the paradigms that govern how mycobacteria grow are different than the systems governing growth in other rod-shaped organisms.

How, then, is cell wall synthesis directed to this specific space (the cell pole)? A major factor that spatially determines growth at the pole is Wag31, the mycobacterial DivIVA homologue. DivIVA proteins in other species are known to direct new cell wall synthesis at the cell pole or hyphal tip [2–4]; proper spatial orientation occurs through DivIVA's recognition of membrane curvature [5,6]. Analogously, Wag31 recognizes the curvature of the mycobacterial pole and promotes its extension [6]. However, Wag31 has

no enzymatic activity and is located in the cytoplasm. Therefore, it must form complexes with or direct cell wall biogenesis factors to the cell pole to for the construction of new cell wall.

Several pieces of evidence point to an intriguing possibility that Wag31 and PonA1 could physically interact. Wag31 has been shown to interact with the cytoplasmic tail of a different penicillin binding protein, PBP3, at the cell septum [7] – where Wag31 localizes as the septum is maturing into a pole [8]. It is possible that Wag31 also interacts with PonA1, through PonA1's long cytoplasmic domain. The overexpression of enzymatically inactive PonA1 generates ectopic polar growth (Chapter 3). These data suggest that excess PonA1 protein is able to stimulate the formation of viable elongation complexes – which are likely formed upon the Wag31 anchor, as Wag31 is required for normal polar growth [6]. However, it is possible that these viable elongation complexes are built through an indirect interaction with Wag31. While the majority of PonA1's cytoplasmic tail can be truncated without diminishing cell survival (Chapter 3), a full deletion of this region has not been assessed (twenty-three cytoplasmic amino acids remain in the $PonA1_{\Delta cyto}$ construct). Further experiments are required to determine whether PonA1 and Wag31 do indeed interact and where in PonA1's cytoplasmic tail, if at all, this interaction occurs.

My work on PonA1 and RipA demonstrates that these proteins localize to certain subcellular sites, suggesting that specific mechanisms exist to spatially organize these proteins in mycobacteria. RipA localizes to the cell's septum, where it cleaves the peptidoglycan that joins the nascent daughter cells [9]. PonA1 localizes to both the cell pole and septum, where it interacts with RipA [10], indicating it functions in both cell septation and cell elongation. The specific mechanisms by which RipA and PonA1 are localized at the cell pole or septum remain unknown. Because septal peptidoglycan must first be synthesized before it can be hydrolyzed to birth nascent daughter cells, one hypothesis is that PonA1 could facilitate RipA's recruitment to the septum, possibly through physical interactions. While my work showed that the PonA1-RipA interaction is not required for viability, loss of this interaction did diminish normal cell separation (Figure 2.10), indicating that RipA's activity at the septum was abnormal. Hence, PonA1 could play a role in properly recruiting or activating RipA at the cell septum.

RipA may also modulate the spatial organization of cell elongation through its specific enzymatic activity at the septum. The septum becomes the cell pole in the next cell cycle, and the physical state of the cell pole's peptidoglycan influences new peptidoglycan synthesis at that site. New peptidoglycan synthesis requires the generation of crosslinks between the glycan strands. However, RipA's enzymatic activity precludes further crosslinking (Figure 5.2). This inhibits new peptidoglycan synthesis at the very tip of the cell pole, leaving the tip static. This inert peptidoglycan could thereby "direct" cell elongation complexes to a region just below the tip for new cell wall synthesis [11]. Indeed, a recent study demonstrated that cell wall synthesis complexes and cell wall precursor incorporation occurred at this sub-polar region [6].

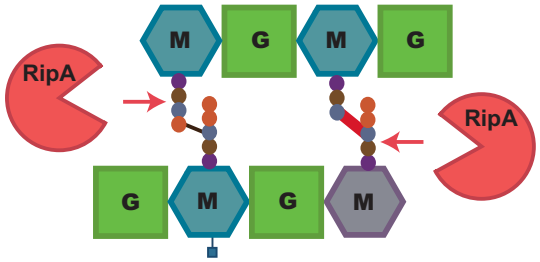

Figure 5.2 RipA's hydrolytic activity prevents further peptidoglycan crosslinking. RipA cleaves the bond between the second (D-Glu) and third (meso-DAP) amino acids of the peptide tail (colored circles) that descend from the glycan strands (colored squares and hexagons). RipA's hydrolysis precludes any new transpeptidation reactions, which require a tetrapeptide (for 3–3 crosslinks) or a pentapeptide (for 4–3 crosslinks) tail.

Temporal control of cell wall synthesis

RipA's activity at the septum must also be governed in time. If RipA is activated too early, destruction of cell wall peptidoglycan could occur, leading to lysis and cell death. The mechanism of RipA's activation remains unknown. It may be that the cell orchestrates RipA's proteolysis at the septum once a signal for septum completion has been received. The nature of this signal and how it is propagated remains uncharacterized. However, it is feasible that a series of protein-protein interactions temporally modulates when RipA's processing occurs. Many of the enzymes that function in the divisome are recruited in a certain order [12], suggesting that the timing of divisome formation is regulated and that specific patterns of protein localization to the divisome are important for proper activity. RipA's activation at the septum

could also rely on specific protein-protein interactions, not only for its proper recruitment to and localization within the divisome, but also for its proteolysis. The factor responsible for proteolyzing RipA is unknown, as is the spatiotemporal regulation of RipA's processing. Much remains to be discovered about how the cell controls RipA's processing in both time and space.

A major finding of my work was the temporal regulation of PonA1's enzymatic activity. This is the first illustration that a post-translational modification impacts activity of a penicillin binding protein, the workhorses of cell wall synthesis in walled bacteria. Phosphorylation plays a key role in governing cell growth and division in mycobacteria, which have evolved a complex network of phosphorylated targets [11]. Indeed, all steps of the peptidoglycan synthesis pathway are regulated by phosphorylation (GlmU for precursor synthesis [13], MviN for precursor export [14], and PonA1 for polymerization [Chapter 3]). Phosphorylation also regulates the synthesis of the other major cell wall macromolecules as well as the formation of cell growth and division complexes [11]. Why have mycobacteria evolved to so heavily use phosphorylation? It is perhaps because phosphorylation can quickly alter protein conformation or activity [14] . Quick responses facilitate malleability in the face of environmental stresses, and such plasticity may have aided the adaptation of *Mtb* [15] to the variable environment of the human host [11]. Alternatively, mycobacteria may have evolved a widespread phosphorylation network [16] as a method to regulate the timing of cell division. Several studies suggest that mycobacterial cell division is regulated more by time than by cell size [8,17], as is common in other bacteria [18]. The phosphorylation of many cell growth and division proteins could relay the information to commence cell elongation or division.

PonA1 may additionally modulate the timing of cell wall biogenesis through its dual role in septation and elongation. Mycobacteria face the complex problem of growing from the site of former cell division. How does the cell transition the division site, occupied by the large divisome, into a site productive for cell elongation, which requires a separate protein machine? Does the divisome dissolve? Is its composition altered or localized to a sub-polar space? PonA1's activity in both the divisome and elongation complex hints it could play a role in the cell's segue from division to elongation in the same subcellular space. Further experiments are required to test this model. Timelapse imaging of fluorescently tagged PonA1 in

cells treated with small molecule inhibitors of specific cell elongation and division proteins may begin to address these questions. However, technological advancement is required as fluorescent tagging of cell wall associated proteins is technically challenging in mycobacteria, and current cell biological reagents are geared more towards *E. coli*.

Temporal regulation of 4–3 and 3–3 crosslinking must also occur during cell wall synthesis. Although several works postulated that 3–3 crosslinking enzymes facilitate the transition into stationary phase [19,20], a comprehensive study of mycobacterial PG from multiple growth stages showed that 3–3 crosslinking is equally prevalent in vegetative and stationary phase growth [21]. These data suggest that 3–3 crosslinking enzymes are active during vegetative growth and are likely critical for normal cell elongation. Indeed, a recent study demonstrated that lack of the 3–3 transpeptidases LdtA and LdtB resulted in shorter cells [22]. I also observed decreased length in addition to increased cell width in cells that lack LdtB (Chapter 4). These data suggest that 3–3 crosslinking enzymes are active during vegetative growth and are important in maintaining normal cell shape. How does the cell determine whether a 4–3 or 3–3 enzyme crosslinks the nascent PG? Do these enzymes act sequentially? Several pieces of evidence suggest that 3–3 transpeptidases use a tetrapeptide substrate for their crosslinking reaction [23,24], which means another enzyme must first cleave the ultimate amino acid from pentapeptide tail of nascent peptidoglycan [25]. What are the temporal dynamics of those proteins in cell wall synthesis? Furthermore, it remains unclear whether previously 4–3 crosslinked peptide tails can later be used in a 3–3 transpeptidation reaction.

However, my work showed that the function of PonA1 and PonA2 is correlated with LdtB during growth, which indicates that 4–3 and 3–3 crosslinking are temporally and/or spatially connected. Do these enzymes physically interact? Are their respective crosslinking activities coordinated? Much remains to be understood about the spatiotemporal interplay between 4–3 and 3–3 crosslinking enzymes and how the cell governs their activity.

Section 5.3 Future Directions

My work has uncovered several common themes for how cell wall biogenesis is governed in mycobacteria – many which exist at the protein level of control. However, many questions remain for how the cell specifically defines sites and times of growth.

Interaction Partners of PonA1

As a major bifunctional peptidoglycan synthase that promotes cell elongation, PonA1 likely has interacting partners in the elongation complex in addition to its known partner in the divisome (RipA). Because of the dearth of information about the composition of the elongation complex, identifying PonA1 partners would greatly expand our understanding of how cell elongation is controlled in mycobacteria. These experiments would answer fundamental questions such as whether Wag31 interacts directly with PonA1, even transiently. The identified genetic interaction between PonA1 or PonA2 and LdtB may be a result of physical interaction. Identifying PonA1's protein-protein interactions could determine whether 3–3 transpeptidases exist in the classical elongation complex. Further experiments could address whether PonA1's protein-protein interactions impact its retention in or the stability of the elongation complex.

Additionally, it remains unknown whether PonA1's phosphorylation mediates interactions with other factors. Pull down experiments with wildtype or phosphorylation mutants would test the importance of PonA1's phosphorylation for any protein-protein interactions. Our model of PonA1's phosphorylation regulating its TG activity needs experimental evidence. Analysis of peptidoglycan from cells that produce differently phosphorylated PonA1 protein could demonstrate whether the length of glycan chains, and hence PonA1's TG activity, is impacted by its phosphorylation status.

Investigation of 3–3 Transpeptidases

Why have mycobacteria evolved to crosslink their peptidoglycan mainly with 3–3 bonds? Is there an advantage to 3–3 peptide crosslinks? Do they lend greater stability to the cell wall or more antibiotic tolerance? These transpeptidases are of biological interest because of the unusual prevalence of 3–3 crosslinks in mycobacterial peptidoglycan, but also because classic beta-lactam antibiotics, such as

penicillin, do not inhibit these enzymes. Further work on these enzymes could be fruitful for chemotherapeutic development in *Mtb* (Chapter 4).

Because *Mtb* encodes five of these enzymes (Appendix 1), much work is required to understand the biological roles of the individual proteins. One study suggested that *ldtB* was the most highly transcribed [20] , and presumably the most active, and failed to find enzymatic activity for three of the other 3–3 transpeptidases, a finding which was recently challenged [23]. Furthermore, the majority of studies on these proteins focused on *in vitro* protein structure, biochemical activity, or drug inhibition [19,23,26-30]. Few works have investigated the activity or regulation of these enzymes in the cell or in the host [20,22,31]. Therefore, there is room for examining the individual importance of these proteins during growth and cell wall biogenesis. Directed knockouts, cell biological assays (population growth, cell shape, cell wall labeling [6,8,17], protein localization), biochemical analysis of isolated sacculi, and macrophage or mouse infections constitute straightforward first steps to determine the relative importance of each of *Mtb*'s L,D-transpeptidases to growth and cell wall synthesis in culture and during infection.

Because of the frequency of 3–3 crosslinks in mycobacterial peptidoglycan, I hypothesized that these enzymes may exist in the traditional elongation complex or in distinct complexes that are also active at sites of growth [11]. Protein interaction studies have the potential to resolve whether these enzymes interact with known members of the cell wall biogenesis machinery, and localization of fluorescently tagged L,D-transpeptidases would spatially resolve these enzymes' activity. My work demonstrated that loss of LdtB impacted cell width and cell length (also reported in another study [22]). Timelapse microscopy of cell-surface- or cell-wall- labeled *Δldtb* cells would determine whether the observed cell shape changes are due to alterations in cell elongation and/or in cell septation. Both processes impact cell length, and it is feasible that alterations in cell septation impact cell width. These experiments could define whether LdtB is more active in either process or whether it functions in peptidoglycan metabolism throughout the cell cycle.

Major Unanswered Questions on the Spatiotemporal Control of Mycobacterial Cell Growth and Division

Several major questions remain unanswered in the field of mycobacterial cell growth and division. Studies investigating these questions would substantially expand our understanding of prokaryotic cell division, as mycobacteria have evolved to control their growth and division in different ways than many currently studied organisms. Additionally, resolving these questions has the potential to further our knowledge of how *Mtb* remains such a successful pathogen.

How are the various layers of the cell wall synthesized in concert? How do all of these enzymes function together? Many factors involved in cell wall biogenesis are not essential for growth of *Mtb* in culture, which eases investigation of their activity during cell wall biogenesis. Genetic interrogation of these enzymes is relatively facile in *Mtb*. Transposon mutagenesis is efficient, and it is feasible to obtain highly complex libraries of transposon-disrupted loci [32], which could be manually ordered to facilitate downstream studies of individual factors. Additionally, several labs, including the Rubin lab, are currently constructing a whole-genome mutant collection wherein each locus is deleted or, for essential genes, conditionally expressed. Such resources will promote the study of how *Mtb* specifically organizes its cell wall synthesis. Additionally, the development of chemical probes for the arabinogalactan and mycolic acid layers would distinguish mutants in peptidoglycan, arabinogalactan, and mycolic acid synthesis (peptidoglycan probes exist [33] but optimization and probes targeting other PG moieties would be useful). These additional probes would greatly advance our understanding of AG and MA cell wall incorporation and the coordinated synthesis of the cell envelope.

One major question in mycobacterial cell biology is how the division site is selected[1]. Mycobacteria have no known homologues to the systems widely present in other bacteria that regulate selection of the division site (Chapter 1). A combination of genetic and visual screens could identify factors that modulate division site selection in mycobacteria. Because the factors that govern division site selection may be

[1] Some of the ideas presented in this paragraph stem from conversations with Dr. Cara Boutte, a postdoc in the Rubin lab.

essential, an overexpression library could be used to search for mutants in cell division (a whole genome library, with some exceptions, exists). Alternatively, division site regulators may not be essential, and a whole genome transposon mutagenesis screen could query which genes impact division site localization. These libraries would need to be visually screened for cell division mutants. Mutant populations of interest could first be enriched for different cell sizes via filtering (unlike *M. tuberculosis*, *M. smegmatis* is quite long; single cells are on average 5 μm. Mutants in cell division may fail to divide and hence become longer; alternatively, mutants may become shorter if division is activated earlier than normal. Filtering with a 5μm filter could enrich for both classes of mutants). Alternatively, cell sorting (using a microfluidic based platform [34] or a cell sorter [35,36]) could also enrich for differentially sized cells. Any mutants with widely different cell size compared to wildtype could be further investigated to determine whether the division site is aberrantly formed or matured. Determination of division site localization and stability can be assessed with timelapse microscopy of fluorescently-tagged FtsZ [37], the major cell division protein, in the mutant cells.

Another significant unanswered question in the field is whether the apparent asymmetric growth and division of mycobacterial cells (Chapter 1) is important during infection. Timelapse microscopy of single cells during growth in macrophages is a first step to illuminating whether certain lineages of daughter cells survive better during growth in macrophages or in different host-like conditions. For example, do new pole daughter cells fare worse in host-like conditions? The seminal study on this work examined the survival of daughter cells in one condition – antibiotic stress – and many unanswered questions remain about whether asymmetric growth and division impacts the fitness of single cells in other stresses. A recent study examined the partitioning of irreversibly oxidized proteins during mycobacterial cell division and found asymmetric partitioning of the protein aggregates; the progeny with a greater proportion of the aggregates had diminished fitness during antibiotic stress [38]. These findings support the hypothesis that asymmetric growth and division, with its impacts on cell wall composition and protein content for each daughter cell, could impact the fitness of individual cells. Changes in individual cell fitness could have direct consequences on their survival in the human host. These hypotheses need to be tested in models that more closely resemble human infection. Ultimately, mutants that exhibit an altered symmetry of

growth and division should be analyzed for their ability to robustly survive in macrophage, mouse, or non-human primate models. Do global changes to the spatiotemporal pattern of *Mtb* growth impact its survival in the host? Such findings would illuminate whether *Mtb*'s unusual mode of growth contributes to its extraordinary success as a human pathogen and aid the development of novel chemo- or immuno-therapeutics.

Section 5.4 References

1. Meisner J, Llopis P, Sham L, Garner E, Bernhardt T, et al. (2013) FtsEX is required for CwlO peptidoglycan hydrolase activity during cell wall elongation in Bacillus subtilis. Molecular Microbiology 89: 1069–1083.

2. Hempel A, Wang S, Letek M, Gil J, Flärdh K (2008) Assemblies of DivIVA Mark Sites for Hyphal Branching and Can Establish New Zones of Cell Wall Growth in Streptomyces coelicolor. J Bacteriol 190: 7579–7583.

3. Letek M, Ordóñez E, Vaquera J, Margolin W, Flärdh K, et al. (2008) DivIVA Is Required for Polar Growth in the MreB-Lacking Rod-Shaped Actinomycete Corynebacterium glutamicum. J Bacteriol 190: 3283–3292.

4. Brown P, Kysela D, Brun Y (2011) Polarity and the diversity of growth mechanisms in bacteria. Semin Cell Dev Biol 22: 790–798.

5. Ramamurthi K, Losick R (2009) Negative membrane curvature as a cue for subcellular localization of a bacterial protein. Proc Natl Acad Sci USA 106: 13541–13545.

6. Meniche X, Otten R, Siegrist M, Baer C, Murphy K, et al. (2014) Subpolar addition of new cell wall is directed by DivIVA in mycobacteria. Proc Natl Acad Sci USA 111: E3243–E3251.

7. Mukherjee P, Sureka K, Datta P, Hossain T, Barik S, et al. (2009) Novel role of Wag31 in protection of mycobacteria under oxidative stress. Mol Microbiol 73: 103–119.

8. Santi I, Dhar N, Bousbaine D, Wakamoto Y, McKinney J (2013) Single-cell dynamics of the chromosome replication and cell division cycles in mycobacteria. Nat Commun 4: 2470-3470.

9. Hett E, Chao M, Deng L, Rubin E (2008) A Mycobacterial Enzyme Essential for Cell Division Synergizes with Resuscitation-Promoting Factor. PLoS Pathog 4. doi:10.1371/journal.ppat.1000001.

10. Hett E, Chao M, Rubin E (2010) Interaction and Modulation of Two Antagonistic Cell Wall Enzymes of Mycobacteria. PLoS Pathog 6. doi:10.1371/journal.ppat.1001020.

11. Kieser K, Rubin E (2014) How sisters grow apart: mycobacterial growth and division. Nat Rev Microbiol 12: 550–562.

12. Goehring N, Beckwith J (2005) Diverse Paths to Midcell: Assembly of the Bacterial Cell Division Machinery. Current Biology 15. R514-R526.

13. Parikh A, Verma S, Khan S, Prakash B, Nandicoori V (2009) PknB-mediated phosphorylation of a

novel substrate, N-acetylglucosamine-1-phosphate uridyltransferase, modulates its acetyltransferase activity. J Mol Biol 386: 451–464.

14. Gee C, Papavinasasundaram K, Blair S, Baer C, Falick A, et al. (2012) A phosphorylated pseudokinase complex controls cell wall synthesis in mycobacteria. Sci Signal 5: ra7.

15. Galagan J (2014) Genomic insights into tuberculosis. Nat Rev Genet 15: 307–320.

16. Baer C, Iavarone A, Alber T, Sassetti C (2014) Biochemical and Spatial Coincidence in the Provisional Ser/Thr Protein Kinase Interaction Network of Mycobacterium tuberculosis. J Biol Chem 289: 20422-33.

17. Aldridge B, Fernandez-Suarez M, Heller D, Ambravaneswaran V, Irimia D, et al. (2012) Asymmetry and aging of mycobacterial cells lead to variable growth and antibiotic susceptibility. Science 335: 100–104.

18. Robert L, Hoffmann M, Krell N, Aymerich S, Robert J, et al. (2014) Division in Escherichia coli is triggered by a size-sensing rather than a timing mechanism. BMC Biol 12: 17. doi:10.1186.

19. Lavollay M, Arthur M, Fourgeaud M, Dubost L, Marie A, et al. (2008) The peptidoglycan of stationary-phase Mycobacterium tuberculosis predominantly contains cross-links generated by L,D-transpeptidation. J Bacteriol 190: 4360–4366.

20. Gupta R, Lavollay M, Mainardi J-L, Arthur M, Bishai W, et al. (2010) The Mycobacterium tuberculosis protein LdtMt2 is a nonclassical transpeptidase required for virulence and resistance to amoxicillin. Nat Med 16: 466–469.

21. Kumar P, Arora K, Lloyd J, Lee I, Nair V, et al. (2012) Meropenem inhibits D,D-carboxypeptidase activity in Mycobacterium tuberculosis. Molecular Microbiology 86: 367–381.
22. Schoonmaker M, Bishai W, Lamichhane G (2014) Nonclassical Transpeptidases of Mycobacterium tuberculosis Alter Cell Size, Morphology, the Cytosolic Matrix, Protein Localization, Virulence, and Resistance to β-Lactams. J Bacteriol 196: 1394–1402.

23. Cordillot M, Dubée V, Triboulet S, Dubost L, Marie A, et al. (2013) In vitro cross-linking of Mycobacterium tuberculosis peptidoglycan by L,D-transpeptidases and inactivation of these enzymes by carbapenems. Antimicrob Agents Chemother 57: 5940–5945.

24. Mainardi J-L, Legrand R, Arthur M, Schoot B, Heijenoort J, et al. (2000) Novel Mechanism of β-Lactam Resistance Due to Bypass of DD-Transpeptidation in Enterococcus faecium. J Biol Chem 275: 16490–16496.

25. Sacco E, Hugonnet J, Josseaume N, Cremniter J, Dubost L, et al. (2010) Activation of the l,d-transpeptidation peptidoglycan cross-linking pathway by a metallo-d,d-carboxypeptidase in Enterococcus faecium. Mol Microbiol 75: 874–885.

26. Correale S, Ruggiero A, Capparelli R, Pedone E, Berisio R (2013) Structures of free and inhibited forms of the l,d--transpeptidase LdtMt1 from Mycobacterium tuberculosis. Acta Crystallogr D Biol Crystallogr 69: 1697–1706.

27. Erdemli S, Gupta R, Bishai W, Lamichhane G, Amzel L, et al. (2012) Targeting the cell wall of Mycobacterium tuberculosis: structure and mechanism of L,D-transpeptidase 2. Structure 20: 2103–2115.

28. Böth D, Steiner E, Stadler D, Lindqvist Y, Schnell R, et al. (2013) Structure of LdtMt2, an l,d-transpeptidase from Mycobacterium tuberculosis. Acta Crystallogr D Biol Crystallogr 69: 432-41.

29. Kim H, Kim J, Im H, Yoon J, An D, et al. (2013) Structural basis for the inhibition of

Mycobacterium tuberculosisl,d-transpeptidase by meropenem, a drug effective against extensively drug-resistant strains. Acta Crystallogr D Biol Crystallogr 69: 420-31.

30. Dubée V, Triboulet S, Mainardi J-L, Ethève-Quelquejeu M, Gutmann L, et al. (2012) Inactivation of Mycobacterium tuberculosis l,d-Transpeptidase LdtMt1 by Carbapenems and Cephalosporins. Antimicrob Agents Chemother 56: 4189–4195.

31. Sanders A, Wright L, Pavelka M (2014) Genetic characterization of mycobacterial l,d-transpeptidases. Microbiol 160: 1795–1806.

32. Long J, DeJesus M, Ward D, Baker R, Ioerger T, et al. (2015) Identifying Essential Genes in Mycobacterium tuberculosis by Global Phenotypic Profiling. Methods Mol Biol 1279: 79–95.

33. Siegrist M, Whiteside S, Jewett J, Aditham A, Cava F, et al. (2012) d-AminoAcid Chemical Reporters RevealPeptidoglycan Dynamics of an Intracellular Pathogen. ACS Chem Biol 8: 500-05.

34. MacDonald M, Spalding G, Dholakia K (2003) Microfluidic sorting in an optical lattice. Nature 426: 421–424.

35. Zhang X, Zhang Q, Yan T, Jiang Z, Zhang X, et al. (2014) Surface Free Energy Activated High-Throughput Cell Sorting. Anal Chem 86: 9350-55.

36. Vahey M, Voldman J (2008) An equilibrium method for continuous-flow cell sorting using dielectrophoresis. Anal Chem 80: 3135–3143.

37. Rajagopalan M, Maloney E, Dziadek J, Poplawska M, Lofton H, et al. (2005) Genetic evidence that mycobacterial FtsZ and FtsW proteins interact, and colocalize to the division site in Mycobacterium smegmatis. FEMS Microbiol Lett 250: 9–17.

38. Vaubourgeix J, Lin G, Dhar N, Chenouard N, Jiang X, et al. (2015) Stressed Mycobacteria Use the Chaperone ClpB to Sequester Irreversibly Oxidized Proteins Asymmetrically Within and Between Cells. Cell Host & Microbe 17: 178-90.

Appendices

Appendix 1. Mycobacterial cell wall synthesis enzymes.

Enzyme	Gene	Function
Lipid II Synthesis		
MurA	*rv1315*	adds enoyl pyruvate to UDP—NAG
MurB	*rv0482*	reduces enoyl pyruvate to generate UDP—NAM
MurC	*rv2152*	adds L-Ala to UDP—NAM
MurD	*rv2155*	adds D-Glu to UDP—NAM—L-Ala
MurE	*rv2158*	adds DAP to UDP—NAM—L-Ala—D-Glu
MurF	*rv2157*	adds D-Ala—D-Ala to UDP—NAM—L-Ala—D-Glu—DAP to form UDP—NAM—pentapeptide
Ddl	*rv2981*	D-Ala—D-Ala ligase
Alr	*rv3423*	alanine racemase
MurX	*rv2156*	generates Lipid I by appending UDP—NAM—pentapeptide to decaprenol phosphate (DP)
NamH	*rv3818*	glycolates NAM moieties
MurG	*rv2153*	generates Lipid II by adding NAG to Lipid I
MviN (MurJ)	*rv3910*	putative lipid II flippase
FhaA	*rv0020*	modulates MviN functionality
Peptidoglycan Synthesis		
PonA1	*rv0050*	transglycosylation and 4→3 transpeptidation of PG
PonA2	*rv3682*	transglycosylation and 4→3 transpeptidation of PG
PBPA	*rv0016*	4→3 transpeptidation of PG
PBPB	*rv2163*	4→3 transpeptidation of PG
LdtA (LdtMt1)	*rv0116*	3→3 transpeptidation of PG
LdtB (LdtMt2)	*rv2518*	3→3 transpeptidation of PG
LdtC (LdtMt5)	*rv0483*	3→3 transpeptidation of PG
LdtD (LdtMt3)	*rv1433*	3→3 transpeptidation of PG
LdtE (LdtMt4)	*rv0192*	3→3 transpeptidation of PG
possible penicillin binding lipoprotein	*rv2864*	putative 4→3 transpeptidation of PG
putative homologue of *E. coli* PBP4	*rv3627*	putative 4→3 endopeptidase
DacB1	*rv3330*	4→3 carboxypeptidase
DacB2	*rv2911*	4→3 carboxypeptidase
Arabinogalactan Synthesis		
RmlA	*rv0334*	transfers dTDP to glucose (Glu)
RmlB	*rv3464*	dehydrates dTDP-Glu to dTDP-4-keto-6-deoxy-D-Glu
RmlC	*rv3465*	epimerizes dTDP-4-keto-6-deoxy-D-glucose to dTDP-4-keto-rhamnose
RmlD	*rv3266*	generates dTDP-rhamnose from dTDP-4-keto-rhamnose
WecA	*rv1302*	transfers NAG*p* from UDP—NAG to DP
WbbL	*rv3265*	adds dTDP-rhamnose to DP—NAG*p* to form the linker unit of AG synthesis
Glf	*rv3809*	isomerizes UDP—Gal*p* to form UDP—Gal*f*
GlfT1	*rv3782*	transfers initial Gal*f* to DP—NAG*p*—Rha
GlfT2	*rv3808*	transfers Gal*f* residues to DP—NAG*p*—Rha—Gal*f*
RfbE	*rv3781*	putative ABC transporter (with RfbD) that translocates lipid-linked galactan chains across the plasma membrane

Appendix 1 (Continued)

RfbD	*rv3783*	putative ABC transporter (with RfbE) that translocates lipid-linked galactan chains across the plasma membrane
UbiA	*rv3806*	transfers 5-phosphoribose 1-diphosphate (pRpp) to DP to form DP-5-phosphoribose (DPPR)
Rv3807	*rv3807?**	dephosphorylates DPPR to form DP-5-ribose (DPR)
DprE1	*rv3790*	oxidizes DPR to form DP-2-keto-erythro-pentose (DPX)
DprE2	*rv3791*	reduces DPX to form DP-Ara*f* (DPA)
AftA	*rv3792*	transfers first Ara*f* group to DP—NAG*p*—Rha—Galf_{30}
EmbA	*rv3794*	transfers Ara*f* groups to DP—NAG*p*—Rha—Galf_{30}—Ara*f*
EmbB	*rv3795*	transfers Ara*f* groups to DP—NAG*p*—Rha—Galf_{30}—Ara*f*
AftB	*rv3805*	transfers final Ara*f* to DP—NAG*p*—Rha—Galf_{30}—Araf_{64}
AftD	*rv0236*	generates the branched 1,3-Ara*f* motif
Rv1459	*rv1459*	generates the branched 1,3-Ara*f* motif
AftC	*rv2673*	generates the branched 1,3-Ara*f* motif
Mycolic Acid Synthesis		
Fas	*rv2524*	synthesizes C_{20}-C_{26} fatty acid precursors from acetyl-CoA and malonyl-CoA
FabD	*rv2243*	transfers malonyl residue to acyl carrier protein (ACP)
AcpM	*rv2244*	facilitates fatty acid elongation by carrying growing acyl chains between enzymes of the Fas system
FabH	*rv0533*	condenses malonyl-ACP to produce β-ketoacyl-ACP
MabA (FabG1)	*rv1483*	reduces β-ketoacyl-ACP to β-hydroxyacyl-ACP
HadAB	*rv0635/ rv0636*	dehydrates β-hydroxyacyl-ACP to form 2-*trans*-enoyl-ACP
HadBC	*rv0636/ rv0637*	dehydrates β-hydroxyacyl-ACP to form 2-*trans*-enoyl-ACP
InhA	*rv1484*	reduces 2-*trans*-enoyl-ACP for final chain elongation
KasA	*rv2245*	initial extension of β-ketoacyl chain to C_{40} by condensing with malonyl-ACP
KasB	*rv2246*	extends β-ketoacyl chain to C_{54} by condensing with malonyl-ACP
EchA10*/EchA11*	*rv1142/ rv1141*	isomerizes 2-*trans*-enoyl-ACP to generate *cis* unsaturated precursors
DesA2/DesA3	*rv1094/ rv3229*	Desaturates the 2-*trans*-enoyl-ACP to generate unsaturated precursors
MmaA2	*rv0644*	generates a cyclopropane ring into the distal chain; also cyclopropanates MmaA4's product at the proximal *cis* site
PcaA	*rv0470*	generates a cyclopropane ring into the proximal chain

Appendix 1 (Continued)

MmaA4	*rv0642*	alters the distal *cis* unsaturation to an alcohol and adds a methyl group to generate *cis*-oxygenated precursors
MmaA1	*rv0654*	alters the proximal *cis* unsaturation to an allylic methyl branch with *trans* saturation to generate *trans*-oxygenated meroacid precursors
MmaA3	*rv0643*	transfers methyl group to secondary alcohols of MmaA4 and MmaA1's products to generate *cis*- and *trans*-methoxy-meroacids
CmaA2	*rv0503*	introduces *trans* cyclopropanation at proximal site of MmaA1's product
Rv0161*	*rv0161*	oxidizes MmaA4's hydroxy-meroacid in the first step of keto-meroacid precursor generation
AdhE1*/Rv3057*	*rv0162/ rv3057*	reduces the oxidized product of Rv0161* to generate keto-meroacid precursors
AccD4	*rv3799*	carboxylates the meromycolate precursor
AccD5	*rv3280*	carboxylates the product of AccD4 to generate a precursor for Pks13 condensation
FadD32	*rv3801*	acyl-adenylates the α-branch Fas precursor and loads it onto Pks13
Pks13	*rv3800*	synthesizes mature α-mycolates from AccD5 and FadD32 products
CmrA	*rv2509*	reduces β-ketoacyl from Pks13 condensation for ligation to AG
Rv3802*	*rv3802*	putatively transfers mature mycolates to mannopyranosyl-1-phosphoheptaprenol (PL) to form myc-PL
Rv1288*/Rv0519*	*rv1288/ rv0519/*	putatively transfers myc-PL to trehalose 6-phosphate forming TMM-phosphate for extracellular transport
OtsB1*	*rv2006*	putatively dephosphorylates TMM-6-P for extracellular transport
Mmpl3	*rv0206*	putative transporter for TMM export
FbpA/FbpB/FbpC/FbpD (Ag85 complex)	*rv3804/ rv1886/ rv0129/ rv3803*	transfers mycolic acid from TMM to arabinogalactan to mycolate the cell wall

*Biochemical function of these enzymes have not been verified in the processes indicated.
* Unsaturation could occur through two distinct mechanisms (see Barry *et al*, Infect Disord Drug Targets, 2007).

Appendix 2. Supplementary Data for Chapter 3.

Overview

These data are the supplementary information for the manuscript under review that comprises Chapter 3.

Attributions

I performed the experiments and analyzed the data in S1, S2, S4, S5, S6, S7 (A,B,C), S8, S9, S10, and S11. I made all the strains for the experiments except for the *E. coli* overexpression vectors for wildtype and TG- PonA1, which were made by Michael Chao. Cara Boutte made the *E. coli* strains for the phospho-transfer experiments done in S7D. Christina Baer and Cara Boutte purified the *Mtb* kinases for the phosphorylation experiments. Amy Barczak performed the lipidomic analysis and analyzed the data in S3. Xavier Meniche performed the mass spec and analyzed the data in S7D. Jemila Caplan Kester made the microfluidic devices I used for experiments in S8. Hesper Rego helped set up the experiment in her CellASIC microfluidic device that is displayed in S5.

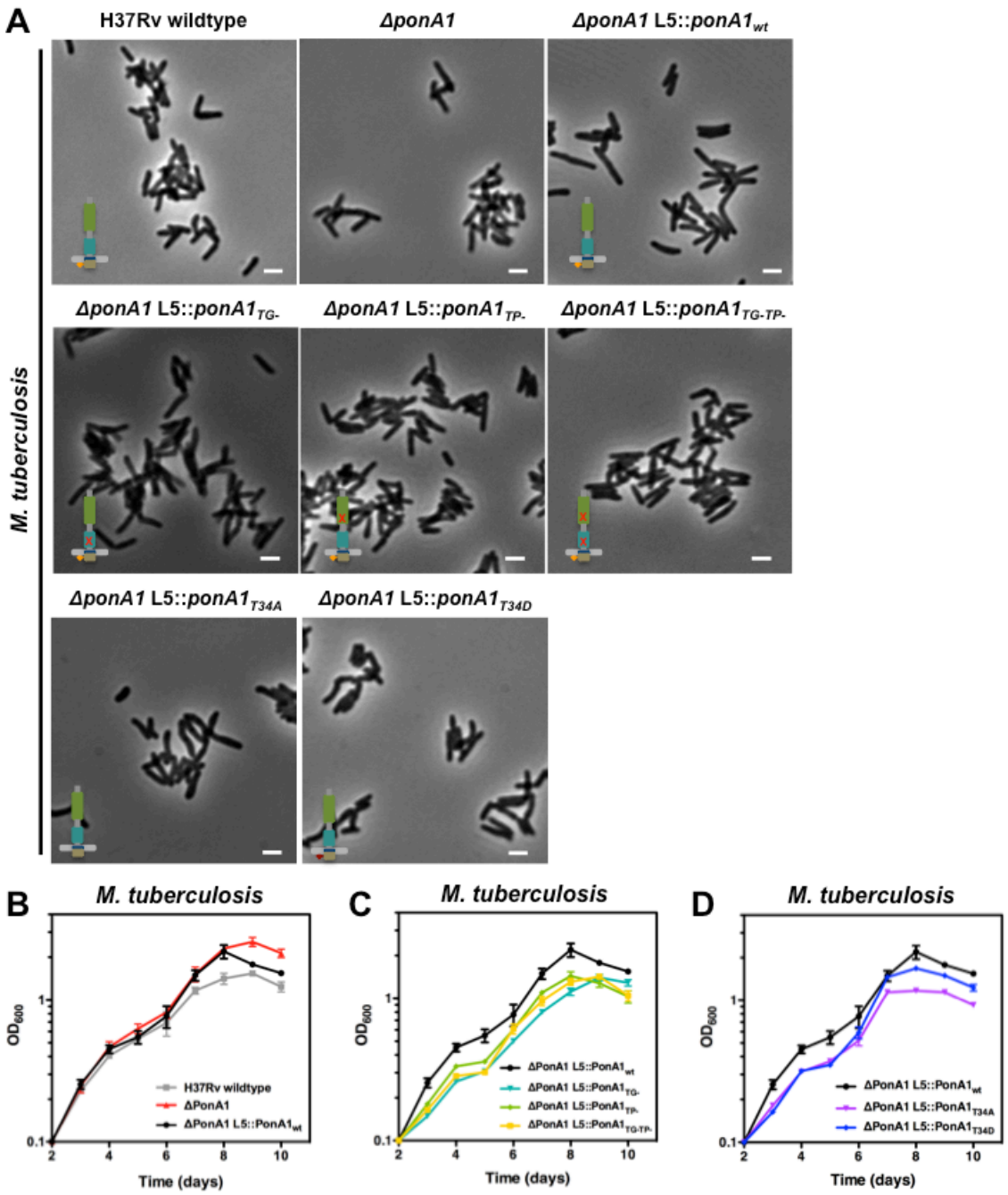

S1 Figure. Changes to PonA1 function modestly impacts *Mtb* morphology.
(A) Cells that no longer express PonA1 or that express PonA1 catalytic or regulatory mutants exhibit no gross morphological changes. Scale bar, 2 μm. **(B)** Population doubling is not severely impacted by loss of PonA1 when cells are grown in standard laboratory conditions. **(C)** Expression of catalytic mutants of PonA1 does not significantly impact population doubling rates, suggesting that the defect observed during infection is not due to changes in growth rate. **(D)** Similarly, changes to PonA1's regulatory activity do not significantly change population doubling rates.

S2 Figure. Normal cell growth requires a fully functional PonA1.
(A) A panel of PonA1 mutants was constructed to investigate the cellular role of PonA1. Catalytic mutations in the TG or TP domain replace the active site serine with an alanine to abolish enzymatic activity (red X). The phosphorylation mutations either remove the phosphorylation site (yellow bar) by replacing the phosphorylated threonine with an alanine (lack of yellow bar) or attempt to mimic the phosphorylation with a threonine to aspartic acid muation (dark red bar). The truncation mutations were deletion of the majority of the cytoplasmic tail (*Msm* $PonA1_{95\text{-}827}$) or of the TP domain (*Msm* $PonA1_{1\text{-}360}$). **(B)** Expression of $PonA1_{TP\text{-}}$-FLAG complements bacterial growth, although population doubling rates are slightly dampened. **(C)** During exponential growth, the TP- cells have an average doubling time of 4.21 hours, whereas isogenic wildtype doubles on average every 3.40 hours (p-value < 0.0001 by the unpaired two-tailed t-test). **(D)** The $PonA1_{TP\text{-}}$-FLAG isoform is stable, suggesting the phenotype of short cell length is due to lack of PonA1's PG crosslinking. **(E)** Expression of an allele that encodes only PonA1's TG domain ($PonA1_{1\text{-}360}$-FLAG) complements bacterial survival, although it dampens population doubling rates. **(F)** During exponential growth, $PonA1_{1\text{-}360}$ cells double on average every 4.23 hours, whereas isogenic wildtype doubled every 3.45 hours in this experiment (p-value < 0.0001 by the unpaired two-tailed t-test). **(G)** The $PonA1_{1\text{-}360}$-FLAG protein is stable, suggesting the cell shape changes observed are due to changes in PonA1 function because of the truncated allele and not due to an unstable protein isoform.

S2 Figure (Continued)

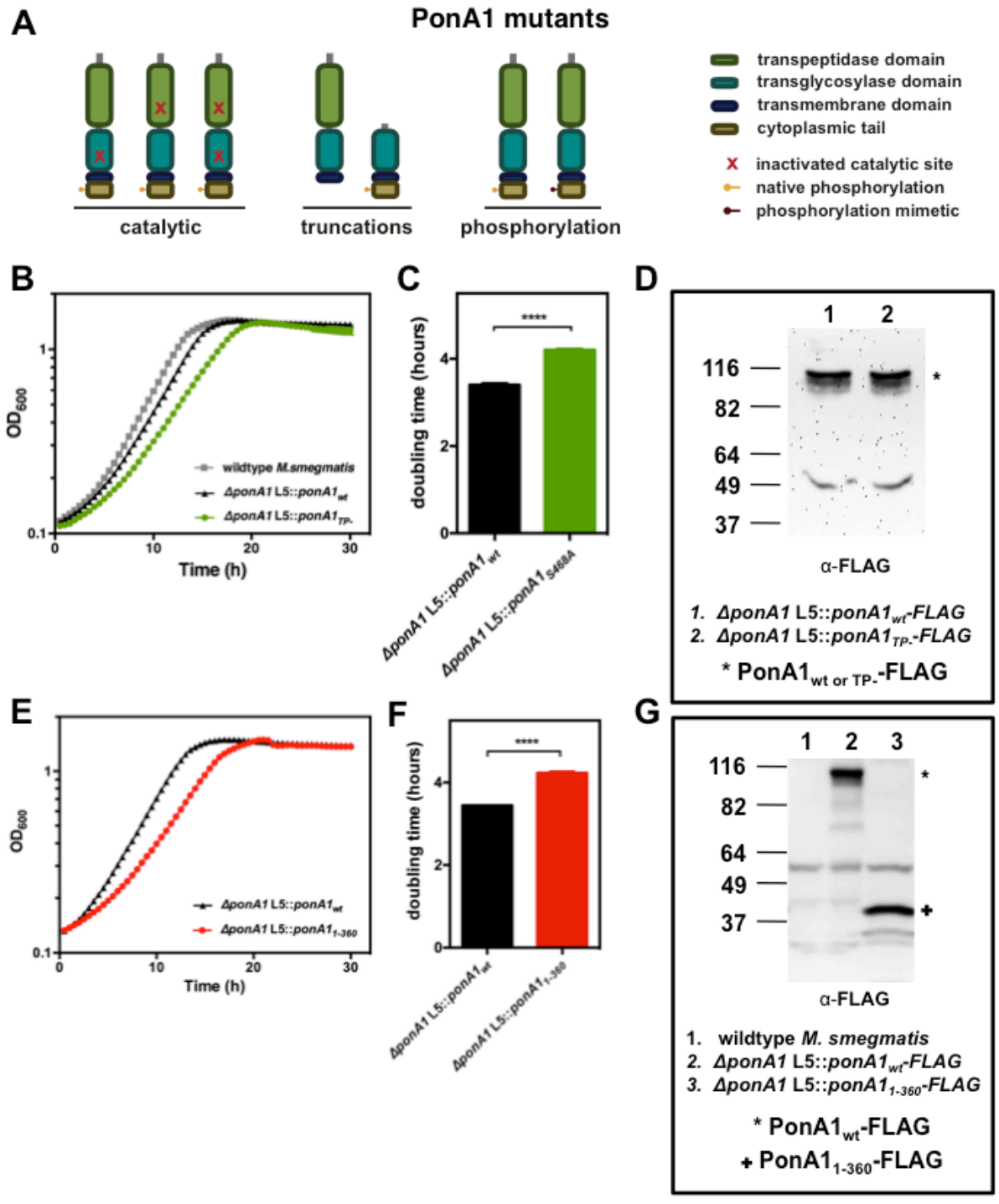

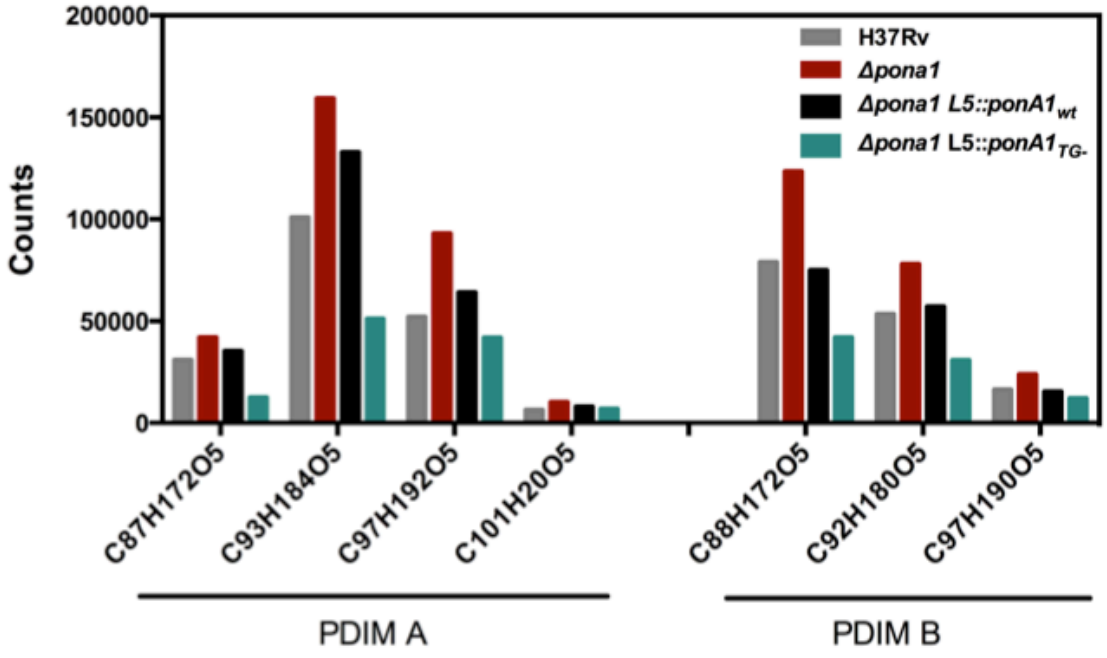

S3 Figure. Mass spectrometric quantitation of pthiocerol dimycocerosate (PDIM) for strains used for mouse infections. Total cell wall lipids from *M. tuberculosis* in mid-log phase growth were extracted with chloroform:methanol and quantitated using established liquid chromatography-mass spectrometry protocols [43]. Individual PDIM A and PDIM B species were identified based on characteristic retention times and highly accurate mass matching (NH4+ adducts).

S4 Figure. Overproduction of PonA1 mutants changes *Msm* cell shape.
(A) Cells that overexpress different catalytic variants of PonA1 exhibit cell shape changes, including ectopic polar growth, bulging poles, and altered cell length. Cells were imaged six hours of induction. Scale bar, 2 μm. **(B)** Quantitation of cell length of cells in (A). A TG- allele of PonA1 negatively impacts cell length more than other catalytic variants, perhaps because these cells also produce the highest frequency of ectopic poles. Cells that do not exhibit an ectopic pole are shorter than wildtype, however, which may suggest a role for balanced PG synthesis in productive activity of the elongation complex (control: 237 cells; wildtype: 226 cells; TG-: 244 cells; TP-: 163 cells; TG-TP-: 234 cells; representative data. Significance was assessed by the Kolmogorov-Smirnov test. $PonA1_{wt}$ compared to $PonA1_{TG-}$ approximate p-value < 0.0001; $PonA1_{wt}$ compared to $PonA1_{TP-}$ approximate p-value < 0.0001; $PonA1_{wt}$ compared to $PonA1_{TG-TP-}$ approximate p-value < 0.0001). **(C)** Overexpression of PonA1 leads to ectopic poles usually at one pole; rare cells are observed with both poles having formed ectopic poles. However, these cells usually exhibit multiple septa (white arrows), indicating these cells are not truly uni-cellular and are not an accurate reflection of 'symmetrically' active growth poles. **(D)** Endogenous PonA1 tagged with RFP on the chromosome localizes to the cell pole and mid-cell in *M. smegmatis*.

S4 Figure (Continued)

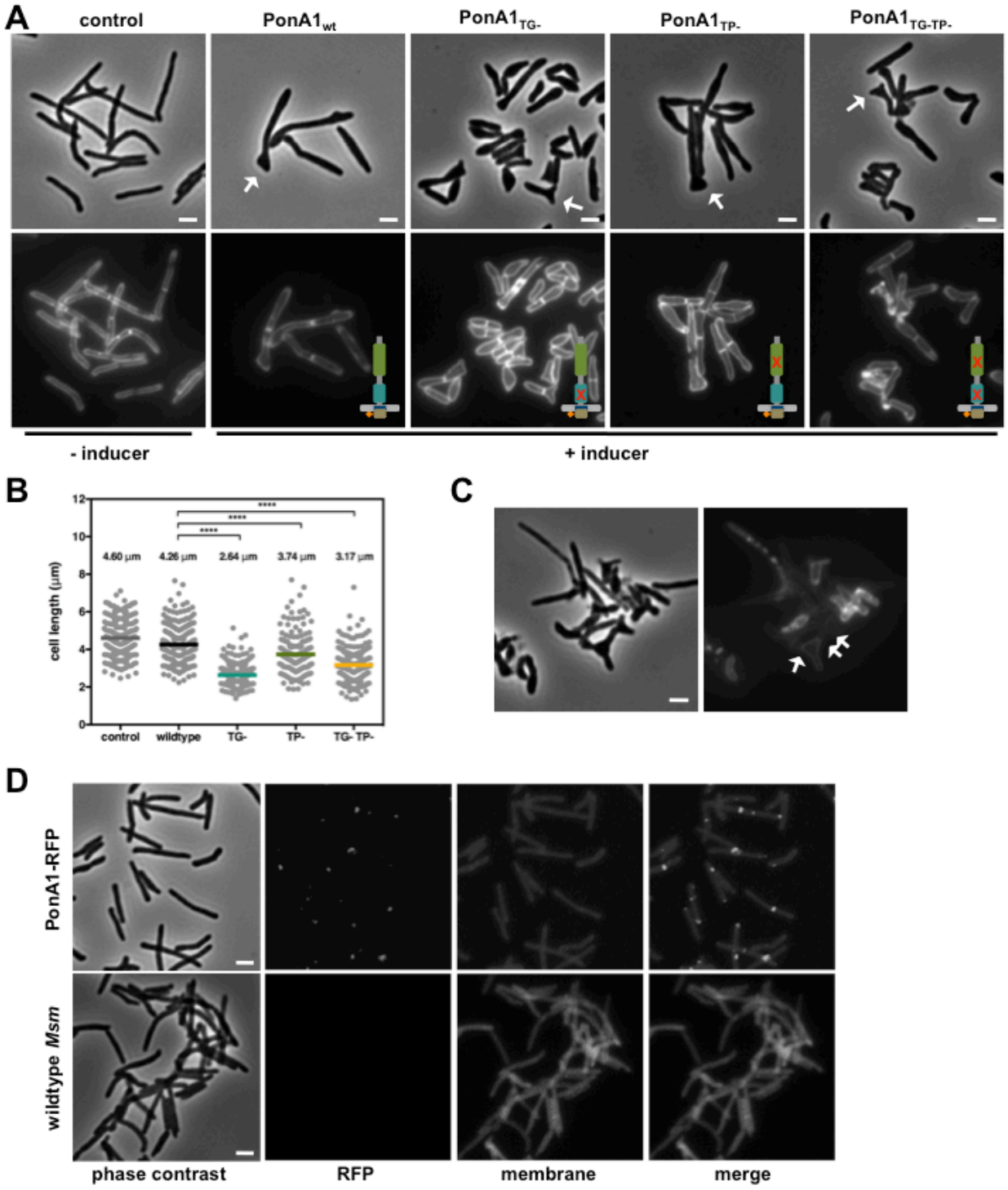

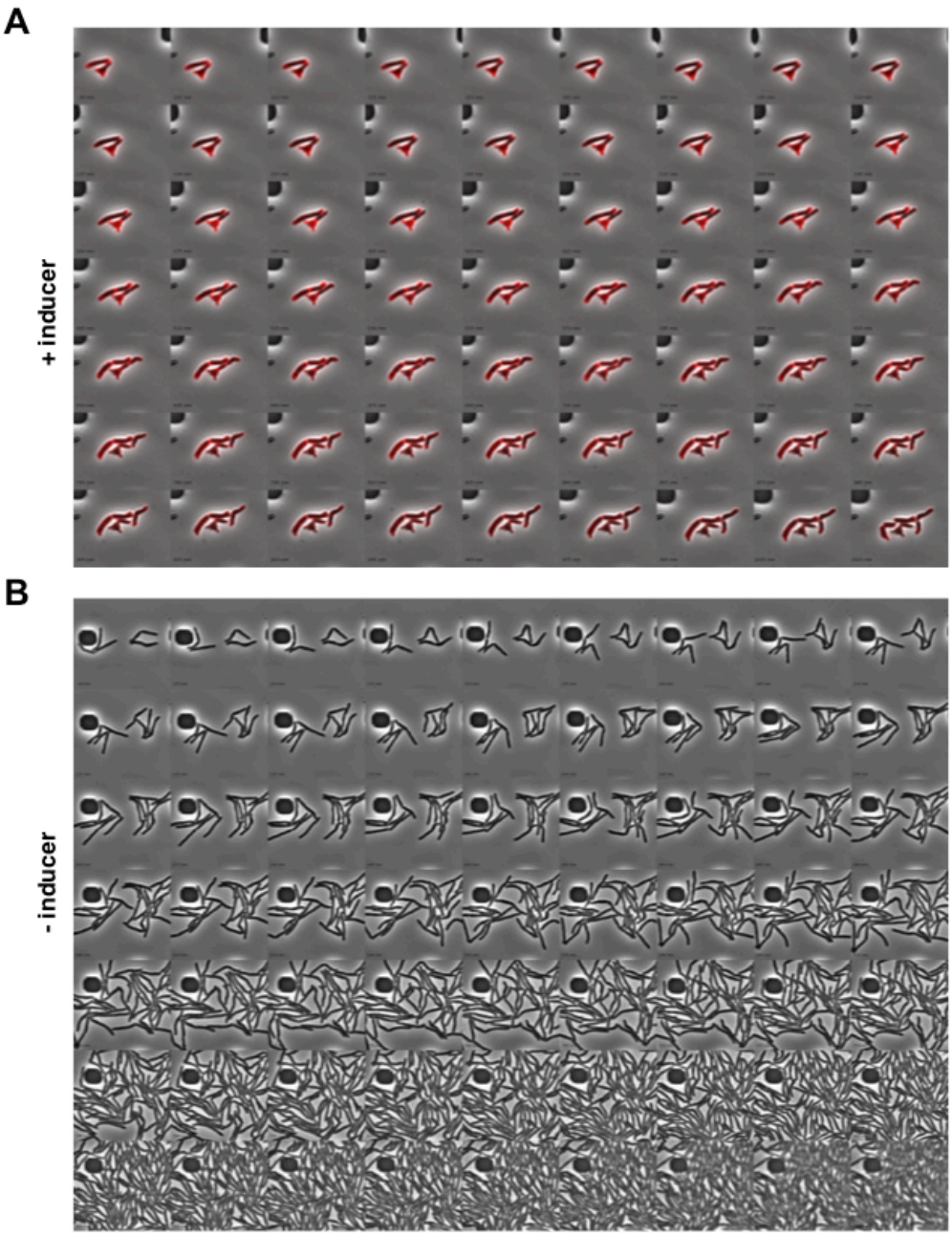

S5 Figure. PonA1 is an early polar localizing factor that drives polar growth.
(A) *Msm* cells that encode an overexpression vector for the TG- allele of PonA1-RFP were grown ± inducer to overproduce $PonA1_{TG-}$-RFP for four hours. The cells were then imaged for 17 hours ± inducer in the CellASIC microfluidic system to visualize cell growth. Cells that overexpress $PonA1_{TG-}$-RFP exhibit slow population growth as previously observed. PonA1 localizes to the pole prior to budding of the ectopic pole (follow cell with white arrow), suggesting that PonA1 is an early localizing factor at the growth tip and drives growth of the pole or ectopic pole upon PonA1 overproduction. Scale bar, 2 μm. **(B)** $PonA1_{TG-}$-RFP cells grown without inducer exhibit normal morphology in the CellASIC microfluidic system and grow robustly. Scale bar, 2 μm.

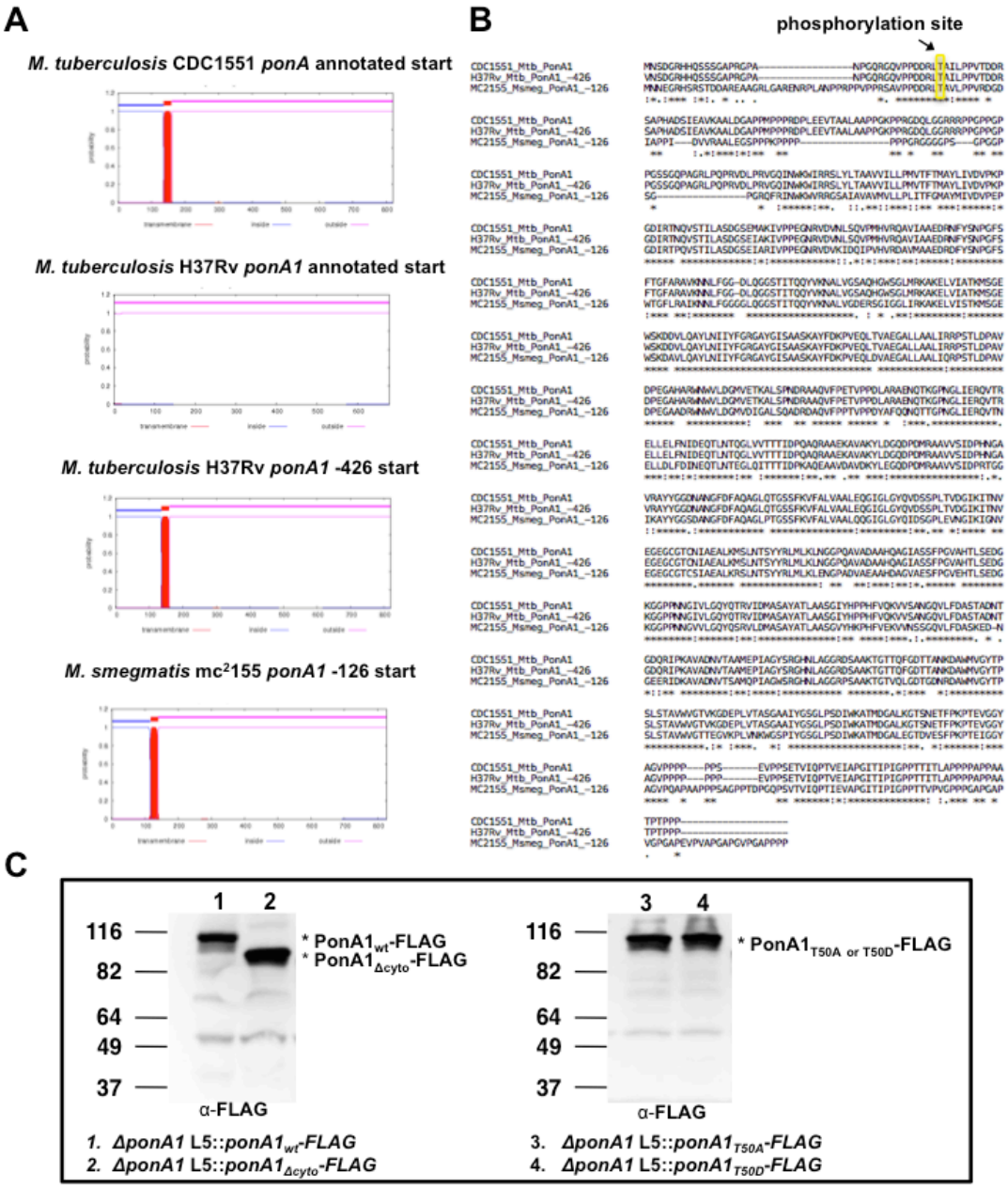

S6 Figure. Mycobacterial PonA1 encodes a phosphorylated cytoplasmic domain.
(A) We used an H37Rv PonA1 (*rv0050*) construct with a start site 426 nucleotides upstream of the annotated start. This start site generates a protein with a predicted transmembrane pass, as expected for PBPs, and captures the translational start site. Alignment of the start site for *Msm* PonA1 (MSMEG_6900) with the *Mtb* genes shifts the start site by 126 nucleotides upstream. **(B)** The -426 *Mtb* PonA1 and -126 *Msm* PonA1 protein align well with the CDC1551 sequence for PonA (proteins were aligned with ClustalO on the EBI server). These proteins contain a phosphorylated threonine (H37Rv PonA1 T34A; *Msm* PonA1 T50A, yellow box). **(C)** Truncation of PonA1's cytoplasmic tail or alteration of its phosphorylation site do not alter protein stability, suggesting the observed phenotypes are not due to aberrant protein production or folding.

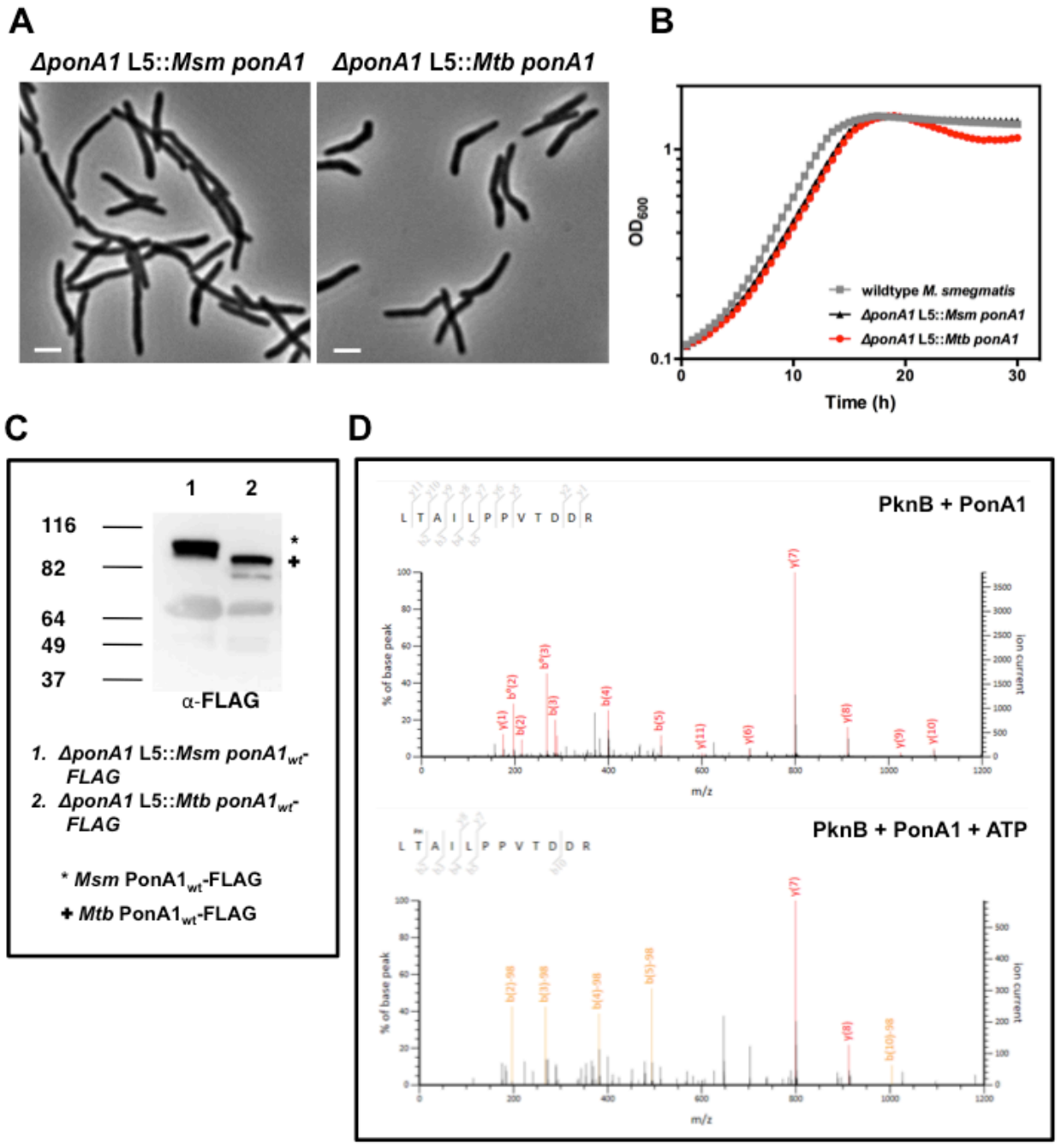

S7 Figure. *M. tuberculosis* PonA1 complements *M. smegmatis* survival.
(A) *Msm* cells that express *Mtb* -426 PonA1 show no morphological differences. Scale bar, 2 μm. **(B)** The *Msm* cells that only express *Mtb* -426 PonA1 also double at rates identical to isogenic wildtype, suggesting that -426 PonA1 fully complements growth of *Msm* that lacks endogenous PonA1. **(C)** The *Mtb* PonA1 allele is produced at similar levels to *Msm* PonA1 (the nonspecific band demonstrates lane 2 has less protein loaded). **(D)** Mass spectrometric analysis confirms that PknB phosphorylates *Mtb* MBP-PonA1$_{cyto}$ (with the -426 start site) *in vitro*.

S8 Figure. PonA1 phosphorylation regulates single cell elongation rates.
(A) *Msm* cells that express phosphorylation mutants (T50A and T50D) or a truncation of the cytoplasmic tail of PonA1 (*Δ*cyto) exhibit similar population doubling rates to isogenic wildtype or wildtype *Msm*. **(B)** To investigate the impact of PonA1's phosphorylation on cell elongation and division, cells were stained with a green fluorescent dye that binds to the cell surface. After staining, single cells were imaged in custom microfluidic devices, and new cell wall elongation and division events were measured. **(C)** The increase in single cell elongation rate of cells that express $PonA1_{T50A}$ correlates with an increased length of single cells at division, as expected. ($PonA1_{wt}$ compared with $PonA1_{T50A}$ approximate p-value < 0.0001 by the Kolmogorov-Smirnov test. $PonA1_{wt}$ compared with $PonA1_{\Delta cyto}$ approximate p-value < 0.0001 by the Kolmogorov-Smirnov test). **(D)** Expression of T50A or *Δ*cyto PonA1 do not impact single cell generation times. This suggests that the observed increased cell length is due to faster single cell elongation rates alone and is not impacted by altered septation timing. Significance was assessed by the Kolmogorov-Smirnov test, and neither mutant population was statistically different than $PonA1_{wt}$. **(E)** Cell elongation still occurs predominantly from the old pole in the absence of PonA1's phosphorylation or cytoplasmic tail. ($PonA1_{wt}$ compared with $PonA1_{T50A}$ approximate p-value < 0.0001 by the Kolmogorov-Smirnov test. $PonA1_{wt}$ compared with $PonA1_{\Delta cyto}$ approximate p-value < 0.0001 by the Kolmogorov-Smirnov test). **(F)** The new pole exhibits mild increased elongation in cells that express T50A or *Δ*cyto PonA1 compared to wildtype. ($PonA1_{wt}$ compared with $PonA1_{T50A}$ approximate p-value = 0.0036 by the Kolmogorov-Smirnov test. $PonA1_{wt}$ compared with $PonA1_{\Delta cyto}$ approximate p-value = 0.0261 by the Kolmogorov-Smirnov test). Together with (E), these data suggest that loss of PonA1's phosphorylation does not impact subcellular distribution of elongation complexes or PonA1's localization within the elongation complex itself, since the majority of cell elongation still occurs at the old pole.

S8 Figure (Continued)

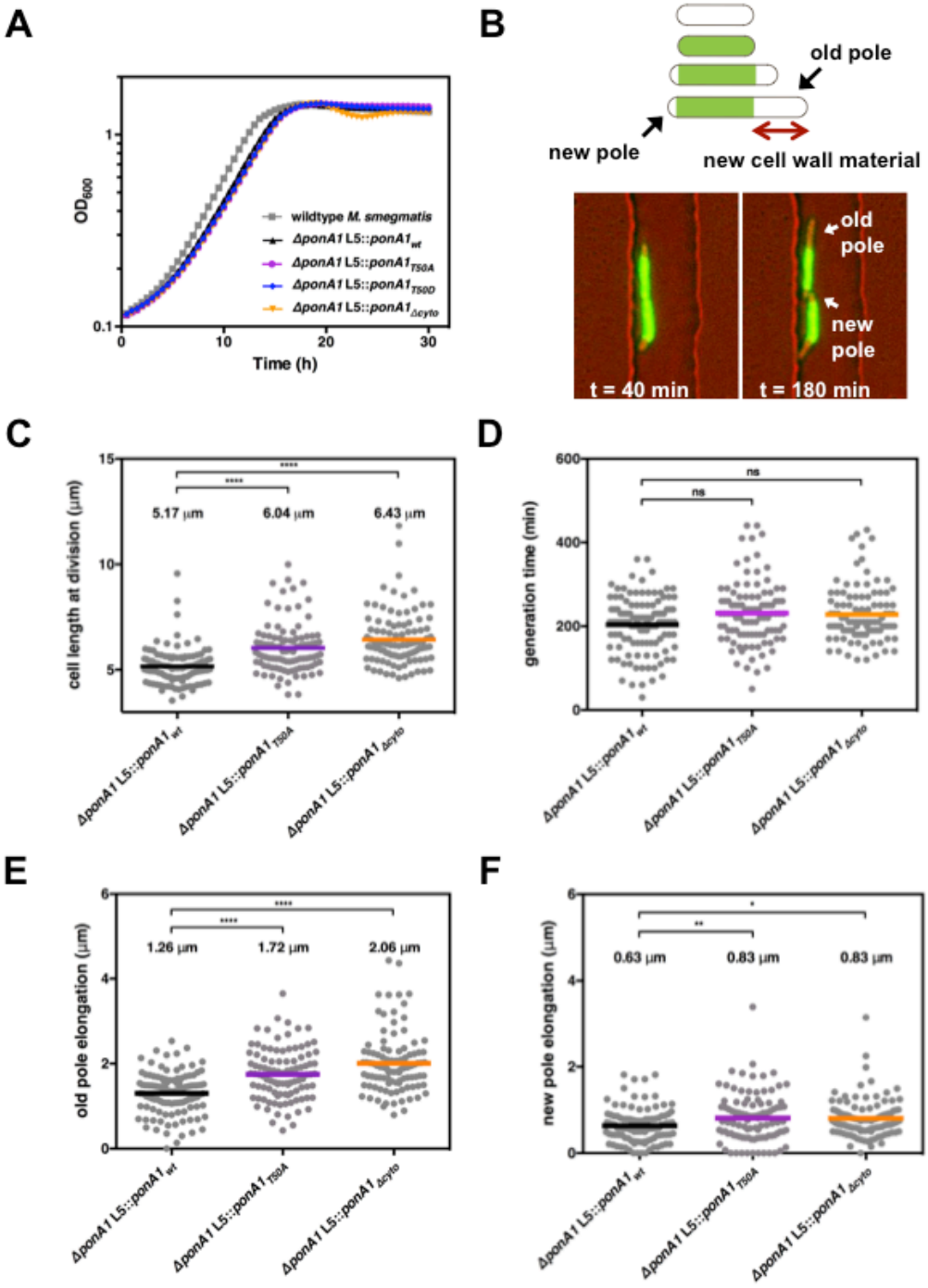

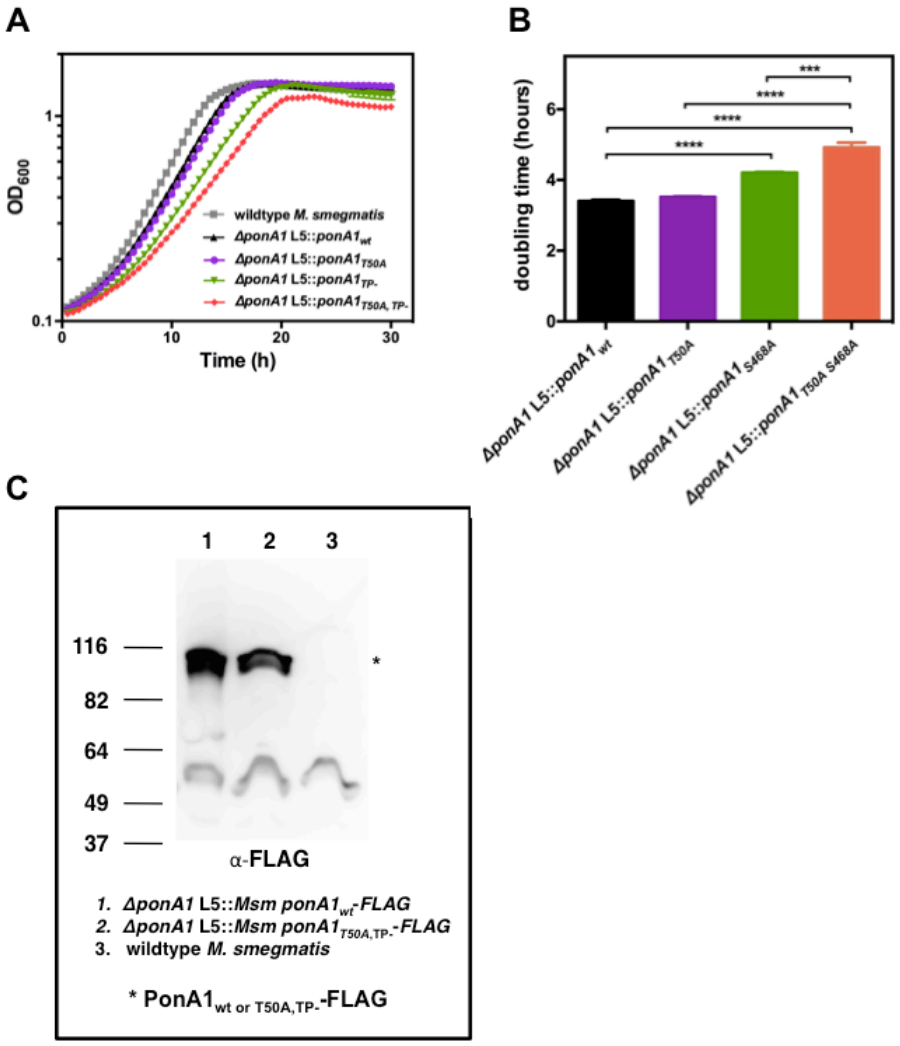

S9 Figure. Inactivating PonA1's phosphorylation site and TP active site together impacts cell growth.
(A) Cells that express a T50A,TP- allele of PonA1 exhibit slower population doubling time as compared to the single point mutants or isogenic wildtype, suggesting that PonA1's phosphorylation may regulate TG activity to promote normal cell elongation and division. **(B)** T50A cells double on average every 3.52 hours, TP- cells double every 4.21 hours (p-value < 0.0001 by the unpaired t-test compared to isogenic wildtype), and T50A,TP- cells double every 4.92 hours (p-value < 0.0001 by the unpaired t-test compared to isogenic wildtype; p-value = 0.0008 compared to TP- cells; p-value < 0.0001 by the unpaired t-test compared to T50A cells), whereas isogenic wildtype doubles every 3.40 hours. **(C)** The T50A,TP- allele is translated into a stable protein.

A

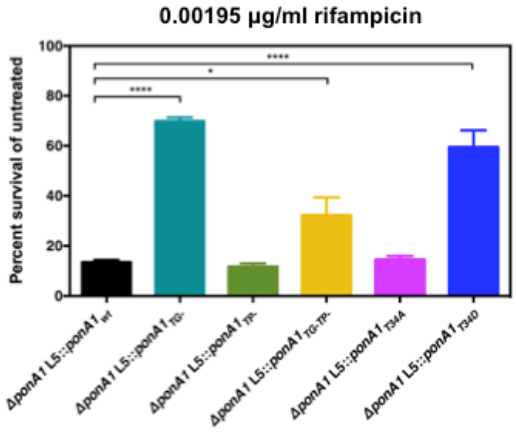

B

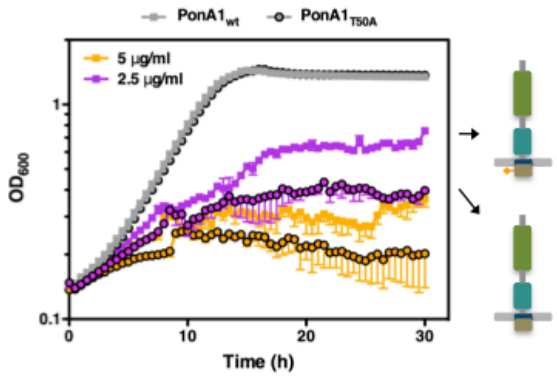

C

Strain	moenomycin A MIC (µM)
M. smegmatis mc²155	39
M. tuberculosis H37Rv	79
M. tuberculosis H37Rv *ΔponA1*	158
M. tuberculosis H37Rv *ΔponA1* L5::*ponA1*$_{wt}$	79
M. tuberculosis H37Rv *ΔponA1* L5::*ponA1*$_{TG-}$	158

S10 Figure. Antibiotic tolerance shifts when PonA1's activity changes.
(A) The impact of rifampicin on *M. tuberculosis* cell fitness of PonA1 catalytic and regulatory mutants was measured by assessing growth by OD_{600} after six days ± drug treatment. (Statistical significance was assessed by one-way analysis of variance with Bonferroni's multiple comparison test, and multiplicity adjusted p-values are reported. $PonA1_{wt}$ compared to $PonA1_{TG-}$ p-value < 0.0001; $PonA1_{wt}$ compared to $PonA1_{TG-TP-}$ p-value = 0.0295; $PonA1_{wt}$ compared to $PonA1_{T34D}$ p-value < 0.0001). **(B)** Changes in *M. smegmatis* cell fitness in the presence of TP domain inhibitors was evaluated by measuring population growth by OD_{600} after treatment with meropenem. **(C)** The minimum inhibitory concentration (MIC) of the TG inhibitor moenomycin was determined for both *Msm* and *Mtb*.

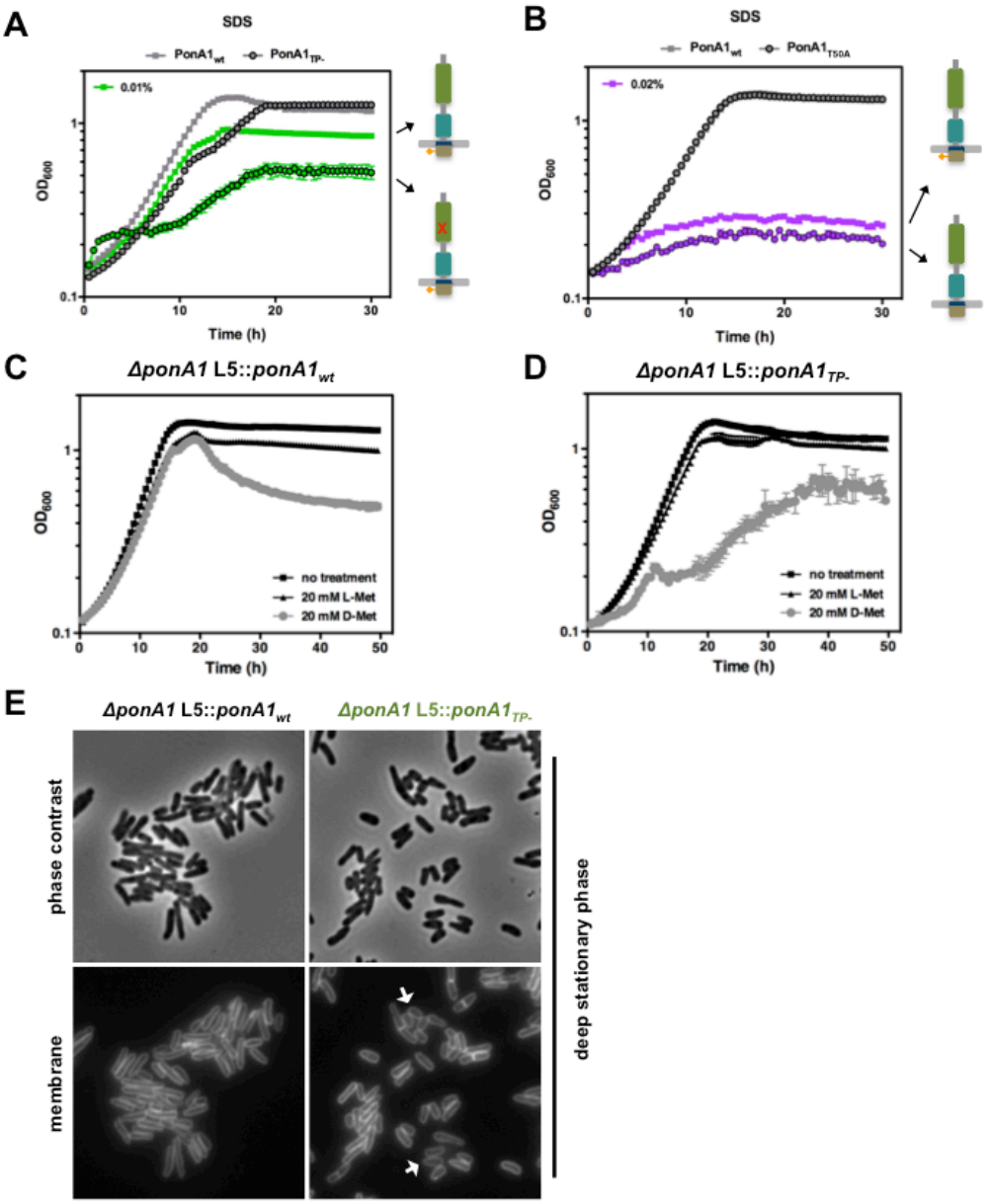

S11 Figure. Normal PonA1 activity is required for cell fitness during stress.
(A) Fitness of *Msm* cells that lack PonA1's TP activity (black outlined circles) during incubation with SDS was compared to isogenic wildtype cells (gray squares). Population growth was measured by OD_{600}. **(B)** Fitness of *Msm* cells that lack PonA1's phosphorylation site (black outlined circles) during incubation with SDS was compared to isogenic wildtype cells (gray squares). Population growth was measured by OD_{600}. **(C)** Fitness of *Msm* cells during incubation with D-Met, L-Met or no treatment was measured by OD_{600}. **(D)** Fitness of *Msm* TP- PonA1 cells during incubation with D-Met, L-Met or no treatment was measured by OD_{600}. **(E)** Cells that express a TP- PonA1 grown until deep stationary phase (cultured for four days) were visualized via light microscopy.

Appendix 3. *Mycobacterium smegmatis* PonA1 suppressor screen.

Overview

These data comprise results from a screen I performed searching for suppressors of *ponA1* essentiality in *M. smegmatis*.

Attributions

I performed the suppressor screen and isolated the genomic DNA from the strains. Dr. Thomas Ioerger at Texas A&M University performed the whole genome sequencing and alignment to the *M. smegmatis* genome.

Rationale

ponA1 is required for the growth of *M. smegmatis* but not for the growth of *M. tuberculosis*. We undertook a suppressor screen to determine whether we could identify a mutation that would relieve the requirement for *ponA1* in *M. smegmatis*. This screen could potentially identify an important interaction that would illuminate PonA1 biology.

S12 Figure. A frameshift mutation in *lpqU* suppresses the essentiality of *ponA1* in *M. smegmatis.* **(A)** Alignment of whole genome sequencing reads to the *M. smegmatis* genome. The *ΔponA1* L5::*ponA1*$_{wt}$ strain (red) has many reads that map to the *ponA1* locus (black dashed box). The *ΔponA1* L5::*tetR M. smegmatis* strain (blue) has no reads that map to the *ponA1* locus. **(B)** Whole genome sequencing reveals genetic mutations unique to a strain of *M. smegmatis* lacking *ponA1* and confirms that *ponA1* is deleted from the genome. The experimental strains differ from the wildtype *M. smegmatis* genome used for whole genome sequencing by several single nucleotide polymorphisms (SNPs) in MSMEG_0510 and MSMEG_4862. The most unique SNP in the suppressor strain (blue) was identified in LpqU. **(C)** Partial sequence of *lpqU* in the wildtype complement strain (red) and the *ponA1* suppressor strain (blue). The single nucleotide deletion in *lpqU* (signified as "– ") occurs approximately at the 18th amino acid, resulting in a frameshift and a likely truncated gene product. **(D)** BLASTp results from the *M. tuberculosis* LpqU homologue (*rv1022*). LpqU exhibits high homology to a lytic transglycosylase.

S12 Figure (Continued)

(A)

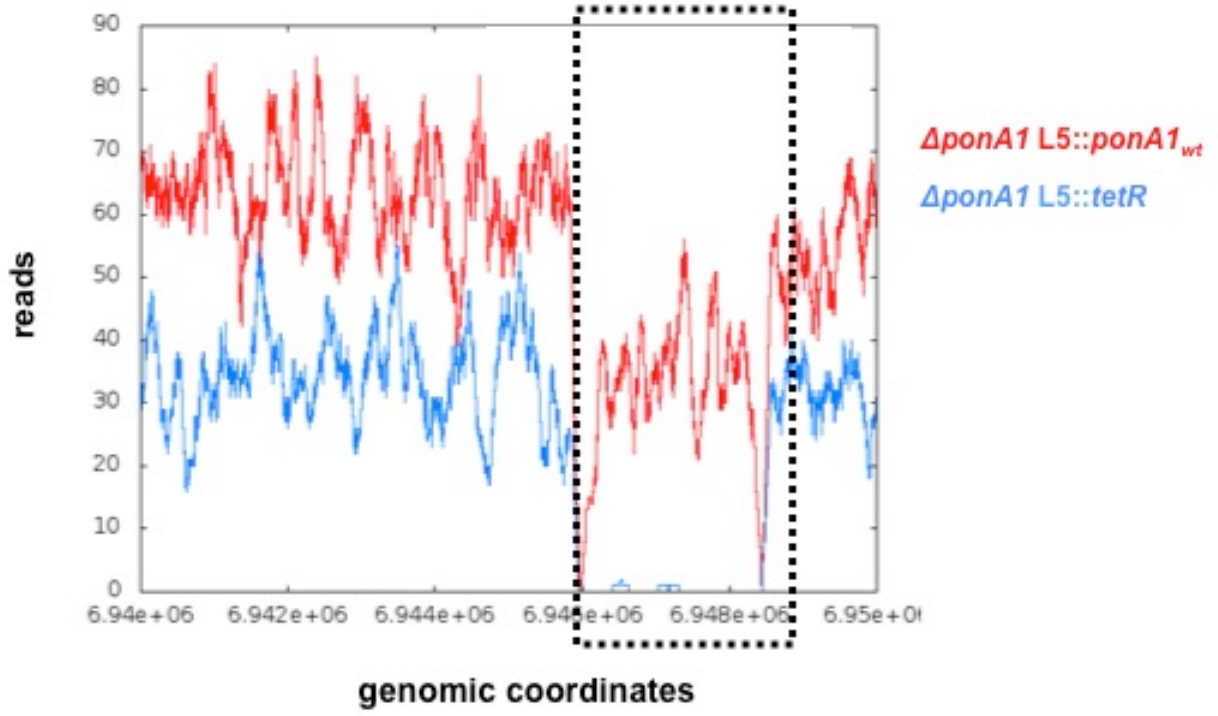

(B)

Strain	Locus	Name	Genetic Changes
ΔponA1 L5::*ponA1*$_{wt}$	MSMEG_0510	Tagatose-1,6-bisP aldolase	+g
	MSMEG_4862	FabG ortholog	+c
	MSMEG_6900	PonA1	S644S, V753V
ΔponA1 L5::*tetR*	MSMEG_0510	Tagatose-1,6-bisP aldolase	+g
	MSMEG_4862	FabG ortholog	+c
	MSMEG_5416	LpqU	-g
	MSMEG_6538	FabG ortholog	T84A (74%)
	MSMEG_6900	PonA1	deletion of entire ORF

(C)

ATGGCTTCCAGCTGCTCGTGGCAGCTCGGCACGCCGATCCCGGAAGGTGTGCCGCCCCGGCCGGT
GATCCGGTCCCCGCGATCGACACCTA

ATGGCTTCCAGCTGCTCGTGGCAGCTCGGCACGCCGATCCCGGAAGGTGTGCCG–CCCGGCCGGT
GATCCGGTCCCCGCGATCGACACCTA

S12 Figure (Continued)

(D)

MULTISPECIES: murein transglycosylase [Actinomycetales]

Sequence ID: ref|WP_033335617.1| **Length:** 246 **Number of Matches:** 1

Range 1: 7 to 241 GenPept Graphics ▼ Next Match ▲ Previous Match

Score	Expect	Method	Identities	Positives	Gaps
238 bits(606)	2e-74	Compositional matrix adjust.	127/235(54%)	155/235(65%)	4/235(1%)

```
Query  8    RAVAVIG-ATAMLLASSCT---WQLSLFITDGVPPPPGDPVPPVDTHAGGRPADQLREWA  63
            R VAV   A+AM L + C     +  + I +G+PP PG PVP +D +  GR A+ LR+WA
Sbjct  7    RTVAVTAIASAMFLTAGCLDLPSKSKVAIPEGIPPNPGAPVPYIDINTPGRTAELLRDWA  66

Query  64   EKRAAALGIPVIALEAYAYAARVAEVENPKCHLAWTTLAGIGRVESHHGTYRGATIAPNG  123
               +    IP++ALEAY  AA +   ++P+C + WTTLAGI  VES HG YRGA IA NG
Sbjct  67   TPISEQTRIPLVALEAYGNAAEIQRQQHPECGITWTTLAGIAGVESKHGRYRGADIAANG  126

Query  124  DVSPPIRGVRLDGTGGTLRIVDRDGGGLDGDAAVERAMGPMQFISETWRLYGVAARNDGI  183
            DVSP IRGV LDGT G   I D DGG LDGD  ++RAMGP QFI  TW  +GV A  DG
Sbjct  127  DVSPEIRGVPLDGTQGNATINDTDGGVLDGDDQLDRAMGPFQFIPTTWERFGVDANGDGR  186

Query  184  ANVDNIDDAALSAAGYLCWRGKDLATPRGWITALRAYNNSVIYARAVRDWATAYA  238
            A++DNIDDAALSAA YLC  G D+ TP GW  A++ YNNS+ Y   VRD A AY+
Sbjct  187  ADMDNIDDAALSAARYLCVSGGDMTTPEGWENAVKVYNNSMQYVLDVRDHANAYS  241
```

Methods

The *ΔponA1* L5::*ponA1*$_{wt}$ strain (Kan^{R}) was transformed with an L5 integrating vector that encoded the *tetR* negative control gene. A positive control transformation with an L5 vector that encoded *ponA1* was performed simultaneously. Of the surviving 7 colonies on the *tetR* transformation plate, one tested negative for the majority of the *ponA1* locus by PCR. Genomic DNA was purified from both the putative suppressor strain and the *ΔponA1* L5::*ponA1*$_{wt}$ strain and analyzed via whole genome sequencing.

Appendix 4. PonA1 mediates low-level rifampicin resistance in *Mycobacterium tuberculosis*.

Overview

These data were published in the manuscript titled *Genomic analysis identifies targets of convergent positive selection in drug-resistant Mycobacterium tuberculosis* by Maha R Farhat*, B Jesse Shapiro*, Karen J Kieser, Razvan Sultana, Karen R Jacobson, Thomas C Victor, Robin M Warren, Elizabeth M Streicher, Alistair Calver, Alex Sloutsky, Devinder Kaur, Jamie E Posey, Bonnie Plikaytis, Marco R Oggioni, Jennifer L Gardy, James C Johnston, Mabel Rodrigues, Patrick K C Tang, Midori Kato-Maeda, Mark L Borowsky, Bhavana Muddukrishna, Barry N Kreiswirth, Natalia Kurepina, James Galagan, Sebastien Gagneux, Bruce Birren, Eric J Rubin, Eric S Lander, Pardis C Sabeti, and Megan Murray in Nature Genetics in September 2013.

*authors contributed equally

Attributions

Maha Farhat and B. Jesse Shapiro performed the whole genome sequencing and data analysis of the *M. tuberculosis* clinical strains that identified the SNPs in *ponA1* associated with drug resistance. I generated the *M. tuberculosis* mutant strains and performed the drug susceptibility assays.

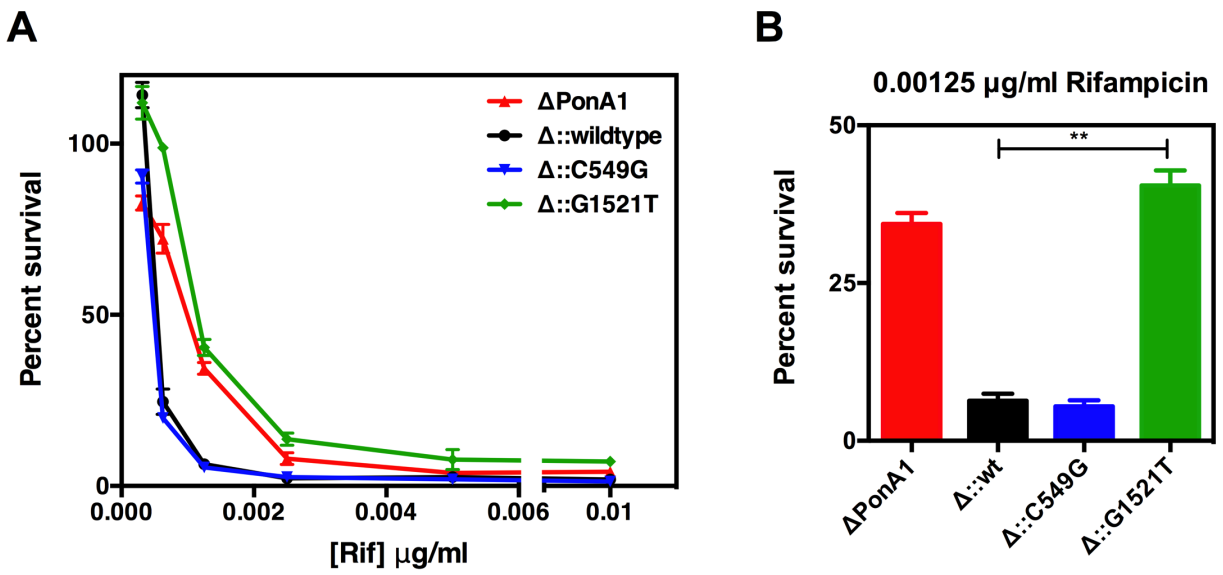

S13 Figure. Clinically identified single nucleotide polymorphisms in *ponA1* mediate low-level tolerance to rifampicin in *M. tuberculosis*.
(A) Bacterial survival (percent of untreated control OD600 absorbance) under increasing concentrations of rifampicin for Δ*ponA1* (ponA1 deletion mutant), Δ::*wildtype* (ponA1 deletion mutant complemented with the wildtype *ponA1* gene), Δ*::G1521T* (*ponA1* deletion mutant complemented with *ponA1* carrying the c.1521G>T allele) and Δ*::C549G* (*ponA1* deletion mutant complemented with *ponA1* carrying the c.549>G allele). **(B)** Bacterial survival as in A) of strains cultured in the presence of 0.00125 µg/ml rifampicin. Two-sided t tests were used to evaluate significance. The difference in survival between the Δ*::wildtype* and Δ*::G1521T* strains was significant (**), with a p-value of 0.006. Error bars, s.d. Four replicate experiments were performed with similar results; representative data are shown.

Methods

M. tuberculosis *strain generation*

Rv0050, encoding *ponA1*, was replaced with a hygromycin resistance cassette using mycobacterial recombineering. The PonA1::Hyg^R replacement was confirmed by PCR and whole genome sequencing. PonA1 SNP alleles C549G and G1521T were generated by site directed mutagenesis and sequence confirmed. Taking into account *ponA1*'s misannotated start site (see Chapter 3), the mutations were generated at nucleotide positions of -426. The C549G SNP is the identified C123G SNP; the G1521T SNP is the identified G1095T SNP. PonA1 wildtype or SNP alleles were cloned under the control of a constitutive promoter and integrated in the *M. tuberculosis* genome as single copies at the L5 phage integration site.

Drug susceptibility assays

All strains were grown in Middlebrook 7H9 medium supplemented with 0.25% glycerol, 10% oleic acid–albumin-dextrose-catalase, and 0.05% Tween-80. For MIC calculations, the strains *ΔponA1*, *ΔponA1* L5::$ponA1_{wildtype}$, *ΔponA1* L5::$ponA1_{C549G}$, and *ΔponA1* L5::$ponA1_{G1521T}$ were grown until mid-log phase (0.5 – 0.8 OD_{600}) and then diluted to a calculated starting OD_{600} of 0.006 and grown ± drug for 6 days at 37°C with shaking. All conditions were done in duplicate. Percent survival is calculated by normalizing the OD_{600} measurements of each strain to its respective untreated control.

Appendix 5. PonA1 is critical for normal tolerance to transpeptidase inhibitors.

Overview

These data will be published in a manuscript titled *Structure of the transpeptidase domain of penicillin-binding protein PonA1 from antibiotic resistant strain of Mycobacterium Tuberculosis* by E.V. Filippova, K.J. Kieser, C.H. Luan, Z. Wawrzak, O. Kiryukhina, E.J. Rubin, and W.F. Anderson. The manuscript will be submitted soon.

Attributions

I generated the mutant *M. tuberculosis* and *M. smegmatis* strains. I performed the antibiotic susceptibility assays and analyzed the data.

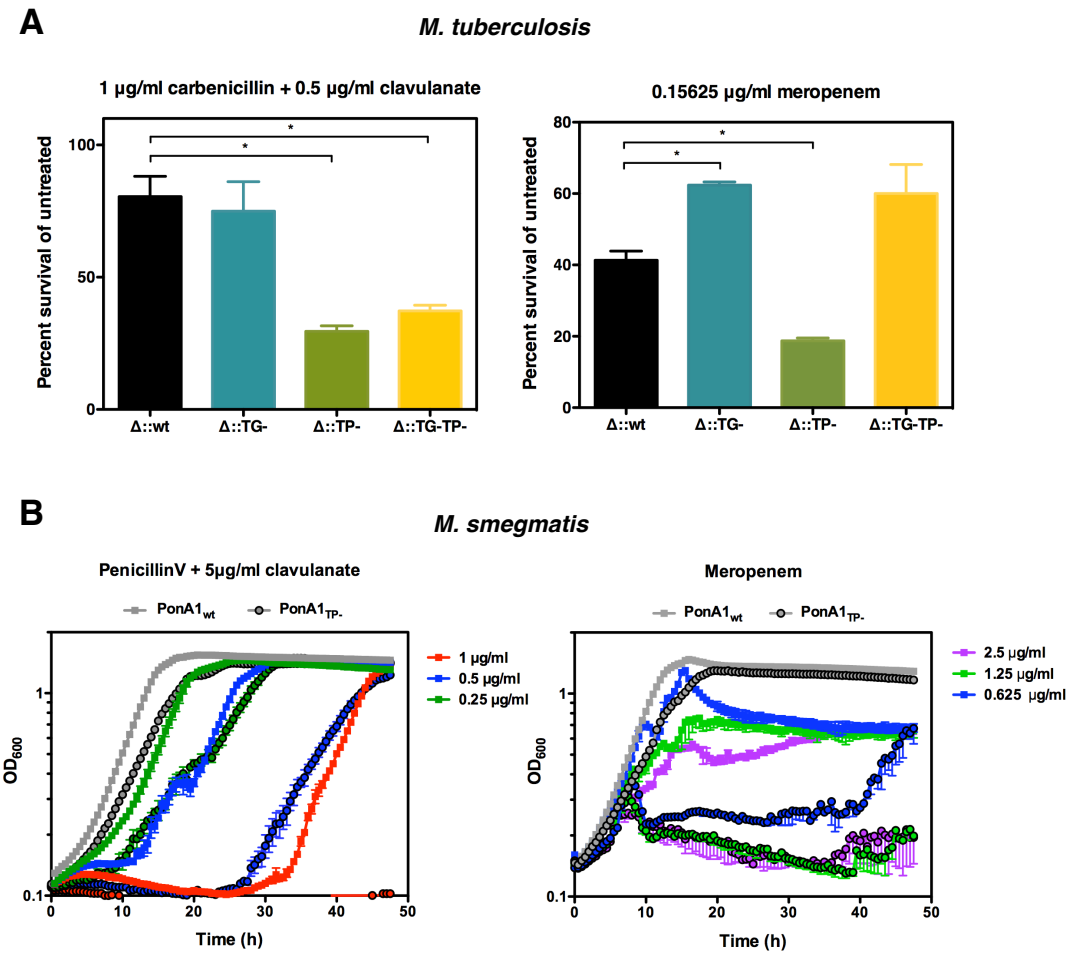

S14 Figure. PonA1 is important for normal tolerance to transpeptidation inhibitors in *M. tuberculosis* and *M. smegmatis*.
(A) Loss of PonA1's transpeptidase activity renders *M. tuberculosis* cells more susceptible to carbenicillin and meropenem (green bars). Transglycosylase, TG; transpeptidase, TP. Two-tailed t-test assessed significance (*, p-value <0.05; **, p-value <0.01). **(B)** Loss of PonA1's transpeptidase activity renders *M. smegmatis* cells more susceptible to treatment of penicillinV and meropenem. Squares, wildtype PonA1. Black-outlined circles, TP- PonA1 (S468A,S469A).

Methods

M. tuberculosis *antibiotic susceptibility assays*

Log phase *M. tuberculosis* H37Rv strains were back-diluted to a calculated OD600 of 0.01 and grown in 7H9 + OADC complete medium ± drug for six days in 24 well plates. Cells were grown at 37°C with shaking. Each strain was cultured in triplicate. Control wells contained no drug. Optical density of each

well measured after six days. Triplicate wells treated with drug were averaged and then normalized to the average of triplicate untreated wells to calculate the percent survival in the presence of drug. Carbenicllin (1 μg/ml) was co-treated with clavulanate (0.5 μg/ml). Meropenem was used at 0.15625 μg/ml.

M. smegmatis *antibiotic susceptibility assays*

Log phase *M. smegmatis* mc^2155 strains were back-diluted to a calculated OD600 of 0.01 and grown in 7H9 + ADC complete medium ± drug for 48 hours in 96 well plates. Cells were grown at 37°C with shaking. Control wells contained no drug. Optical density of each well measured every 30 minutes. All data was plotted without normalization to untreated control strains. Cells were treated with penicillinV at 1 μg/ml, 0.5 μg/ml, 0.25 μg/ml in the presence of 5 μg/ml clavulanate (cultured in triplicate) or meropenem at 2.5 μg/ml, 1.25 μg/ml, and 0.625 μg/ml (cultured in duplicate).